# Sol-Gel Derived Hydroxyapatite, Fluorhydroxyapatite and Fluorapatite Coatings for Titanium Implants

**A thesis submitted for the degree of**

**Doctor of Philosophy**

by

**Christopher Jeremy Tredwin**

UCL Eastman Dental Institute

Divisions of Biomaterials and Tissue Engineering &

Restorative Dental Sciences

University College London

256 Gray's Inn Road

London

WC1X 8LD

**-March 2009-**

**Acknowledgements**

I would like to extend my extreme gratitude to Professor Jonathan Knowles for his continued help, support, assistance, guidance and good humour. I would also like to thank Dr Anne Young for her help, support and assistance.

I would like to thank Dr George Georgiou for taking the time to provide me with support and training in various techniques and uses of equipment.

I would also like to extend my thanks to Dr Derrick Setchell for his help in constructing the Instron Jig and Michael Weisbloom for his help with the photography.

I would like to extend my thanks to David Moles and Peter Howell for their statistical advice. I would also like to thank Ensanya Abou Neel for her help, patience and guidance with the cellular techniques and analysis.

Lastly, I would like to thank my dear wife Sandra, children Harry and Gemma and parents for their continued support, encouragement and understanding throughout my time at The Eastman.

**Declaration**

Except for the help listed in the acknowledgements, the contents of this thesis are entirely my own work. This work has not been previously submitted, in part or in full, for a degree or diploma of this or any other University or examination board.

_____

Christopher Tredwin

Divisions of Biomaterial and Tissue Engineering &

Restorative Dental Sciences,

UCL Eastman Dental Institute,

University College London,

256 Gray's Inn Road,

London

WC1X 8LD

**Abstract**

Currently, most titanium implant coatings are made using hydroxyapatite and a plasma-spraying technique. There are however limitations associated with the plasma-spraying process including; poor adherence, high porosity and cost. An alternative - the sol-gel technique offers many potential advantages but is currently lacking research data for this application.

Hydroxyapatite (HA), fluorhydroxyapatite (FHA) and fluorapatite (FA) have been synthesised by a sol-gel method. Calcium nitrate and triethyl phosphite were used as precursors under an ethanol-water based solution. Different amounts of ammonium fluoride ($NH_4F$) were incorporated for the preparation of the FHA and FA sol-gels. Optimisation and characterisation of the sol-gels was carried out using, X-ray Diffraction (XRD), High Temperature X-Ray Diffraction (HTXRD), Fourier Transform Infrared Analysis (FTIR) and Differential Thermal Analysis (DTA).

Rheology and hydrophilicity of the sol-gels showed that increasing fluoride ion substitution caused an increase in viscosity and contact angle.

The dissolution ($Ca^{2+}$ and $PO_4^{3-}$rates) rates of the fluoride-substituted powders from the sol-gels were considerably lower than that of HA and all rates could be decreased by increasing the sintering temperature. This suggests the possibility of tailoring the solubility of any coatings made from the sol-gels through fluoride ion substitution and increased sintering temperature.

A spin coating protocol has been established for coating the sol-gels onto titanium. Increasing the coating speed decreased the porosity and thickness of the coatings. Bond strengths to titanium were investigated. Fluoride substitution and sintering temperature were shown to be important factors.

Cellular proliferation studies revealed that increasing the level of fluoride substitution in the apatite structure significantly increased the biocompatibility of the material.

The sol-gel technique may be an alternative to plasma spraying for coating titanium implants. Furthermore it may also be suitable for producing HA, FHA and FA as bone grafting materials.

## 1. Contents

## List of Figures

## List of Tables

# Chapter 1:

# Introduction &

# Literature Review

## 1. INTRODUCTION

Titanium (Ti) and its alloys have long been recognized as dental and orthopedic implant materials. To improve the implant-tissue osseointegration, considerable effort has been exerted to modify the Ti surface structure both physically and chemically (Adell et al., 1981; Ratner, 1993; Nanci et al., 1998). Hydroxyapatite [HA, $Ca_{10}(PO_4)_6(OH)_2$] coatings on Ti substrate have attracted significant attention for several years aimed at combining the excellent biocompatibility of HA and load-bearing ability of Ti (Block et al., 1989; McPherson et al., 1995). Currently, most HA coatings are produced by a plasma-spraying technique (Bloebaum et al., 1993; Overgaard et al., 1996). In vivo reports on the system have shown good bone-bonding ability and fast osseointegration when compared with pure Ti implants. This was mainly attributed to the osteoconductivity and chemical and biological similarities of HA with the human hard tissues (Hench, 1991; Ducheyne et al., 1992; McPherson et al., 1995).

There are some parameters to be improved in the plasma spraying process, such as coating strength, chemical homogeneity, and residual porosity. These are related to the high fabrication temperature and coating thickness (Overgaard et al., 1996). Recently, alternative methods have been developed to produce thin HA films. The sol-gel technique, being one of the thin film methods provides some benefits over the plasma spraying method, such as chemical homogeneity, fine grain structure, and low processing temperature (Brinker et al., 1990). Moreover, when compared with other thin film methods, it is simple and cost efficient, as well as effective for the coating of complex-shaped implants. Pure fluorapatite (FA, $Ca_{10}(PO_4)_6F_2$) is known to have a much lower solubility than HA, because FA possesses a greater stability than HA,

both chemically and structurally (Morono et al., 1974; Larson et al., 1989). Moreover, the FA is able to form fluorhydroxyapatite (FHA, $Ca_{10}(PO_4)_6F_1OH_1$) with the substitution of $OH^-$ by $F^-$. Hence, modulation of the extent of fluoride substitution provides an effective way of controlling the solubility of the apatite. In practice, the fluoride ion itself has been studied widely in dental restorative areas, due to its advantages over other ions in that it can reduce the formation of caries in bacterially contaminated environments and promotes mineralisation and crystallisation of calcium phosphates in the formation of bone (Morono et al., 1974; Marie et al., 1986). Nevertheless, there have been few reports concerning the fabrication or characterisation of the FA or FHA materials produced via the sol-gel route.

This thesis sought to produce, characterise and optimise hydroxyapatite and fluorapatite sol gels, investigate and characterise the parameters for producing such coatings on titanium and investigate the biological performance in terms of dissolution behaviour and *in vitro* cellular response.

# 1. LITERATURE REVIEW

## *1.1. Bone composition*

Bone is a specialised connective tissue composed of an extracellular matrix that is part organic and part inorganic within which lie bone cells. 35 per cent constitutes the organic part of bone and of that, 95 per cent is made up of mainly type I collagen fibres, the rest consists of non-collagen proteins of bone, such as osteocalcin, osteonectin and osteopontin, plasma proteins, lipids, and glycosaminoglycans. The inorganic mineral component of bone makes up 65 per cent of the bone matrix, and consists of crystalline salts, that are mainly calcium and phosphate based. A well known form of crystalline salt that is a constituent of bone is hydroxyapatite [$(Ca)_{10}(PO4)_6(OH)_2$] (Evans et al., 1990; Aoki, 1991; Narasaraju & Phebe, 1996; Athanasou, 1999).

## 1.2. Apatites

### *1.2.1. Introduction*

Apatites have significant importance to biologists, mineralogists, and inorganic and industrial chemists. Apatites form the mineral component of bone and teeth and as such have much significance in biomedical applications. Due to their biocompatible nature these materials are constantly used for bone replacement or for coatings of bone prostheses. The involvement of apatites and related calcium phosphates in the mineralisation processes and pathological calcifications is attributed to the versatility of these minerals in accepting a large variety of substitutional ions (Verbeek et al., 1995; Narasaraju & Phebe, 1996; Barralet et al., 1998; Merry et al., 1998 ; Ferraz et al., 1999; Lopes et al., 2000; Rendon-Angeles et al., 2000).

The structure and chemistry of the apatites and related calcium phosphates has only recently been, to some extent, fully understood. The basic apatite structure was determined in the early half of the 20$^{th}$ century, however, the structure of the other calcium phosphates has come under some considerable scrutiny. The location of the carbonate group within the structure of biological, mineral and synthetic apatites was also a major debate at the time. Furthermore, the idea that apatites could be precipitated from solution to give Ca/P ratios ranging from 1.6667 to 1.5 without any significant changes in the x-ray diffraction pattern was also ambiguous.

Analytical tools such as single crystal X-ray diffraction have been utilised to determine the structural aspects and crystal chemistry of the apatites and other calcium phosphates. However, due to the lack of suitable single crystals, the application of infra-red and nuclear magnetic spectroscopy have provided other ways of understanding the relationship between carbonate and apatites and the variation in the Ca/P ratios of precipitated apatites.

### *1.2.2. The chemistry of the calcium orthophosphates*

Calcium orthophosphates are salts of phosphoric acid, $H_3PO_4$. The conditions in which the calcium orthophosphates contribute to the development of biological systems depend on the compounds that the phosphoric acid form. $H_3PO_4$ can produce compounds that consist of $H_2PO_4^-$, $HPO_4^{2-}$ or $PO_4^{3-}$ ions. Compounds that contain $H_3PO_4^-$ ions are not normally found in biological systems, and this is due to the acidic conditions needed for the formation of these particular compounds (Elliot, 1994). The mineral part of bone and teeth however contain both $HPO_4^{2-}$ and $PO_4^{3-}$ ions (Penel et al., 1998). More importantly, calcium phosphates occur as minerals in the apatitic form, for

instance hydroxyapatite, where the basic apatitic calcium phosphate can consist of hydrated calcium phosphates that contain $OH^-$ ions (Elliot, 1994).

Other members of this phosphate family include pyrophosphates ($P_2O_7^{2-}$) and polyphosphates that are less significant biologically, however, calcium pyrophosphates are known to occur in some pathological calcifications. Furthermore, the nucleation and crystal growth of calcium phosphates in aqueous systems can be greatly inhibited by the presence of pyrophosphates (Elliot, 1994).

### *1.2.3. The general chemistry and structure of apatites*

The general formula associated with apatites is expressed as $Ca_5(PO_4)_3X$ or as $Ca_{10}(PO_4)_6X_2$, where X can represent a number of ions namely $F^-$, $Cl^-$ or $OH^-$ to give apatites of the fluorapatite, chlorapatite and hydroxyapatite form respectively (LeGeros & LeGeros, 1993).

The apatite structure can accommodate a variety of ionic substitutions, which include the partial or full substitution of $Ca^{2+}$ by $Ba^{2+}$, $Sr^{2+}$ or $Pb^{2+}$ ions (Elliot, 1994). $Pb^{2+}$ exchange can result in apatite structures that are commonly referred to as lead minerals such as $Pb_5(PO_4)_3Cl$ (pyromorphite), $Pb_5(VO_4)_3Cl$ (vanadite) and $Pb_5(AsO_4)_3Cl$ (mimetite). Another common feature of the apatites is the occurrence of halide and $OH^-$ ions present in the same structure. These are normally abbreviated as OH FAp (hydroxyl fluoroapatite), Cl,OHAp (chloro hydroxylapatite) *etc*. Other substitutions that can occur include coupled substitutions whereby one ion is exchanged for another that has the same sign but differs in charge. An example of this is the coupled substitution of a calcium ion, $Ca^{2+}$ for sodium ion, $Na^+$, accompanied by the substitution of a phosphate ion, $PO_4^{3-}$, by a carbonate ion, $CO_3^{2-}$ to give $Ca_9Na(PO_4)_5CO_3(X)_2$. This coupled substitution is necessary to ensure that the neutrality of the apatite structure is

maintained. This type of substitution can be termed a type B substitution and such structures can be found in biological apatites in particular carbonate apatites (Verbeek et al., 1995; Barralet et al., 1998; Penel et al., 1998; Schramm et al., 1998).

Carbonate apatites, which include the minerals francolite, dahllite and the rock phosphates, are an important but controversial group of apatites (Verbeeck et al., 1995). Whether it is viewed from a mineralogical, synthetic or biological perspective the exact nature and crystal structure of carbonate substitution into calcium phosphates has stimulated a great debate since the 1930's. The crystal structure and the effects of carbonate substitution into calcium phosphate apatites was not fully investigated until the 1960's. LeGeros had found that the two type of substitutions, namely type A and type B, had induced changes in the lattice parameters in the carbonate hydroxyapatite crystal lattice (Verbeek et al., 1995; Barralet et al., 1998; Penel et al., 1998; Schramm et al., 1998).

Type A substitution involves the substitution of the $OH^-$ ion for a $CO_3^{2-}$ ion. This exchange results in an increase in the a-axis. This is largely due to the fact that the smaller $OH^-$ is replaced by a larger and more planar $CO_3^{2-}$ ion. In contrast, what was observed for type B substitution is a reduction in the a-axis, which is attributed to the exchange of large tetrahedral phosphate group, $PO_4^{3-}$, for a comparatively small $CO_3^{2-}$ ion (LeGeros & LeGeros, 1993)

The manner in which the carbonate ion substitutes into synthetic apatites appears to differ from that of biological or natural apatites under similar conditions. What is observed in geological mineral apatites is a shorter a-axis compared to stoichiometric HA when formed at high temperatures and pressures, this is associated with B type substitution. In synthetic carbonate

apatite, however, the opposite occurs when formed at high temperatures i.e. type A substitution resulting in a longer a-axis.

The comparison of the lattice dimensions that occur between carbonate hydroxyapatite (CHA) formed by low temperature precipitation reactions and the apatite phases of biological tissues, such as enamel, also exhibit differences to what is expected. What was confirmed by LeGeros is an increase in the a-axis for enamel containing 2.5wt% of carbonate compared to stoichiometric HA (LeGeros, 1965). The study was carried using x-ray diffraction and the lattice dimensions ascertained for CHA prepared by aqueous precipitation at different reaction temperatures. The resulting single phase apatite structure showed a shrinkage in the a-axis as a function of increasing carbonate content, which was indicative of a B-type substitution. This mode of substitution was substantiated by a linear correlation indicated by a decrease in the phosphate content as the phosphate ions are progressively substituted for carbonate ions.

Precipitation of carbonate hydroxyapatite at 25ºC and 37ºC were also undertaken to simulate biological conditions and also mirror the type of carbonate substitutions that occur in enamel apatite (LeGeros, 1965). Crystallographic analysis showed that the crystallinity of the samples were quite poor and consequently any variation in the lattice parameters that would take place could not be detected. However, a drop in the phosphate content was measured and so this might suggest that it is the type-B substitution which occurs in this case.

The biological environment provides the perfect conditions for a variety of ionic substitutions to take place. In the mineral phase of biological tissues simultaneous substitutions of ions can occur, and therefore might explain why

enamel has an enlarged a-axis. The simultaneous substitution of the $OH^-$ ion for $Cl^-$ and $HPO_4^{2-}$ for $PO_4^{3-}$ inhibits any reduction of the a-axis during carbonate substitution. This is primarily due to the fact that the $Cl^-$ ion has a considerably greater ionic radii to $OH^-$, ($Cl^-$ : 1.81Å ; $OH^-$ : 1.37Å) and also any reduction in the a-axis that occurs as a consequence of substituting phosphate groups for smaller carbonate groups can be compensated by the inclusion of large $HPO_4^{2-}$ groups (Rey, 2000).

The mode of vibration that is associated with the $CO_3^{2-}$ ion in infra-red analysis is the $\nu_2$ mode, which can be used to establish the type of carbonate substitution that takes place. In CHA prepared via the solid state method gave a distinct peak at 877$cm^{-1}$, whereas a low temperature precipitation method gave two peaks at 871$cm^{-1}$ and 878$cm^{-1}$ that are associated with type-B carbonate substitution. These two peaks or doublet of peaks represents $CO_3^{2-}$ substituting for $PO_4^{3-}$ at two different phosphate sites. The $\nu_3$ peak, however, was shifted to higher frequencies in the high temperature apatite compared to the precipitated and was lower in intensity. Similarities between the IR spectrum for human enamel and the low temperature precipitated apatite points towards type-B substitution in enamel apatite (Rey, 2000).

Francolite is a naturally occurring mineral. Francolite-like analogues (B-$CO_3$FAp) (B- Type-B carbonate substitution) can be synthesised and have potential medical and dental applications (Elliot, 1994). Fluoride containing ceramics such as fluorapatite (FAp) for instance can be used as implant materials which may prevent caries in teeth by releasing fluoride ions into the oral environment (Joa et al., 1997).

Another mode of substitution commonly seen in francolites is AB substitution. AB-$CO_3$F,OHAp involves the substitution of $CO_3^{2-}$ for $PO_4^{3-}$ ions (B-type

substitution) as well as $CO_3^{2-}$ ions replacing $OH^-$ ions (A-type substitution) (Joa et al., 1997).

### *1.2.4. Hydroxyapatite*

#### *1.2.4.1. Structure*

Crystallographic structures of crystals can be categorized depending on the type of symmetry inherent to them. These structures can therefore be categorized according to their space group. Hydroxyapatite, in particular calcium hydroxyapatite, has a definite crystallographic structure and composition, based on a repeating unit cell (Figure 1). The unit cell of hydroxyapatite consists of a six fold c-axis perpendicular to three equivalent a-axes ($a_1$,$a_2$,$a_3$) at angles 120ºC to each other. The groups that make up the closely packed hexagonal unit cell are $Ca^{2+}$, $PO_4^{3-}$, and $OH^-$ groups (Kay et al., 1964; Abrahams & Knowles, 1994; Feki et al., 1999; Ikoma et al., 1999; Lopes at al., 2000; Morgan et al., 2000).

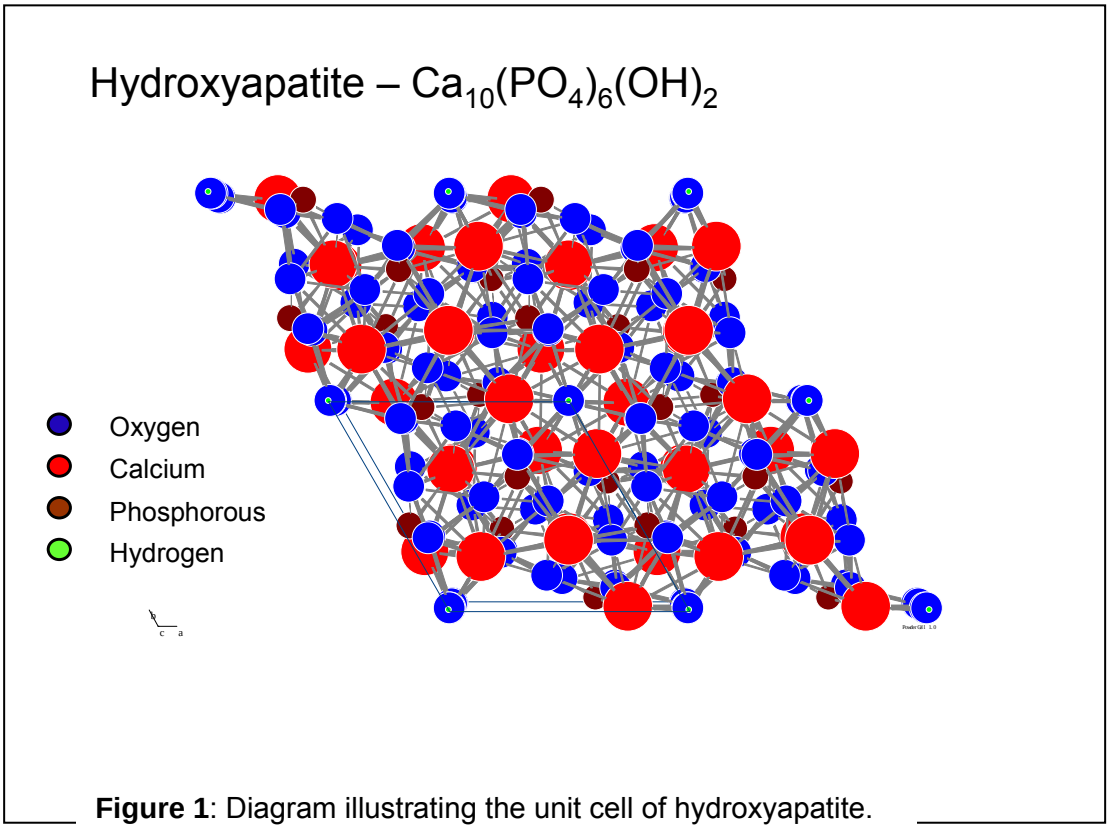


**Figure 1**: Diagram illustrating the unit cell of hydroxyapatite.

The six $PO_4^{3-}$ groups have tetrahedral symmetry and are responsible for the stability of the apatite structure. The atomic arrangements that the atoms adopt in hydroxyapatite are similar to those seen in fluorapatite, ($Ca_{10}(PO_4)_3F_2$), and Cl-Apatite ($Ca_{10}(PO_4)_3Cl_2$), but the $OH^-$ atomic positions in this instance are described for $F^-$ and $Cl^-$ ions that substitute for the $OH^-$ groups (see figure 2).

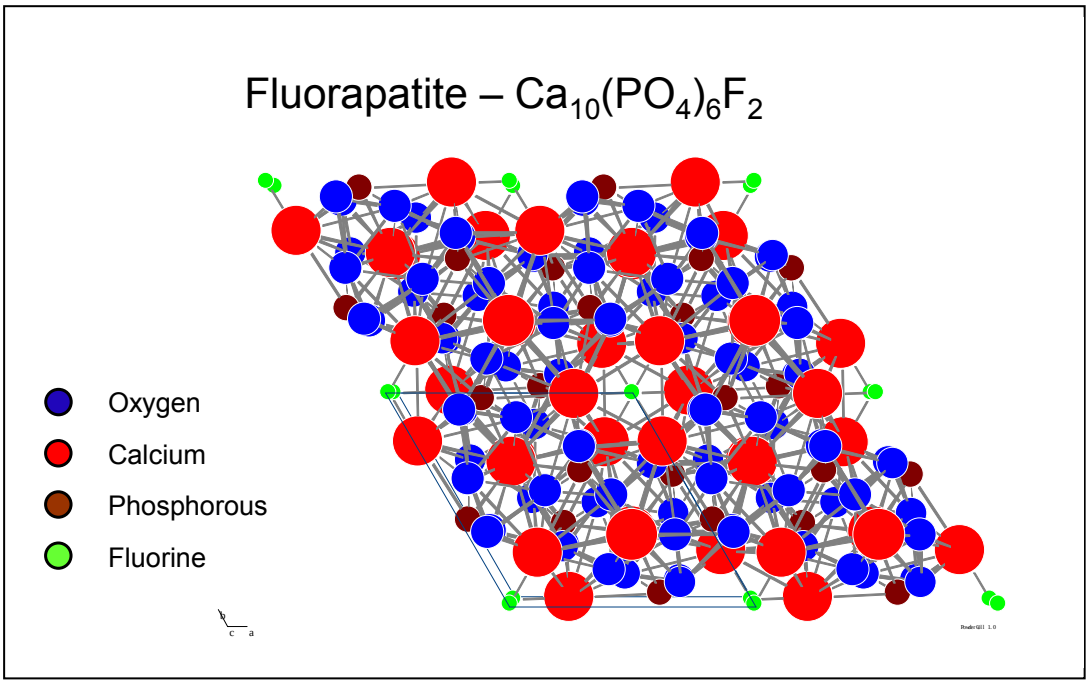


**Figure 2**: Diagram illustrating the unit cell of fluorapatite.

Changes in the properties of Ca-hydroxyapatite can occur as a result of ionic substitutions of $Ca^{2+}$, $PO_4^{3-}$ and $OH^-$ groups within the apatite structure. The changes in properties include lattice parameters, morphology and solubility; however, they can take place without significantly altering the hexagonal symmetry. It has, though, been reported that symmetry changes from hexagonal to monoclinic can occur upon $Cl^-$ substitution for $OH^-$and this is in fact a loss or reduction in symmetry which is thought to reflect the alternating

positions of $Cl^-$ atoms and an expansion of the cell in the b-axis (LeGeros & LeGeros, 1993).

The solubility properties of apatites can give an indication of the crystallinity, stability and crystal size of a particular apatite. Fluoroapatite for instance, exhibits a higher degree of the aforementioned properties, and consequently are less soluble, compared to fluoride free apatites and biological apatites. This can be attributed to a contraction in the a-axis without any change in the c-axis, and arises from substitution of $F^-$ for $OH^-$ (LeGeros & LeGeros, 1993).

Differences in lattice parameters can also be observed for Ca-hydroxyapatite that undergoes cationic substitution. Ions such as strontium ($Sr^{2+}$), magnesium ($Mg^{2+}$), barium ($Ba^{2+}$), lead ($Pb^{2+}$), etc. substitute for $Ca^{2+}$ in the crystal lattice. The extent to which these changes take place reflect the size and amount of the substituting ions. Crystallinity, thermal stability and dissolution properties would consequently alter as cationic substitutions take place, for instance the extent of dissolution would increase for apatites with the substitution of $Sr^{2+}$ or $Mg^{2+}$ for $Ca^{2+}$ (Tonsuaada et al., 1995; Bigi et al., 1996; Golden & Ming, 1999; Kanno et al., 1999; Rangavittal et al., 2000). Furthermore, the presence two substituents such as $Mg^{2+}$ and $CO_3^{2-}$ would have synergistic effects on crystallinity and dissolution properties of synthetic apatites. Alternatively, antagonistic effects can also be seen with the presence of two substituents such as magnesium and fluoride or carbonate and fluoride, with the fluoride effect being the greatest (LeGeros & LeGeros, 1993).

The type of substitutions that have been mentioned are important in understanding how the change in properties of the apatite relate to the way HA behaves as a biomaterial, in particular the manner that HA interacts with bone mineral of the bone-biomaterial interface. HA can be used for clinical

applications such as bone repair, augmentation, substitution and coatings of metals used as dental and orthopaedic implants (LeGeros & LeGeros, 1993).

#### *1.2.4.2. Composition of dense HA*

The theoretical composition of HA whether it is pure, mineral or commercial will undoubtedly vary depending on the phases that are present when sintered. Pure HA is composed of 39.68wt% Ca; 18.45wt% P; giving a Ca/P weight ratio of 2.151 and molar ratio of 1.6667. Dense HA containing only the apatite phase or mixed with other Ca-P phases can exhibit a variation in the Ca/P ratio when sintered, this can be attributed to the presence of secondary phases such as β-TCP. Other factors such as the composition or calcium deficiency in the material before sintering can also influence the Ca/P ratio (LeGeros & LeGeros, 1993). The presence of β-TCP, tetracalcium phosphate, $Ca_4P_2O_9$ or $Ca_4(PO_4)_2O$ along with the HA phase in the sintered material is indicative of a Ca/P ratio which is lower than that of just the HA phase ( Ca/P=1.67 ) and is influenced by the sintering conditions and the temperature. Higher Ca/P ratios than 1.67 would indicate the presence of CaO with the HA phase (LeGeros & LeGeros, 1993). The final composition of dense HA after sintering appears to depend on the sintering temperature, the conditions and Ca/P molar ratio of the apatite preparation prior to sintering (LeGeros & LeGeros, 1993).

Characterisation of HA can be carried out using x-ray diffraction. This technique can give an idea of the other phases present in the sintered material, such as β-TCP, α-TCP, TTCP and CaO, in addition, it can also be used to determine the purity and crystallinity of the HA phase (LeGeros & LeGeros, 1993; Knowles et al., 1996; Georgiou & Knowles, 2001). Furthermore, unit cell parameters of HA and other phases can also be ascertained through XRD and these can give indirect evidence of any substitutions that have taken place.

### *1.2.4.3. Crystallographic properties*

X-ray diffraction can provide information concerning lattice parameters such as **a** and **c** dimensions of a unit cell (LeGeros & LeGeros, 1993). In the case of HA these were found to be around 9.422 and 6.881Å for the a and c dimensions respectively. This method can also give the proportion of other phases present with the HA phase, such as $\beta$ and $\alpha$-TCP, TTCP and CaO (LeGeros & LeGeros, 1993; Knowles et al., 1996; Georgiou & Knowles, 2001).

In physical terms ceramic HA crystals adopt large rhombic shapes that resemble human enamel when sintered at 950°C and are different to smaller acicular apatite crystals before sintering. The presence of lattice defects in the crystal structure of ceramic HA sintered at lower temperatures are known to induce a biological response in vivo compared to those sintered at higher temperatures (LeGeros & LeGeros, 1993). This response is related to the type and amount of defects residing in the material. At 950°C HA contains defects that are hexagonal parallelapiped in shape, as well as other types of defects, and are more predominant than those present at 1250°C. It is therefore expected that a material with a greater number of lattice defects would be more reactive (LeGeros & LeGeros, 1993).

### *1.2.4.4. Infrared*

Infrared spectroscopy is a technique that can often be used to complement x-ray diffraction in the characterisation of hydroxyapatite. The shape and intensity of the absorption bands that arise from the absorption of infrared light by molecules can give a good indication of the chemistry of the material.

Like x-ray diffraction, infrared can be used to detect additional phases in which modes of vibrations belonging to functional groups inherent in the crystal

structure undergo changes in peak shape, intensity and may often involve shifts in vibrational frequency. Infra-red absorption is a technique that can detect vibrational modes corresponding to the energy of a particular bond or group vibration such as $OH^-$ or $PO_4^{3-}$. It can be used to distinguish between different chemical bonds because each absorbs IR radiation of different often characteristic wavenumbers.

The main modes of vibration that hydroxyapatite exhibits are assigned to the hydroxyl stretching mode (~3570$cm^{-1}$), the carbonate $\nu_3$ mode (~1648$cm^{-1}$) and the phosphate $\nu_3$ modes (~1092 and 1042$cm^{-1}$). Additional infrared modes related to these functional groups are given in Table 1 and are assigned to bending and/or deformation modes (Gadaleta et al., 1996; Rehman & Bonfield, 1997; Cheng et al., 1998; Morgan et al., 2000).

Hydroxyapatite can undergo decomposition to secondary phases $\beta$-TCP and $\alpha$-TCP. This can be detected by changes in peak height and shape of the phosphate $\nu_3$ modes accompanied by the loss in intensity of the hydroxyl stretching band.

Infrared spectroscopy can also indicate the presence of substituent ions such as carbonate ($CO_3^{2-}$) and fluoride ($F^-$) (Freund & Knobel, 1977; Rehman & Bonfield, 1997; Barralet et al., 1998). It is commonly known that $CO_3^{2-}$ substitution can occur either as type A substitution in which $CO_3^{2-}$ ions substitute for $OH^-$ groups, or type B substitution in which they substitute for $PO_4^{3-}$ groups. In the former, it is expected to observe an increase in intensity for the vibrational modes related to $CO_3^{2-}$ ions in the hydroxyl sites accompanied by a decrease in intensity for the hydroxyl stretch. In the latter one would expect an increase in the vibrational modes related to the $CO_3^{2-}$ ions in the

phosphate sites accompanied by a decrease in intensity of the phosphate $\nu_3$ modes.

| Peak assignments | Wavenumber |
|---|---|
| HA | ($cm^{-1}$) |
| Hydroxyl stretch | 3568 |
| Carbonate $\nu_3$ | 1650-1300 |
| -(m: medium intensity) | 1648 |
| -(m) | 1454 |
| -(m) | 1419 |
| -(w: weak intensity) | - |
| Phosphate $\nu_3$ | 1190-976 |
| -(vs: very strong intensity) | 1092 |
| -(vs) | 1042 |
| Phosphate $\nu_1$(m) | 962 |
| Carbonate $\nu_2$ (ms: medium strong) | 874 |
| Phosphate $\nu_4$ | 660-520 |
| -(m) | 633 |
| -(vs) | 602 |
| -(vs) | 566 |
| Phosphate $\nu_2$ (w) | 472 |

**Table 1.** Infrared peak assignments of hydroxyapatite (Rehman & Bonfield, 1997).

### *1.2.4.5. Surface chemistry*

The dissolution properties of dense HA ceramic is important in determining the surface chemistry of the material in relation to biological interactions to the HA implant. When the HA ceramic is subjected to an acid environment partial dissolution occurs on the surface forming a hydrated layer consisting of a number of mineral ions. This behaviour is mirrored by the interaction of biological apatites with biological fluids. This suggests that the composition of the ceramic and the pH of the solution influences the surface chemistry, since a more acidic environment will cause greater dissolution on the ceramic HA surface. $Ca^{2+}$, $H_2PO_4^-$, $HPO_4^{2-}$, $PO_4^{3-}$, $H^+$, $OH^-$ and ion pairs $CaH_2PO_4^+$ and

$CaOH^+$ are the type of species that exist in the hydrated layer (LeGeros & LeGeros, 1993).

Surface charges on the HA implant evolve as a result of the electrolytes that exist within biological fluids. Cellular activities involved in bone regeneration on the bone-implant interface are influenced by these surface charges. Surface charges can be expressed by the absolute values of zeta-potential and it has been suggested that differences in these values found for unsintered apatite, Ca-deficient apatite, ceramic HA and stoichiometric HA accounts for the variation in cellular activity on the surface of each material (LeGeros & LeGeros, 1993).

#### *1.2.4.6. Dissolution/precipitation*

Observations made on the surface of ceramic HA after implantation in bony sites indicate the presence of a precipitated layer of microcrystals that are characterized as apatites. Infra-red analysis confirmed these to be crystals of carbonate apatite, similarly, these crystals can be found in bone apatite and are closely linked with the organic matrix (LeGeros & LeGeros, 1993).

The dissolution-precipitation process involves the release of $Ca^{2+}$, $HPO_4^{2-}$ and $PO_4^{3-}$ ions from the surface of the material through partial dissolution of HA brought about by cellular activity in an acidic environment (LeGeros & LeGeros, 1993).

There are three main pathways in which carbonate apatite can form:

- Hydrolysis of calcium phosphates (DCPD, OCP, magnesium substituted β-TCP) by $CO_3^{2-}$ ions in biological fluid.

- Direct formation of carbonate apatite from ions released from partially dissolving ceramic HA ($Ca^{2+}$, $HPO_4^{2-}$ and $PO_4^{3-}$) and biological fluids ($CO_3^{2-}$ and $Mg^{2+}$).

- Uptake of calcium ions from serum results in precipitation of carbonate apatite.

It has been shown that the dissolution-precipitation of biphasic materials such as biphasic calcium phosphate is influenced by the ratio of β-TCP to HA. The $CO_3^{2-}$ apatite crystals tended to be more abundant on the surface of the biphasic calcium phosphate with higher β-TCP/HA ratio. This is due to the greater dissolution of the β-TCP component of the biphasic material to calcium and phosphate ions (LeGeros & LeGeros, 1993).

#### *1.2.4.7. Tissue response*

The biocompatibility of the HA surface allows the cell proliferation and cell attachment of a variety of cell types, these include macrophages, fibroblasts, osteoclasts, osteoblasts and periodontal ligament cells (LeGeros & LeGeros, 1993).

Dissolution of HA crystals from the surface of the ceramic occurs as a result of cellular interactions. This process is carried out in two ways:

- Intracellularly: Phagocytosis

- Extracellularly:Producing an acid environment for dissolution

Bone cells that attach and proliferate on HA and on bone surfaces do not appear to differentiate between the two surfaces. This suggests that the

surface chemistry of HA and bone exhibit similarities (LeGeros & LeGeros, 1993).

The ability of dense HA to promote the attachment and proliferation of matrix-producing bone cells on a $CO^{3-}$ apatite surface is indicative of a material which provides the right surface chemistry and surface charges, and in many respects is considered osteoconductive in nature (LeGeros & LeGeros, 1993).

### 1.3. Titanium

Chemically, titanium is an element in group 4B in the periodic table of elements. It has an atomic number of 22 and an atomic weight of 47.9 (g/mol). Titanium combines the strength of iron and steel with the light weight of aluminium, which accounts for its widespread use in aviation, sports equipment and more relevantly, medical and dental bone replacement devices (Lu et al., 2000). Ti has a low specific gravity (4.5), and a high melting point.

With regards to the chemical composition, commercially pure titanium (cp Ti) contains a very high percentage of titanium (Ti), with the balance being largely oxygen (O), nitrogen (N), hydrogen (H), carbon (C), and iron (Fe) in various amounts. The American Society for Testing Materials (ASTM) classified Ti in 4 grades, according to the chemical composition, variations in which will influence its properties. Alloying elements are commonly added to titanium to improve the physical and chemical properties.

#### *1.3.1. Titanium implants*

Amongst metals and alloys Ti is the most widely used for dental implants. This is due to its biocompatibility and to the fact that it becomes osseointegrated more rapidly than other metals. According to their position and shape the dental implants can be classified as subperiosteal, transosteal, and

endosseous. The most widely used dental implants nowadays are the endosseous ones. They are used widely, as single implants to replace one missing tooth as well as for partially dentate or edentulous patients. The most commonly used endosseous implants are root-form analogues.

The main objective of dental implant treatment is to replace lost teeth in order to restore the function and appearance of the oral cavity.

Insertion of dental implants is based on the “osseointegration” concept that allows dental implants to fuse with bones. This concept was first defined by Brånemark and collaborators in the 1960s as ‘a direct structural and functional connection between ordered, living bone and the surface of a load carrying implant’ (Albrektsson et al., 1986). The authors suggested criteria of success that indicate the clinical performance of a successful dental implant. They are: absence of implant mobility, absence of radiolucent zones on X-ray, annual bone loss after the first year of < 0.2 mm around the implant, absence of signs and symptoms such as pain, infection, neuropathies, damage to the mandibular canal following placement etc. These criteria are now universally accepted. Since the development of the first implants, there has been considerable debate as to when is the best time to load an implant. In the early days the tissues around implants were allowed to heal and osseointegration to occur for up to 6 months before the implant was loaded. The minimum duration allowed for osseointegration has been reduced dramatically since then. Nowadays there are supporters of immediate loading (Esposito, 1998). This is not, however, universally accepted (Misch 1999).

Whatever the protocol, titanium implants may fail with time (Esposito 1998). The majority of implant failures are related to factors including fractures of prosthetic and fixture components as well as iatrogenic factors. In the minority

of the cases implant failures are related to poor osseointegration early on (osseointegration not established) or at a later stage (osseointegration not maintained) Modification of the physical and chemical properties of the Ti surface has been increasingly used as a method of enhancing osseointegration.

The ideal material for hard tissue replacement prostheses should possess the following properties: ‘biocompatibility’ so as to minimise adverse tissue reactions, an excellent resistance to degradation (corrosion) in the human body, acceptable strength, a low modulus to minimize bone resorption, and a high wear resistance to minimise debris generation. Besides the above properties, bioactivity, which determines the osseointegratability of the implant, is very important to facilitate cementless anchoring of artificial bones, joints, and dental implants to bones. In order to avoid adverse tissue reactions arising from hard tissue replacements, a bioinert material, which is stable in the human body and reacts minimally with body fluids and tissues, is preferred. Following implantation into the living body bioinert materials are generally encapsulated by fibrous tissues which isolates them from the surrounding bone. Some bioactive materials, such as hydroxyapatite and bioactive glasses are increasingly used as hard tissue replacements to improve the bonding between implants and bone tissues, because the materials can bond to living bone without the formation of fibrous tissues by creating a bone-like apatite layer on their surface after implantation. Apatite formation is currently believed to be the main requirement for the bone-bonding ability of materials. In this respect, titanium with its native surface oxide, is known to be bioinert, therefore it is difficult to achieve good chemical bonding with bones and form new bone on its surface at the early stage after implantation. Hence, titanium and titanium alloys do not meet all the requirements of the ‘ideal’ material. In addition, longer human life expectancy and younger patients requiring implants have driven

biomedical research from original implant concerns, such as material strength, infection and short-term rejection to consideration of more long-term materials limitations, for instance, wear, fatigue strength, and long-term biocompatibility. The current trend is to use surface modification technologies to address a number of these ever-increasing clinical demands.

Before presenting the Ti modifications, some definitions of the most relevant and frequently used terms mentioned in the area of titanium implants are presented.

A material is defined as 'bio-inert' if it is unable to elicit any response, either favourable or unfavourable, upon contact with the host tissue. The use of this type of material will not harm the host tissue. A material which facilitates tissue growth on its surface and encourages the progression of tissue growth once initiated is defined as 'bio-conductive'. 'Bio-integration' is a term defined as the formation of a biochemical union between the surface of an implant and the host tissue or bone (Steinmann 2000). 'Bio-inductive' materials are materials, which can induce relevant tissue growth.

### *1.3.2. Modifications to titanium*

Osseointegration of titanium implants is thought to be a result of the presence of a very stable oxide layer at the Ti surface. This layer remains intact on contact with the body tissues and serves as the interface for the chemical interaction between Ti and live tissues. The pure titanium metal does not come into contact with the biological environment (Kasemo 1983). The oxide layer also protects the metal against corrosion. This layer appears on contact with air or water (fluids) and is generally around 0.5-7 nm thick, self-repairing, and strongly resists corrosion (Sunny 1991). Manufacturing procedures as well as the cleaning and sterilization process affect the thickness and the structure of

this oxide layer. Osseointegration represents processes that take place between the titanium implant and the bone, at a cellular level. However, processes may occur at a molecular level, between the titanium surface and the organic structures. Improving the titanium surface, by various modifications, the reaction of the inorganic and organic molecules to it may be improved, and clinical results that are more predictable may be obtained when using titanium implants.

Therefore, in order to improve the biological, chemical, and mechanical properties, surface modification is often performed. Various surface modification technologies pertaining to titanium and titanium alloys include mechanical treatment, thermal spraying, sol–gel, chemical and electrochemical treatment, and ion implantation from the perspective of biomedical engineering. Recent work has shown that the wear resistance, corrosion resistance, and biological properties of titanium and titanium alloys can be improved selectively using the appropriate surface treatment techniques while the desirable bulk attributes of the materials are retained. The proper surface treatment expands the use of titanium and titanium alloys in the biomedical fields.

Recent clinical research has focused on developing implant materials that produce predictable and rapid healing of the interfacial tissues, both hard and soft. Events leading to the integration of an implant into bone, and consequently to the clinical performance of the restoration under loading, take place largely at the tissue-implant interface. They are dependent on the material that is used to fabricate the dental implant, the state of the host, the response of the host to the implant, and the behaviour of the material in the host.

### *1.3.3. The tissue-implant interface*

Since the tissue-implant interface plays a major role in osseointegration, a better understanding of events at the interface is needed, and of the effects that biomaterials have on bone and bone cells.

Upon insertion of a titanium implant into the tissues, water adsorption onto the surface results in the formation of an initial hydrated layer known as the 'Helmholtz layer'. The ions and biomolecules present in the surrounding biofluid adhere within this hydrated layer, forming the 'conditioning film' with which cells interact (Lausmaa et al., 1999). The bonding of biomolecules to the surface can occur in several ways, including the long-range and weak van der Waals' interactions and short-range strong chemical bonding, through ionic and covalent bond formation. Inorganic interactions can result in the thickening of the oxide layer through oxidation and hydroxylation, as well as the diffusion of mineral ions or atoms from the bioliquid and tissue into the oxide (e.g. Ca and P-containing mineral ions). Interaction with this conditioning film governs subsequent tissue responses to the implant through the adsorption of larger biomolecules and proteins, which will proceed to form the bone-implant bond. The proteins come first from blood and tissue fluids at the wound site, and later from cellular activity in the interfacial region. Once on the surface, proteins can either desorb, or remain to mediate tissue-implant interactions. If they interact strongly with the surface, they may adopt a structure very different to that in solution (denaturing). The nature of the film deposited on biomaterials, along with the biomechanical conditions surrounding the implantation, can play a major role in the host response (Brunski 2003).

Apart from protein adsorption on the implant's surface, significant changes also occur on the material side of the interface. It is believed that the oxide layer at

the implant surfaces undergoes changes in the physiological environment. Commercially pure titanium (cp Ti) implants have an oxide thickness of 0.5 to 7 nm before implantation, but films on implants removed from human tissues may be 2 to 3 times thicker (Brunski et al, 2003). Analytical studies of the surface showed that the chemical composition of the oxide film also changed with incorporation of calcium, phosphorus, and sulphur. Continued oxide growth after implantation in the body may suggest ongoing events which occur at the tissue-implant interface.

Simultaneously with the events that occur at the titanium surface, ion release from the titanium into the surrounding tissues takes place. Ion release into an experimental medium or any bio-liquid is important because it may be an indication of release into the surrounding tissues *in vitro* and *in vivo*. This may affect the biological and molecular interactions around an implant by inducing hydroxyapatite precipitation and subsequently enhancing bone deposition around the implant. Also, ions released into solution may go through the cell membranes themselves and may have a beneficial effect on the cells but could also have a toxic effect on them. They can also enter the bloodstream and have a systemic effect or potentially be accumulated in the body.

Surface properties play an important role in the dynamics of the interaction between Ti and the surrounding tissues. Various surface modifications have been employed to improve the body reaction to Ti implants.

The bulk properties of biomaterials, such as non-toxicity, corrosion resistance or controlled degradability, modulus of elasticity, and fatigue strength have long been recognized to be highly relevant in terms of the selection of the appropriate biomaterials for a specific biomedical application. The events after implantation include interactions between the biological environment and

artificial material surfaces, and the onset of biological reactions, as well as the particular response paths which occur. The material surface plays an extremely important role in the response of the biological environment to artificial medical devices. In implants made of titanium, the normal manufacturing steps usually lead to an oxidized, contaminated surface layer that is often stressed and plastically deformed, non-uniform and rather poorly defined. Such surfaces are clearly not appropriate for biomedical applications and some surface treatment must be performed. Another important reason for conducting surface modification of titanium medical devices is that specific surface properties that are different from those in the bulk are often required. For example, in order to accomplish biological integration, it is necessary to have good bone apposition. In blood-contacting devices, such as dental implants, blood compatibility is crucial. In other applications, good wear and corrosion resistance are also required. The proper surface modification techniques not only retain the excellent bulk attributes of titanium and its alloys, such as relatively low modulus, good fatigue strength, formability and machinability, but also improve the specific surface properties required by different clinical applications. According to these different clinical needs, various surface modification schemes have been proposed.

These methods are classified into mechanical, chemical and physical methods according to the formation mechanism of the modified layer on the surface of titanium and its alloys. The properties of titanium and its alloys can be upgraded to some extent after their surfaces are modified using suitable surface modification technology. With the development of surface engineering, new surface modification technologies have been introduced to improve the properties of titanium and its alloys for meeting the clinical needs.

An overview of the surface modification methods for titanium and its alloys is presented below.

## 1.4. Mechanical methods of modifying the titanium surface

### *1.4.1. Machining and surface roughness*

Common mechanical surface modification methods, such as machining (Lausmaa et al., 1990; Lucchini et al., 1996), grinding, polishing (Hignett et al., 1987), and blasting (Wennerberg et al., 1996; Buser et al., 1999; Desagne et al., 1999; Baleani et al., 2000; Marinucci et al., 2006; Meirelles et al., 2008) involve physical treatment, shaping, or removal of the surface of the material. The typical objective of mechanical modification is to obtain specific surface topographies and roughness, remove surface contamination, and / or improve adhesion in subsequent bonding steps.

Increased surface roughness has been shown to enhance the mechanical interlocking between the macromolecules of the implant surface and the bone (Cochran 1999). This has resulted in a greater resistance to compression, tension, shear, and stress. All these properties increase the degree of cellular attachment of osteoblast-like cells. They also increase the removal torque, (the torque applied on the implant in order for it to be removed), which demonstrates that implants with roughened surfaces have enhanced contact with bone. Implants with increased surface roughness show higher success rates compared with those with smooth surfaces (Lazzara et al., 1999, Binon, 2000).

## 1.5. Physical methods of modifying the titanium surface

During some surface modification processes, such as thermal spraying and physical vapour deposition, chemical reactions do not occur. In this case, the

formation of a surface modified layer, films or coatings on titanium and its alloys are mainly attributed to the thermal, kinetic, and electrical energy. In the thermal spraying process, the coating materials are thermally melted into liquid droplets and coated on to the substrate at a high speed (kinetic energy). Physical vapour deposition leads to film growth by reaction between a substrate surface and an adjacent vapour which supplies the coating material in the form of atoms, molecules or ions, generated from a target and transported to the substrate surface on which condensation and reaction with atoms of the surface lattice take place. The generation of atoms, molecules or ions from targets can be accomplished by resistance heating, electron beam, laser or electrical discharge in vacuum. Glow discharge plasma treatment and ion implantation are also categorized as physical methods, although they influence the surface chemistry.

### *1.5.1. Thermal spraying*

Thermal spraying is a group of techniques in which materials are thermally melted into liquid droplets and introduced energetically to the surface on which the individual particles stick and condense. The coating is formed by a continuous build-up of successive layers of liquid droplets, softened material domains and hard particles. Thermal spraying requires a device that creates a high temperature flame or a plasma jet. Therefore, thermal spraying is often divided into flame spraying and plasma spraying. The principal difference between flame and plasma spraying is the maximum temperature achievable.

Plasma sprayed hydroxyapatite coating, because of its similarity to the mineral phase of natural hard tissues, is considered to be a bioactive material. Bone can be regarded as an organic matrix with the inclusion of an inorganic filler with a crystal size in the submicron range. About 70% of the mineral fraction of

bone has an HA-like structure and the use of HA as an orthopaedic biomaterial has been suggested and clinically demonstrated. However, the mechanical properties of HA are quite poor, making it unsuitable as bulk a material in applications where high loads or strains occur. The concept of using plasma spraying to produce HA coatings on endoprosthesis was first proposed in Japan in 1975. It has been shown that implants with an HA surface develop a strong connection with the bone tissue in a short time (Lacefield, 1993; Driskell et al., 1994). The relatively poor bonding between a plasma sprayed HA coating and titanium is one of the main disadvantages of the technique. The bonding strength of the HA coating on titanium decreases with longer immersion time in simulated body fluids (SBF) (Kweh et al., 2002). Another disadvantage is the resorption and degradability of HA coatings in a biological environment. This may lead to disintegration of the coating resulting in the loss of both the coating–substrate bonding strength and implant fixation. There also exists the threat of coating delamination and formation of particulate debris (Bauer et al., 1991, Collier et al., 1993). The thickness of the HA coating affects both its resorption and mechanical properties. A thicker coating usually exhibits poorer mechanical properties. The suggested optimum thickness is about 50 μm in order to avoid fatigue failure while still providing reasonable coating resistance to bioresorption and consistent bone growth (Wang et al., 1993, Yang et al., 1997).

A plasma sprayed titanium coating increases the surface area of the bone to implant interface, and increases roughness for initial stability, while the surface has a stronger bond to an implant interface than uncoated implant surfaces (Liu et al., 2004). Plasma-sprayed titanium coatings with porous structure have been used in tooth root, hip, knee and shoulder implants. The porous surface improves fixation via the growth of bone into the coating, forming a mechanical

interlock. Vercaigne et al. (1998) evaluated the biological and mechanical properties of the implant with a titanium coating and investigated the effects of the surface roughness on the bone response. No correlation was observed between the percentage of bone contact and surface roughness. The percentage of bone contact after 3 months of installation was very low. The loosening of particles during or after implant placement endangers the safe application of very rough coatings, but with the advent of improved plasma spraying techniques and post processing, rough coatings that show no particle release have been produced. Lee et al. (2004) investigated the mechanical stability and i*n vivo* behaviour of implants of three surface designs: smooth surface (SS), rough titanium surface with a plasma-sprayed coating (PSC), and an alkali- and heat-treated titanium surface (AHT) after plasma spraying. Four weeks after the implants had been implanted in dog bone, the pull-out forces of the SS, PSC, and AHT implants were determined. The AHT implant showed good bone-bonding strength after 4 weeks of healing because of the mechanical interlocking in the micrometer-sized rough surface and the large bonding area between the bone and implant, as a result of the nanosized porous surface structure. During this healing period, new bone on the surface of AHT implants underwent higher growth than that on the PSC implants, results which have been confirmed by Liu et al., (2004).

### *1.5.2. Physical vapour deposition*

Physical vapour deposition (PVD) is a technique used to deposit thin films of various materials onto various surfaces by physical means, as compared to chemical vapour deposition. The physical vapour deposition process can be described succinctly as follows. In vacuum, the target materials are evaporated or sputtered to form atoms, molecules or ions that are subsequently transported to the substrate surface, on which condensation and sometimes

some reactions with the materials surface take place leading to film growth. Physical vapour deposition processes include evaporation, sputtering, and ion plating.

### *1.5.3. Glow discharge plasma treatment*

Glow discharge plasma is a low-temperature, low-pressure gas in which ionization is controlled by energetic electrons. Glow discharge plasma treatment has been well established for cleaning and surface processing in the microelectronics industry (Mittal, 1979) and has attracted much interest in biomaterials research in which it is used for the surface modification of bulk polymers and production of thin polymer coatings (plasma polymerization).

### *1.5.4. Ion implantation*

Ion implantation is a technique developed for the semiconductor industry to introduce ions into the surface layer of a material (Sze, 1985). It has been proposed as a method of enhancing biological response to the surface. This method is very advantageous because in general it is controllable, fast, homogeneous, reproducible and useful for creating model surfaces of known composition. Ion implantation allows the alteration of the chemical, physical and optical properties of a solid and is commonly used to alter the composition, structure and morphology of the near surface layers. Various surface properties may be modified by ion implantation, like mechanical, chemical, electrical and optical properties (Townsend et al., 1994). Mechanical properties include microhardness, friction, adhesion, and wear. Chemical properties altered by ion implantation include corrosion, passivation, diffusion, and reactivity. Electrical properties include resistivity, photoconductivity, electron mobility, and semiconductivity, meanwhile optical properties include colour, reflectivity, transmission and opteoelectronics.

Different ions have been implanted into titanium with a view to improving its properties, including oxygen, calcium, nitrogen, argon, and fluoride.

Nitrogen implantation results in the formation of titanium nitride (TiN). Its good electrical conductivity and excellent performance as an adhesive layer make TiN an interesting material in microelectronic applications, for example as a diffusion barrier between silicon substrates and aluminium metallisations (Hench & Andersson, 1993; Price et al., 1993). TiN also has high hardness and remarkable resistance to wear and corrosion, and is therefore commonly used in products such as cutting tools. Because of its intrinsic biocompatibility, TiN is also a suitable material for orthopaedic implants and has been used as a coating on the heads of hip prostheses to improve their wear and fatigue resistance (Mandl et al., 2002). TiN is the material of choice as the hard coating on dental implants and dental surgical tools.

Oxygen implantation improves the wear resistance, corrosion resistance, and biocompatibility of titanium and its alloys (Fraker et al., 1983).

Carbon does not worsen the biocompatibility of titanium alloys and is widely used as a coating on metal implants (De Maetzu et al., 2007). Carbon has been implanted to or deposited on titanium using ion implantation and deposition technologies, and found to improve the mechanical properties, corrosion resistance and biocompatibility. The implanted ions are bound either to titanium to form titanium carbides or to carbon atoms to form C-C bonds near the surface. Implantation at moderate doses ($5 \times 10^{15} \times 10^{17}\ cm^{-2}$) creates a layer of nanocrystalline titanium carbide TiC with a cubic lattice (Fm3m) and a-Ti matrix.

Fluorine has been implanted into titanium to improve the antibacterial effect (Yoshinari et al., 2001; Nurhaerani et al., 2006). $F^-$ implanted specimens were

observed to significantly inhibit the growth of both *P. gingivalis* and *A. actinomycetemcomitans* (Yoshinari et al., 2001). It has also been reported that several fluoride salts with polyvalent cations, such as $Cu^{2+}$, $Sn^{2+}$, and $Al^{3+}$ exhibit a direct antibacterial effect, and titanium tetrafluoride seeded with bacteria exhibits similar growth inhibition zones to those of these salts (Skartveit et al., 1990).

It has been shown that the architecture of the tissues adjacent to a titanium implant is greatly affected by the implant surface configuration. This includes both chemical and structural properties. The surface chemistry and energy are reported to determine the type and the orientation of adsorbed molecules, and consequently cellular attachment. It is known that osteoblasts and chondrocytes are sensitive to subtle differences in surface roughness and surface chemistry (Boyan et. al., 1995). As established by Larsson (1996), early phases of cortical bone formation in rabbits are determined by the surface roughness and the oxide film thickness on 99.7% commercially pure titanium (cp Ti). It has been shown that by increasing the surface roughness the mechanical interlocking between the macromolecules of the implant surface and the bone (Cochran 1999) is enhanced. This results in a greater resistance to tension, shear, stress and compression. As a result, the degree of cellular attachment of osteoblast - like cells will increase, as well as the torque removal (the torque applied on the implant in order to break the bond between the implant and the surrounding tissues). This demonstrates that implants with roughened surfaces have enhanced contact with bone. Implants with increased surface roughness show higher success rates compared with those with smooth surfaces (Binon et al., 2000). It has been shown that cells respond differently at a gene level to different surface topography (Brett et al., 2004).

Some attempt has been made in the past to characterise Ti surfaces (Shinawi, 2003), but many of these studies were inconclusive, and the characteristics of Ca implanted Ti (Ca-Ti) are still not fully understood. Those studies however, provided a starting point for this work, which has extended the understanding of the Ca-Ti surface and sub-surface composition and resulting reactivity quite considerably.

## 1.6. Chemical methods of modifying the titanium surface

### *1.6.1. Chemical treatment*

Chemical methods include chemical treatment (acid, alkali, $H_2O_2$, heat, and passivation treatments), electrochemical treatment (anodic oxidation), sol–gel, chemical vapour deposition (CVD), and biochemical modification. During the chemical and electrochemical treatments, and biochemical modification, chemical, electrochemical or biochemical reactions occur, respectively, at the interface between titanium and a solution.

Kasemo & Lausmaa (1986) stated that biologic tissues interact mainly with the outermost atomic layer of an implant, the "primary interaction zone". Modifications are made at this "primary interaction zone". It has been shown that the physico-chemical nature of the implant surface can influence macromolecular binding.

Among the physico-chemical properties that have been modified in order to improve the bone-implant interface are: surface energy, surface charge, and surface composition (Baier & Meyer, 1988). Procedures that have been undertaken to increase the surface energy have included heat treatments in the range of 500º-600ºC, acid cleaning and passivation (Kilpadi et al., 2000), glow

discharge and the use of charged surfaces (Taborelli et al., 1997, Rupp et al., 2006).

Chemical modifications employed include the preparation of sol-gel titania layers, treatment with hydrogen peroxide (Ohtsuki et al., 1997), treatment with alkali solution (with and without heat treatment) and etching with sulphuric and hydrochloric acids (Kim et al., 1996).

Rough surfaces are generally created by the use of coatings, blasting (sand blasting), acid etching, or a combination of the last two (sand blasting and acid etching (SLA)). Other methods of increasing surface roughness include anodic oxidation, machining and grinding.

### *1.6.2. Anodic oxidation*

Anodic oxidation is a simple and effective method to modify the surface of titanium and its alloys for better biocompatibility and bioactivity. The anodic oxide film exhibits a variety of different properties that depend on the composition and microstructure of the materials and processing parameters, such as anode potential, electrolyte composition, temperature, and current. Anodic oxidation encompasses electrode reactions in combination with electric field driven metal and oxygen ion diffusion leading to the formation of an oxide film on the anode surface.

Yang et al. (2004) indicated that anodic oxidation in an $H_2SO_4$ solution combined with subsequent heat treatment was an effective method to prepare bioactive titanium. After anodic oxidation, the surface was observed to be covered with porous titania. In simulated body fluids, the titanium anodically oxidized during spark discharge induced apatite formation on its surface.

### *1.6.3. Chemical vapour deposition*

Chemical vapour deposition is a process involving chemical reactions between chemicals in the gas phase and the sample surface resulting in the deposition of a non-volatile compound on the substrate. It is different from physical vapour deposition (PVD), which typically employs techniques, such as evaporation and sputtering involving no chemical reactions. CVD is widely adopted in the industry to produce organic and inorganic films on metals, semiconductors, and other materials. The application of diamond coatings on cemented tungsten carbide (WC-Co) tools has been the subject of much attention in recent years in order to improve cutting performance and tool life in orthodontic applications (Jackson et al., 2007). Chemical vapour deposition and sol-gel methods are used in the surface engineering of artificial heart valve discs (Jackson et al., 2006).

## 1.7. Sol–gel coatings

### *1.7.1. Definition of a Sol-gel*

By definition, a sol is a suspension of colloidal particles in a liquid (Floch et al., 1995). A sol differs from a solution in that a solution is a single-phase system, whereas a sol is a two-phase, solid-liquid system. Colloidal particles can be in the approximate size range of 1-1000 nm, hence gravitational forces on these particles are negligible and interactions are dominated by short-range forces, such as van der Waals and surface charges. Brownian motion leads to a low energy arrangement, thus imparting stability to the system (Brinker & Scherer, 1990).

The stability of the sol particles can be modified by reducing their surface charge. If the surface charge is reduced sufficiently, gelation is induced and the resultant product is able to maintain its shape without the assistance of a mould. Gels are regarded as composites, since they consist of a solid skeleton or network that encloses a liquid phase or excess of a solvent.

### *1.7.2. Advantages of sol-gel*

Sol-gel processing is unique in that it can be used to produce different forms, such as powders, platelets, coatings, fibers and monliths of the same composition, merely by varing the chemistry, viscosity and other factors of a given solution.

The sol-gel process is exclusively aimed at the deposition of thin (<10 μm) coatings (Haddow et al., 1996). Compared to conventional thin film processing and offers several advantages (Ben-Nissan & Choi, 2006):

- It is of nanoscale.
- It results in stoichiometric, homogenous and pure products owing to mixing on the molecular scale.
- High purity can be maintained as grinding can be avoided.
- It allows reduced firing temperatures due to small particle sizes with high surface areas.
- It has the ability to produce uniform fine-grained structures.
- It allows the use of different chemical routes (alkoxide or aqueous based)
- It is easily applied to complex shapes with a range of coating techniques.

- The costs of the precursors are relatively unimportant owing to the small amounts of material requirements. Furthermore, it is a simpler procedure which requires considerably less equipment and thus again is potentially less expensive than many of the alternative coating techniques.

- Shrinkage up to a certain number of coatings, depending on the chemistry, is fairly uniform perpendicular to the substrate.

- The coating can dry rapidly without cracking.

### *1.7.3. Sol-gel precursors*

All sol-gel processing methods can be classified as aqueous- or alcohol-based. As the names suggest, aqueous-based systems are carried out in the presence of water, while alcohol-based systems generally exclude water build-up until the hydrolysis stage. Similarly, sol-gel precursors can be classified as either alkoxides or nonalkoxides. While alkoxides are the precursors for sol-gel production owing to their volatility, other compounds, such as metal salts, can be used (Pettit et al., 1988).

The preparation of sol solutions involves the use of solvents. These solvents are usually organic alcohols. While the primary objective of the solvent is to dissolve solid precursors, they are also used to dilute liquid precursors and minimise the effect of the concentration gradients. The particular solvent employed can influence factors, such as crystallisation temperatures (de Lambilly & Klein, 1989) and the particle morphology (Harris et al., 1988).

### *1.7.3.1. Nonalkoxide precursors*

Metal salts provide a suitable alternative to alkoxides if they can be transformed readily into their respective oxide by thermal or oxidative decomposition. Nitrates are the most suitable inorganic salts, since chlorides and sulphates are more thermally stable and may be difficult to remove (Schwartz et al., 1986).

### *1.7.3.2. Alkoxide precursors*

Metal alkoxides are probably the best starting material in sol gel preparations (Schroder, 1966). All metals are capable of forming metal alkoxides of the form $M(OR)_x$, where M is a metal, R is an alkyl group and x is the valence state of the metal. Another type of alkoxide that exists is the double alkoxides, which have the general formula $M'_xM''_y(OR)_z$, where M' and M'' are metals, R is an alkyl group and x,y and z are integers, Double alkoxides have the added advantage of retaining their stoichiometry (Thomas, 1988).

While the organic group influences the stability of the alkoxide, precursors should also be chosen so they have sufficient volatility to enable a clean break of the M-OR and MO-R bonds to produce materials free from organics (Mazdiyasni, 1982).

While alkoxides are the most favourable sol-gel precursor, there are two exceptions to this rule. These are the alkoxides of silicon and phosphorous. Silicon alkoxides require an acid or base catalyst for hydrolysis, and even with such an addition, hydrolysis is very slow. Similarly, trialkylphosphates are very stable and can be difficult to hydrolyse (Thomas, 1988).

### *1.7.4. Gelation*

The simplest picture of gelation is that clusters grow by condensation of polymers or aggregation of particles until the clusters collide. Links then form between the clusters to produce a single giant cluster that is called a gel. The gel point can only be estimated by an increase in viscosity since no latent heat is released. The gel consists of a solid skeleton enclosing a continuous liquid phase (Thomas, 1988).

The chemical reactions involved in a sol-gel process are hydrolysis and polymerisation. At high temperatures, the rate of polymerisation is greater than the rate of hydrolysis, and precipitates, such as hydroxides, do not have a chance to form. When the rate of hydrolysis is less than the rate of polymerisation, that is, when the temperature is low, hydroxides form by nucleation and growth. This general rule applies for neutral solutions, but can be overshadowed by changes in pH to acidic or basic solutions. Kim et al. (2005) found a significant improvement in the gelation process of hydroxyapatite sol-gel when the pH was increased with the use of ammonium hydroxide.

### *1.7.5. Drying & firing of gels*

Drying is the process whereby excess solvents are removed from the pore network. During this process, significant shrinkage can take place, with shrinkage being proportional to the moisture content (Anderson & Klein, 1987). Cracking can be a problem owing to the large capillary stresses developed when pores are small and this can be avoided through careful control of the drying conditions. The drying of sol-gel derived nano-films is not such a problem compared with that of monoliths, since they are constrained in the plane of the substrate and all shrinkage takes place normal to the substrate (Pettit et al.,

1988). Films less than approximately 400-500nm thick can usually be dried without cracking, regardless of the drying rate, when the film thickness exceeds approximately 500nm, cracking becomes difficult to avoid (Sakka et al., 1984; Strawbridge & James, 1986; Dislich, 1988; Gan & Ben-Nissan, 1997).

Firing is the final stage in the production of ceramic materials via sol-gel synthesis. By heating dried gels to temperatures (approximately >600$^{o}$C) any remaining organic materials are combusted. By controlling the atmosphere during firing, gel can be converted to oxides (Yoldas, 1984), nitrides (Jimenez & Langlet, 1994), carbides (Hasegawa et al., 1997) and mixtures thereof (Gabriel & Riedel, 1997).

### *1.7.6. Sol-gel coating techniques*

#### *1.7.6.1. Dip-coating*

The dip-coating process is used mainly for the production of coatings on items such as flat glass plates, but can be used for complex objects, such as tubes, rods, pipes and fibers. This deposition method has the advantage of being capable of producing multiple coatings with a high degree of uniformity up to 1000 nm thick (Dislich, 1988).

For a given solution, the film thickness of a single layer is governed by withdrawal speed. However, the thickness can also be modified by changing the physical properties of the solution, that is, viscosity and density, as well as the number of layers (Lee et al., 1993).

#### *1.6.6.2. Spin-coating*

Spin-coating is a process suited to flat shapes, such as disks, plates and lenses. The process can be separated into three stages. As with dip-coating, evaporation can take place throughout the entire coating process.

The first stage involves delivering excess liquid to the substrate while it is stationary or spinning. During the second stage, rotation causes the liquid to move outwards radially, owing to centrifugal forces. In stage three, excess liquid flows to the perimeter and detaches in the form of droplets. As the film thins, flow deceases as drag forces increase, and thinner films are affected more by evaporation, which raises the solution viscosity by concentrating nonvolatiles. Evaporation becomes the dominant process once spin-off has ceased. Film thickness will reach uniformity provided that its viscosity is insensitive to shear. Uniformity will occur when viscous forces balance centrifugal forces.

### 1.8. Research on sol-gels and titanium

#### *1.8.1. Risk vs benefit*

The introduction of an additional interface can reduce the lifetime of an implant, particularly if the adhesive strength of the coating is low. In addition, the method that is used to deposit the coating can have a negative effect on the properties of the substrate (e.g. the elevated temperatures needed to densify a ceramic may be deleterious to the mechanical properties of the substrate) or of the coating itself. A decrease in crystallinity can cause an increase in solubility and reduce the stability of the ceramic *in vivo*. Thus, to obtain the inherent advantages of ceramic coatings on metallic implants, the deposition techniques, as well as the pre-treatment and potential post treatment steps have to be chosen and controlled carefully (Scriven et al., 1998).

Titanium dental implants as a stand alone procedure are currently a very successful treatment modality and any intervention to alter their surface must be thoroughly investigated.

Numerous studies have found hydroxyapatite (HA) to be a favourable material for orthopaedic coatings (Vallet-Regi, 2001; Hermansson et al., 2003; Kokubo et al., 2003; Upasani et al., 2009). HA-coated implants have demonstrated extensive bone apposition in animal models. Development of good implant-bone interfacial strength is thought to be a result of the biological interactions of released calcium and phosphate ions. The long-term performance of a calcium phosphate-coated implant depends on coating properties (thickness, porosity, phases and crystallinity), implant surface roughness and overall design.

### *1.8.2. Properties to determine success*

Three different properties determine the success rate of an implant; bioactivity, bioinertness and biodegradabity. Bioactive coatings are materials (natural or synthetic) that are built up to the surface of an implant to promote and enhance biological interactions and hence accelerate fixation. The goal of HA, as a bioactive coating is to achieve rapid biological fixation to bone. Biological fixation is defined as the process by which prosthetic components become firmly bonded to the host bone by bone in-growth, without the use of adhesive and mechanical fixation.

Since porous HA has unfavourable mechanical properties, it cannot be used for load-bearing purposes (Scriven et al., 1998). This generated an impetus for the production and use of a thin film coating on metallic alloys. Because HA is bioactive, using it as a thin film on biometallic alloys, such as titanium, enables the coupling of the two materials' primary properties to form a functional single component (Chai & Ben-Nissan, 1999).

### *1.8.3. Hydroxyapatite via the sol-gel method*

Various sol-gel routes have been used for the production of synthetic HA. The range of precursors include; calcium acetate, calcium alkoxide, calcium chloride, calcium nitrate, calcium hydroxide and dicalcium phosphate dehydrate.

#### *1.8.3.1. Calcium acetate*

Aqueous sol-gel chemistry routes based on ammonium-hydrogen phosphate as the phosphorous precursor and calcium acetate monohydrate as the source of calcium ions have been developed to prepare HA powder samples with different morphological properties (Bogdanoviciene et al., 2006). In the sol-gel process, an aqueous solution of ethylene diamine tetre-acetic acid (EDTA) or tartaric acid (TA) was added to the reaction mixture as complexing agents. The monophasic $Ca_{10}(PO_4)_6(OH)_2$ samples were obtained by calcination of precursor sol-gels for five hours at 1000$^{o}$C. They proposed that this aqueous sol-gel method was simple, inexpensive and possibly appropriate for the large-scale production of calcium HA ceramics.

#### *1.8.3.2. Calcium alkoxide*

Layrolle and Lebugle (1994) developed a synthesis route of different calcium phosphates, using calcium diethoxide ($Ca(OEt)_2$) and orthophosphoric acid ($H_3PO_4$) as reagents and anhydrous ethanol as a solvent. By a simple variance of the ratio of reagents, calcium phosphates of various compositions $Ca_x(HPO_4)_y(PO4)_z$ are precipitated by ethanol. The solids that formed were characterised by different physico-chemical and thermal analysis. The results indicated that the different solid calcium phosphates are amorphous and nanosized and have large specific surface areas and high reactivity. Layrolle et al., (1998) also described the production of an amorphous, nanosized and

carbonate-containing calcium phosphate powder synthesised from calcium diethoxide and phosphoric acid in ethanol via a sol gel method. They concluded that, after sintering, the decomposition of carbonated HA generated a microporous ceramic with an average pore size of 0.2μm and an open porosity of 15.5% and that this microporous bioceramic could be used as a bone filler.

#### *1.8.3.3. Calcium chloride*

Andersson et al., (2005) developed a degradable porous apatite composite material from a simple low-temperature synthesis. HA was synthesised through a sol-gel method at near-room temperature conditions. Staring materials used in this investigation were $CaCl_2.2H_2O$, $Na_2HPO_4.2H_20$, cetyltrimethylammonium bromide ($C_{16}TAB$), ammonia solution and tetraethoxysilane. The resulting gel was reported to consist of HA and sodium calcium phosphate. The hybrid material was shown to induce calcium phosphate formation efficiently under *in vitro* conditions and work simultaneously as a carrier for drugs.

#### *1.8.3.4. Calcium hydroxide*

Tkalcec et al. (2001) produced HA powders and coatings via the sol gel technique to study the formation mechanism of the crystalline phases in the firing process of coatings with different Ca:P molar ratios. Calcium hydroxide was suspended in ethanol and ethylhexanoic acid (EHA) was added drop-wise to this suspension. The solution was then filtered by pressure filtering to obtain a clear solution of calcium 2-ethylhexanoaote ($Ca(O_2C_8H_{15})_2$. $Ca(O_2C_8H_{15})_2$ and 2-ethyl-hexyl-phosphate which were used as calcium and phosphorous precursors respectively. Coatings were performed on Si-wafer and Ti-alloy substrates by dipping the substrates into sols at room temperature. They concluded that dip-coating and sintering in cycles yielded a homogenous and dense coated film with a thickness of 250nm.

### *1.8.3.5. Calcium nitrate*

Calcium nitrate ($Ca(NO_3)_2$) is the most popular calcium precursor for the synthesis of HA and is the precursor of choice in this study.

The citric acid sol-gel combustion method was used by Han et al. (2004) for the synthesis of HA powder from calcium nitrate, diammonium hydrogen phosphate and citric acid. HA powder was sintered onto a ceramic in order to illustrate its sinterability, open porosity, flexural strength and structural property. Scanning electron micrographs (SEM) revealed that there were many micropore sizes ranging between 1 and 5 μm with irregular shape. Although the open porosity of the resulting ceramic was approximately 19%, the pore size is not good enough for bone in-growth. After sintering at 1200$^{o}$C, the grain size was approximately 3μm, which was approximately 20-times that of HA powder sintered at 750$^{o}$C and with a flexural strength of 37 MPa.

Kim et al. (2004) deposited hydroxyapatite on titanium by means of a titania ($TiO_2$) buffer layer using the sol–gel method. To make the sol-gels, calcium nitrate tetrahydrate ($Ca(NO_3)_2.4H_2O$) and tri-ethyl phosphite ($P(OC_2H_5)_3$) were hydrolysed together with ethanol and distilled water. Ammounium hydroxide ($NH_4OH$) was added stepwise to the mixture. To produce a $TiO_2$ sol titanium propoxide ($Ti(OCH_2CH_2CH_3)_4$) was hydrolysed within an ethanol-based solution containing diethanolamine ($(HOCH_2CH_2)NH$) and distilled water. The HA layer showed a typical apatite phase at 400°C. The phase intensity (crystallinity) increased above 450°C. The HA and $TiO_2$ films of thicknesses of approximately 800 and 200 nm, respectively, adhered tightly to each other and to the Ti substrate. The bonding strength of the HA / $TiO_2$ double layer was markedly improved when compared to that of a single HA coating on Ti. The improvement in the bonding strength with the insertion of a $TiO_2$ buffer layer

was attributed to the enhanced chemical affinity of $TiO_2$ towards the HA layer as well as the Ti substrate. Human osteoblast (HOS)-like cells cultured on the HA/$TiO_2$ coating surface proliferated in a similar manner to those on the single $TiO_2$ coating and Ti. However, the alkaline phosphatase (ALP) activity of the cells on the HA / $TiO_2$ double layer was greater than on the single $TiO_2$ and Ti. The corrosion resistance of Ti was also improved by the presence of the $TiO_2$ coating.

Stoch et al. (2005) produced HA coatings on titanium and its alloy for facilitating and shortening the process towards osseointegration. HA coatings were obtained by the sol-gel method with sol solutions prepared from calcium nitrate tetrahydrate and triammounium phosphate trihydrate as the calcium and phosphorous sources. Two types of gelatine were added to the sol: agar-agar or animal gelatine. Both enhanced the formation and stability of amorphous HA using soluble salts as the source of calcium and phosphate. The chemical composition and structure of HA coatings were found to depend on the pH and final thermal treatment of the layer.

Gan & Pilliar (2004) produced thin sol-gel derived calcium phosphate films on sintered porous-surfaced implants as an approach to increasing the rate of bone in-growth. Porous-surface dental implants were used for the sol-gel coating of sintered porous surface structures. The porous surface was created by sintering Ti-6A1-4V particles of 45-150 μm, onto a machined Ti-6A1-4V substrate. The films were prepared using both an inorganic precursor solution (with calcium nitrate tetrahydrate and ammounium dihydrogen phosphate) and an organic precursor solution (with calcium nitrate tetrahydrate and triethyl phosphite). They reported that both approaches resulted in the formation of carbonated HA but with different Ca:P ratios and structures.

A simple rapid-heating method was developed by Hsieh et al. (2002) for calcium phosphate coatings on Ti-6A1-4V substrates by using a sol-gel-derived precursor. The preparation of the precursor was carried out by mixing $Ca(NO_3)_2.4H_2O$ and $(C_2H_5O)_3PO$ in 2-methoxy ethanol. Upon aging, the as-prepared solution was closely capped and placed in an oil bath for sixteen hours. Upon gelation (drying), the solvent evaporated in the same oil bath so that a viscous precursor was obtained. Adhesive strength tests were conducted and the results indicated that, as the first coating layer, using either spin or dip coating, the breakages occurred at the glue-coating interface, representing an adhesive strength of higher than 90MPa. Thus the first layer was adhered firmly to the substrate.

### *1.8.4. Fluorapatite via the sol-gel method*

A sol gel method was utilised by Cheng et al. (2004) to synthesize a fluoridated HA (FHA) phase. Calcium nitrate tetrahydrate, phosphoric pentoxide and ammonium hexafluorophosphate were used as precursors. The Ca, P and F precursors were mixed under designated proportions to form solutions with a Ca:P ratio of 1.67. To obtain an FHA phase with various fluorine contents, different amounts of ammounium hexafluorophosphate were added in the Ca-P mixed solutions.

A method has also been developed using a sol-gel method to synthesise a HA/fluoroapatite (FA) solid solution (Cheng et al., 2001). Calcium nitrate-4 hydrate, phosphorous pentoxide and trifluoroacetic acid (TFA) were used as precursors. Triethanolamine (TEA) was used as a promoter for incorporating fluorine into Ca phosphates. Mixed ethanol solutions of Ca and P precursors in the Ca:P ratio of 1.67 with different amounts of TFA and TEA were prepared; the mixed solutions were dried on a hot plate to convert them to the as-

prepared powders. After the powders were calcined at temperatures up to 900$^{o}$C, HA/FHA solid solutions were obtained.

Kim et al. (2004) synthesised fluorhydroxyapatite (FHA) powders by a sol-gel method. Calcium nitrate and triethyl phosphite were used as precursors under an ethanol-water-based solution. Different amounts of ammounium fluoride ($NH_4F$) were incorporated for the preparation of FHA powders. With heat treatment above 400$^{o}$C a characteristic apatite phase was observed for all the sol-gel powders. However, the crystallization temperature decreased with increasing fluoride addition. The tricalcium phosphate (TCP) phase formed in the HA powder above 800$^{o}$C was attenuated in the FHA powders, confirming an enhanced stability of the FHA powders. Increasing the fluoride addition improved crystallinity and increased the crystallite size. The powders substituted with fluoride exhibited reduced dissolution rates in an *in vitro* solution as compared with pure HA powder. The authors suggested that this may raise the possibility of tailoring bioactivity with fluoride substitution.

Fluorapatite coatings have attracted a great deal of attention in areas requiring long-term chemical and mechanical stability (Legeros et al., 1983; Okazaki et al., 1998; Kim et al., 2002b; Wang et al., 2008). Previous studies have suggested that Fluorapatite ($Ca_{10}(PO_4)_6F_2$) has a similar biocompatibility with HA in terms of its fixation to bone and bone in-growth (Heling et al., 1981; Slosarczyk et al., 1996; Overgaard & Lind, 1997; Wang et al., 2008). Qu & Wei (2006) studies discs doped with various amounts of fluorine ion ($F^-$) to investigate the effect of $F^-$ content on oesteoblastic cell behaviour. They concluded that FHA is biocompatibile and that the amount of $F^-$ affects cell attachment, proliferation, morphology and differentiation of osteoblastic cells.

### *1.8.5. Other sol gel titanium coating materials*

#### *1.8.5.1. Silica and collagen*

Meretoja et al., (2007) compared titania ($TiO_2$-coated), titania-silica (TiSi)-coated, and uncoated (cp Ti) titanium fibre meshes as scaffolds for bone engineering. The authors noted that the sol-gel coatings resulted in enhanced initial bone contact and distribution of bone tissue, whereas uncoated implants showed bone formation mainly in the centre of the scaffolds. They concluded that $TiO_2$-based sol-gel coatings may be used in tissue engineering to gain more uniform distribution of bone throughout titanium fibre mesh scaffolds.

The role of silica gel in the formation of bone-like apatite on the substrate has been investigated by many researchers. Karlsson et al., (1989) proposed that silicate chelation was an essential step in the formation and mineralisation of hard tissues. Yoshida et al. (1999) investigated the silica coatings produced on titanium by the sol–gel technique. The formation of both thin $SiO_2$ and $SiO_2/F^-$ hybrid films by the sol–gel dipping process gave rise to excellent surface properties including high bonding strength to the metal substrate, small amounts of leached titanium ions and high hydrophobicity. With these important findings, the bond strength of dental resin cements to titanium can be improved, the release of titanium ions from the substrate can be mitigated, and accumulation of dental plaque on intraoral dental devices can be reduced.

Collagen coatings on Ti alloys improve the early cells adhesion of cell. $TiO_2$ coating (titania coatings) synthesised by the sol–gel process are widely used in the optical, electrical, and catalytic fields (Samuneva et al., 1993, Trapalis et al., 1993).

### *1.8.6. Bond strengths of sol-gel coatings*

The bonding strength of titania coatings synthesised on titanium substrates using the sol–gel technique was investigated by Pätsi et al., (1998). In their work, different pretreatments were used, namely sodium hydroxide treatment and titanium nitride coating. The effects of the temperature, heating in vacuum, and titanium surface roughness were studied. The maximum attachment strengths were achieved by a 1 h treatment in 10 M sodium hydroxide solution. All the samples showed the ability to form a calcium phosphate layer in simulated body fluids (Pätsi et al., 1998). It is believed that the sol–gel titania rich in Ti–OH groups can induce calcium phosphate formation and may therefore be able to contribute to enhanced bonding to bones.

The possibility of modifying the surface area, porosity, composition, adsorption capacity, and dissolution rate using the sol–gel technique is very attractive in the fields of medicine and dentistry. Calcium phosphate coatings, especially hydroxyapatite coatings, are commonly used in orthopaedic applications. The sol–gel method is a relatively simple way to prepare hydroxyapatite coatings on titanium alloys because of the easy formation of the oxide coatings at a relatively low temperature.

The hydroxyapatite coatings synthesized by the sol–gel method are typically bioactive but have poor adhesion strength to the substrate. On the other hand, titanium dioxide ($TiO_2$) coatings strongly adhere to titanium but their bioactivity is limited. Hence, a composite titania/hydroxyapatite coating can take advantage of the high adhesion strength of $TiO_2$ and bioactivity of calcium phosphate.

### *1.8.7. Coating thickness of hydroxyapatite sol-gels*

A coating thickness in the range of 70 – 9000 nm has been reported. Table 2 summarises the thickness of the sol-gel derived HA coatings that are available in the literature, as well as the substrate materials used in their studies.

| Authors | Substrate material | Thickness of coating |
|---|---|---|
| Chai et al. (1999) | $Al_2O_3$, Vycor glass, Ti-6Al4V | 70 nm |
| Zreiqat et al. (2005) | Ti-6Al4V | 70 nm |
| Tkalcec et al. (2001) | Silicon wafers, Ti-30Nb-3Al | 250 nm |
| Kim et al. (2004c) | Commercially pure Ti | 800-900 nm |
| Gan & Pilliar (2004) | Ti-6Al4V | 1-2 μm |
| Hsieh et al. (2002) | Ti-6Al4V | 3-9 μm |
| Lim et al (2003) | Ti-6Al4V | 0.12-0.13 μm |

**Table 2:** Summary of the thickness of the sol-gel derived hydroxyapatite coatings and substrate materials used.

## 1.9 Biochemical modification of titanium and titanium alloys

Biochemical modification of biomaterials utilises biological and biochemical knowledge of cellular function, adhesion, differentiation and remodelling. The objective of modification is to induce specific cell and tissue response by means of surface-immobilised peptides, proteins, or growth factors. However, it is also important that biochemical modification improves the biocompatibility of the surface, the bulk properties cannot be adversely affected, and so the

concept of a biomimetic surface to guide cell behaviour on an ultra thin layer consisting of bioactive molecules has been introduced (Xiao et al., 2001). A variety of techniques, such as silanised titania (Xiao et al., 1997, 1998), photochemistry, self-assembled monolayers (Iwasaki et al., 2003; Abe et al., 2005; Majewski et al., 2006; Schuler et al., 2006; Mani et al., 2008) protein resistance, and protein immobilization (Tosatti et al., 2003) have been used on titanium and titanium alloys. These technologies exploit either physical adsorption via van der Waals', hydrophobic, or electrostatic forces, or chemical bonding. On account of the existence of a surface $TiO_2$ film, the modified layer does not make direct contact with the substrate. Since $TiO_2$ is a relatively inert surface, only a few organic reagents, such as organosilanes, organophosphates, and photosensitive chemicals, are able to form strong chemical bonds.

Covalent attachment of organosilanes has proven to be a simple and versatile method to enhance surface properties, such as wettability, adhesion, and surface activity. Silane chemistry is used on the titanium surface to enhance metal–metal and metal–polymer adhesion, convert semiconducting $TiO_2$ films into electrodes (Finklea et al., 1979), immobilise enzymes, and conduct chromatography. It is also useful to graft biomolecules onto the titanium implant surface for improvement in biocompatibility. Photochemistry can also be used to graft biomolecules onto titanium surfaces (Xiao et al., 2001).

Self-assembled monolayers (SAMs) have become an important research technique to produce surfaces with a very well defined chemical composition. SAMs have often been used as model surfaces for various biological assays including the study of cell-surface interaction and the influence of the surface chemistry on the spontaneous mineralisation caused by contact with simulated body fluid (Tanahashi et al., 1997; Scotchford et al., 1998). Self-assembled

monolayers of alkaline phosphates or phosphonates have been used on titanium surfaces to tailor selected physico-chemical properties of the surface, such as wettability and electrical charge. The effects of the surface chemistry on protein adsorption and cell adhesion have also been studied (Sigal et al., 1998, Tegoulia et al., 2001). Protein-resistant and protein immobilisation technologies are often used to modify the surface of titanium and titanium alloys. In many cases, integration of the implant with the newly formed tissue is desired. Thus, the adsorption of cell-adhesive proteins or bioactive proteins is an important aspect of the healing process. Bone morphogenetic protein can be immobilised on the surface of Ti–6Al–4V to enhance the bioactivity (Puleo et al., 2002). Plasma polymerisation of allyl amine has also been used to provide functional groups for immobilisation of biomolecules on Ti–6Al–4V surfaces. The amount of protein weakly and strongly bound to metallic biomaterials can be controlled by the choice of the surface treatment and immobilization chemistry. BMP-4 bound to Ti–6A–AL4V having a high density of amino groups using a two-step carbodiimide immobilization scheme appears to induce significant osteoblastic activity in pluripotent C3H10T1/2 cells. In other applications, protein adsorption may lead to a deleterious physiological response depending on the type and nature of the adsorbed proteins (Xiao et al., 2001). For example, non-specific protein adsorption may impair the performance of blood or serum in contact with stents or diagnostic sensors.

The native oxide on titanium is beneficial to the adhesion of many proteins. However, in some applications, it is necessary to reduce surface protein adsorption, for example in blood-contacting devices, such as stents and sensors. The simplest approach to controlling protein adsorption is to passivate the surface with a layer of an inert protein, such as albumin (Xiao et al., 2001).

### *1.9.1. 3D structures*

Silica based sol–gel derived bioactive glasses have been foamed to produce macroporous 3D resorbable scaffolds for tissue engineering applications. A hierarchical structure was obtained, with macropores in excess of 500 μm connected by pore windows with diameters in excess of 100 μm, and a mesoporous texture (pore diameters of 10–20 nm). Many processing variables can be used to control the pore network structure, such as the glass composition, surfactant and gelling agent concentrations and the foaming temperature (Sepulveda et al., 2002).

Sol–gel derived bioactive glasses tend to have more simple compositions than the melt-derived bioactive glasses and exhibit enhanced bioactivity and resorbability, due to a mesoporous texture (pore diameters in the range 2–50 nm) inherent to the sol–gel process (Sepulveda et al., 2002).

Bioactive silica glasses are class A bioactive materials, that is they can bond to both bone and soft tissue and can stimulate bone growth (Hench et al., 1991, 1993). The bone bonding ability of the glasses has been attributed to their ability to form a surface layer of hydroxycarbonate apatite (HCA) (Hench et al., 1993). Melt-derived bioactive glasses are commercially available for bone repair in a powder form (Hench et al., 1993).

# Chapter 2:

# Characterisation Techniques

## 2. Characterisation techniques

In this thesis several characterisation methods have been adopted;

### *2.1. Thermal analysis*

The thermal events that occur in a sol gel as a function on temperature can be monitored using thermoanalytical methods such as differential thermal analysis (DTA) (Willard, 1981; Braun, 1987). In DTA, the temperature difference between the sample and a non-reactive reference is monitored as a function of temperature. Commonly used inert reference materials include alumina and silicon carbide. The reference and the sample are held in two separate containers (typically Pt), which are identically heated. The difference in the temperature between the sample and the reference is monitored by thermocouples placed on pedestals that support each container (see Figure 3).

DTA can be used to control or study any exothermic or endothermic events during heating or cooling. Melting, boiling, sublimation and crystallisation can be exothermic events. The temperatures at which peaks are observed can be used to identify the glass transition ($T_g$), crystallisation ($T_c$), eutectic and melting temperatures ($T_{en}$ and $T_m$) if appropriate.

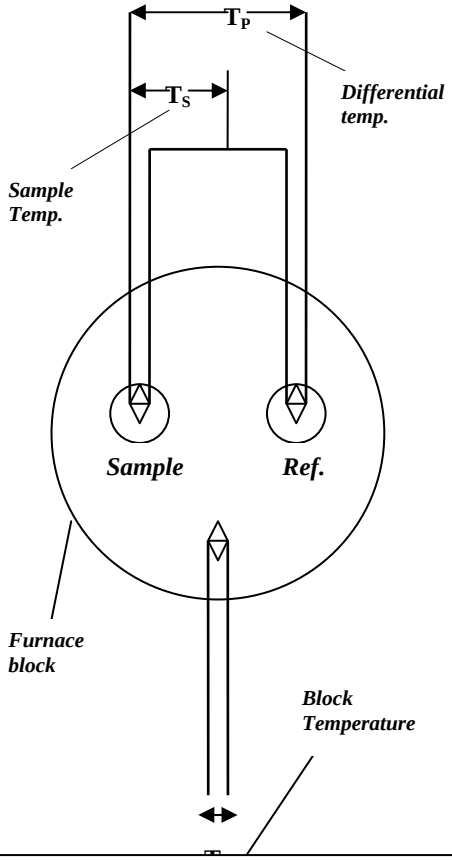


**Figure 3**: Schematic representation of DTA

### *2.2. Infrared spectroscopy*

The infrared region of the electromagnetic spectrum can provide chemists and material scientists with information about the energy of molecular vibrations. This is a useful tool for distinguishing the different functional groups inherent within a material. When ceramics are heated to very high temperatures they usually undergo either a change in structure and/or may undergo a loss of atoms or functional groups. This behaviour can be detected using infrared and is reflected in the changes of vibrational mode, a shift in vibrational mode frequency or intensity and shape of the peak to which a mode is assigned (Williams & Fleming, 1995; Hollas, 1996).

### *2.2.1. Infrared spectrometer*

The application of infrared spectroscopy involves the emission of infrared light from a source throughout the whole frequency range of the instrument (Williams & Fleming, 1995; Hollas, 1996). The infrared light is then split into two equally intense beams, in which one beam is passed through the sample. Absorption of energy of this frequency may occur provided the frequency of vibration of a sample or molecule lies within the range of the instrument, in which case the intensity of the beam passing through the sample is compared against the other beam. A prism or grating within the instrument will spread this information in the form of transmittance peaks across a wavelength range over which this comparison is made. Each peak will correspond to a characteristic absorption at the wavelength or frequency to which it is assigned. Compounds may be examined in vapour phase, as pure liquids, in solution, and in the solid state.

At an atomic level, the process of infrared is considered as the absorption of infrared radiation by a molecule or solid resulting in the promotion of a photon from a lower vibrational energy state to a higher one (Figure 4). The energy of separation of vibrational states must be equivalent to the energy of the photon

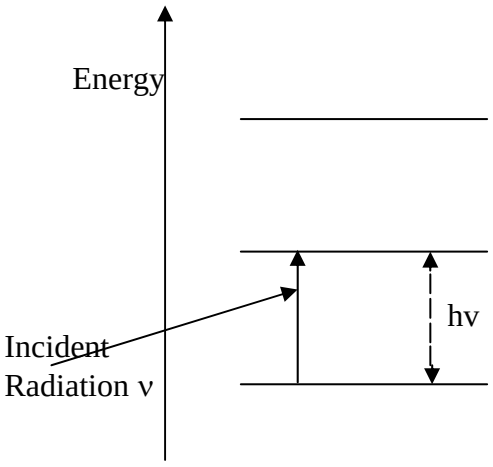


**Figure 4**: Infrared absorption.

for this to occur.

Raman spectroscopy, however, concerns the use of visible light. In contrast to infrared the energy here is not absorbed. Since the energy of a visible photon is much greater than the fundamental vibrational transitions in molecules and solids, the spectrum that is obtained measures the scattering of photons. This is where the photon loses some of its energy. This loss corresponds to the vibrational transition energy and also correlates to a shift to lower frequency of the visible photon (Figure 5).

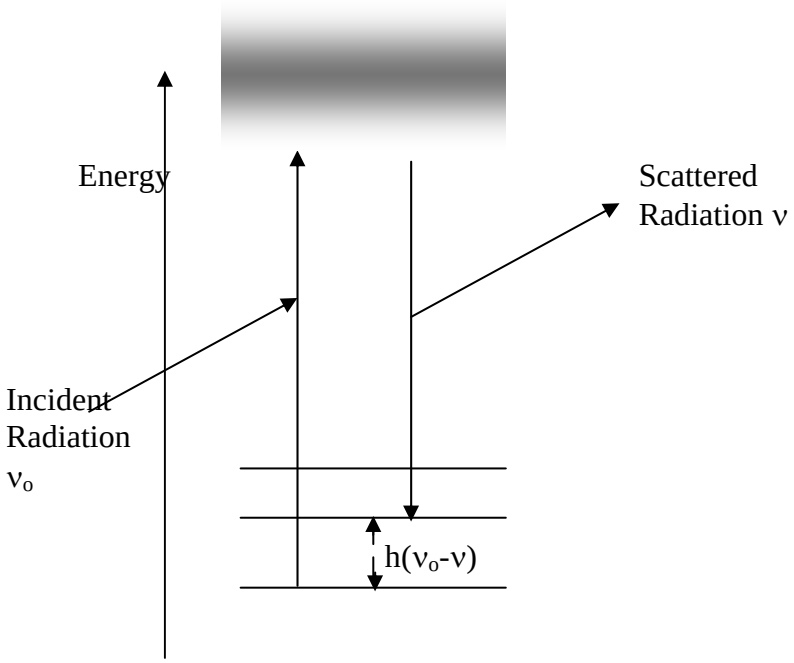


**Figure 5**: Photon scattering (Raman) (Hollas, 1996)

### *2.2.2. Fourier transform infrared (FTIR)*

Fourier transform infrared has become a widely used technique, this is due to its high sensitivity and the digital data handling capability. This technique provides the user with the same information as traditional infrared, however, it

utilises the interference effects between two rays from a broad band source, as a result what is detected is a signal that oscillates in time and is referred to as an interferogram. This signal is converted using a mathematical technique so that it can be interpreted as a function of frequency so that it resembles a normal infrared spectrum (Williams & Fleming, 1995).

### *2.2.3. Selection rules*

Molecular vibrations that occur can result in an oscillating dipole moment. When this interacts with the oscillating electric vector of the infrared beam infrared light is then absorbed. The requirement for this can be explained by a simple rule; if there is a difference in dipole moments between the two extremes of a vibration then the interaction will occur. Raman, however, involves the interaction of the light with the molecule's polarizability, this requires different selection rules (Williams & Fleming, 1995).

The difference in selection rules for infrared and Raman are simple to envisage. If the vibration about the centre of symmetry of a molecule is symmetric then the interaction is active in the Raman and inactive in the infrared, if it is anti-symmetric then it is inactive in Raman and active in the infrared (Figure 6).

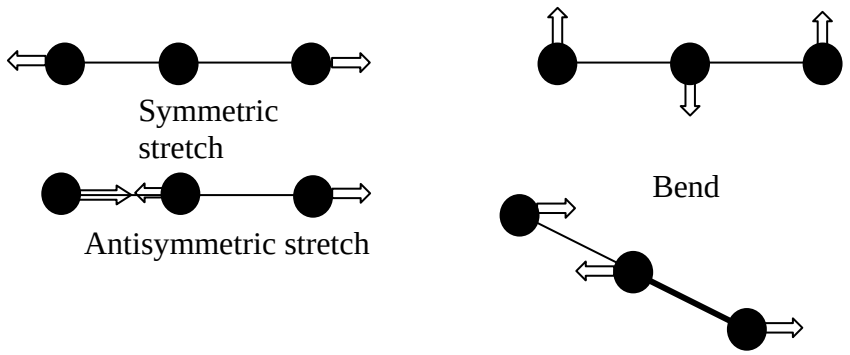


**Figure 6**: Symmetric and antisymmetric modes. Symmetrical stretches are active in Raman, anti-symmetric stretches are active in infrared

### *2.3. X-ray diffraction Crystal structure*

#### *2.3.1. Lattice and unit cells*

In order to understand the concept of a lattice in crystal structure, one must be able to visualise this crystal as a structure that contains individual entities of a certain pattern that form the building block of a crystal (Cullity, 1978; Shriver et al., 1995). A crystal is constructed from atoms, ions or molecules which are termed asymmetric units. The locations of the asymmetric units that form the pattern can be represented by points that are referred to as the space lattice, which in effect is considered as an abstract scaffolding for the crystal structure.

The basic three dimensional crystal structure consists of a theoretically infinite array of points that defines a basic repeating pattern and vice-versa. This scaffold does not necessarily imply that an asymmetric unit must be centred on each lattice point, in essence, the space lattice and the identical asymmetric unit are associated when one uses these terms to define the crystal structure.

The pattern within a crystal structure, can be thought of as an imaginary structure that contains one unit or **unit cell** that is translationally repeated (Figure 7). The unit cell is the smallest (fundamental) repeating unit that makes up the entire structure. Primitive unit cells are composed of neighbouring lattice points that are joined by straight lines, in which each unit cell has one lattice point at its origin. Non-primitive unit cells can also be depicted; however, the lattice points in this case are located at their centres or on pairs of faces.

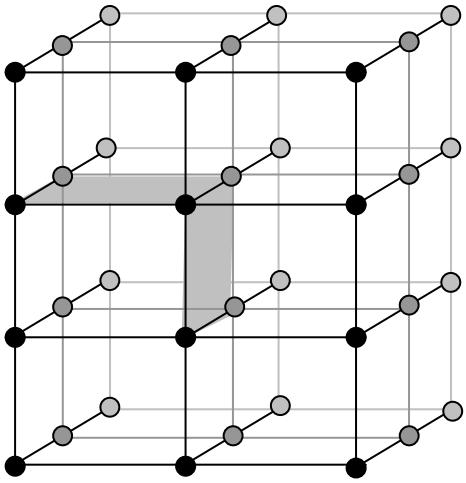

**Figure 7**: Translationally repeating unit cell.

Unit cell parameters are used to define the length of the sides and the angles between them, these are given as a, b and c (lengths) and $\alpha$,$\beta$ and $\gamma$ (angles) –

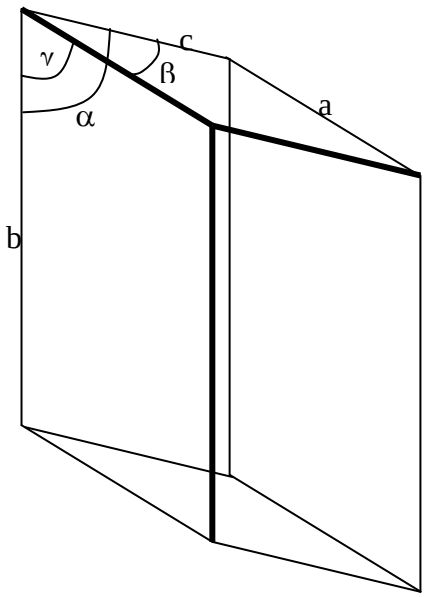


see figure 8.

**Figure 8**: Unit cell defined by its parameters (Shriver et al., 1995).

A unit cell has an inherent rotational symmetry to which it belongs. The rotational symmetry of unit cells can be otherwise referred to as crystal systems of which there are seven. A cubic lattice, the simplest structure, has unit cells that have a rotational symmetry in which there are four threefold axes in a tetrahedral array (Figure 9).

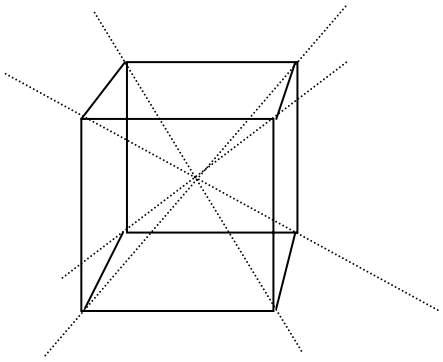

**Figure 9**: Rotational symmetry of a cube.

### *2.3.2. X-Rays*

The emission of x-rays arise from the bombardment of a metal with high energy electrons (Shriver et al., 1995). The radiation produced is electromagnetic. Bremsstrahlung is a term that refers to the deceleration of electrons as they bombard the metal upon which radiation is generated with a continuous range of wavelengths. The collision of the incoming high electrons with inner-shell electrons from the atoms result in a few sharp high intensity peaks that are superimposed on the continuum, these correspond to the emission of excess energy in the form of an x-ray photon.

### *2.3.3. The Bragg law*

The application of x-rays as a means of establishing the crystal properties of a material was not realised until the early part of the $20^{th}$ century. Max von Laue suggested that when x-rays are passed through a crystal they are diffracted, and that there was a relationship between their wavelengths and the separation of planes (quoted from Shriver et al., 1995).

A crystal can be considered as being made up of stacks of reflecting planes that are separated by d-spacing, with each lattice plane regarded as a mirror in which x-rays can be reflected.

An incoming beam of x-rays may be reflected if the crystal is orientated at a given angle, this is known as constructive interference and appears as an intense spot. The angle at which this interference occurs can be easily calculated and is based on the model of lattice planes (Figure 10). Thus, a plane at a given angle in a crystal is responsible for this constructive interference.

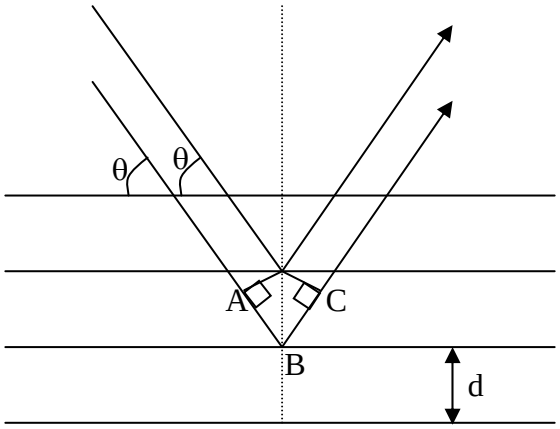


**Figure 10**: Bragg model of lattice planes (Shriver et al., 1995).

This diagram depicts the path length difference of two rays. The path length difference is related to the glancing angle of the ray and the d-spacing through the following relationship:

$$AB + BC = 2d\sin\theta \qquad \textbf{Equation 1}$$

The path length difference can be comparable to the wavelength of the incoming ray, however, most rays do not interfere constructively and are out of phase. This infers that the path length difference is not an integral number of wavelengths. During constructive interference the path length difference is an integral number of wavelengths, hence AB + BC = $n\lambda$. When the glancing angle satisfies the Bragg law then a bright reflection should be observed, therefore:

$$n\lambda = 2d\sin\theta \qquad \textbf{Equation 2}$$

The separation of planes d are associated to an integral number of planes at angle $\theta$, in which the x-rays are reflected and so for reflections corresponding to n = 1,2,3,4…etc, the Bragg law can be simplified:

$$\lambda = 2d\sin\theta \qquad \textbf{Equation 3}$$

Hence, the $n^{th}$ order of reflection corresponds to the (nh, nk, nl) planes.

### *2.3.4. The Debye-Scherrer method*

This technique, which was developed by Peter Debye and Paul Scherrer, used a powdered sample instead of a single crystal and monochromatic radiation (Shriver et al., 1995). The orientation of some of the crystallites in the powdered sample should satisfy the Bragg condition for each set of planes (h k l). For instance, the set of (111) planes, with plane separation $d_{111}$, belonging to some crystallites of given orientation will give rise to diffracted intensity at glancing angle $\theta$. Crystallites having the same glancing angle $\theta$ will be orientated at all possible angles around the incoming beam, giving rise to diffracted beams that lie on a cone around the incident beam of half angle $2\theta$.

This applies to other crystallites with orientation of different planes that satisfy the Bragg law. Therefore, each set of (h k l) planes will give rise to a diffraction cone of associated diffracted intensity and half angle.

The Debye-Scherrer method uses a rotating capillary tube to give a random orientation of crystallites, in which the diffraction cones are detected by a

photographic film. Modern diffractometers utilise a flat plate for mounting the sample, the intensities of the reflections and the diffraction patterns are collected and interpreted electronically.

The identification of a sample can be made by using powder diffraction, this can be done by comparing the positions of the diffraction lines and their associated intensities with a large data bank. Phase diagrams can also be determined using this technique. A powder may contain a mixture of phases and so the relative amounts of each phase may be determined also. Identification of different phases are distinguished by the different diffraction patterns that they exhibit.

### *2.3.4. High-temperature X-ray diffraction (HTXRD)*

At higher temperature, there is often little chemical change seen in samples; however significant crystallisation events can be seen and detected with a high temperature XRD system. It allows crystallisation to be measured as a function of both composition and also as a function of temperature, it also allows measurement of changes in unit cell dimension versus temperature. A linear power spectrum dentsity allows fast transitions to be investigated.

## 2.4. Rheology

Rheology is thought of as the study of flow and deformation of matter. The principles involved can be explained by the behaviour of fluid flow and its relationship with viscosity (Richerson, 1992).

### *2.4.1. Viscosity*

The viscosity of a fluid is a measure of its resistance to flow (Richerson, 1992). A fluid is considered a substance consisting of a number of different layers

sliding past each other at different velocities during flow. Essentially the viscosity of a particular fluid is a measure of the internal friction or shear between two adjacent component layers.

A common example of the variation in velocities of layers can be described by the flow of a viscous fluid through a pipe. Layers flowing close to the pipe wall will tend to move slower than those at the centre, which move the fastest. This is due to the friction between the wall and the fluid near the wall.

A simple profile can be given to illustrate differences in velocities of a fluid across the pipe (Figure 11) (Breithaupt, 1990).

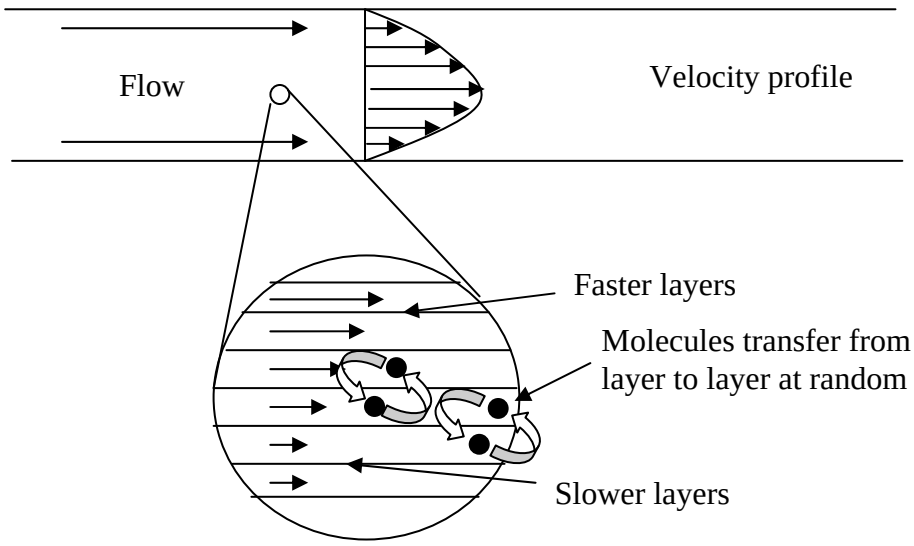


**Figure 11**: Fluid flow across a pipe.

Viscosity is attributed to molecular motion, which can be described as the transfer of molecules from layers of varying velocities, which as a consequence causes a transfer of momentum between layers. This is the reason why the frictional force between layers occurs.

The difference in velocities across the pipe radius, therefore, can be expressed as the velocity gradient dv/dr where d/dr refers to the change per unit distance.

The tangential stress, T, can be described as the viscous force acting per unit area along the boundary of two adjacent fluid layers (Figure 12) (Breithaupt, 1990).

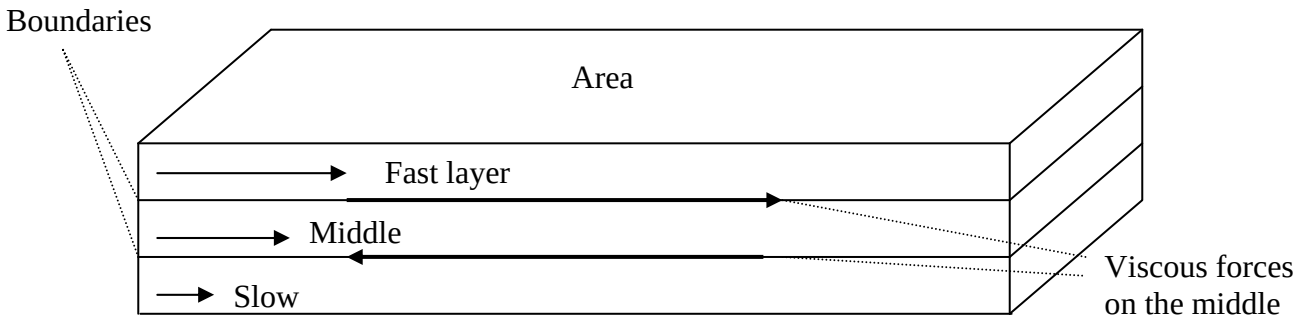


**Figure 12**: Diagram illustrating the viscous force acting along the boundary of adjacent layers.

In a Newtonian fluid the velocity gradient at any point in the fluid across the pipe is proportional to the tangential stress.

The Newtonian relationship between stress and velocity gradient does not hold true for the majority of ceramic materials in suspension. In fact at constant temperature most suspensions show a curve for shear rate against shear stress. Such suspensions can be considered non-Newtonian. Paint for example becomes less viscous the more it is stirred (Worrall, 1975).

### *2.4.1.1. Pseudo-plasticity, Bingham plasticity and dilitancy*

Examples of non-Newtonian behaviour are pseudo-plasticity, Bingham plasticity and dilatancy.

Pseudo-plasticity describes systems that give flow curves that pass through the origin and are similar to those expressed for plastics. The difference between pseudo-plasticity and plastic flow is that plastic flow gives a yield value that is indicated by a minimum stress value that intersects the stress axis (Figure 13) (Worrall, 1975).

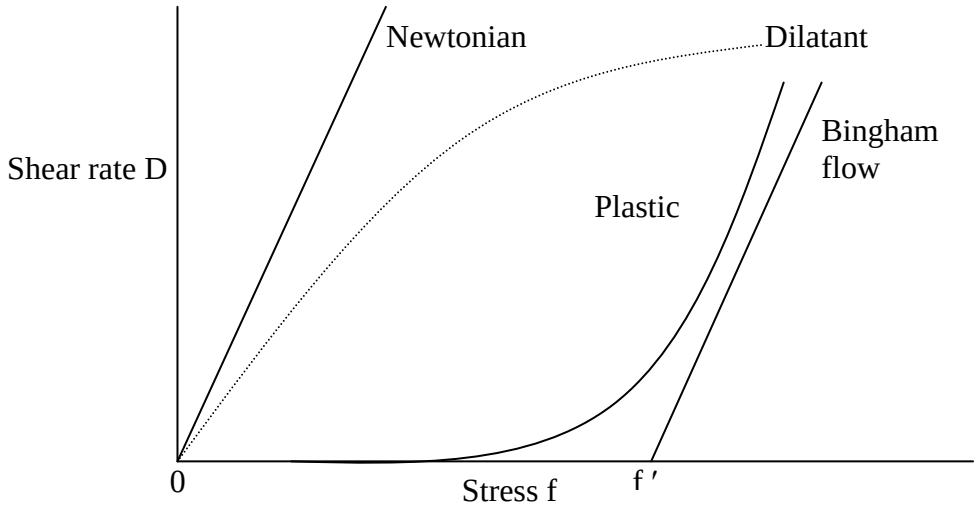


**Figure 13**: Graph displaying different flow systems (Worrall, 1975).

Dilatancy is the term that describes systems that have a tendency to increase in viscosity as a function of shear rate and where no yield is given (Worrall, 1975).

Dilatancy, although not fully understood, might be attributed to the 'squeezing out' of water. This phenomenon is most likely to occur at parts of the suspension that experience the greatest shear and is commonly associated with suspensions containing coarse particles. Alternatively, dilatancy might occur through the formation of large voids when a suspension undergoes shearing. This consequently makes it difficult for water to sufficiently fill these voids and hence might explain why viscosity increases with increasing shear (Worrall, 1975).

#### *2.4.1.2. Thixotropy*

Thixotropy is a term that refers to suspensions that break up to form loose structures of low viscosity as shear rate increases, but have a tendency to thicken and increase in viscosity if left unstirred (Ring, 1996). In many respects this behaviour resembles a hysteresis curve when shear rate is plotted against stress and so thixotropy can be considered a reversible, time dependent property.

The thixotropic property of a suspension can be measured stepwise. Since thixotropy is time dependent, a selection of shear rates can be used with the resulting stress measured 10 seconds after shearing is stopped. This process is carried out from the smallest shear rate in increasing steps to a maximum practical value and then repeated with decreasing shear rates.

Before a suspension is stirred the particles are built up in a kind of three-dimensional network consisting of particle linkages, and accounts for the yield value given when a suspension is initially stirred. Furthermore, the break up of the network structure requires a measurable time. This is indicated by the greater stress needed for this to occur with respect to 'equilibrium stress' and suggests this process is not instantaneous. For a decrease in shear, what is

usually observed is a downward curve that follows the 'equilibrium stress' curve, however, is slightly less in stress which indicates that the structure is attempting to build up rather than remaining broken down (Figure 14) (Worrall, 1975).

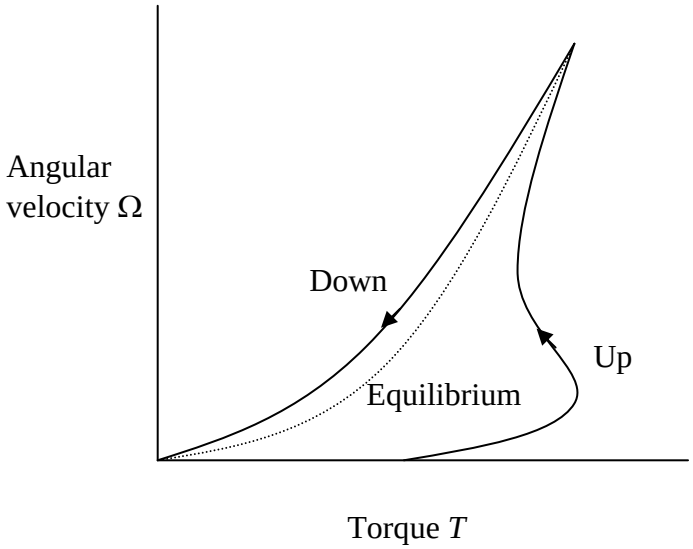


**Figure 14**: Graph showing thixotropic behaviour.

### *2.4.1.3. Measurement of viscosity*

There are a number of methods for measuring viscosity, the simplest of which is modelled around determining the rate at which a liquid flows through a tube, with the application of constant pressure (Breithaupt, 1990).

Changing the rate of flow requires a change in pressure or change of tube length. By recording the volume (V) of fluid passing through the tube over time (t), and knowing the pressure applied, radius and length of tube, the viscosity ($\eta$) can therefore be determined.

The rotating-cylinder viscometer consists of two concentric cylinders that are immersed in a liquid. The outer cylinder is driven by an electric motor that

creates a viscous drag in the liquid as a result of its angular velocity. This in turn exerts a torque on the inner cylinder which is suspended from a light spring and therefore is able to rotate through an angle of twist $\theta$. A pointer, a component of the inner cylinder, records the angle of twist, which may then be calculated as stress or viscosity.

### *2.4.2. Contact Angle*

Contact angle measurements are a simple and inexpensive method of determining basic information on the wettability of a material. Contact angle measurements are often used as a primary characterisation technique (Ratner, 1996).

Contact angle ($\theta$) is a quantitative measure of the wetting by liquid of a solid. Contact angle can be defined as the geometric angle formed between the liquid surface and solid surface when liquid and solid have made contact (see figure 15).

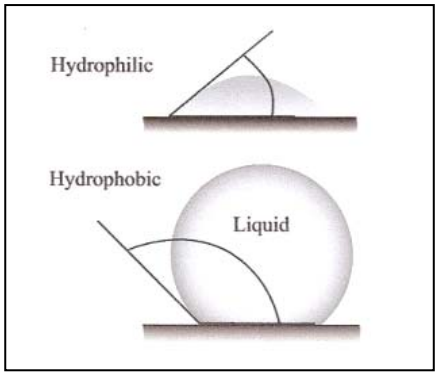


**Figure 15**: Schematic drawing to show hydrophilic and hydrophobic contact angle.

If θ is less than 90$^{o}$, this indicates that the solid exhibits good wettability, and can also be used as an indicator that the surface of the solid or the liquid are relatively hydrophilic. For solids where complete or perfect wetting occurs, θ will be zero degrees. If θ is greater than 90$^{o}$, it is said to be non-wetting, indicative that the material surface is relatively more hydrophobic (Van Noort, 2006).

### 2.5. Ion Chromatography

Ion chromatography (IC) is a system for ion analysis of a sample that can use either suppressed or non suppressed conductivity detection.

An IC system can comprise of a high pressure pump, sample injector/auto sampler, a guard and separator column, a chemical suppressor, liquid eluent, a detection cell, along with a data collection system (see figure 16).

Eluent is the fluid used to aid with the separation of the sample ions. The delivery of eluent which is the first stage of the ion analysis process, is the distribution of the eluent through the ion chromatography system.

The next stage of ion chromatography is injecting the sample (in solution). The sample is then loaded into the sample loop, either manually or via an automated autosampler. After being triggered, the sample is injected into the eluent stream. This eluent and sample are then pushed with the aid of the pump through the guard and separator columns. Both of these columns are chemically inert tubes which contain a polymeric resin. The guard column removes any harmful contaminants which may damage the separator column, while the separator column is where the ion separation process occurs.

Following on from this, the eluant and sample ions are pumped through the suppressor, which enhances the detection of the sample ions whilst suppressing the conductivity of the eluant. As the sample ions emerge from the suppressor, the detection cell measures their properties and produces a signal based either on the physical or chemical property of the ion. The detection cell then transmits this data to the data collection system. The data collection system works by identifying the ions based on retention time. The quality of measured ion is determined by the software which integrates the peak and/or peak height. This data is then compared against peaks produced from the standard solutions of predetermined quantities of ions. The result is then finally displayed as a chromatogram (Dionex, 2003).

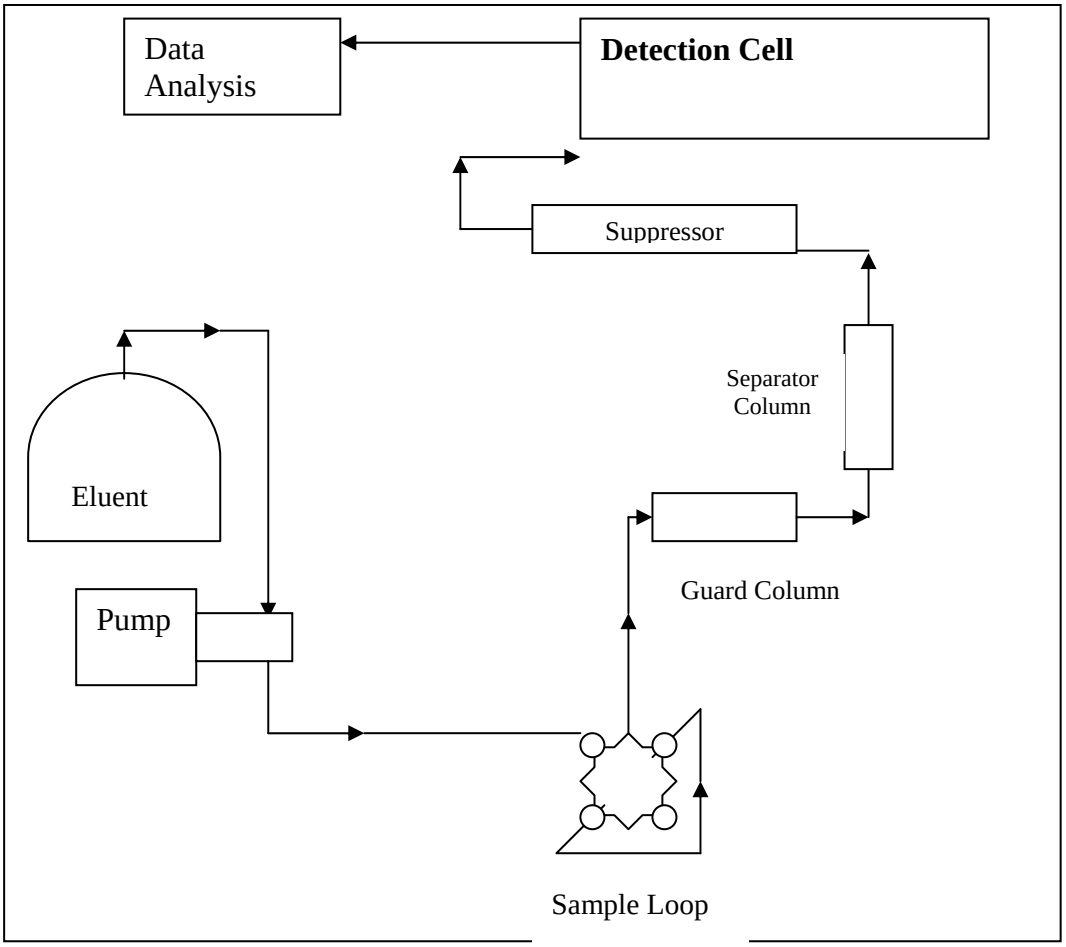


**Figure 16**: Schematic representation of a typical ion analysis

### 2.6. Ball milling

Ball milling is a commonly used route for obtaining the desired particle size distribution (Richerson, 1992). This step involves particle size reduction, where the particles are ground in a closed cylindrical container with grinding balls, rods or short cylinders which is continually rotated. In order to obtain effective milling the cylinder is placed horizontally so as to allow the grinding media to cascade. Ceramic particles are effectively broken down into smaller particles

through their movement between the grinding media and between the media and the mill wall (Figure 17).

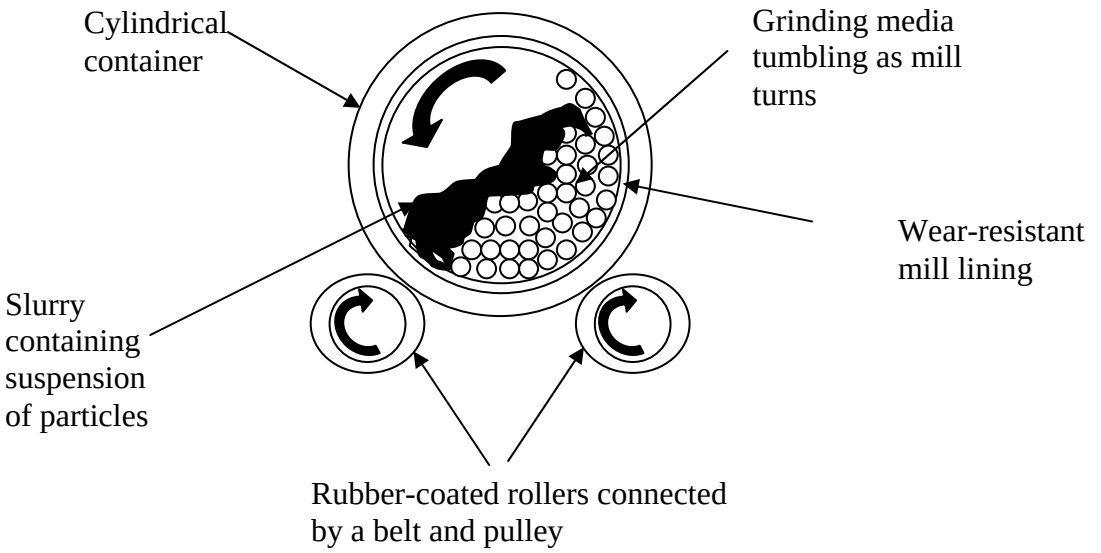


**Figure 17**: Diagram representing the ball milling process.

The type of grinding media that can be utilised are WC, steel, $ZrO_2$, $Al_2O_3$ and $SiO_2$. These media have a different specific gravity and it is the specific gravity amongst other factors (relative size and hardness) that dictates the rate of milling. A higher rate of milling can be achieved through a higher specific gravity media and consequently leads to a specific size reduction being reached more quickly (Richerson, 1992).

Milling can be carried out under either wet or dry conditions. Some of the main advantages of wet milling over dry milling is that it can achieve a smaller particle size than dry, higher rotational speeds, a narrower particle size and also allows wet screening of particles through a fine screen. However, the resulting powder after dry milling does not require separation from a liquid (Richerson, 1992).

Overall, the effect of milling achieves a broader particle size distribution compared to screening alone. The particle size distribution can be illustrated as a cumulative mass percent against the equivalent spherical diameter as a function of milling time for silicon powder (Richerson, 1992).

## 2.7 Cellular methods and analysis

### 2.7.1 Bone healing

The ability to maintain and manipulate cells in culture is a valuable tool for research. Before the *in vitro* use of cells is discussed there needs to be a simple overview of bone healing. All bone healing processes are similar to the healing process that occurs in fractured long bones and can effectively be divided into stages (Frost, 1989):

(1) Within the first few days of healing, the inflammatory process begins to remove any debris and form a hematoma. If it is a fracture repair, then simultaneously, a callus is formed over the fracture site on both the periosteum (outside) and the endosteum (inside) of the bone. This inflammatory phase lasts 3 – 4 days.

(2) Between 7 and 10 days after injury, the space between the fragments is filled with tissue that forms fibrocartilage. Osteoblasts begin to lay down collagen. The blood supply that provides the needed oxygen and nutrients for growth, comes from the periosteal and endosteal vessels, and from the intercortical blood supply.

(3) Three to four weeks following injury, calcification of the fibrocartilage begins. This is when radiographic evidence of healing becomes noticeable.

(4) Between 6 and 8 weeks after injury, the calcification escalates, more blood vessels supply the area, and the fibrocartilage is gradually replaced by fibrous bone. In the final stage, the fibrous bone is gradually transformed to lamellar bone via osteoclastic and osteoblastic activity (remodelling).

### 2.7.2. Human Osteosarcoma Cells

Osteoblasts are mononucleate cells, and as has been previously discussed, are responsible for bone repair and formation. In *in vitro* studies osteoblasts can be slow and difficult to culture and grow, clearly any cells that mimic the effect of these cells, but can be grown quickly and are less sensitive to *in vitro* conditions, can be useful to test the biocompatibility of a material. One such group of cells are human osteosarcoma cells.

The osteosarcoma cell line has been well characterised and validated as a model to test biocompatibility of various materials (Francheschi et al., 1985; Boyan et al., 1989; Lajeunesse et al., 1991). Osteosarcoma cell lines have been used in many studies, particularly with in vitro work with titanium surface topographies, potential bone grafting materials and implant coating materials. Despite being a tumour cell line, which proliferates more rapidly than human bone derived cells, osteosarcoma cells exhibit many osteoblastic traits which are characteristic for bone forming cells (Bachle & Kohal, 2003). Osteosarcoma cells exhibit an increased alkaline phosphatase activity following I,25-dihydroxyvitamin $D_3$ (I,25$(OH)_2D_3$) administration, which is a characteristic for bone derived cells (Clover & Gowen, 1994). These cells are thought to be relatively immature osteoblasts. However they exhibit a number of osteoblast-like phenotypic markers, including response to parathyroid hormone (Aisa et al., 1996) and inhibition of proliferation with I,25$(OH)_2D_3$ (Boyan et al., 1989).

### 2.7.3 Cellular proliferation

Cell culture models permit the study of a single cell type. Cell culture models also allow the measurement of cell responses to conditions which are more tightly regulated than the complex environment presented by an entire

organism. One of the most fundamental measurements that can be made with cells in culture is cell proliferation.

To study cell proliferation several methods are available. The methods either detect an antigen which is present in proliferating cells but absent in non-proliferating cells (e.g. monoclonal antibody Ki-67), measure DNA synthesis (quantification of $^{3}$H-thymidine or 5-bromodeoxyuridine incorporation; monitoring DNA quantity with fluorescent dye Hoechst 33258) or monitor the reducing environment of the cells (quantification of tetrazolium salt or alamarBlue™ reduction).

One of the most common methods used for assessing cellular proliferation is using alamarBlue™ (BioSource Inc, USA) reduction (Ahmed et al., 1994). The internal environment of proliferating cells is more reduced than that of non-proliferating cells (Mossmann, 1983). Specifically the ratios of NADPH/NADP and NADH/NAD, increase during cell proliferation. AlamarBlue™ is reduced by these metabolic intermediates and hence is useful in monitoring cell proliferation because its reduction is accompanied by a measurable shift in colour (Ahmed et al., 1994). The site of reduction of alamaBlue™ is still the cause of controversy and both the mitochondria and cytoplasm have been suggested as potential sites (O'Brien et al., 2000). Because alamarBlue™ is soluble, stable in culture medium and is non-toxic, the continuous monitoring of cells in culture is permitted (Ahmed et al., 1994).

Proliferation measurements with alamarBlue™ may be measured either spectrophotometrically or fluorometrically (Biosource, 2003).

# Chapter 3:

# Statement of the Problem

## 3. STATEMENT OF THE PROBLEM

Hydroxyapatite [HA, $Ca_{10}(PO_4)_6(OH)_2$] has attracted much interest as an implant material for teeth and bones, due to the similarity of its crystallography and chemical composition to that of human hard tissues (Block et al., 1989; McPherson et al., 1995). The idea of coating HA on Ti substrate appears very appealing combining the excellent biocompatibility of HA and load-bearing ability of Ti.

Traditional methods for providing coatings on materials, such as plasma spraying, are associated with many problems such as coating strength, chemical homogeneity, residual porosity, expense and difficulty with coating complex shapes (Overgaard et al., 1996). The sol-gel technique has been suggested as a potential method to overcome many of these problems. The medical application of materials and devices containing sol-gel coatings is already becoming widespread and has been proposed to increase in the next 10 years to be used in implantable materials, skin products, slow-drug-delivery systems, bone grafts, stem cells and biogenic material-containing scaffolds and biologically active membranes (Ben-Nissan & Choi, 2006).

In the sol-gel HA coatings, various precursors have been tried in the pursuit of obtaining a well developed HA layer; $Ca(NO_3)_2$, CaO, $Ca(OH)_2$ and Ca alkoxide as a Ca sources, P alkoxide such as triethyl phosphite [$P(OC_2H_5)_3$] (TEP) and triethyl phosphate [$PO(OC_2H_5)_3$], ($P_2O_5$) and $H_3PO_4$ as a P-source, with differing successes (Layrolle & Lebugle, 1994; Layrolle et al., 1998; Tkalcec et al., 2001; Gan & Pillar, 2004; Han et al., 2004; Hsieh et al., 2004; Kim et al., 2004; Andersson et al., 2005; Stoch et al., 2005; Bogdanoviciene et al., 2006). The $Ca(NO_3)_2$ and TEP combination has shown the most promising results but to date has still had difficulty in obtaining phase pure HA.

Pure fluorapatite [(FA, $Ca_{10}(PO_4)_6F_2$)] is known to have a much lower solubility than HA, because FA possesses a greater stability than HA, both chemically and structurally (Larsen & Jensen, 1989). Moreover, the FA forms fluorhydroxyapatite (FHA, $Ca_{10}(PO_4)_6OH,F_1$) solid solutions with HA through the replacement of $OH^-$ by $F^-$. Hence, modulation of the extent of fluoride substitution provides an effective way of controlling the solubility of the apatite. There have been few reports concerning the fabrication or characterisation of the FA or FHA materials (Cheng et al. 2001, 2004; Kim et al., 2004). Most studies discussed the fabrication of FA powders by precipitation methods or films by thermal spraying techniques (Joa et al., 1997; Overgaard et al., 1997). However, the properties and qualities of the powders and films were not so satisfactory due to the formation of byproducts or to other technical problems. The sol-gel approach has been suggested as a potential method to overcome these difficulties (Kim et al. 2004) but requires further investigation.

# Chapter 4:

# Aims

## 4. AIMS

The aims of this PhD thesis are as follows:

(1) Optimisation and charaterisation of hydroxyapatite [HA, $Ca_{10}(PO_4)_6(OH)_2$] produced by the sol-gel method using calcium nitrate $Ca(NO_3)_2$ and triethyl phosphite [$P(OC_2H_5)_3$] (TEP) as the precursors. This is with a view to establishing phase pure HA.

(2) Investigation of fluorapatite [(FA, $Ca_{10}(PO_4)_6F_2$)] production via sol-gel synthesis using calcium nitrate $Ca(NO_3)_2$ and triethyl phosphite [$P(OC_2H_5)_3$] as the precursors and ammonium fluoride ($NH_4F$) as the source of fluoride. Optimisation and charaterisation of FA produced.

(3) Investigation of fluorhydroxyapatite (FHA, $Ca_{10}(PO_4)_6(OH,F)_2$) production via sol-gel synthesis using calcium nitrate $Ca(NO_3)_2$ and triethyl phosphite [$P(OC_2H_5)_3$] as the precursors and ammonium fluoride ($NH_4F$) as the source of fluoride. Optimisation and charaterisation of FHA produced.

(4) Investigation of morphology, phase and structural changes of the HA, FA and FHA sol-gels, with thermal treatment.

(5) Investigation of the in vitro dissolution rates to examine bioactivity of the HA, FA and FHA produced.

(6) Investigation of the rheology and surface coating characteristics (wettability) of the HA, FA and FHA sol-gels.

(6) Investigation and establishment of a prototcol for coating HA, FA and FHA sol-gels onto titanium.

(7) Investigation of the surface morphology and coating thickness and surface interaction of HA, FA and FHA sol-gel coatings produced on titanium.

(8) Investigation of the adhesive strength and failure mechanisms of the HA, FA and FHA sol-gels.

(9) Investigation of the *in vitro* biological properties of the HA, FA and FHA produced, with a particular emphasis on cell proliferation.

# Chapter 5:

# Overview of the PhD

## 5. OVERVIEW OF PhD

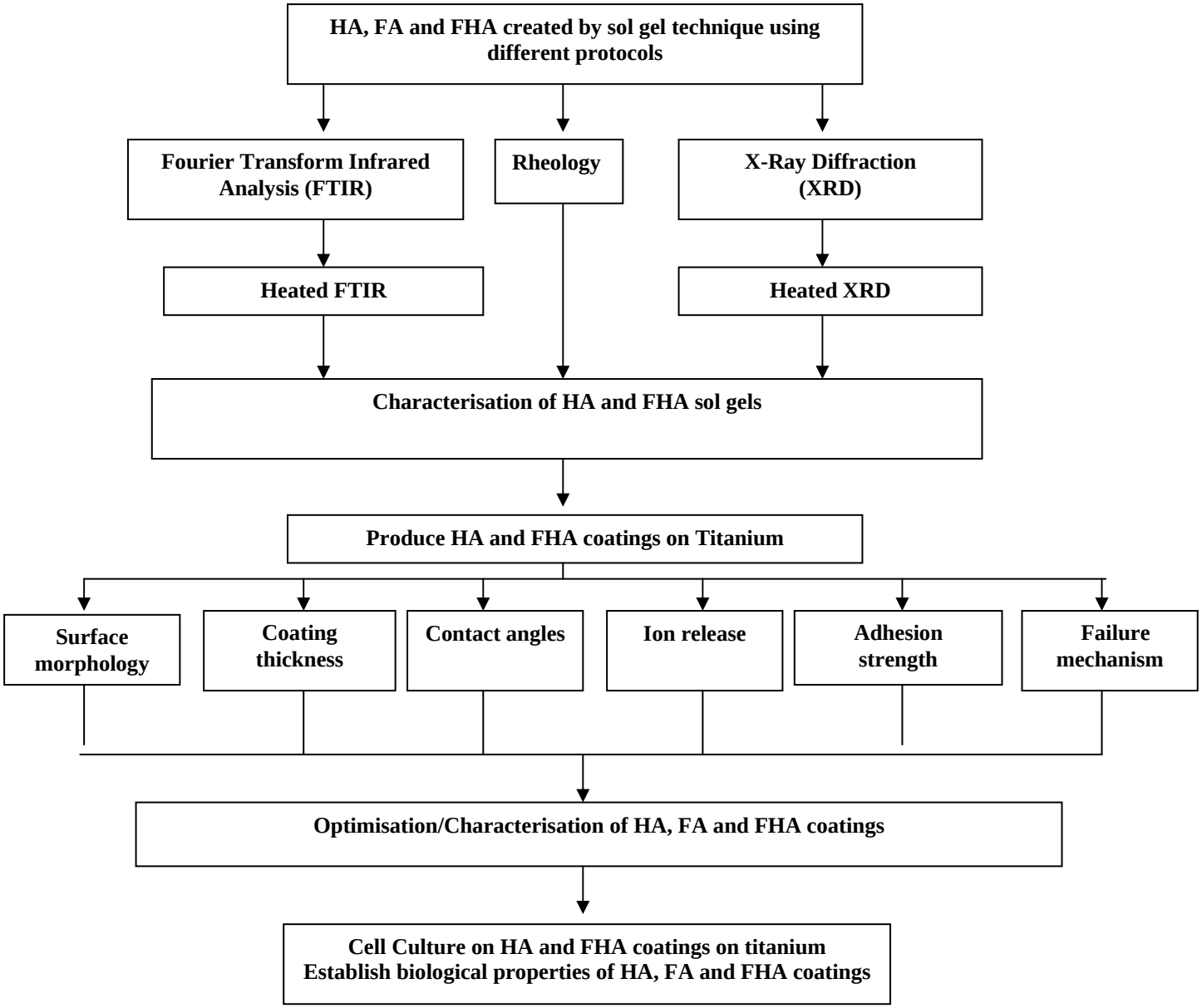

# Chapter 6:

# Characterisation & Optimisation Of

# Hydroxyapatite $Ca_{10}(PO_4)_6(OH)_2$

# Sol-gels

## 6.1. Methods & Materials

### *6.1.1. Preparation of HA sol-gel films*

With reference to the literature, while use of triethyl phosphite and calcium nitrate as precursors have been the most successful method for the production of HA-sol gel, the majority of the sol-gel produced is β-TCP and not HA. It was the intention of this chapter to try and optimise the production of HA sol-gel using triethyl phosphite and calcium nitrate as precursors.

Triethyl phosphite ($[P(C_2H_50)_3]$, Aldrich, USA) of 0.1 moles (16.16g) was hydrolyzed in 33.12g of ethanol (0.72 moles) with 5.04g of distilled water (0.28 moles) for 12 hours, and then slowly added to a 0.16 mole (39.36g) solution of calcium nitrate [$Ca(NO_3)_2.4H_20$, Aldrich USA] and allowed to mix for a further 12 hours. A 5% solution of ammonium hydroxide ($NH_4OH$, BDH, UK) was added to the solution in order to improve gelation and the polymerization of an apatite structure, followed by aging for 72 hours at room temperature and pressure. Oven drying was undertaken for a further 24 hours. This is summarised in table 3.

**Table 3:** Variation of constituents (amount of water)

| **Constituents** | **$Ca(NO_3)_2.4H_20$** | **$P(C_2H_50)_3$** | **$C_2H_5OH/H_2O$** |
|---|---|---|---|
| 1 mole | $236.15gmol^{-1}$ | $166.16gmol^{-1}$ | 46+18 (64) |
| Ideal ratio | 0.1667 mole | 0.1mole | 1 mole |
| Amount (grams) | 39.36g | 16.16g | 33.12g/5.04g |
| Ammonium hydroxide(5%) - 25ml | | | |

Following the above protocol it was found that a sol-gel was produced, but it was it was very dry. So to produce a sol-gel with a usable consistency, following addition of ammonium hydroxide, 30ml, 60ml, 75ml and 100ml of water was added.

### *6.1.2. Variation of Hydrolysation Time of TEP.*

Triethyl phosphite ([$P(C_2H_50)_3$], Aldrich, USA) of 0.1 moles (16.16g) was hydrolyzed in 33.12g ethanol (0.72 moles) with 5.04g of distilled water (0.28 moles) for 24, 48 and 72 hours and then slowly added to a 0.16 mole (39.36g) solution of calcium nitrate [$Ca(NO_3)_2.4H_20$, Aldrich USA] and allowed to mix for a further 12 hours. A 5% solution of ammonium hydroxide ($NH_4OH$, BDH, UK) and 100ml of water was added to the solution in order to improve gelation and the polymerization of an apatite structure, followed by aging for 72 hours at room temperature. Oven drying was undertaken for a further 24 hours. This is summarised in table 4

**Table 4:** Variation of hydrolysation time of TEP in ethanol prior to mixing with Calcium Nitrate.

| **Constituents** | **$Ca(NO_3)_2.4H_20$** | **$P(C_2H_50)_3$** | **$C_2H_5OH/H_2O$** |
|---|---|---|---|
| 1mole | $236.15gmol^{-1}$ | $166.16gmol^{-1}$ | 46+18 (64) |
| Ratio | 0.1667 moles | 0.1 moles | 1 moles |
| Amount (grams) | 39.36g | 16.16g | 33.12g/5.04g |
| Ammonium hydroxide (5%) - 25ml | | | |
| **Run 1** | 24 hours hydrolysation time | | |
| **Run 2** | 48 hours hydrolysation time | | |
| **Run 3** | 72 hours hydrolysation time | | |

### *6.1.3. Increased mixing time of hydrolysed TEP and calcium nitrate.*

Triethyl phosphite ([$P(C_2H_50)_3$], Aldrich, USA) of 0.1 moles (16.16g) was hydrolyzed in 33.12g of ethanol (0.72 moles) with 5.04g distilled water (0.28 moles) for 24 hours and then slowly added to a 0.16 mole (39.36g) solution of calcium nitrate [$Ca(NO_3)_2.4H_20$, Aldrich USA] and mixed for 12, 24 and 72 hours. A 5% solution of ammonium hydroxide ($NH_4OH$, BDH, UK) was added to the solution with 100ml of water in order to improve gelation and the polymerization of an apatite structure, followed by aging for 24, 48 & 72 hours at room temperature. Oven drying was undertaken for a further 24 hours. This is summarised in table 5.

**Table 5:** Variation in aging time following gelation

| **Constituents** | **$Ca(NO_3)_2.4H_20$** | **$P(C_2H_50)_3$** | **$C_2H_5OH/H_2O$** |
|---|---|---|---|
| 1 mole | 236.15gmol$^{-1}$ | 166.16gmol$^{-1}$ | 46+18 (64) |
| Ratio | 0.1667 moles | 0.1 moles | 1 moles |
| Amount (grams) | 39.36g | 16.16g | 33.12g/5.04g |
| Ammonium hydroxide (5%) - 25ml | | | |
| **Run 1** | 12 hours aging time | | |
| **Run 2** | 24 hours aging time | | |
| **Run 3** | 72 hours aging time | | |

### *6.1.4. Aging at an increased temperature.*

Triethyl phosphite ([$P(C_2H_50)_3$], Aldrich, USA) of 0.1 moles (16.16g) was hydrolyzed in 33.12g of ethanol (0.72 moles) with 5.04g of distilled water (0.28 moles) for 24 hours and then slowly added to a 0.16 mole (39.36g) solution of calcium nitrate [$Ca(NO_3)_2.4H_20$, Aldrich USA] and allowed to mix for 24 hours. A 5% solution of ammonium hydroxide ($NH_4OH$, BDH, UK) was added to the solution with 100ml of water in order to improve gelation and the polymerization of an apatite structure, followed by aging for 24 hours at room temperature or at 40$^oC$. Oven drying was undertaken for a further 24 hours. This is summarised in table 6.

**Table 6:** Variation in aging temperature following gelation

| **Constituents** | **$Ca(NO_3)_2.4H_20$** | **$P(C_2H_50)_3$** | **$C_2H_5OH/H_2O$** |
|---|---|---|---|
| 1 mole | 236.15gmol$^{-1}$ | 166.16gmol$^{-1}$ | 46+18 (64) |
| Ratio | 0.1667 moles | 0.1 moles | 1 moles |
| Amount (grams) | 39.36g | 16.16g | 33.12g/5.04g |
| Ammonium hydroxide (5%) - 25ml | | | |
| **Run 1** | 24 hours aging time at R.T.P. | | |
| **Run 2** | 24 hours aging time at 40$^oC$. | | |

### *6.1.5. Powder Preparation*

Following successful preparation of a sol-gel, proportions of the sol-gels were heated at 400$^{o}$ – 1000$^{o}$C for 2 hours in air using a hot air oven (Lenton Furnace, Lenton Thermal Designs Limited, UK) with a ramp of 5$^{o}$C per minute, dwell time of 60 minutes and cool down rate of 10$^{o}$C per minute.

Following heating in the hot air oven the samples were ground to a powdery form for 20 minutes using a vibrating agate ball mill (Fritsch, Germany) and to ensure similar particle sizes ≈ 20μm were passed through a sieve (Fritsch, Germany).

## 6.2 Methods & Materials - Characterisation Techniques

### *6.2.1. Powder X-ray diffraction (XRD)*

Following preparation of the hydroxyapatite sol-gels and subsequent powdering, X-ray diffraction was undertaken. Because of the nature of the powder, which consists of many tiny randomly oriented crystals, Bragg's law for each set of lattice planes is always satisfied (see literature review). The probability for at least some of those crystallites being at the Bragg angle is very high. Therefore, by varying the incident angle $\theta$, each particular set of lattice planes diffracted the radiation at the corresponding $\theta$ angle. In flat plane geometry the sample is placed in a flat holder and the angle of the sample holder and detector was slowly changed keeping the X-ray beam fixed ($\theta$ / $2\theta$ geometry).

X-ray diffraction data were collected using an automated Bruker D8 Advance system equipped with a sample changer and Ni filtered CuK$\alpha$ ($\lambda$ = 1.5418 Å) in a flat plane $\theta$ - $\theta$ geometry in the range 10-100$^{o}$ $2\theta$, in steps of 0.02$^{o}$, with a count time of 12 seconds per step. From the data obtained, unit cell size was calculated using the TOPAS programme.

Once the X-ray pattern had been recorded, the data obtained was compared to standard patterns in the Powder Diffraction File (PDF, 1998) and analysed using TOPAS software.

### *6.2.2. High-temperature X-ray diffraction (HTXRD)*

The High-temperature X-ray diffraction (HTXRD) was measured on a Bruker D8 Advance diffractometer equipped with a LynxEye detector and an Anton Paar HTK1600 heating stage fitted with a Pt electrode. XRD patterns were collected from $2\theta$ = 21-36$^{o}$ with a step of 0.02$^{o}$ and counting time of 37.8 seconds per point using Ni-filtered CuK$\alpha$ radiation generated at 35 kV and 45

mA. Data were collected between 20 and 1200$^{o}$C at intervals of 10oC using air as a purge gas. The heating rate between temperature points was 6$^{o}$Cs$^{-1}$.

### *6.2.3. Differential thermal analysis (DTA)*

The sol-gels were evaluated using differential thermal analysis (DTA) to elucidate the crystallisation kinetics, using a Labsys TG/DTA 1600$^{o}$C (Setaram instruments, Caluire, France. Weighed (100mg) sol-gel samples were placed into platinum sample holders and tested in an inert nitrogen atmosphere, and compared with a platinum pan only as a reference. Samples were run from 20$^{o}$C to 1000$^{o}$C at a rate of 20$^{o}$C / minute. The data was baseline corrected by carrying out a blank run and subtracting this from the plot obtained.

### *6.2.4. Fourier transform infra red (FT-IR)*

FT-IR spectra were obtained for all the samples investigated. Three readings at various places were taken per sample, and all were checked to ensure that samples were homogeneous in composition by checking that identical chemical groups were present in all three readings. A Perkin Elmer series 2000 Attenuated Total Reflectance (ATR) FTIR spectrometer was used. The samples were placed on the diamond ATR specimen holder. The source that reflected off the specimen was in the mid infrared range. The incident beams were split using a KBr beamsplitter and the resolution was set at 8 cm$^{-1}$, wavenumber was set between 500 and 4000 cm$^{-1}$, and 4 scans were taken for each sample as selected. A background reading was taken before collecting spectra from the samples and was subtracted from the sample spectra.

## 6.3. Results

### *6.3.1. Variation of constituents (amount of water)*

Following the initial protocol resulted in a sol-gel being produced that was very dry. So to try to produce a sol-gel with a usable consistency, following addition of ammonium hydroxide, 30ml, 60ml, 75ml and 100ml of water was added. Use of 30, 60 and 75 ml of water did not result in the production of a sol-gel.

Use of 100ml of water did result in a sol-gel. This was heated to 600$^{o}$C, powdered and following ball milling resulted in the XRD pattern shown in Figure 18.

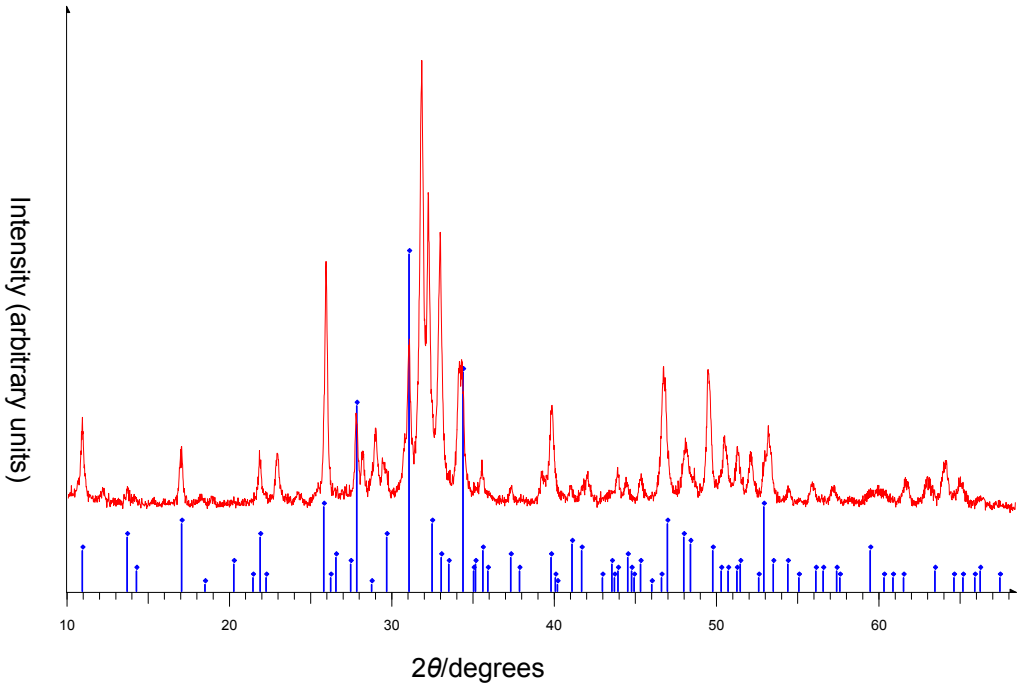


**Figure 18**: X-ray diffraction pattern found for sol-gel produced with 100ml of water. Lower key; blue lines are HA

The X-ray diffraction pattern revealed that the sol-gel consisted of ß-tricalcium phosphate (ß-TCP) and hydroxyapatite. TOPAS software was used to determine the exact amounts of the phases contained in the sol-gel – the results of this are shown in table 7.

| Constituent | Percentage (%) |
|---|---|
| ß-tricalcium phosphate | 87 |
| hydroxyapatite | 13 |

**Table 7**: Percentage constituents of sol-gel produced with 100ml of water.

Thus further modifications were required to the chemistry in order to produce a hydroxyapatite sol gel. However the protocol for the initial amount of water required (100ml) to obtain a sol-gel was established.

### *6.3.2. Variation of Hydrolysation Time of TEP.*

The next parameter in the chemistry that was investigated to try and establish a hydroxyapatite sol-gel was varying the hydrolysation time of TEP. The hydrolysation time of TEP was increased from the initial 12 hours used in the protocol and increased to 24, 48 and 72 hours. All of the hydrolysation times used resulted in production of a sol-gel. These were heated to 600°C, powdered and following ball milling resulted in the XRD pattern shown in Figure 19.

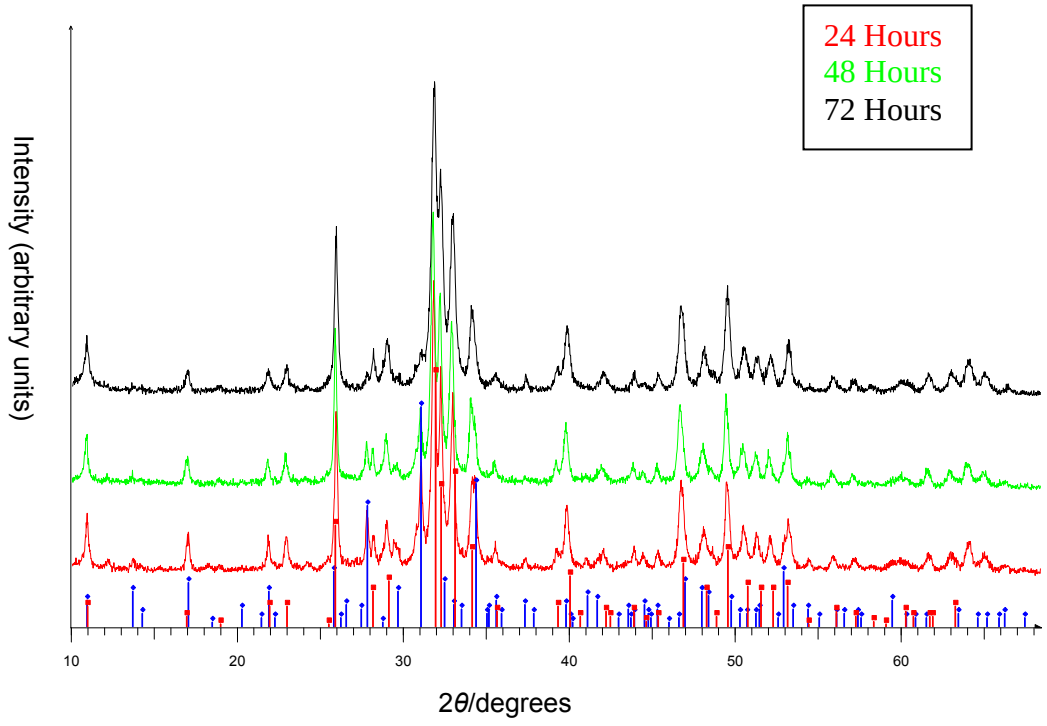


**Figure 19**: X-ray Diffraction pattern found for sol-gel when hydrolysing TEP for 24, 48 and 72 hours. Lower key; red lines (HA), blue line β-TCP.

The results of the X-ray diffraction revealed that the sol-gels now consisted of a mixture of ß-TCP and hydroxyapatite. With increased hydrolysation time the amount of ß-TCP decreased indicating that the longer the hydrolysation times the better. TOPAS software was used to reveal the exact constituents contained in each of the sol-gels – the results of this are shown in table 8.

| **Hydrolysation Time (Hours)** | **Constituents** | **Percentage (%)** |
|---|---|---|
| 24 | ß-tricalcium phosphate | 75 |
| | hydroxyapatite | 15 |
| 48 | ß-tricalcium phosphate | 48 |
| | hydroxyapatite | 52 |
| 72 | ß-tricalcium phosphate | 18 |
| | hydroxyapatite | 82 |

**Table 8**: Percentage constituents with varying hydrolysation time.

### *6.3.3. Variation in mixing time of hydrolysed TEP and calcium nitrate*

The next parameter in the chemistry that was investigated to try and establish a hydroxyapatite sol-gel was varying the mixing time of the hydrolysed TEP and calcium nitrate. Following mixing the solution was aged for 12, 24 & 48 hours at room temperature, prior to the addition of ammonium hydroxide. All of the mixing times resulted in production of a sol-gel. These were heated to 600$^{o}$C, powdered and following ball milling X-ray diffraction undertaken. The sol gel obtained after 12 hours was identical to the patterns shown in figure 17. However, the x-ray diffraction patterns obtained for 24 and 48 hours both confirmed the presence of hydroxyapatite, with minimal amounts of ß-TCP and are shown in figures 20 & 21.

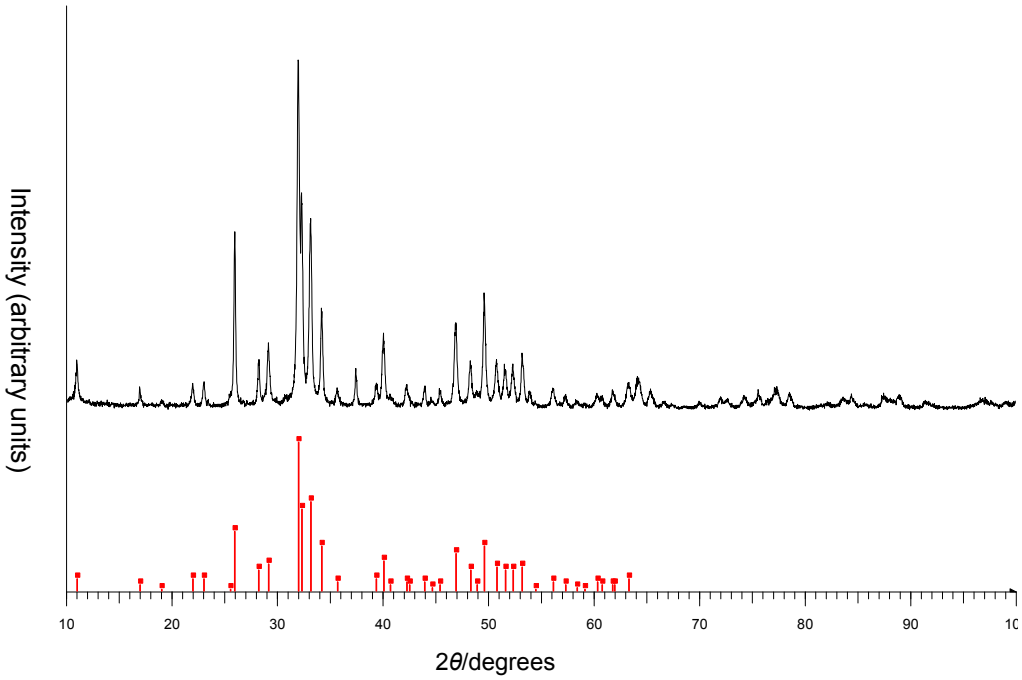


**Figure 20**: X-ray Diffraction pattern confirming the presence of hydroxyapatite – mixing time of 24 hours.

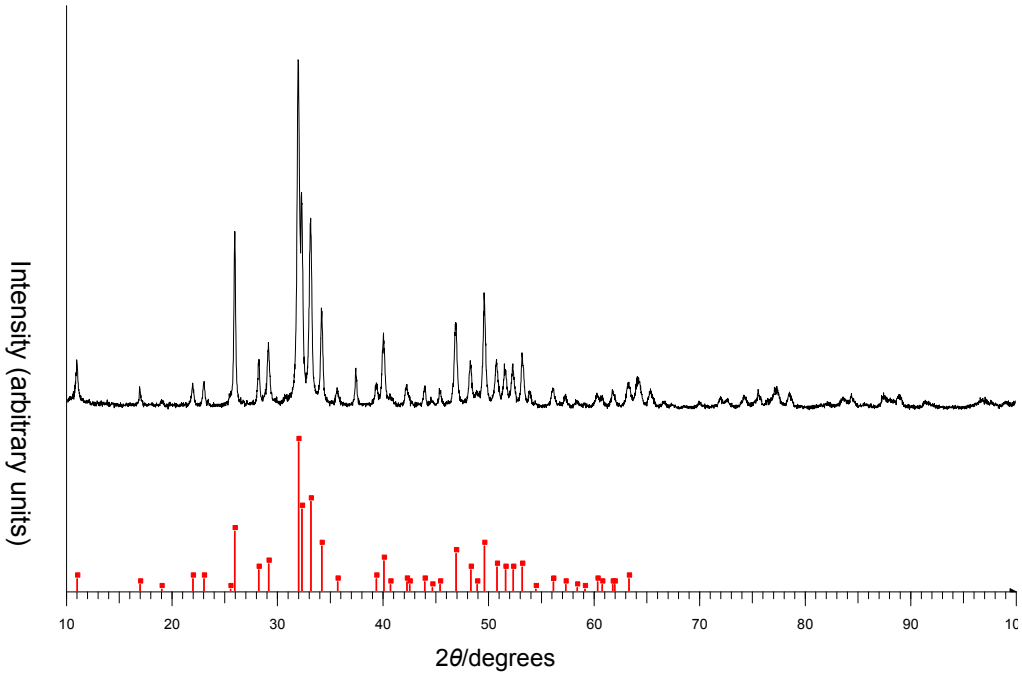


**Figure 21**: X-ray Diffraction pattern confirming the presence of hydroxyapatite – mixing time of 48 hours.

TOPAS software was used to reveal the exact constituents contained in each of the sol-gels – the results of this are shown in table 9.

| Mixing Time (Hours) | Constituents | Percentage (%) |
|---|---|---|
| 12 | ß-tricalcium phosphate | 18 |
| | hydroxyapatite | 82 |
| 24 | ß-tricalcium phosphate | 1 |
| | hydroxyapatite | 99 |
| 48 | ß-tricalcium phosphate | 0.3 |
| | hydroxyapatite | 99.7 |

**Table 9**: Percentage constituents with varying mixing time.

### *6.3.4. Aging at an increased temperature*

The final initial parameter tested was investigating the effect of aging the sol-gel produced at an increased temperature. Aging at room temperature and pressure or at 40$^{o}$C resulted in a pattern that was identical that that in figure 21. Use of TOPAS software revealed that both sol-gels were 99.4% HA / 0.6% β-TCP.

## 6.4. Discussion of the Preparation of HA sol-gels

### *6.4.1. Use of X-Ray Diffraction*

X-ray diffraction proved to be an excellent method for characterising the materials in this study and for monitoring changes in the constituent make up of the materials are changes in the chemistry were made.

As early as 1912 Maxwell von Laue recognised that crystalline solids consist of a geometric arrangement with inter-atomic distances that are sufficient to affect

a diffraction pattern when electromagnetic radiation (such as x-rays) are directed at it. Constructive interference is said to occur when the waves are in phase and reinforce each other. However if the waves are out of phase destructive interference will take place. The patterns generated can be mathematically analysed to reveal the geometry of the solid. The positions and intensity of the lines that make up the distinctive x-ray diffraction pattern correspond to the lattice spacing and phase of the material respectively. It is this knowledge that has provided the grounding for the x-ray diffraction used in this study. Investigation of the variation of constituents and subsequent analysis by x-ray diffraction allowed a definitive protocol for the production of hydroxyapatite sol-gel to be established.

### *6.4.2. Sol-gel technique*

The sol-gel technique offers many advantages for the production of coatings that can be deposited on to materials including titanium implants, among many these include; it results in particles of nanoscale, it results in an homogenous product, it allows reduced firing temperatures, it results in a uniform fine-grained structure, it is easily applied to complex structures, it has a low production and coating cost, it has a uniform shrinkage when heated and can rapidly dry without cracking.

Review of the literature revealed that no other study had been able to produce a phase pure hydroxyapatite (HA) when using the sol-gel technique. Several sol-gel processing methods have been investigated to produce phase pure HA. These have been based on an aqueous system (water) or an alcohol system. Potential precursors for the source of the calcium in the HA sol-gel are; calcium acetate, calcium alkoxide, calcium chloride, calcium nitrate and calcium hydroxide. Potential precursors for the phosphate have been triethyl phosphite

and triethyl phosphate. From the literature the most promising combination for the precursors has been calcium nitrate and triethyl phosphite (TEP) using alcohol at the hydrolysis stage (Kim et al., 2004). However Kim et al. (2004) could not produce phase pure HA and were unable to reduce the significant amounts of beta tricalcium phosphate (β-TCP) formed. It was thus the initial intention of this thesis to look at the variables that were used in the production of the HA sol-gel using calcium nitrate and triethyl phosphite as precursors and if modifications to all the variables in the chemistry used, could result in changes which could be used to optimise the resultant HA sol-gel.

With reference to the literature there were many factors in the chemistry which had not been investigated – the amount of water required to hydrolyse the TEP, the time that the TEP should be hydrolysed for, the mixing time for the TEP and calcium nitrate, the aging time of the initial sol-gel and the effect of temperature on aging and the resultant effects that these may have on the HA sol-gel. The unknown variables in the reaction can be summarised in figure 22.

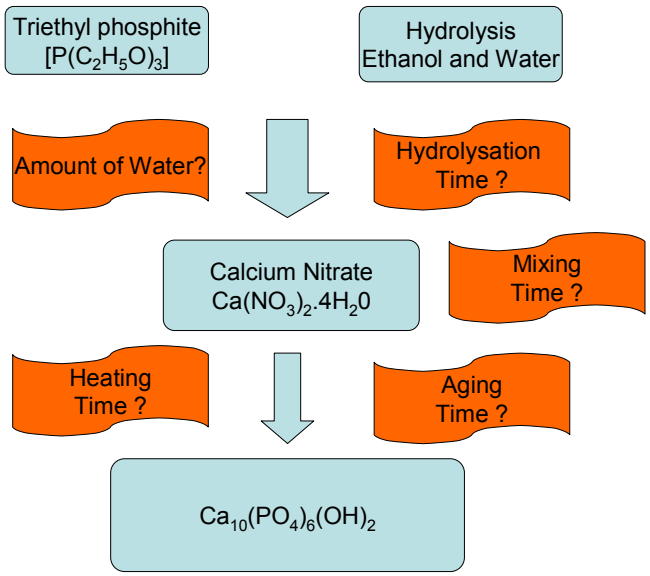


**Figure 22:** Schematic diagram to show unknown variables in the reaction to produce HA sol-gel.

### *6.4.3. Varying the amount of water*

Initial hydrolysation of the TEP is required to increase its reactivity so that it can react readily with the calcium nitrate. Varying the amount of water used to hydrolyse the TEP in ethanol using the basic protocol from the literature (Kim et al., 2004) illustrated that use of less than 30, 60 and 75ml of water did not result in a sol gel production. With reference to figure 23 it can be seen that in the process of hydrolysation the electrons from the water attack the phosphate in the TEP and cause the terminal group with organically bound oxygen to be displaced and replaced with an –OH group.

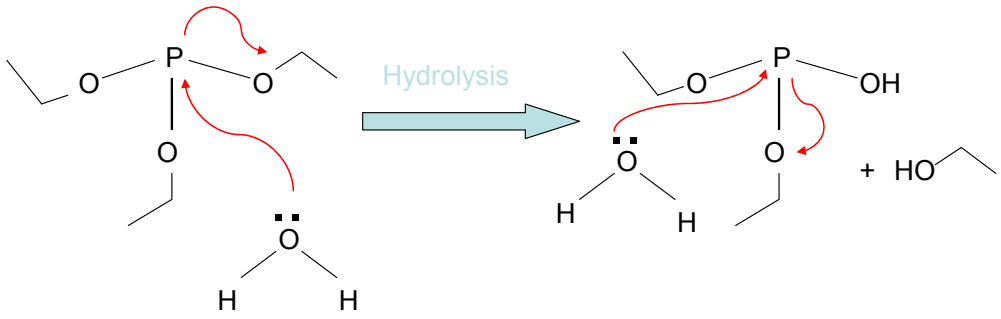


**Figure 23:** Schematic diagram showing the initial process that is undergone during the hydrolysation of TEP.

It can be proposed that 30, 60 and 75ml of water did not allow adequate amounts of available water to donate sufficient electrons to attack the phosphate groups in the TEP and thus the TEP was not sufficiently reactive when mixed with the calcium nitrate and as a result an HA sol-gel was not produced.

Use of 100ml of water did result in a sol-gel and proved to be an adequate amount for the hydrolysis of the TEP. However, the resultant sol-gel produced when analysed by x-ray diffraction consisted largely of ß-TCP (87%) with only

13% being HA. This indicated that further modifications were required to the initial chemistry / protocol in order to produce a hydroxyapatite sol-gel. However from this thesis, initial use of 100ml of water had been established.

### *6.4.4. Varying the hydrolysation time of TEP*

Increasing the hydrolysation time of TEP (in 100ml of water) from the initial 12 hours used to 24, 48 and 72 hours all resulted in the production of a sol-gel. X-ray diffraction revealed that the sol-gels now consisted of a mixture of ß-TCP and hydroxyapatite. The ß-TCP proportions decreased with increased mixing time such that it was almost phase pure after 72 hours of mixing. This suggested that hydrolysation time for the TEP in ethanol and water (100ml) should be undertaken for a period of 72 hours.

Figure 24 shows the chemical processes that can be proposed to be happening with the increased hydrolysation time.

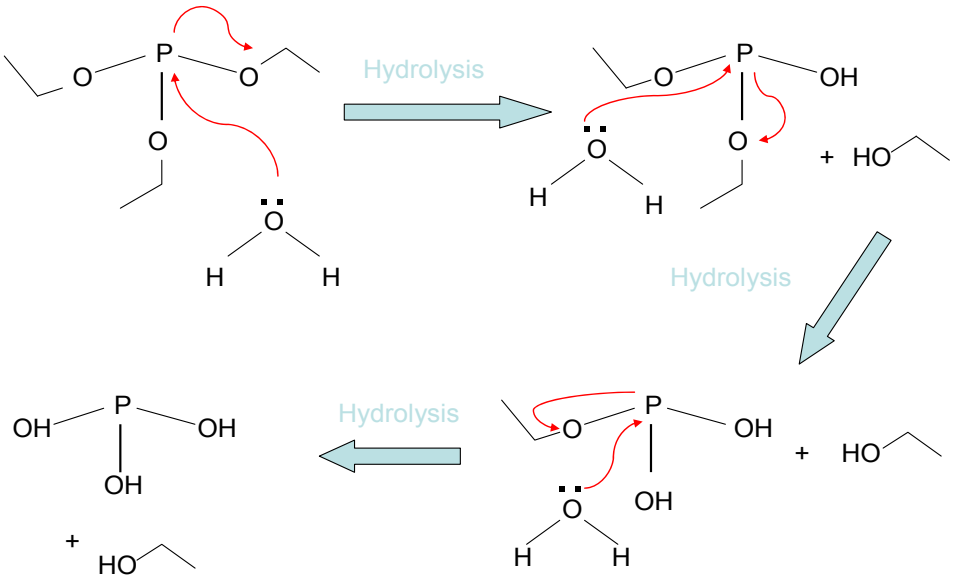


**Figure 24:** Schematic diagram showing the chemical process that is taking place as TEP is hydrolysed.

With reference to figure 24 and the results found it can be proposed that the longer the reaction has to take place the more of the groups that are substituted. In its form where total substitution has taken place the hydrolysed TEP is now ready to completely react with the calcium nitrate to form hydroxyapatite. If not enough time is allowed for hydrolysis, then the incompletely hydrolysed TEP, can be proposed to be more likely to react to form β-TCP. The ethanol produced as a side product from this reaction has a boiling point of 78$^{o}$C and can be easily driven off once the sol-gel is heated.

### *6.4.5. Variation in mixing time of hydrolysed TEP and calcium nitrate*

The next parameter investigated was varying the mixing time following addition of the hydrolysed TEP to the calcium nitrate. The mixed solution was mixed for 12, 24 and 48 hours at room temperature prior to the addition of ammonium hydroxide. Figure 25 shows a schematic representation of the reaction that is occurring during the formation of HA.

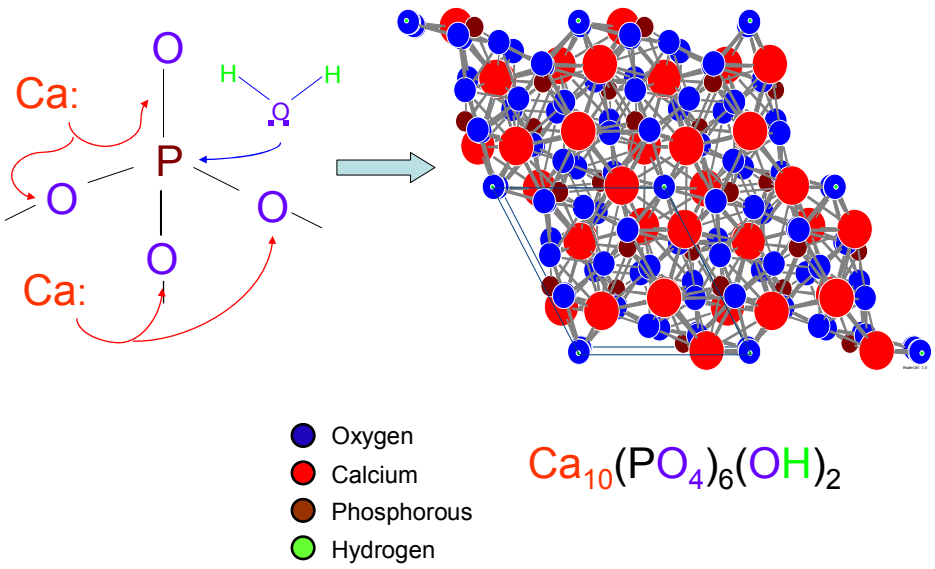


**Figure 25:** Schematic diagram showing the formation of HA from the precursors.

With reference to the results it can be seen that all of the aging times resulted in the production of a sol gel. X-ray diffraction of the sol gel obtained after 12 hours revealed the presence of ß-TCP and hydroxyapatite (18% and 82% respectively). However increasing the mixing time from 12 to 24 and 48 hours resulted in the presence of just much less ß-TCP (reducing to 1% and then 0.3% respectively).

It is known that calcium nitrate and TEP can react together rapidly to produce ß-TCP (Kim et al., 2004). It can be proposed that the reduction of the ß-TCP with increased mixing time occurs because, the ratio of Ca:P in ß-TCP are 1:5, and effectively a calcium deficient phase is initially formed (ß-TCP), as more time is allowed more calcium is released and HA is formed. It can be proposed that in contrast to figure 25 the actual reaction that is occurring can be illustrated in figure 26.

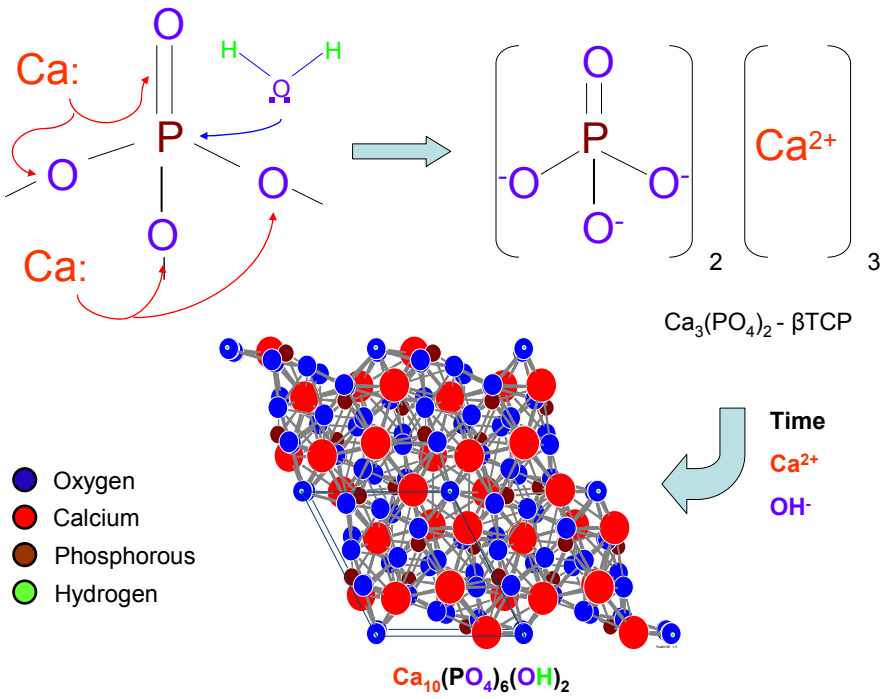


**Figure 26:** Schematic diagram to show formation of the intermediary β-TCP, which given more reaction time then becomes HA.

The results of this thesis indicate that the longer the mixing time of calcium nitrate and TEP that is allowed the more phase pure HA the final sol-gel will be. This now clearly illustrates a method of controlling the final constituents of the HA sol-gel.

### *6.4.6. Aging at increased temperature*

The final parameter investigated was the effect of aging the sol-gel produced at an increased temperature. Usually conducting a reaction at a higher temperature delivers more energy into the system and increases the reaction rate by causing more collisions between particles. However, the main reason why it increases the rate of reaction is that more of the colliding particles will have the necessary activation energy resulting in more successful collisions (Conners, 1990). As a rough rule of thumb, reaction rates for many reactions double for every 10$^{o}$C increase in temperature (Conners, 1990), though the effect of temperature may be very much larger or smaller than this (to the extent that reaction rates can be independent of temperature or decrease with increasing temperature).

As one of the advantages of the sol-gel technique is that it is simple and cost effective, it was decided that only a simple increase in temperature that could be well controlled over a long period would be undertaken. Furthermore, temperatures in excess of 40$^{o}$C may cause some of the reactants (especially ethanol) to be lost through evapouration and thus adversely interfere with the chemical reactions taking place. Room temperature and heating at 40$^{o}$C were compared to see if there was any effect on the resultant sol-gel obtained.

Analysis of the x-ray diffraction patterns obtained revealed that aging for 24 hours at room temperature versus aging for 24 hours at 40$^{o}$C revealed no difference. Both of the sol-gels were found to be 99.4% HA and 0.6% TCP. The

probable explanation for no influence of the temperature change on the reaction, is that because the amount of HA formed at room temperature was so high there was little additional effect that temperature could have in terms of HA formation. It can be postulated that if the amount of HA formed at room temperature was lower then heating during the aging process may be seen to have had more of an effect.

It is possible to conclude from the results of this thesis that it is satisfactory to make the HA sol-gels with a high purity at room temperature.

### *6.4.7. Addition of ammonium hydroxide*

The addition of ammonium hydroxide can catalyse the reaction between TEP and calcium nitrate. The schematic diagram in figure 27 illustrates how this may be occurring.

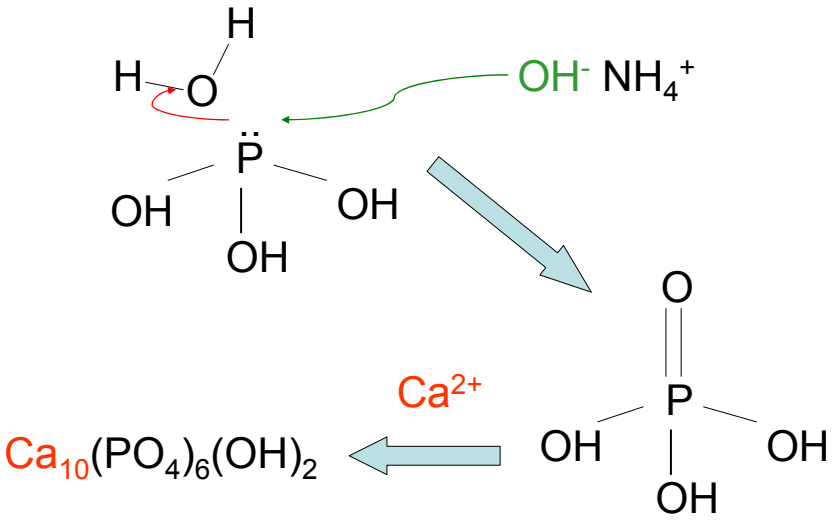


**Figure 27:** Schematic diagram showing how ammonium hydroxide catalyses the reaction between TEP and calcium nitrate.

With reference to figure 27 it can be seen that $OH^-$ ions from ammonium hydroxide can attack the hydrolysed TEP, this places the TEP into a more reactive form which can then react with $Ca^{2+}$ to form the hydroxyapatite. Without the addition of ammonium hydroxide this reaction will still eventually take place, but occurs less completely and much more slowly.

### 6.5. Summary of the results for preparation of HA sol-gels

These initial results allowed a definitive protocol for the production of phase pure hydroxyapatite sol-gels as follows:

(1) Triethyl phosphite ([$P(C_2H_50)_3$], Aldrich, USA) of 0.1 mole is hydrolyzed in ethanol with 100ml distilled water (100ml) for 72 hours.

(2) The hydrolysed TEP is then slowly added to a 0.16 mole solution of calcium nitrate [$Ca(NO_3)_2.4H_20$, Aldrich USA] and allowed to mix for 24 hours.

(3) A 5% solution of ammonium hydroxide ($NH_4OH$, BDH, UK) and 100ml of water is added to the solution in order to improve gelation and the polymerization of an apatite structure.

(4) Subsequent aging is allowed for 24 hours at room temperature.

(5) Oven drying is undertaken for a further 24 hours.

This established protocol was now used for the production of all further hydroxyapatite sol-gels in this thesis.

### 6.6. Differential thermal analysis (DTA)

The hydroxyapatite sol-gel was evaluated using differential thermal analysis (DTA) to elucidate the decomposition and crystallisation kinetics. Figure 28 shows the DTA trace obtained.

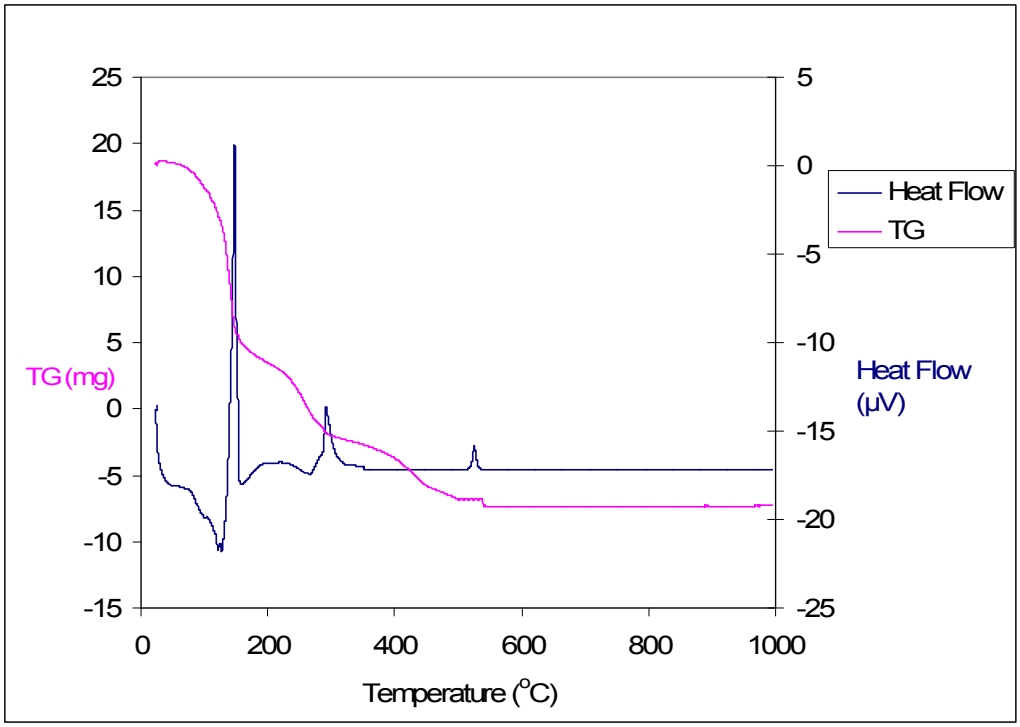


**Figure 28**: Differential thermal analysis tracing obtained for hydroxyapatite sol-gel.

From the graph seen in figure 28 it can be seen that there are three main regions where changes are taking place:

(1) Between 88°C and 200°C (Peak at 130°C).

(2) Between 260°C and 357°C (Peak at 294°C).

(3) Between 490°C and 503°C (Peak at 499°C).

There are no further significant changes in heat flow or TG after 454$^{o}$C. The experiment was completed three times so a mean and standard deviation could be obtained for the crystallisation temperature.

## 6.7. Discussion of results of the differential thermal analysis (DTA)

### *6.7.1. Differential thermal analysis (DTA)*

The thermoanalytic technique of DTA was employed in this thesis to elucidate the crystallisation kinetics of the HA produced via the sol-gel technique. The HA sol-gel was heated in an atmosphere of nitrogen and compared to an inert reference (platinum pan only) and the temperature difference between the HA and the reference recorded. The differential temperature was then plotted against temperature. The DTA allowed changes in the sample, either exothermic or endothermic to be detected relative to the inert reference.

### *6.7.2. DTA of hydroxyapatite sol-gels*

With reference to the results it can be seen that three major changes were discovered. It can be proposed that the first change (both endothermic and exothermic) i.e. between 88$^{o}$C and 200$^{o}$C – with a peak at 130$^{o}$C are due mainly to the loss of water, un-bound and bound in the structure, a corresponding weight loss is seen. The second change (exothermic) between 260$^{o}$C and 357$^{o}$C (Peak at 294$^{o}$C) be proposed to be the decomposition of nitrate from the Ca precursor (this can be evidenced in the FT-IR data seen later), a corresponding weight loss is seen.

The third change between 490$^{o}$C and 503$^{o}$C (Peak at 499$^{o}$C) can be proposed to be the crystallisation temperature of the hydroxyapatite from the sol-gel (this is confirmed in the XRD data seen later). There is no corresponding weight loss seen.

This indicates that using the HA sol-gel produced has completed crystallisation by 499$^{o}$C (+/-0.65$^{o}$C) and that any further crystallisation investigation should involve heating the HA sol-gel to at least this temperature.

The other noteworthy point is that there were no further changes following 503$^{o}$C up to 1000$^{o}$C. This indicates that the hydroxyapatite produced via the sol-gel method is thermally stable to at least 1000$^{o}$C and that the material can be heated up to this temperature without degradation.

### 6.8. Further investigation of any structural changes.

#### *6.8.1. Heating powders from 600$^{o}$C to 900$^{o}$C analysed using X-ray diffraction*

The results of the DTA suggested that the HA sol-gels produced were thermally stable up to 1000$^{o}$C with little exothermic of endothermic changes or changes in weight taking place after 499$^{o}$C (+/-0.65$^{o}$C). Structural changes at different temperatures after crystallisation were further investigated using XRD.

Following preparation of the HA sol-gel using the established protocol, proportions of the sol-gel were heated to 600, 700, 800 and 900$^{o}$C for 2 hours in a hot air oven (Lenton Furnace, Lenton Thermal Designs Limited, UK) with a ramp of 5$^{o}$C per minute, dwell time of 60 minutes and cool down rate of 10$^{o}$C per minute. Subsequent X-ray diffraction was undertaken and a typical result of this is shown in figure 29.

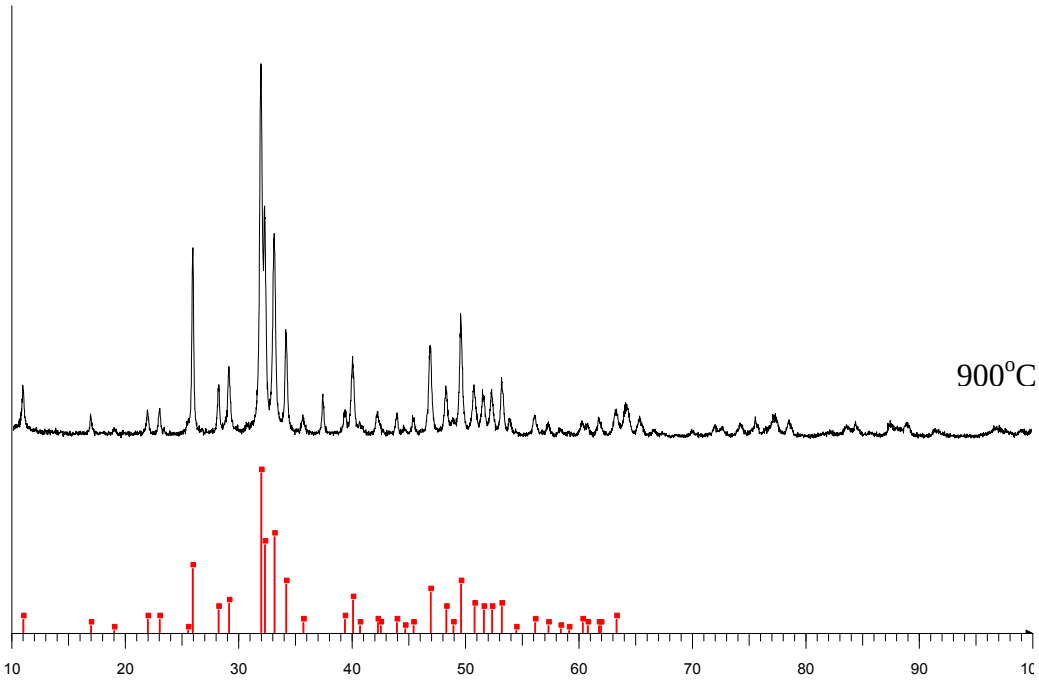


**Figure 29**: Typical X-ray diffraction pattern obtained after heating the HA sol-gel up to 900°C (Red lines on bottom of graph represent HA).

TOPAS software was used to reveal the exact constituents contained in the HA sol-gel at varying temperatures after crystallisation – the results of this are shown in table 10.

| Heating Temperature (°C) | Constituents | Percentage (%) |
|---|---|---|
| 600 | ß-tricalcium phosphate | 0.4 |
| | hydroxyapatite | 99.6 |
| 700 | ß-tricalcium phosphate | 0.4 |
| | hydroxyapatite | 99.6 |
| 800 | ß-tricalcium phosphate | 0.4 |
| | hydroxyapatite | 99.6 |
| 900 | ß-tricalcium phosphate | 0.4 |
| | hydroxyapatite | 99.6 |

**Table 10:** Table to show relative percentages of HA and β-TCP at heating temperatures up to 900°C.

High-temperature X-ray diffraction (HTXRD) was then undertaken using the sol-gel and measured on a Bruker D8 Advance diffractometer equipped with a LynxEye detector and an Anton Paar HTK1600 heating stage fitted with a Pt electrode. XRD patterns were collected from $2\theta$ = 21-36$^{o}$ with a step of 0.02$^{o}$ and counting time of 37.8 seconds per point using Ni-filtered CuK$\alpha$ radiation generated at 35 kV and 45 mA. Data were collected between 20 and 1200$^{o}$C at intervals of 10$^{o}$C using air as a purge gas. The heating rate between temperature points was 6$^{o}$Cs$^{-1}$.

This data obtained from the HTXRD of the HA sol-gel is shown graphically in Figure 30, utilisation of this technique allows the data at 10$^{o}$C intervals to be visualised clearly. This again confirms the crystallisation temperature.

**Figure 30**: 3 Dimensional graphical representation of high temperature X-ray diffraction of the HA sol-gel heated at 10°C intervals from 200 – 1000°C.

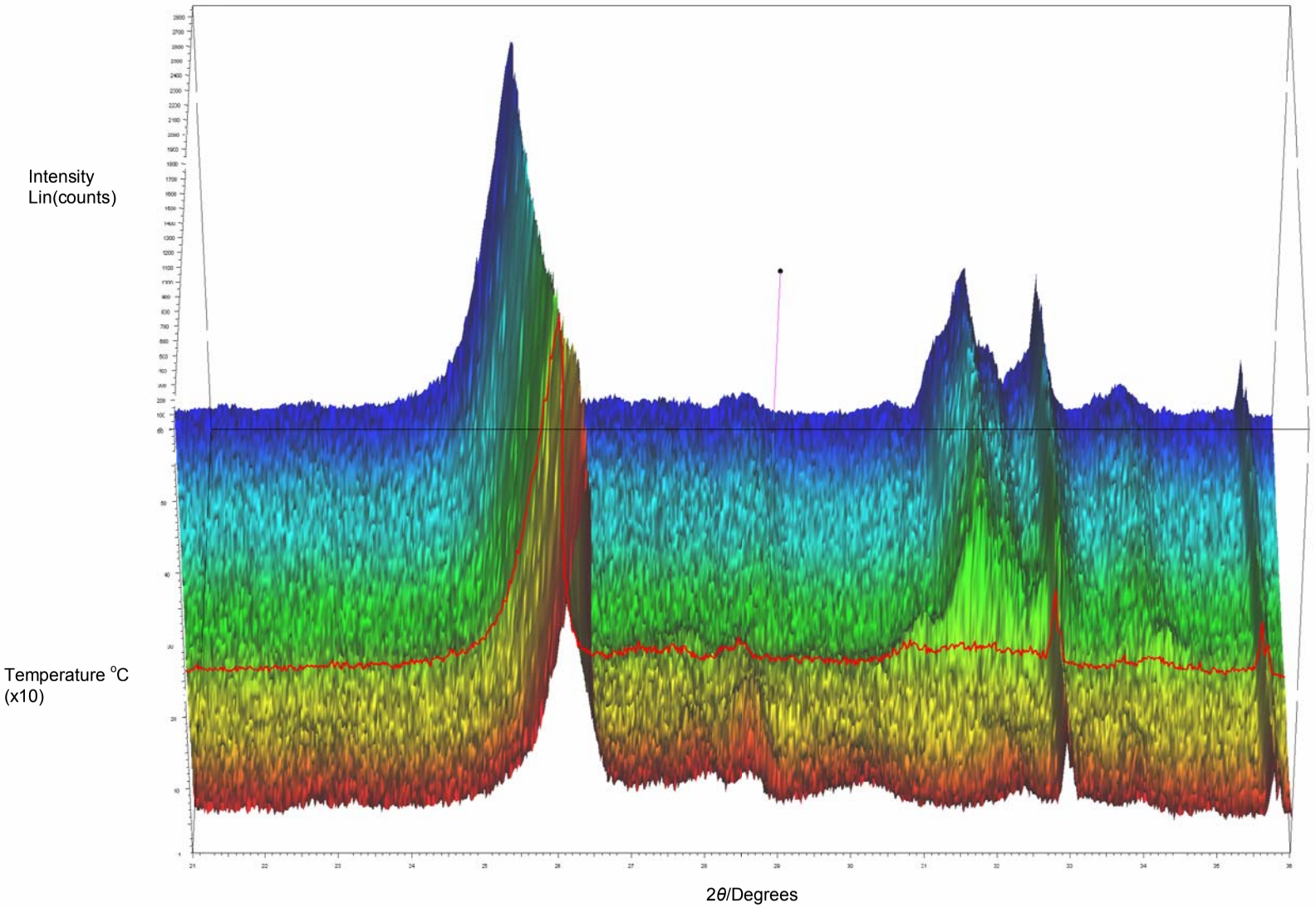

Unit cell measurements (a-axis, c-axis and unit cell volume) of the hydroxyapatite structure were undertaken at these six different heating temperatures after crystallisation and the results of these are summarised in Table 11 and shown graphically in figures 31, 32 and 33.

| Heating Temperature (°C) | a-axis(Å) | a-axis SD | c-axis (Å) | c-axis SD | Volume (Å$^3$) | Volume SD |
|---|---|---|---|---|---|---|
| 500 | 9.419 | 0.001 | 6.881 | 0.001 | 528.748 | 0.145 |
| 600 | 9.418 | 0.001 | 6.882 | 0.001 | 528.612 | 0.125 |
| 700 | 9.418 | 0.001 | 6.884 | 0.001 | 528.609 | 0.11 |
| 800 | 9.418 | 0.001 | 6.884 | 0.001 | 528.600 | 0.102 |
| 900 | 9.418 | 0.001 | 6.883 | 0.001 | 528.550 | 0.111 |
| 1000 | 9.415 | 0.001 | 6.881 | 0.001 | 528.340 | 0.111 |

**Table 11**: Unit cell measurement of sol-gel produced hydroxyapatite at heating temperatures of 500 – 1000°C.

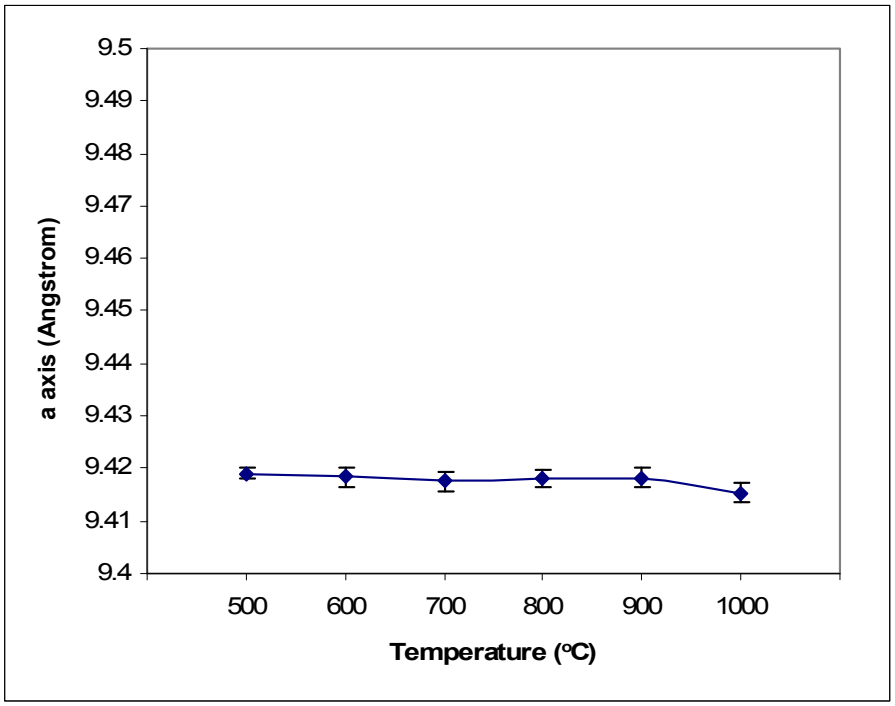


**Figure 31**: Graph to show a-axis changes with heating of HA sol-gel, mean +/- standard deviation.

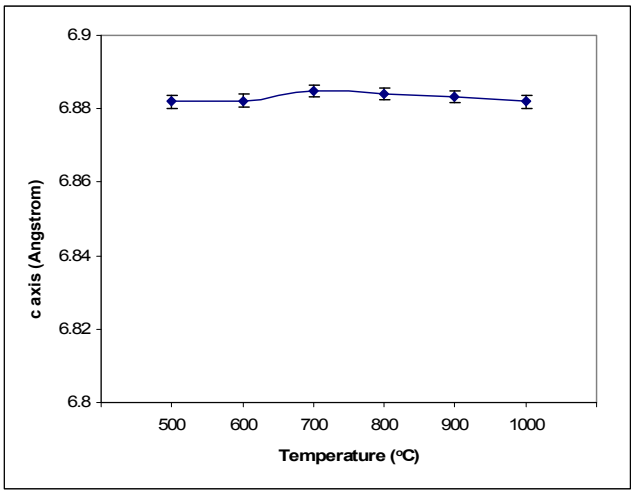


**Figure 32**: Graph to show c-axis changes with heating of HA sol-gel, mean +/- standard deviation.

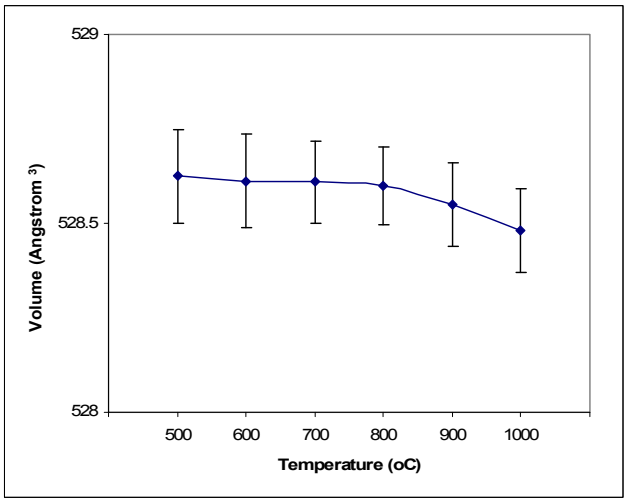


**Figure 33**: Graph to show changes in unit cell volume with heating of HA sol-gel, mean +/- standard deviation.

### 6.8.2. Discussion of Structural Changes

#### *6.8.2.1. Effect of Heating*

From the results it can be seen that using XRD there is minimal if any degradation of the hydroxyapatite sol-gel as heating is increased. This indicates that the HA produced by the sol-gel method used is thermally stable up to 900°C. This is important as it indicates that when heating the HA produced following coating on to titanium, it can be heated to a least 900°C

without degradation. Raynaud et al., 2002 reported that HA at temperatures starting at 880$^{o}$C can start to degrade and form β-TCP, this becomes more pronounced and complete at temperatures over 1200$^{o}$C. Analysis of temperatures up to 900$^{o}$C using the TOPAS software showed that there was no change at all in the relative compositions of HA and β-TCP, with the relative percentages being maintained at 99.6 and 0.4% respectively.

The XRD patterns obtained for the HA obtained remain broadly similar as the sol-gels were heated from 600 to 900$^{o}$C, however the resolution and intensity of the characteristic HA peaks increased with increasing temperature and confirms the results of a similar study which assessed the effect of heating on HA (Mobasherpour et al., 2007), furthermore this is indicative that the Ca/P ratio must be close to the ideal 1.67 ratio, as in this form it is at its most thermally stable (Mobasherpour et al., 2007). The reason for the increase in resolution and intensity with increasing temperature seen with the XRD is that the samples are becoming more crystalline. This implies that as the samples are heated from 600 to 900$^{o}$C the heating process is very effective in transforming the amorphous phase to HA crystalline phase.

The high temperature XRD (HTXRD) confirmed the above results and proved to be a very useful piece of equipment for such heating investigations. The HTXRD also allowed the samples to be heated directly from their sol-gel state and thus the pre-crystallisation XRD properties of the material to be assessed. With reference to the HTXRD data shown it can be seen that the XRD pattern seen in the as-prepared sol-gel bears with it the characteristic patterns of HA but not with much resolution and intensity. As discussed above once the crystallisation temperature is reached the resolution and intensity of the characteristic peaks increase with increasing temperature.

### *6.8.2.2. Unit Cell*

Analysis of the unit cell data suggests that there are minimal changes in the a-axis and c-axis after heating the hydroxyapatite sol-gel at 500, 600, 700, 800, 900 and 1000$^{o}$C. Both the a and c values are within the range for the reported values for pure HA (9.41 – 9.42 Å for the a axis and 6.87 – 6.88 Å for the c axis) (Elliot et al., 1994). This again provides evidence to suggest that the Ca/P ratio must be close to the ideal 1.67 ratio, as in this form it is at its most thermally stable (Mobasherpour et al., 2007)

With regard to unit cell volume there is a small downward trend as the temperature increases from 500$^{o}$C to 1000$^{o}$C, however it must be noted that as all the error bars overlap this could be an anomaly. Abrahams and Knowles (1994) investigated the effects of sintering conditions on hydroxyapatite using X-Ray Diffraction. They were investigating temperatures in excess of 1000$^{o}$C and found small but significant decreases in unit-cell volume as temperature increased. They proposed this is to be due to a loss of small amounts of carbonate ion from channels within the structure. It is possible to suggest that the pattern seen in the unit cell volume here is similar and may be due either to the loss of small amounts of carbonate ion at the lower temperatures investigated, or general shrinkage of the unit cell.

What is interesting about the data in found in this thesis is that the changes in the unit cell appear to be occurring at temperatures under a 1000$^{o}$C. There appears to be an initial drop in unit cell volume between 500 and 600$^{o}$C and a second drop between 900 and 1000$^{o}$C – this finding contributes to the literature already established by Abrahams and Knowles (1994), it seems reasonable to assume that these changes at the lower temperatures than previously reported

could be explained in a similar fashion to the higher temperature changes i.e. due to a loss of small amounts of carbonate ions from within the HA structure.

### 6.9. Fourier transform infra red (FTIR) analysis of HA sol-gel

Using the Perkin Elmer series 2000 Attenuated Total Reflectance (ATR) FTIR spectrometer three readings at various places were taken of the HA sol gel as received and following heating to 500°C. This is shown in figure 34.

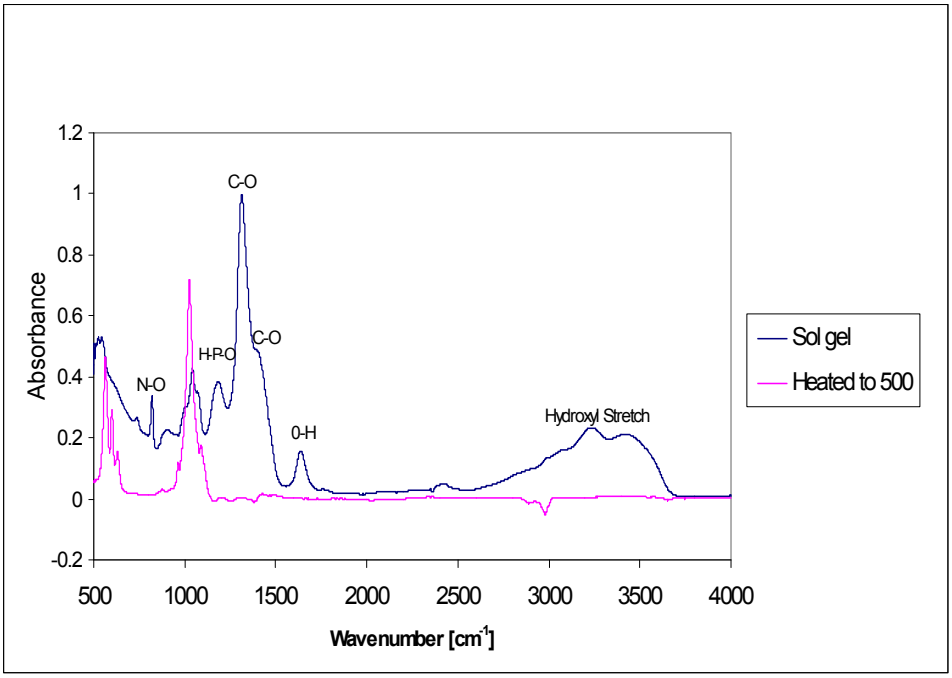


**Figure 34**: FTIR of HA sol-gel as received and heated to 500°C.

### 6.10 Discussion of FTIR analysis of HA sol-gel

#### *6.10.1. FTIR analysis – the principle*

FTIR is a widely used tool in analytical chemistry and is based on the fundamental principles of molecular spectroscopy. The basic principle behind molecular spectroscopy is that specific molecules absorb light energy at specific wavelengths, known as their resonance frequencies. An FTIR

spectrometer works by taking a small quantity of sample (in the case the HA sol-gel) and introducing it to the infrared cell, where it is subjected to an infrared light source, which is scanned from 4000 $cm^{-1}$ to around 600$cm^{-1}$. The intensity of light transmitted through the sample is measured at each wavenumber allowing the amount of light absorbed by the sample to be determined as the difference between the intensity of light before and after the sample cell. This is known as the infrared spectrum of the sample. In the infrared region of the spectrum, the resonance frequencies of a molecule are due to the presence of molecular functional groups specific to the molecule.

FTIR is a highly complementary technique to x-ray diffraction and allows the chemical changes occurring in the sol-gel to be investigated and explored as the sol-gel is heated.

### *6.10.2. HA sol-gel*

With reference to the FTIR in figure 34 it can be seen that the original sol-gel still has carbonate bonds (C-0) present and (N-O) and (H-P-O) bonds present potentially indicating the presence of unreacted calcium nitrate and TEP, there is also a pronounced hydroxyl stretch (around 3568 $cm^{-1}$) indicating the presence of water. The characteristic infrared peak assignments of hydroxyapatite are present (see table 1). On heating all calcium nitrate, TEP and water are lost leaving just the presence of hydroxyapatite. This is important as clearly the biocompatibility of HA could be affected if the primary unreacted constituents of calcium nitrate and TEP remained in the sol-gel after it was heated when coating on to titanium.

Figure 35 shows an FTIR of the primary constituents i.e. TEP, calcium nitrate, ammonium hydroxide and water that were originally used in making the sol-gel.

With reference to this, the correlation with the original bonds present and those in the new sol-gel can be visualised.

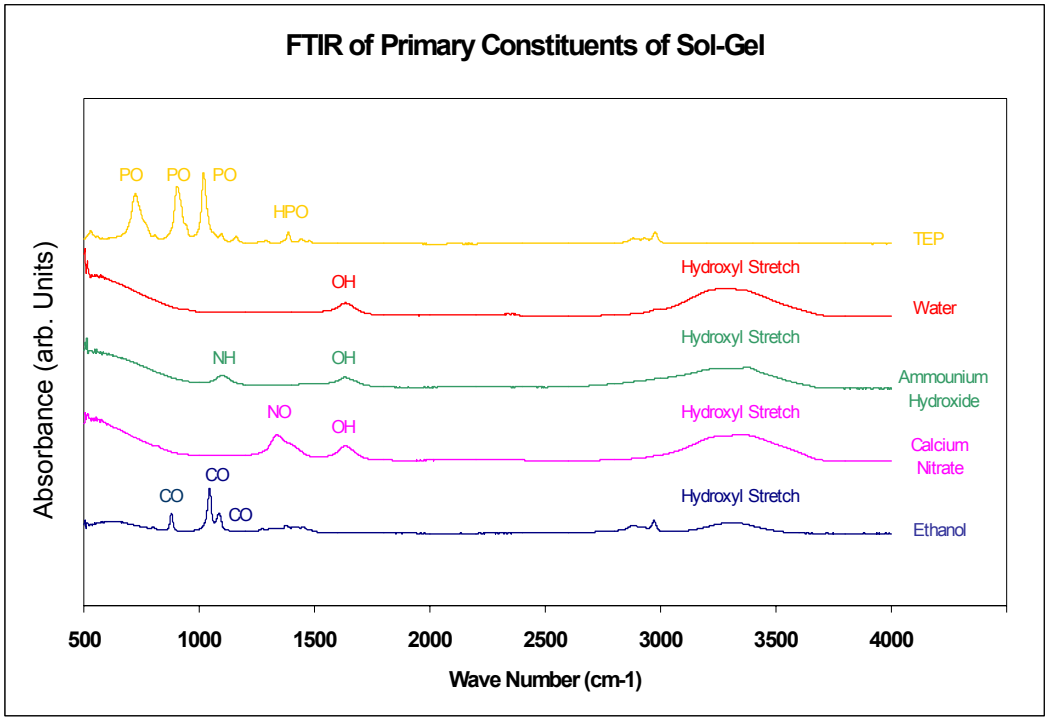


**Figure 35:** FTIR of all the primary constituents used for the HA sol-gel.

Additional heating of the samples and subsequent FTIR analysis of the powders confirmed that no subsequent changes take place when heating up to 900$^{o}$C (see Figure 36). Of interest is that when the sol-gel is heated to 1000$^{o}$C there seems to be some evidence that there is loss of –OH bond in the structure. It is well established that at temperatures of over 900$^{o}$C HA can start to break down / decompose, one of these such products can be oxyapatite ($Ca_{10}(PO_4)_6O$) (Zhou et al., 1993). Neither water nor –OH groups can enter the crystal lattice of oxyapatite and the FTIR data seen seems to suggest that at 1000$^{o}$C oxyapatite has been formed here.

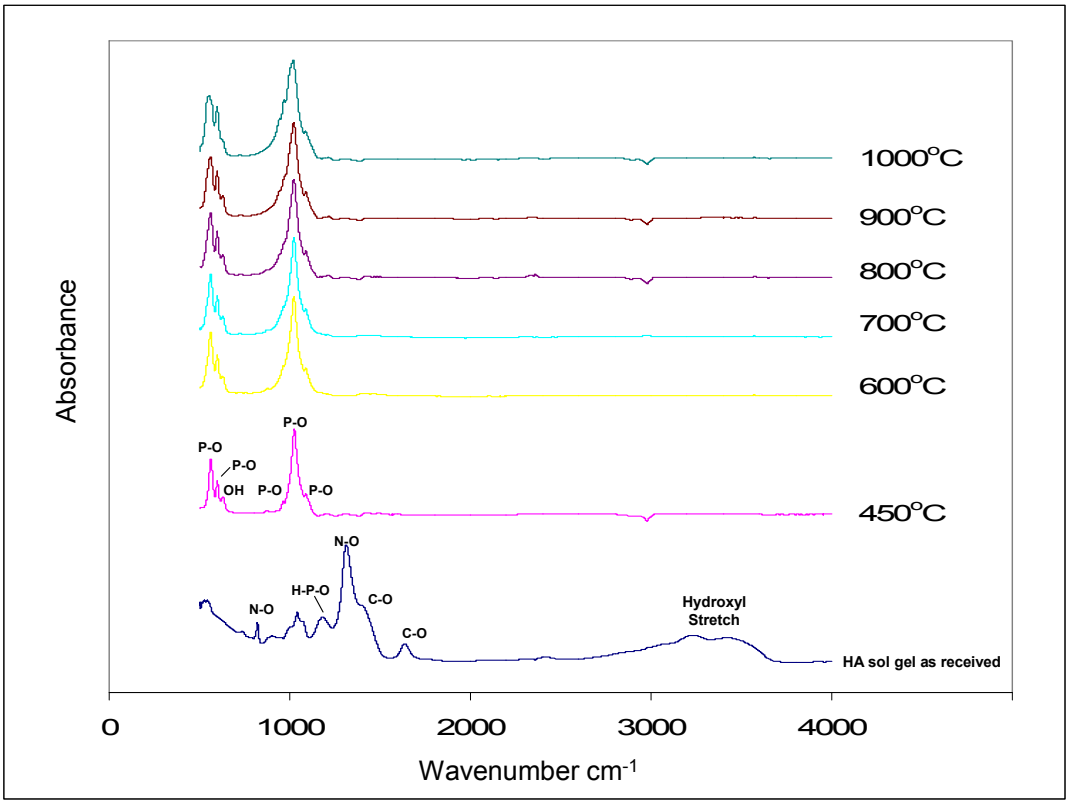


**Figure 36:** FTIR analysis of HA sol-gel as received and after subsequent heating to 450, 600, 700, 800, 900 and 1000°C. The characteristics peaks of Calcium Nitrate, TEP, Water and Hydroxyapatite are shown.

The FTIR data here provides further confirmation that the HA sol-gel is thermally stable up to 900°C, but suggests that there may be initial break down of the HA into oxyapatite at temperature approaching 1000°C. It can be proposed that temperatures up to 900°C can be used when preparing to coat the HA sol-gel produced onto a titanium implant, however caution should be exhibited in temperatures beyond this as decomposition of the HA may start to occur.

# Chapter 7:

# Characterisation & Optimisation Of

# Fluorapatite $Ca_{10}(PO_4)_6F_2$ &

# Fluor-hydroxyapatite $Ca_{10}(PO_4)_6OH_xF_y$

# Sol-gels

## 7.1. Method & Materials

The sol-gel production protocols that had been established for hydroxyapatite production were utilised as the basic methodology for production of the fluorapatite sol-gels.

### *7.1.1. Preparation of fluorhydroxyapatite ($Ca_{10}(PO_4)_6F_1OH_1$)*

To produce FHA sol-gel with a composition of $Ca_{10}(PO_4)_6F_1OH_1$, the following precursors were used:

Calcium nitrate - $Ca(NO_3)_2.4H_20$, Aldrich USA.

Triethyl phosphite - $[P(C_2H_50)_3]$, Aldrich, USA.

Ammonium fluoride - $NH_4F$, Aldrich USA.

Distilled $H_2O$.

Controlled amounts (see below) of triethyl phosphite ($[P(C_2H_50)_3]$, Aldrich, USA) and ammonium fluoride ($NH_4F$, Aldrich, USA) were first dissolved in ethanol and distilled water and then the solution stirred vigorously for 24 hours at room temperature and pressure.

In a separate container, a stoichiometric amount (see below) of calcium nitrate ($Ca(NO_3)_2.4H_20$, Aldrich USA) was dissolved in distilled water with vigorous stirring for 24h. The Ca-containing solution was added slowly to the P-containing solution and then aged at RTP for 24 hours at $40^oC$. Each composition ratio in the FHA sol was adjusted to have [Ca]/[P] = 1.67, [OH]/[P] = 10, and [P]/[F] = 6. A 5% solution of ammonium hydroxide ($NH_4OH$, BDH, UK) and 100ml of water was added to the solution in order to improve gelation and the polymerization of an apatite structure (see table 12).

**Table 12**: Constituents used for the preparation of fluorhydroxyapatite ($Ca_{10}(PO_4)_6F_1OH_1$)

| **$Ca_{10}(PO_4)_6(F_1OH_1)_2$** | | | | |
|---|---|---|---|---|
| **Constituents** | **$Ca(NO_3)_2.4H_20$** | **$P(C_2H_50)_3$** | **$NH_4F$** | **$C_2H_5OH/H_2O$** |
| 1mole | 236.15gmol$^{-1}$ | 166.16gmol$^{-1}$ | 37 | 46+18 (64) |
| Ratio | 0.1667 moles | 0.1 moles | 0.0167 moles | 1 mole |
| Amount (grams) | 39.36g | 16.16g | 0.62g | 33.12g/5.04g |
| Ammonium hydroxide (5%) - 25ml. | | | | |

### *7.1.2. Preparation of fluorhydroxyapatite [$Ca_{10}(PO_4)_6F_{0.5}OH_{1.5}$]*

To produce FHA sol-gel with a composition of $Ca_{10}(PO_4)_6F0_{.5}OH_{1.5}$, the following precursors were used:

Calcium nitrate - $Ca(NO_3)_2.4H_20$, Aldrich USA.

Triethyl phosphite - $[P(C_2H_50)_3]$, Aldrich, USA.

Ammonium fluoride - $NH_4F$, Aldrich USA.

Distilled $H_2O$.

Controlled amounts (see below) of triethyl phosphite ($[P(C_2H_50)_3]$, Aldrich, USA) and ammonium fluoride ($NH_4F$, Aldrich, USA) were first dissolved in ethanol and distilled water and then the solution was stirred vigorously for 24 hours at room temperature and pressure.

In a separate container, a stoichiometric amount (see below) of calcium nitrate ($Ca(NO_3)_2.4H_20$, Aldrich USA) was dissolved in distilled water with vigorous stirring for 24h. The Ca-containing solution was added slowly to the P-containing solution and then aged at RTP for 24 hours at 40$^{o}$C. Each composition ratio in the FHA sol was adjusted to have [Ca]/[P] = 1.67, [OH]/[P] = 10, and [P]/[F] = 12. A 5% solution of ammonium hydroxide ($NH_4OH$, BDH,

UK) and 100ml water was added to the solution in order to improve gelation and the polymerization of an apatite structure (see table 13).

**Table 13**: Constituents used for the preparation of fluorhydroxyapatite $Ca_{10}(PO_4)_6F_{0.5}OH_{1.5}$

| **$Ca_{10}(PO_4)_6(F_{0.5}OH_{1.5})_2$** | | | | |
|---|---|---|---|---|
| **Constituents** | **$Ca(NO_3)_2.4H_20$** | **$P(C_2H_50)_3$** | **$NH_4F$** | **$C_2H_5OH/H_2O$** |
| 1mole | 236.15gmol$^{-1}$ | 166.16gmol$^{-1}$ | 37 | 46+18 (64) |
| Ratio | 0.1667 moles | 0.1 moles | 0.00835 moles | 1 mole |
| Amount (grams) | 39.36g | 16.16g | 0.31g | 33.12g/5.04g |
| Ammonium hydroxide (5%) - 25ml. | | | | |

### *7.1.3. Preparation of fluorhydroxyapatite [$Ca_{10}(PO_4)_6F_{1.5}OH_{0.5}$]*

To produce FHA sol-gel with a composition of $Ca_{10}(PO_4)_6F_{1.5}OH_{0.5}$, the following precursors were used:

Calcium nitrate - $Ca(NO_3)_2.4H_20$, Aldrich USA.

Triethyl phosphite - $[P(C_2H_50)_3]$, Aldrich, USA.

Ammonium fluoride - $NH_4F$, Aldrich USA.

Distilled $H_2O$.

Controlled amounts (see below) of triethyl phosphite ($[P(C_2H_50)_3]$, Aldrich, USA) and ammonium fluoride ($NH_4F$, Aldrich, USA) were first dissolved in ethanol and distilled water and then the solution was stirred vigorously for 24 hours at room temperature and pressure.

In a separate container, a stoichiometric amount (see below) of calcium nitrate ($Ca(NO_3)_2.4H_20$, Aldrich USA) was dissolved in distilled water with vigorous stirring for 24h. The Ca-containing solution was added slowly to the P-containing solution and then aged at RTP for 24 hours at 40$^{o}$C. Each composition ratio in the FHA sol was adjusted to have [Ca]/[P] = 1.67, [OH]/[P]

= 10, and [P]/[F] = 4. A 5% solution of ammonium hydroxide ($NH_4OH$, BDH, UK) and 100ml water was added to the solution in order to improve gelation and the polymerization of an apatite structure (see table 14).

**Table 14**: Constituents used for the preparation of fluorhydroxyapatite $Ca_{10}(PO_4)_6F1_{1.5}OH_{0.5}$.

| **$Ca_{10}(PO_4)_6(F1_{1.5}OH_{0.5})_2$** | | | | |
|---|---|---|---|---|
| **Constituents** | **$Ca(NO_3)_2.4H_20$** | **$P(C_2H_50)_3$** | **$NH_4F$** | **$C_2H_5OH/H_2O$** |
| 1 mole | 236.15gmol$^{-1}$ | 166.16gmol$^{-1}$ | 37 | 46+18 (64) |
| Ratio | 0.1667 moles | 0.1 moles | 0.025 moles | 1 mole |
| Amount (grams) | 39.36g | 16.16g | 0.93g | 33.12g/5.04g |
| Ammonium hydroxide (5%) - 25ml | | | | |

### *7.1.4. Preparation of fluorapatite ($Ca_{10}(PO_4)_6F_2$)*

To produce FA sol-gel with a composition of $Ca_{10}(PO_4)_6F_2$, the following precursors were used:

Calcium nitrate - $Ca(NO_3)_2.4H_20$, Aldrich USA.

Triethyl phosphate - $[P(C_2H_50)_3]$, Aldrich, USA.

Ammonium fluoride - $NH_4F$, Aldrich USA.

Distilled $H_2O$.

Controlled amounts (see below) of triethyl phosphite ($[P(C_2H_50)_3]$, Aldrich, USA) and ammonium fluoride ($NH_4F$, Aldrich, USA) were first dissolved in ethanol and water and then the solution was stirred vigorously for 24 hours at room temperature and pressure.

In a separate container, a stoichiometric amount (see below) of calcium nitrate ($Ca(NO_3)_2.4H_20$, Aldrich USA) was dissolved in distilled water with vigorous stirring for 24h. The Ca-containing solution was added slowly to the P-

containing solution and then aged at RTP for 24 hours at 40$^{o}$C. Each composition ratio in the FHA sol was adjusted to have [Ca]/[P] = 1.67, [OH]/[P] = 10, and [P]/[F] = 3. A 5% solution of ammonium hydroxide ($NH_4OH$, BDH, UK) and 100ml water was added to the solution in order to improve gelation and the polymerization of an apatite structure (see table 15).

**Table 15**: Constituents used for the preparation of fluorapatite $Ca_{10}(PO_4)_6F_2$.

| **$Ca_{10}(PO_4)_6F_2$** | | | | |
|---|---|---|---|---|
| **Constituents** | **$Ca(NO_3)_2.4H_20$** | **$P(C_2H_50)_3$** | **$NH_4F$** | **$C_2H_5OH/H_2O$** |
| 1 mole | 236.15gmol$^{-1}$ | 166.16gmol$^{-1}$ | 37 | 46+18 (64) |
| Ratio | 0.1667 moles | 0.1 moles | 0.0334 moles | 1 mole |
| Amount (grams) | 39.36g | 16.16g | 1.24g | 33.12g/5.04g |
| Ammonium hydroxide (5%) - 25ml | | | | |

## 7.2. Characterisation techniques

The following characterisation and techniques were used:

- Differential Thermal Analysis (DTA)
- Powder X-ray Diffraction (XRD)
- High-temperature X-Ray Diffraction (HTXRD)
- Fourier Transform Infra Red (FTIR)

The methodology undertaken with these has already been described under hydroxyapatite.

## 7.3. Results

Utilising the basic sol-gel production methodology established for hydroxyapatite sol-gel production and modifying it with varying amounts of ammonium fluoride resulted in the production of sol-gels. For completeness results found during the characterisation and optimisation of the HA sol-gels have been included where possible so that direct comparisons can be made with the results found for the for the fluorapatite and fluorhydroxyapatite sol-gels.

### *7.3.1. Differential Thermal Analysis*

The fluorapatite and fluorhydroxyapatite sol-gels were evaluated using differential thermal analysis (DTA) to elucidate the crystallisation kinetics. Figures 37, 38, 39 and 40 show the DTA traces obtained.

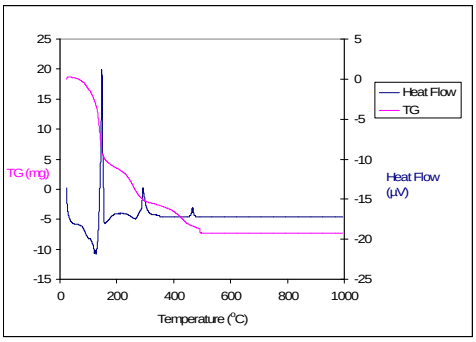


Figure 37: DTA of sol gel constituting $Ca_{10}(PO_4)_6F_2$.

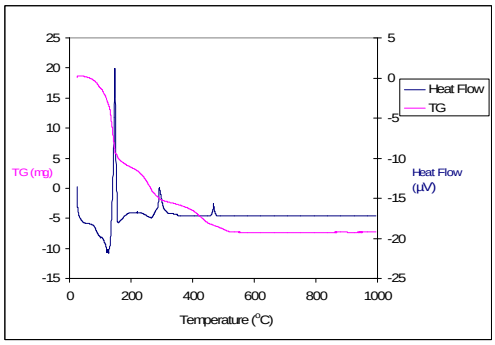


Figure 38: DTA of sol gel constituting $Ca_{10}(PO_4)_6OH_{0.5}F_{1.5}$.

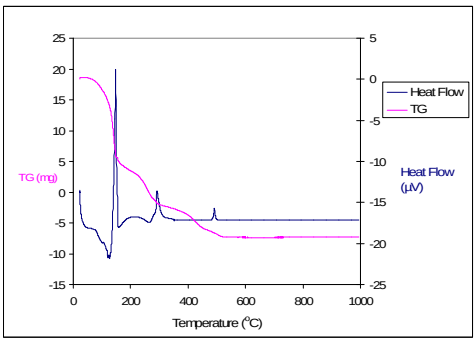


Figure 39: DTA of sol gel constituting $Ca_{10}(PO_4)_6OH_1F_1$.

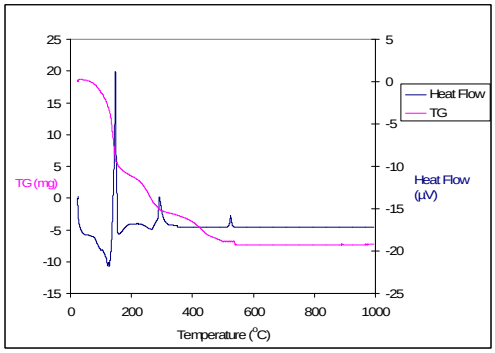


Figure 40: DTA of sol gel constituting $Ca_{10}(PO_4)_6OH_{1.5}F_{0.5}$.

The experiment was completed three times so a mean and standard deviation could be obtained for the crystallisation temperature (see table 16).

| Composition | Crystallisation Temperature Mean +/- SD (°C) |
|---|---|
| $Ca_{10}(PO_4)_6F_2$ | 467 +/- 0.21 |
| $Ca_{10}(PO_4)_6OH_{0.5}F_{1.5}$ | 470 +/- 0.43 |
| $Ca_{10}(PO_4)_6OH_1F_1$ | 492 +/- 1.22 |
| $Ca_{10}(PO_4)_6OH_{1.5}F_{0.5}$ | 498 +/- 0.23 |

**Table 16**: Crystallisation temperature of fluoride substituted apatite compositions as determined by DTA.

### *7.3.2. X-Ray Diffraction (XRD)*

After heating to 500$^{o}$C and powdering all four of the fluoride substituted apatites produced similar X-ray diffraction. Using TOPAS software patterns were identified as fluorapatite / fluorhydroxyapatite. Figures 41, 42, 43 and 44 show the XRD patterns found.

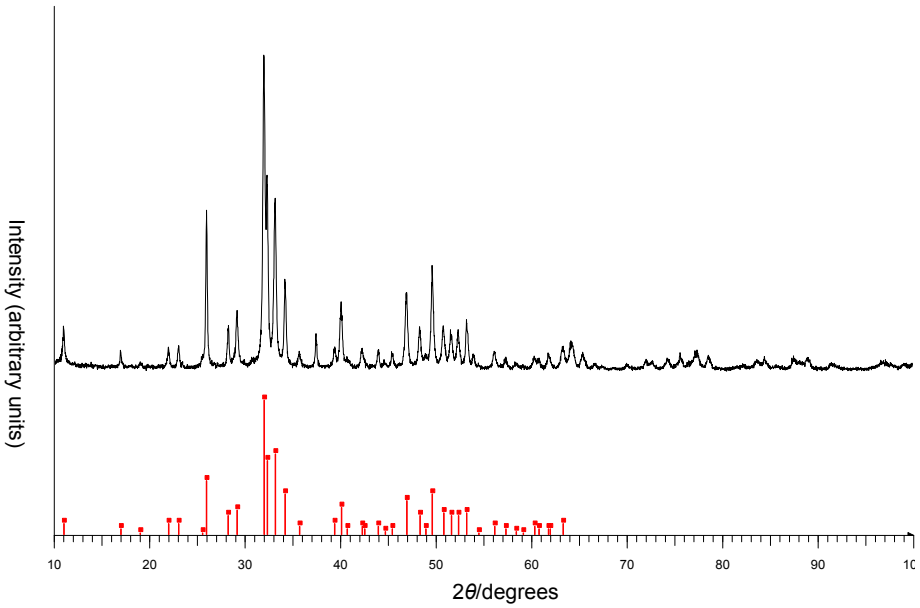


Figure 41: XRD of sol gel constituting $Ca_{10}(PO_4)_6OH_{0.5}F_{1.5}$.

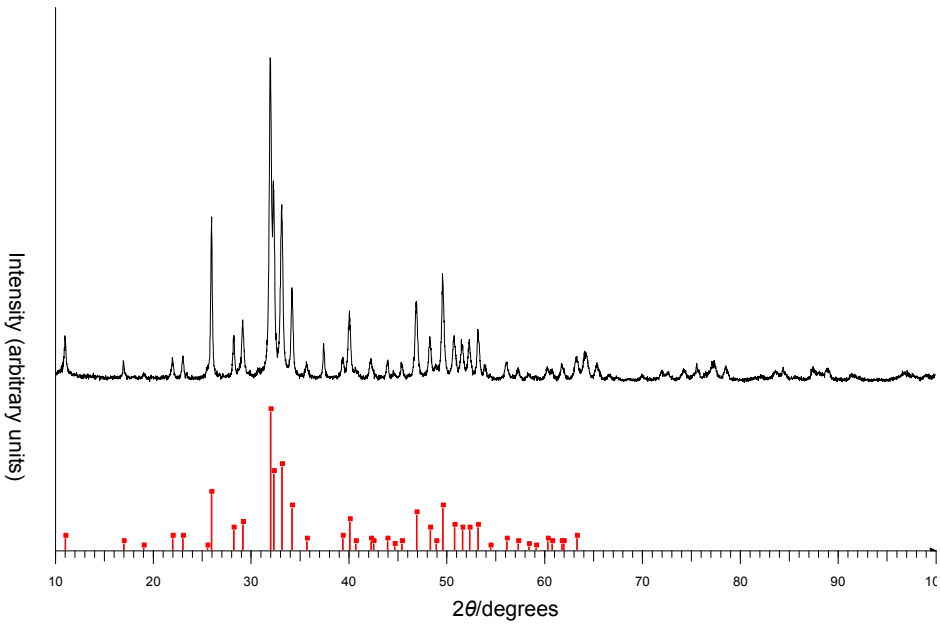


Figure 42: XRD of sol gel constituting $Ca_{10}(PO_4)_6OH_1F_1$.

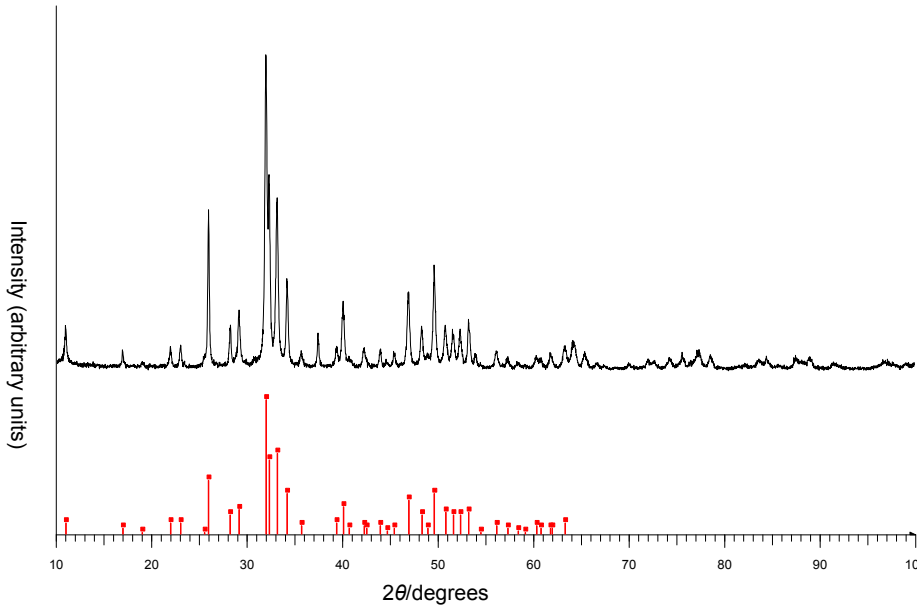


Figure 43: XRD of sol gel constituting $Ca_{10}(PO_4)_6OH_{1.5}F_{0.5}$.

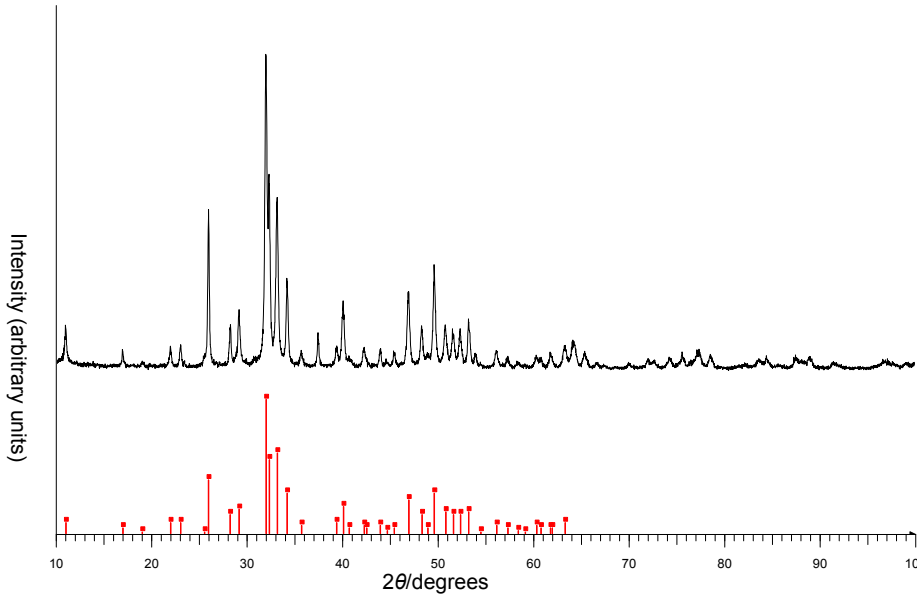


Figure 44: XRD of sol gel constituting $Ca_{10}(PO_4)_6F_2$.

Use of the TOPAS software confirmed all the sol-gels to be at least 99.7% fluorapatite (less than 0.3% ß-TCP).

### *7.3.3. X-ray diffraction on heated powders*

Following preparation of the FHA/FA sol-gels using the established protocol, proportions of the sol-gel were heated to 600, 700, 800 and 1000°C for 2 hours in a hot air oven (Lenton Furnace, Lenton Thermal Designs Limited, UK) with a ramp of 5°C per minute, dwell time of 60 minutes and cool down rate of 10°C per minute. Subsequent X-Ray diffraction was undertaken and the results of this are shown in figures 45, 46, 47, 48 and 49.

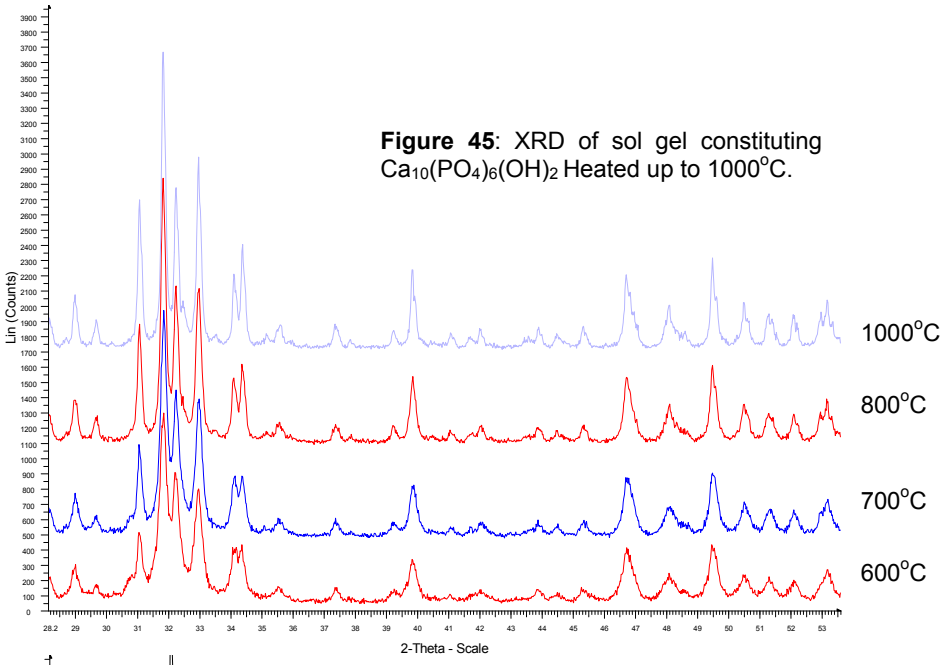


**Figure 45**: XRD of sol gel constituting $Ca_{10}(PO_4)_6(OH)_2$ Heated up to 1000°C.

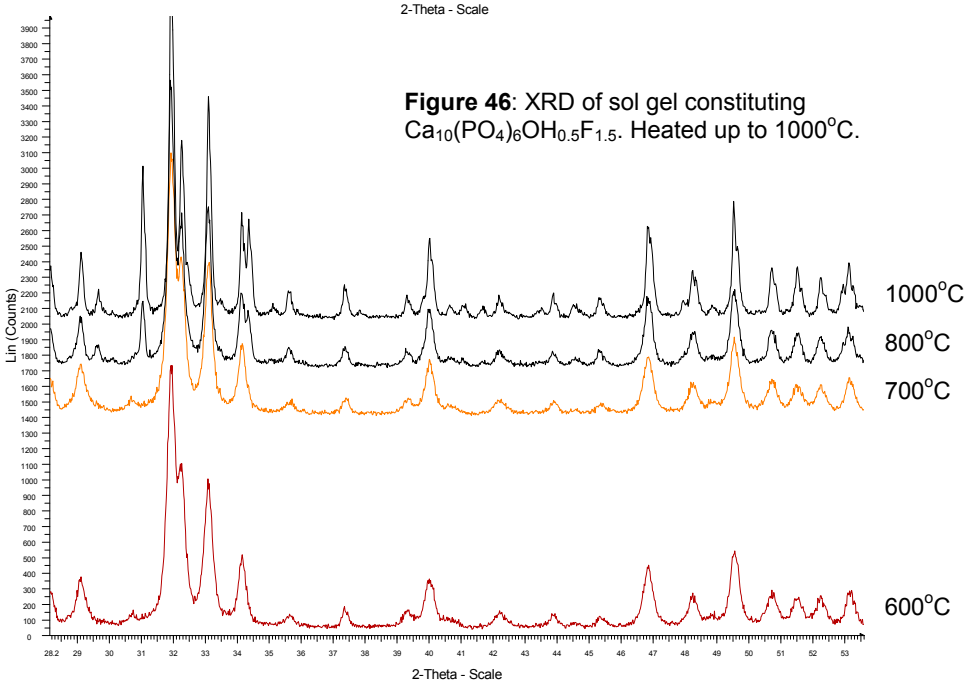


**Figure 46**: XRD of sol gel constituting $Ca_{10}(PO_4)_6OH_{0.5}F_{1.5}$. Heated up to 1000°C.

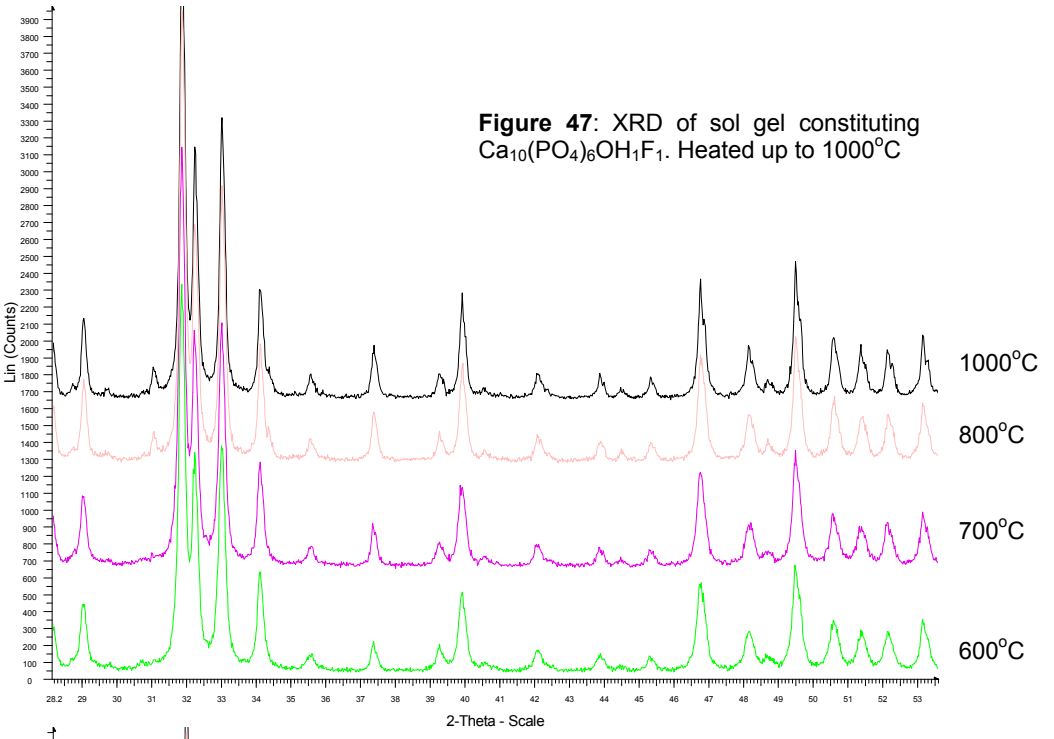


**Figure 47**: XRD of sol gel constituting $Ca_{10}(PO_4)_6OH_1F_1$. Heated up to 1000°C

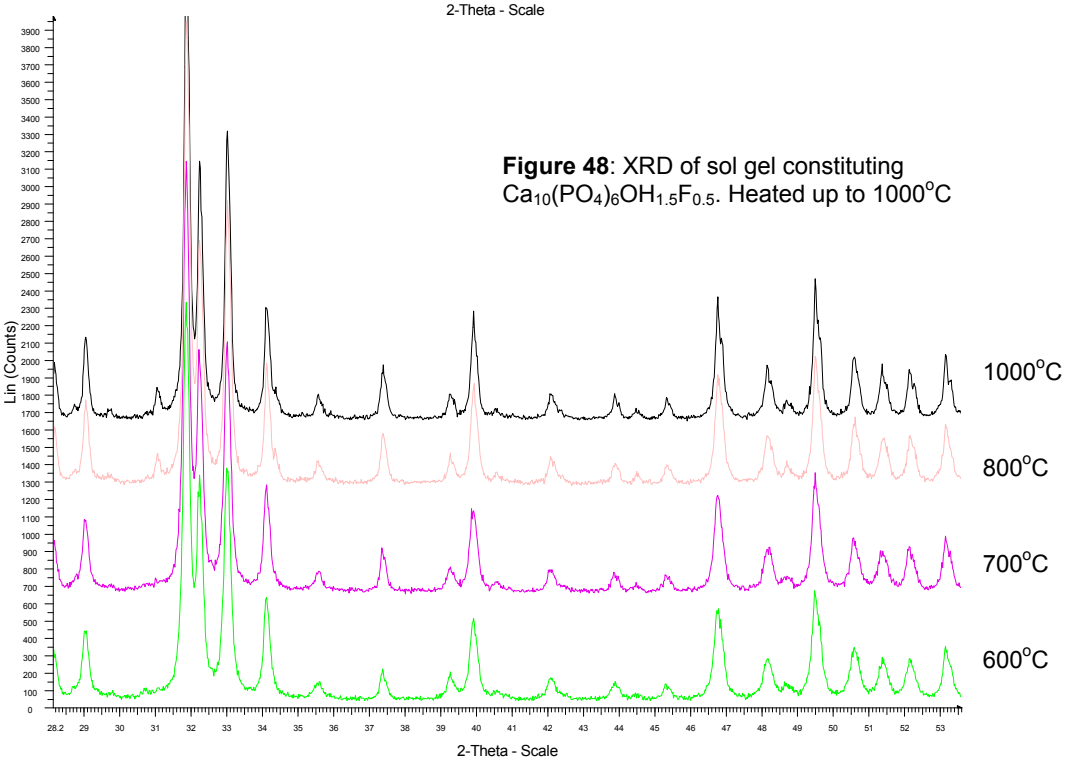


**Figure 48**: XRD of sol gel constituting $Ca_{10}(PO_4)_6OH_{1.5}F_{0.5}$. Heated up to 1000°C

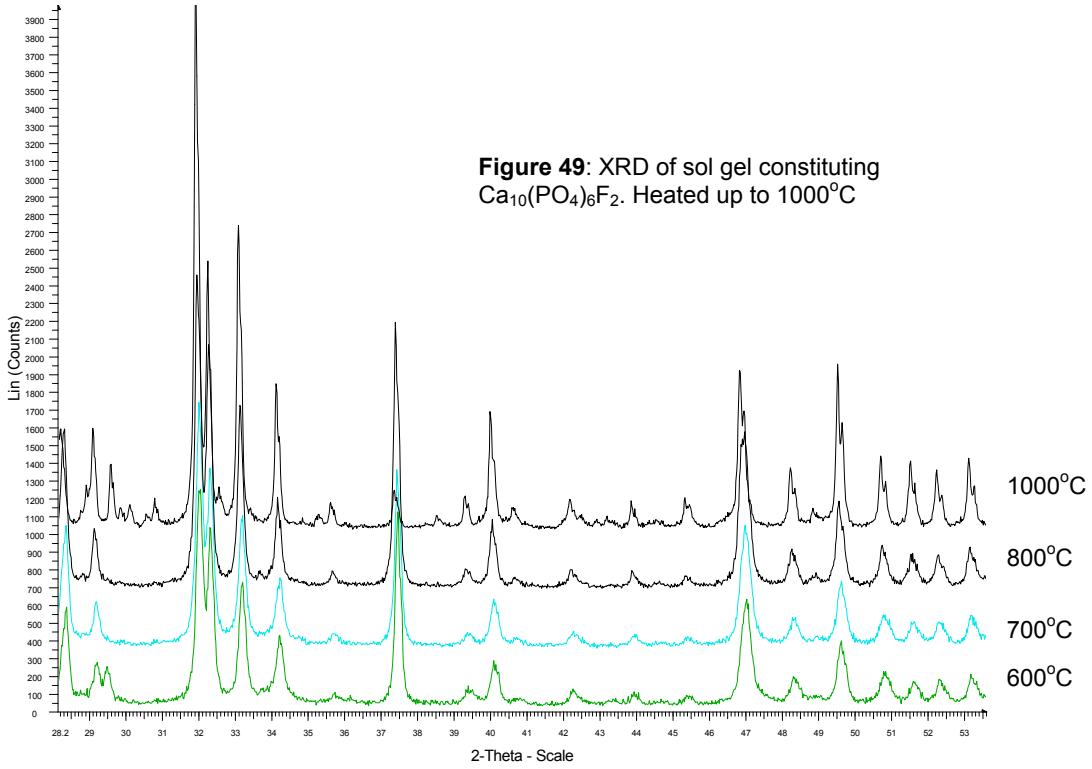


**Figure 49**: XRD of sol gel constituting $Ca_{10}(PO_4)_6F_2$. Heated up to 1000°C

TOPAS software was used to reveal the exact constituents contained in the sol-gels at different heating temperatures and these are summarised in table 17.

| Temp (°C) | Sol-gel $Ca_{10}(PO_4)_6$…. (%) | | | | | | | | | |
|---|---|---|---|---|---|---|---|---|---|---|
| | $(OH)_2$ | | $OH_{1.5}F_{0.5}$ | | $OH_1F_1$ | | $OH_{0.5}F_{1.5}$ | | $F_2$ | |
| | $(OH)_2$ | β-TCP | $OH_{1.5}F_{0.5}$ | β-TCP | $OH_1F_1$ | β-TCP | $OH_{0.5}F_{1.5}$ | β-TCP | $F_2$ | β-TCP |
| 600 | 99.7 | 0.3 | 99.8 | 0.2 | 99.7 | 0.3 | 99.8 | 0.2 | 99.8 | 0.2 |
| 700 | 99.7 | 0.3 | 99.8 | 0.2 | 99.7 | 0.3 | 99.8 | 0.2 | 99.8 | 0.2 |
| 800 | 99.7 | 0.3 | 92.1 | 7.9 | 93.2 | 6.8 | 94.6 | 5.4 | 99.8 | 0.2 |
| 1000 | 99.7 | 0.3 | 88.9 | 11.1 | 81.1 | 18.9 | 92.3 | 7.7 | 94.3 | 5.7 |

**Table 17**: Table to constituents of the powders from the sol-gel after heating at temperatures up to 1000°C.

### *7.3.4. High-temperature X-ray Diffraction*

High-temperature X-ray diffraction (HTXRD) was then undertaken using the FA/FHA sol-gels and measured on a Bruker D8 advance diffractometer equipped with a LynxEye detector and an Anton Paar HTK1600 heating stage fitted with a Pt electrode. XRD patterns were collected from $2\theta$ = 21-36$^{o}$ with a step of 0.02$^{o}$ and counting time of 37.8 seconds per point using Ni-filtered CuK$\alpha$ radiation generated at 35 kV and 45 mA. Data were collected between 20 and 1000$^{o}$C at intervals of 10$^{o}$C using air as a purge gas. The heating rate between temperature points was 6$^{o}$Cs$^{-1}$.

An example of data obtained from the HTXRD of the FA/FHA sol-gels is shown graphically in Figure 50, utilisation of this technique allows the data at 10$^{o}$C intervals to be visualised clearly.

**Figure 50**: Example of a 3 dimensional graphical representation of high temperature X-Ray diffraction of the FA sol-gel heated at 10°C intervals from 20 – 1000°C.

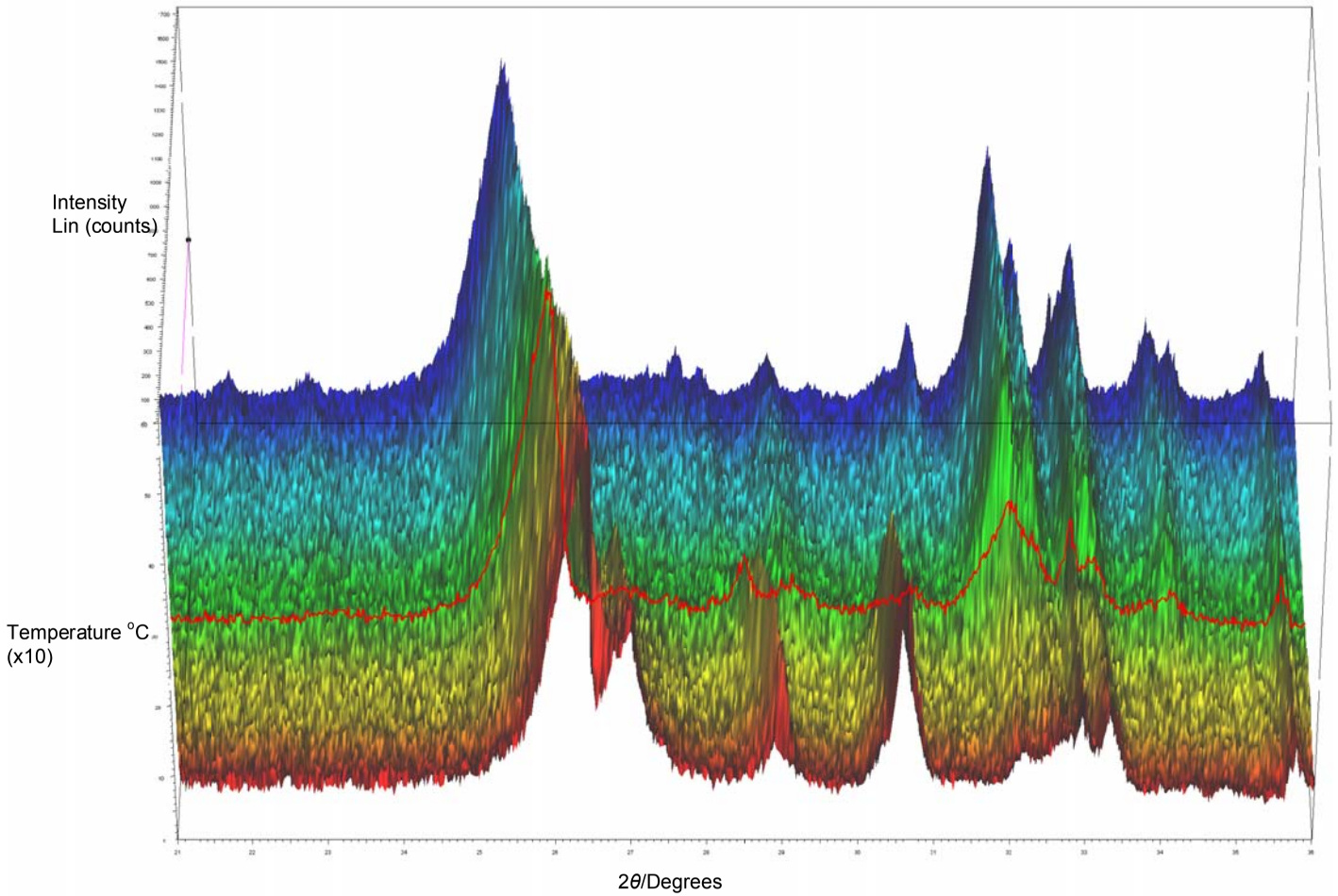

### *7.3.5. Unit cell measurements*

Unit cell measurements (a-axis, c-axis and unit cell volume) of the hydroxyapatite structure were undertaken at these six different heating temperatures after crystallisation and the results of these are summarised in Tables 18, 19, 20 and 21.

| Heating Temperature (°C) | a-axis(Å) | a-axis SD | c-axis (Å) | c-axis SD | Volume (Å$^3$) | Volume SD |
|---|---|---|---|---|---|---|
| 500 | 9.380 | 0.001 | 6.885 | 0.001 | 524.060 | 0.06 |
| 600 | 9.376 | 0.001 | 6.887 | 0.001 | 523.466 | 0.065 |
| 700 | 9.376 | 0.001 | 6.888 | 0.001 | 523.459 | 0.091 |
| 800 | 9.376 | 0.001 | 6.883 | 0.001 | 523.447 | 0.059 |
| 900 | 9.374 | 0.001 | 6.882 | 0.001 | 523.21 | 0.064 |
| 1000 | 9.372 | 0.001 | 6.882 | 0.001 | 523.116 | 0.062 |

**Table 18**: Unit cell measurements of sol-gel produced $Ca_{10}(PO_4)_6OH_{0.5}F_{1.5}$ at heating temperatures of 500 – 1000°C.

| Heating Temperature (°C) | a-axis(Å) | a-axis SD | c-axis (Å) | c-axis SD | Volume (Å$^3$) | Volume SD |
|---|---|---|---|---|---|---|
| 500 | 9.383 | 0.001 | 6.885 | 0.001 | 525.004 | 0.092 |
| 600 | 9.381 | 0.001 | 6.886 | 0.001 | 524.795 | 0.091 |
| 700 | 9.381 | 0.001 | 6.888 | 0.001 | 524.790 | 0.09 |
| 800 | 9.375 | 0.001 | 6.886 | 0.001 | 524.268 | 0.098 |
| 900 | 9.374 | 0.001 | 6.886 | 0.001 | 523.968 | 0.099 |
| 1000 | 9.372 | 0.001 | 6.885 | 0.001 | 523.753 | 0.11 |

**Table 19**: Unit cell measurements of sol-gel produced $Ca_{10}(PO_4)_6OH_1F_1$ at heating temperatures of 500 – 1000°C.

| Heating Temperature (°C) | a-axis(Å) | a-axis SD | c-axis (Å) | c-axis SD | Volume (Å$^3$) | Volume SD |
|---|---|---|---|---|---|---|
| 500 | 9.409 | 0.001 | 6.883 | 0.001 | 527.770 | 0.08 |
| 600 | 9.401 | 0.001 | 6.883 | 0.001 | 526.782 | 0.064 |
| 700 | 9.401 | 0.001 | 6.882 | 0.001 | 526.780 | 0.062 |
| 800 | 9.401 | 0.001 | 6.884 | 0.001 | 526.771 | 0.06 |
| 900 | 9.401 | 0.001 | 6.884 | 0.001 | 526.76 | 0.023 |
| 1000 | 9.377 | 0.001 | 6.887 | 0.001 | 524.468 | 0.101 |

**Table 20**: Unit cell measurement of sol-gel produced $Ca_{10}(PO_4)_6OH_{1.5}F_{0.5}$ at heating temperatures of 500 – 1000°C.

| Heating Temperature (°C) | a-axis(Å) | a-axis SD | c-axis (Å) | c-axis SD | Volume (Å$^3$) | Volume SD |
|---|---|---|---|---|---|---|
| 500 | 9.377 | 0.001 | 6.887 | 0.001 | 523.833 | 0.104 |
| 600 | 9.373 | 0.001 | 6.888 | 0.001 | 522.906 | 0.146 |
| 700 | 9.373 | 0.001 | 6.884 | 0.001 | 522.891 | 0.146 |
| 800 | 9.374 | 0.001 | 6.888 | 0.001 | 522.861 | 0.137 |
| 900 | 9.372 | 0.001 | 6.884 | 0.001 | 522.323 | 0.081 |
| 1000 | 9.370 | 0.001 | 6.885 | 0.001 | 521.906 | 0.146 |

**Table 21**: Unit cell measurement of sol-gel produced $Ca_{10}(PO_4)_6F_2$ at heating temperatures of 500 – 1000°C.

Comparable graphs of the a-axis, c-axis and volume changes as a reflection of material type and temperature are shown in figures 51, 52 and 53.

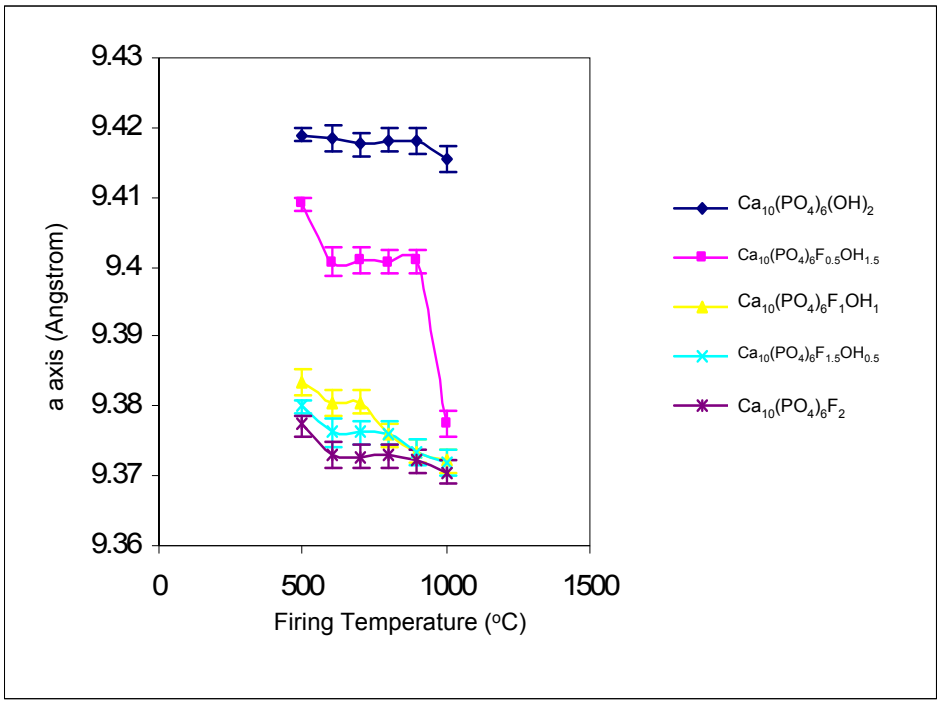


Figure 51: Graph to show a-axis changes with heating of the sol-gels (mean +/- SD).

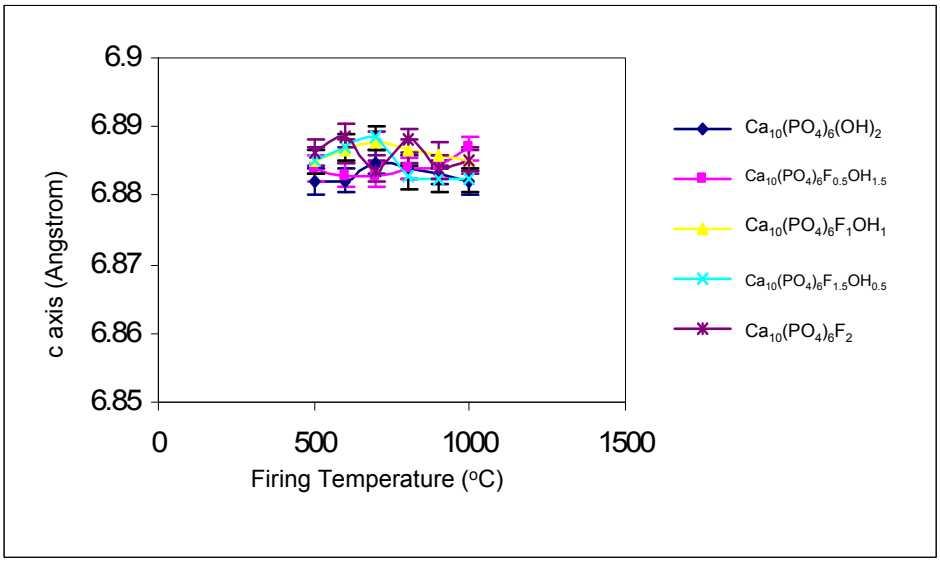


Figure 52: Graph to show c-axis changes with heating of the sol-gels (mean +/- SD).

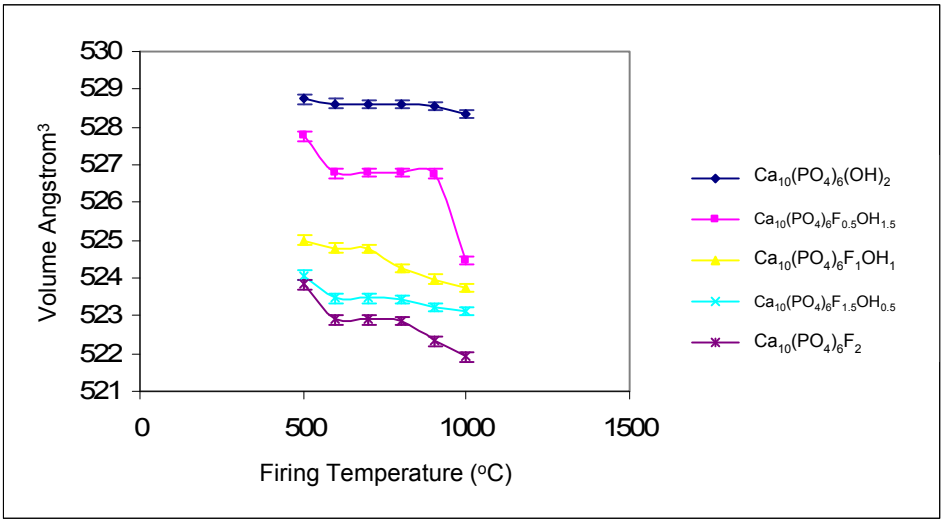


Figure 53: Graph to show changes in unit cell volume with heating of the sol-gels from 500°C – 1000°C (mean +/- SD).

## 7.4 Discussion

### *7.4.1. Chemistry*

The sol-gel production protocols that had been established for HA sol-gel production were utilised as the basic methodology for the production of the fluoride substitute apatite sol-gels. With reference to the literature (Kim et al., 2004) ammonium fluoride was chosen as the donor for the fluoride ions. After preliminary pilot experiments it proved that this should initially be added to the TEP and mixed for 24 hours and then both subsequently added to the calcium nitrate. With attention to the chemistry and controlling the amounts of ammonium fluoride initially added attempt was made to control the level of fluoride substitution in the apatite structure.

From the results obtained it became quickly evident that it was possible to control the amount of fluoride substitution in the apatite structure, and this directly correlated to the initial amounts of ammonium fluoride added. This is a novel finding for this thesis and appears to be the first which has been able to

control the amount of fluoride substitution in the apatite structure with such precision.

### *7.4.2. Differential thermal analysis (DTA)*

With reference to the DTA traces obtained, regardless of the sol-gels, the curves behaved in a similar manner. The first strong peaks at 100$^{o}$C (endothermic and exothermic) correspond to the loss of water. The second strong peak at around 280$^{o}$C, corresponds to the decomposition of nitrate from the Ca precursor (this can be evidenced in the FT-IR data). The temperature of the third exothermic weak peak represents the formation of crystalline apatite (and is further confirmed by the XRD data obtained).

There is a clear trend in the crystallisation temperatures seen. As the level of fluoride substitution increased the crystallisation temperature decreased. The work in this thesis appears to be the first where it has been possible to precisely control the level of fluoride substitution in to the apatite structure and appears to be the first to show this phenomenon so clearly. During substitution the $F^{-}$ occupies to varying degrees (depending on the level of substitution) the position of $OH^{-}$ in the apatite, it is also known that increasing the level of fluoride substitution in the apatite structure produces a smaller more compact crystal structure (Song et al., 2004). The results of this thesis suggest that the increasing levels of fluoride allow the structure to crystallise more easily and hence have a lower crystallisation temperature. This finding could be attributed to the fact that increasing fluoride substitution results in a more stable, compact structure that is capable of crystallising quicker than HA.

Comparison of the crystallisation temperature results to those found of HA sol-gel earlier reveal that the temperature that the HA crystallised at was around

499(+/-0.65)$^{o}$C showing a clear trend that increasing fluoride substitution resulted in a decreasing crystallisation temperature.

The other noteworthy point from the DTA data obtained is that there were no further changes following the crystallisation temperature up to 1000$^{o}$C. This indicates that these fluoride substituted apatites produced via the sol-gel method are thermally stable to at least 1000$^{o}$C and that these materials can be heated up to this temperature without decomposition.

### *7.4.3. X-ray Diffraction*

Structural changes at different temperatures were further investigated using XRD. From the XRD results when the powders had been heated to 500$^{o}$C it can be seen that less than 0.3% of all the samples obtained were β-TCP, this illustrates the efficacy of the chemistry that has been used to makes the sol-gel and illustrates the high purity of the samples obtained. The ability to make such pure fluoride substituted apatites from the sol-gel method is novel to this thesis and has not been reported in the literature using this sol-gel technique.

From the results of the XRD on the heated powders, it can be seen that there were some changes in the patterns observed, with some breakdown to ß-TCP at higher temperatures. The most stable at higher temperatures was the pure FA [$Ca_{10}(PO_4)_6F_2$] and pure HA [$Ca_{10}(PO_4)_6(OH)_2$].

Utilisation of this technique again confirmed the crystallisation temperatures found during the DTA (see table 16) and the stability of the FA/FHA sol gels produced from this sol-gel method. Some of the thermal stability results obtained with the XRD were in slight contrast to the DTA results, this may be indicative of the higher sensitivity of the XRD technique and TOPAS software, furthermore if there were no exothermic, endothermic or weight changes in the

sample this would not be detected by DTA. From the results in table 17 it can be seen that $Ca_{10}(PO_4)_6(OH)_2$ (HA) was thermally stable at all temperatures up to 1000°C. $Ca_{10}(PO_4)_6OH_{1.5}F_{0.5}$, $Ca_{10}(PO_4)_6OH_1F_1$ and $Ca_{10}(PO_4)_6OH_{0.5}F_{1.5}$ were thermally stable up to 700°C, after which there was degradation and increasing amounts of β-TCP were formed. The reason for these being less thermally stable may be that the structure of the molecule may be less stable when OH and F are combined and hence the quicker that it will breakdown as it is heated. $Ca_{10}(PO_4)_6F_2$ (FA) was thermally stable up to 900°C but at temperatures approaching 1000°C was seen to start to degrade with the amounts of β-TCP rising from 0.2% to 5.7%. The data seen here infers that the HA was more stable at temperatures approaching 1000°C than the HA.

### *7.4.4. Unit cell*

Analysis of the unit cell data reveals some very clear patterns as follows:

#### *7.4.4.1. a-axis*

All of the sol-gel produced fluoride substituted apatites had manifestly smaller a-axis than the HA produced from the sol-gel. This is in line with the published literature, which reported in the case of FHA powders, there were significant decreases in the a-axis when compared to HA (Smith, 1994; Larsen & Jensen, 1989; Kim et al., 2002).

The more fluoride substitution the smaller the a-axis, such that the a-axis decreases in size as follows: $Ca_{10}(PO_4)_6F_{0.5}OH_{1.5}$ > $Ca_{10}(PO_4)_6F_1OH_1$ > $Ca_{10}(PO_4)_6F_{1.5}OH_{0.5}$ > $Ca_{10}(PO_4)_6F_2$. The fluoride ion has a smaller size than $OH^-$, being 1.28 Å compared to 1.37 Å (Shannon et al., 1976), and as such is able to pack more closely into the apatite structure. Based on this, the above finding follows this principle, such that the more fluoride that is incorporated

into the apatite structure the smaller the overall size. The results from this thesis constitute the first known data that is able to show this pattern so clearly.

There is a downward trend in the size of the a-axis as the firing temperature is increased. Abrahams and Knowles (1994) investigated the effects of sintering conditions on hydroxyapatite using X-Ray diffraction. They were investigating temperatures in excess of 1000$^{o}$C and found small but significant decreases in unit-cell volume as temperature increased. They proposed this to be due to a loss of small amounts of carbonate ion from channels within the structure. It is possible to suggest that the pattern seen in the unit cell volume here is similar and may be due to loss of small amounts of carbonate ion at the lower temperatures investigated. Furthermore heating the apatite structure to temperatures above the crystallisation temperature, but below the decomposition temperature, vibrates the atoms and allows them to move to a more optimal position. The more optimal position of the atoms the smaller the a-axis and overall unit cell volume will be.

The a-axis values for the $Ca_{10}(PO_4)_6F_2$ (FA) were similar to the reported values for pure FA (a-axis 9.3684 Å) (Elliot, 1994; Smith, 1994). The similarity of the values obtained in this thesis to reported values provides further support for the purity of the samples that have been produced by the sol-gel method adopted.

The changes seen in the unit cell pattern obtained for $Ca_{10}(PO_4)_6F_{0.5}OH_{1.5}$ have a slightly different trend than the other patterns seen. Initially there is a marked drop between 500 and 600$^{o}$C and this is proportionally larger when compared to the other heated sol-gels. It is possible that this combination of $F^-$ and $OH^-$ when heated to 500$^{o}$C form an apatite structure whose structure is far from optimal, heating further to 600$^{o}$C allows the atoms to rearrange and become much more ordered. There is a second different trend seen between 900 and

1000°C. Here there is again a marked drop which is proportionally larger when compared to the other heated sol-gels. It can be postulated that the large drop here could be attributed to the formation of oxyapatite ($Ca_{10}(PO_4)_6O$), there is some indication from the earlier FTIR data in this thesis seen with HA that at around 900°C this may start to occur.

#### *7.4.4.2. c-axis*

While there were manifest changes in the a-axis, there were little changes observed in the c-axis. This is well reported in the literature for fluoride substituted apatites (Larsen & Jensen, 1989; Kim et al., 2002; Smith, 1994). Within the apatite structure there is no spare volume for the structure to change in dimensions along the c axis, therefore it is to be expected that little change would be seen, however again, these findings give further confidence to the data.

#### *7.4.4.3. Volume (Å$^3$)*

All of the sol-gel produced fluoride substituted apatites had manifestly smaller unit cell volumes than the HA produced from the sol-gel. The more fluoride substitution the smaller the a-axis, such that the volume (Å$^3$) decreases in size as follows: $Ca_{10}(PO_4)_6(OH)_2$ > $Ca_{10}(PO_4)_6F_{0.5}OH_{1.5}$ > $Ca_{10}(PO_4)_6F_1OH_1$ > $Ca_{10}(PO_4)_6F_{1.5}OH_{0.5}$ > $Ca_{10}(PO_4)_6F_2$.

In direct proportion to the changes seen in the a-axis, there is a downward trend in the unit cell volume seen as the firing temperature is increased.

Because of the clear correlations above it can be proposed that the controlled incorporation of fluoride in the sol-gel protocol used leads to the successful formation of FHA solid solutions with differing levels of fluoride substitution.

## 7.5. Fourier Transform Infra Red (FT-IR) analysis of HA sol-gel

Using the Perkin Elmer series 2000 Attenuated Total Reflectance (ATR) FTIR spectrometer three readings at various places were taken of the fluoride substituted sol gel as received and following heating to 450°C. These were all identical and an illustrative example is shown in figures 54, 55, 56 and 57.

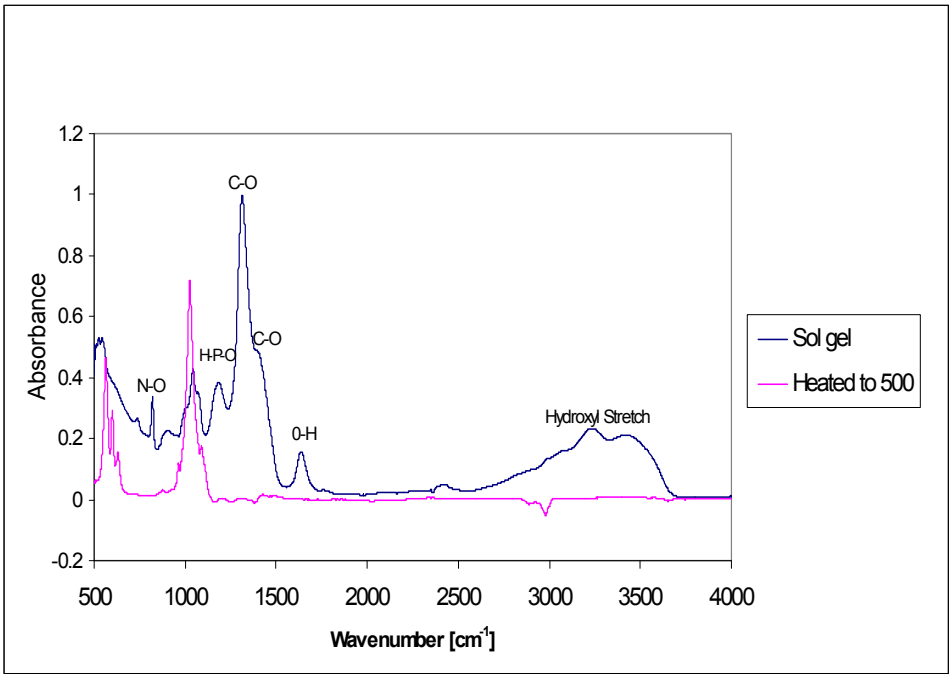


**Figure 54**: FTIR of $Ca_{10}(PO_4)_6F_2$ as received (a.r) and heated to 500°C

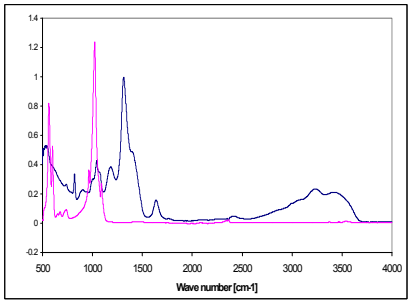


**Figure 55**: FTIR $Ca_{10}(PO_4)_6F_{0.5}OH_{1.5}$ a.r. and 500°C

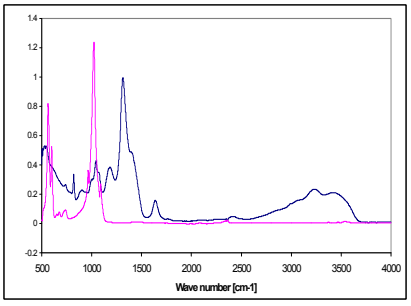


**Figure 56**: FTIR $Ca_{10}(PO_4)_6F_1OH_1$ a.r. and 500°C

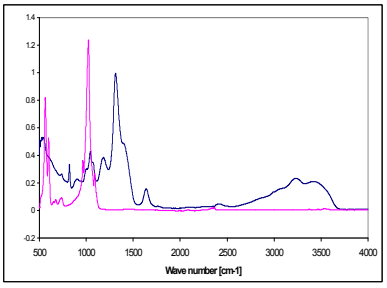


**Figure 57**: FTIR $Ca_{10}(PO_4)_6F_{1.5}OH_{0.5}$ a.r. and 500°C

With reference to the FTIR in figures 54 - 57 it can be seen that the original sol-gels still has carbonate bonds (C-0) present and (N-O) and (H-P-O) bonds present potentially indicating the presence of unreacted calcium nitrate and TEP, there is also a pronounced hydroxyl stretch (around 3568 $cm^{-1}$) indicating the presence of water. These are identical to the peaks found in the HA produced sol-gel. On heating all calcium nitrate, TEP and water are lost leaving just the presence of an apatite structure. This is important as clearly the biocompatibility of FHA/FA could be affected if the primary unreacted constituents of calcium nitrate and TEP remained in the sol-gel after it was heated when coating on to titanium.

Figure 58 shows an FTIR of the primary constituents i.e. TEP, calcium nitrate, ammonium fluoride and water that were originally used in making the sol-gel. With reference to this, the correlation with the original bonds present and those in the new sol-gel can be visualised.

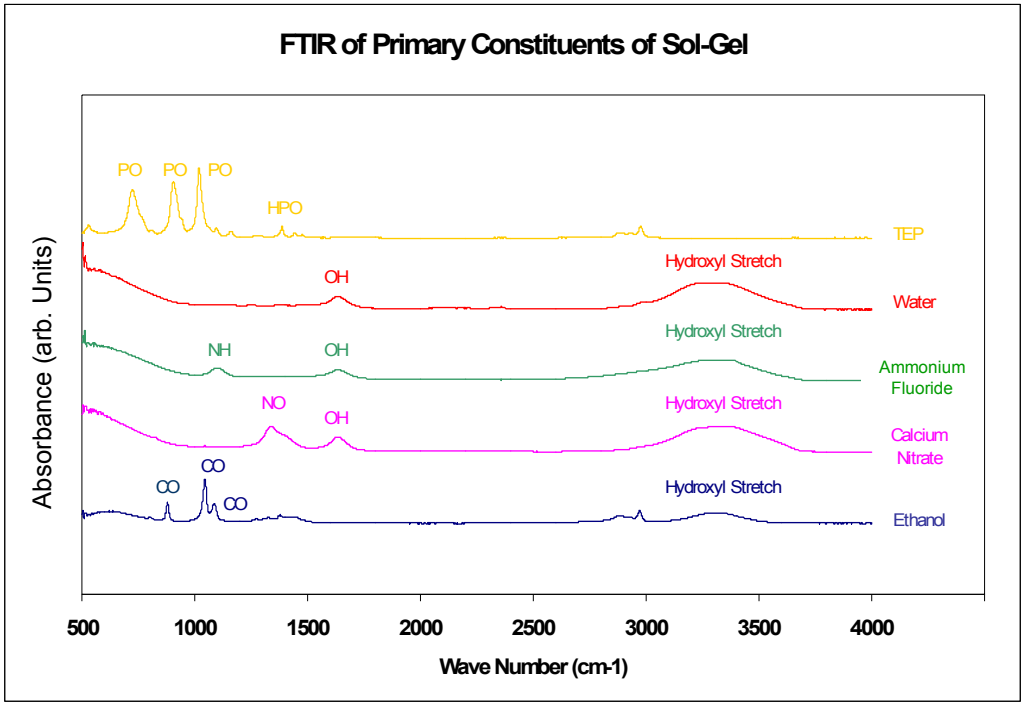


**Figure 58**: FTIR of primary constituents of FHA sol-gels.

Additional heating of the samples and subsequent FTIR analysis of the powders confirmed that no subsequent changes take place when heating up to 1000°C (see Figure 59).

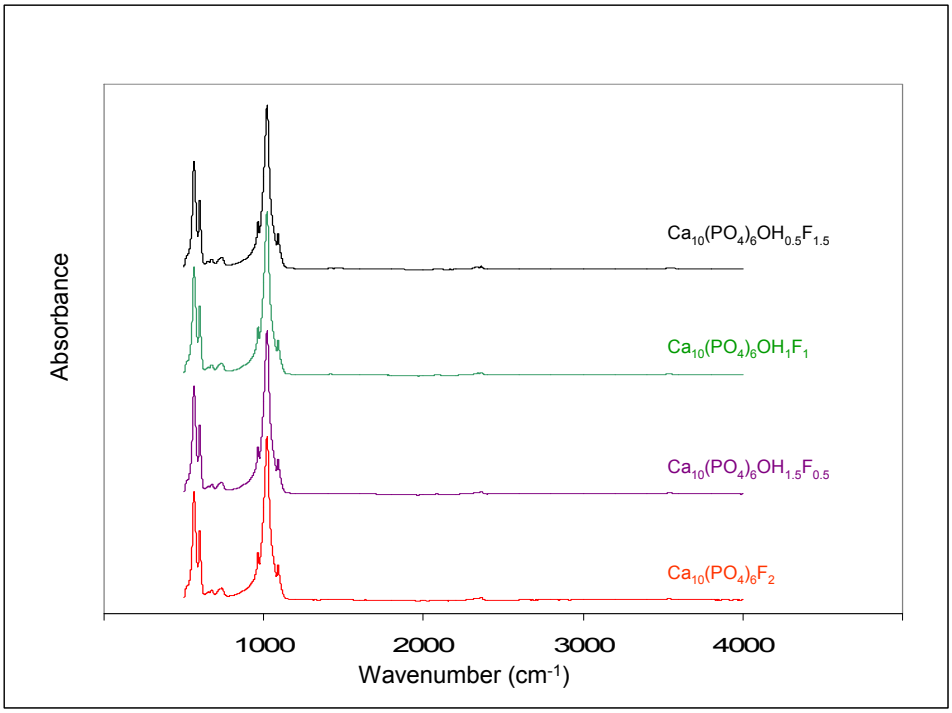


**Figure 59**: FTIR analysis of FA/FHA sol gels after heating to 1000°C. Confirming the stability of the sol-gel produced fluoride substituted apatites.

In combination with the XRD data obtained this FTIR data provides further confirmation that the FHA/FA sol-gels are thermally stable up to 900°C, but suggests that there may be initial break down of the HA into oxyapatite at temperature approaching 1000°C (from XRD data). Thus is seems that temperatures up to 900°C can be used when preparing to coat the FHA/FA sol-gel produced onto a titanium implant, however caution should be exhibited in temperatures beyond this as decomposition of the FHA/FA may start to occur particularly with $Ca_{10}(PO_4)_6F_{0.5}OH_{1.5}$.

# Chapter 8:

# Rheology Of

# Hydroxyapatite $Ca_{10}(PO_4)_6OH_2$,

# Fluorapatite $Ca_{10}(PO_4)_6F_2$ &

# Fluor-hydroxyapatite $Ca_{10}(PO_4)_6OH_xF_y$

# Sol-gels

## 8.1. Methods & Materials

Viscosity is a measure of a fluids resistance to flow. Rheology was studied and contact angle measurement was made of the five sol-gels as follows:

### *8.1.1. Rheology*

Rheology investigations were undertaken using a viscometer (Model DV-III, Brookfield, USA). The principle of operation of the viscometer is to drive a spindle (which was immersed in the sol-gels) through a calibrated spring. The viscous drag of the fluid against the spindle was measured by the spring deflection. Spring deflection was measured with a rotary transducer (see figure 60).

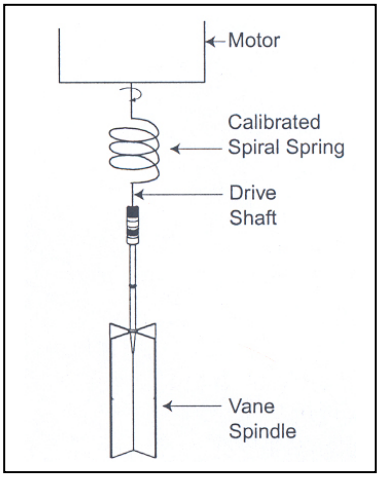


**Figure 60**: Schematic representation of Viscometer. Reproduced from DV-111 manual.

40ml of the sol-gel sample was placed in the container supplied with the viscometer. An appropriate spindle was selected by trial and error using two principles:

- Viscosity range is inversely proportional to the size of the spindle.
- Viscosity range is inversely proportional to the rotational speed.

In other words, to measure high viscosities choose a small spindle and / or a slow speed. Choice of the appropriate spindle resulted in a measurement of 10-100% on the torque scale (RV2 was found to be appropriate for the sol-gels being tested).

Two parameters were investigated:

(1) The varying viscosity of the sol-gels after a set aging time at various shear rates. A period of 24 hours was chosen because of the data found in the early characterisation and optimisation of the gels. Each sol-gel i.e. $Ca_{10}(PO_4)_6(OH)_2$, $Ca_{10}(PO_4)_6OH_{0.5}F_{1.5}$, $Ca_{10}(PO_4)_6)OH_1F_1$, $Ca_{10}(PO_4)_6OH_{1.5}F_{0.5}$ and $Ca_{10}(PO_4)_6F_2$ was measured at various shear rates (from 20 to 200 $s^{-1}$ with intervals of $10s^{-1}$), each for 20 seconds at a constant temperature of 25$^{o}$C. This was repeated 3 times.

(2) Measuring changes in viscosity at a constant shear rate as the sample is aged. After mixing the hydrolysed Triethyl Phosphite [$P(C_2H_50)_3$] Calcium Nitrate [$Ca(NO_3)_2.4H_20$] and ammonium hydroxide ($NH_4OH$) the viscosity at a constant shear rate $150s^{-1}$ was measured every 6 hours up to 72 hours. This was repeated 3 times.

### *8.1.2. Contact angle measurement*

Contact angle measurements were undertaken with a CAM 200 Optical Contact Light Meter (KSV, Instruments Limited, Finland) – see figure 61.

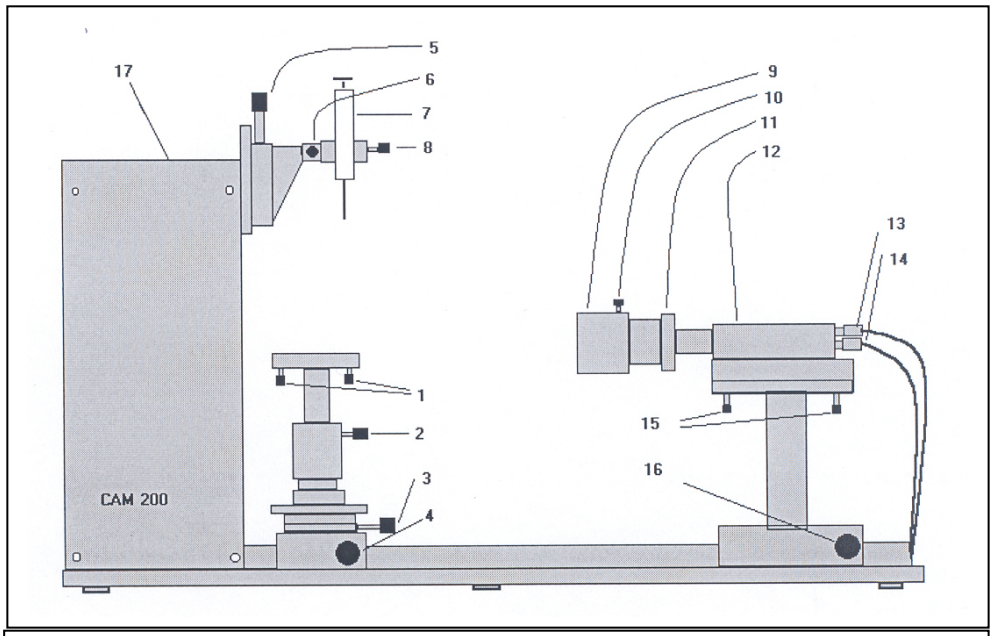


**Key:** (1) Stage level adjustment, (2) Stage height adjustment, (3) Stage lateral adjustment, (4) Stage linear adjustment, (5) Syringe height adjustment, (6) Syringe lateral adjustment, (7) Syringe, (8) Syringe clamp, (9) Camera lens zoom, (10) Camera zoom lock, (11) Lens aperture adjustment, (12) CCD Camera, (13) Light Synchronizing cable, (14) Video Out cable, (15) Camera level adjustment, (16) Camera Linear adjustment, (17) Light source and Interface Unit.

**Figure 61**: CAM 200 Optical Contact Light Meter. Reproduced (with kind permission) from CAM 200 Manual (KSV, Instruments Limited, Finland).

The CAM 200 light source is LED based. The LEDs are housed in a reflective sphere which integrates their light and directs it towards the sample. CAM 200 uses a Jai CV-M50 monochrome video camera using a CCD solid state image sensor with a 55 mm focus length.

5ml of the sol-gel sample was loaded into a syringe provided with the CAM 200 and positioned in place. The camera software was opened and the syringe tip positioned into the upper area of the image screen. A commercially pure titanium disk (10mm by 10mm) was placed on the lower apparatus and

positioned such that it could be seen in the lower part of the image. The camera was focused on the syringe tip and the set up such that when a drop of the sol-gel was made on the titanium disk it started to recording. The syringe tip was subsequently depressed and a drop of sol-gel released on to the titanium and recording commenced.

The CAM 200 was set up to measure the contact angle every second for 30 seconds. The measurements were repeated three times for each sol-gel.

## 8.2. Results

### 8.2.1. *Varying viscosity of the sol-gels after 24 aging time at various shear rates*

Figure 62 shows the viscosity changes (mean +/- standard deviation) of the sol-gels after aging for 24 hours, as represented with respect to shear rate.

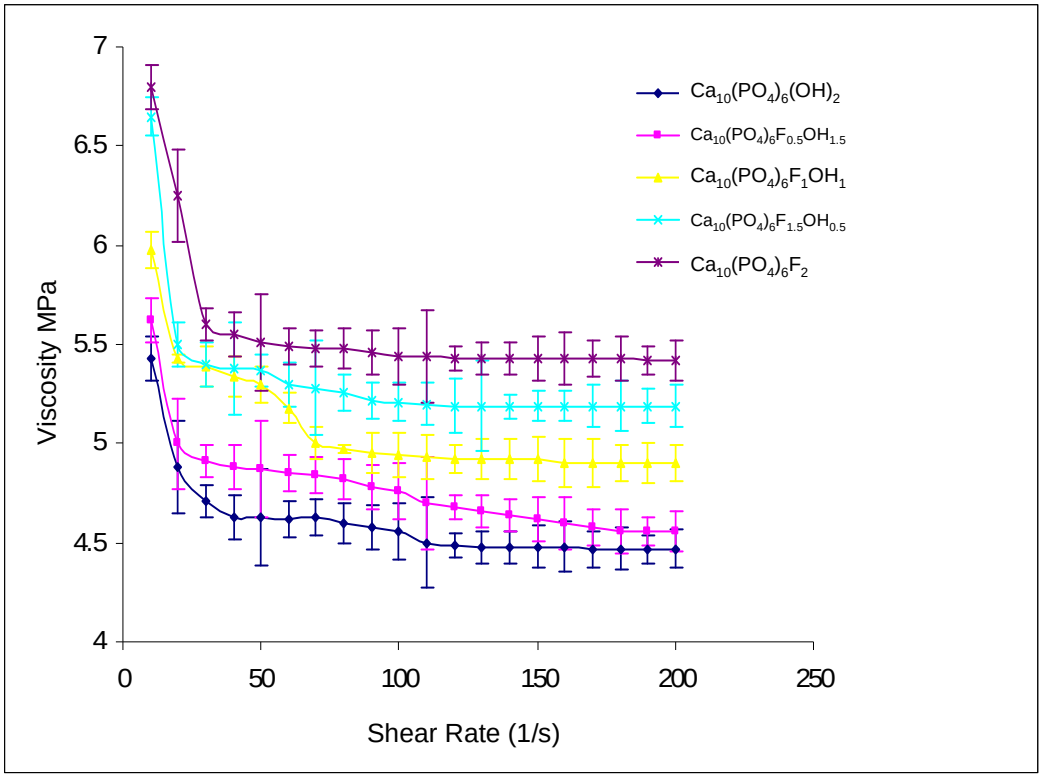


**Figure 62**: Mean viscosity changes in the HA, FA and FHA sol-gels after aging for 24 hours, as represented with respect to shear rate (mean +/- SD).

With reference to figure 62 several clear patterns can be seen. The initial viscosity of the sol-gels is such that the higher the concentration of fluoride in the sol-gel the higher the viscosity i.e. the viscosity of the sol-gels was as follows; $Ca_{10}(PO_4)_6F_2$ > $Ca_{10}(PO_4)_6OH_{0.5}F_{1.5}$ > $Ca_{10}(PO_4)_6)OH_1F_1$ > $Ca_{10}(PO_4)_6OH_{1.5}F_{0.5}$ > $Ca_{10}(PO_4)_6(OH)_2$. This pattern in viscosity was consistent throughout the entire time period tested.

Over the first 24 hour period there were rapid decreases in the viscosity of the sol-gels. Following the first 24 hours there were minimal downward changes in the viscosity of the materials.

### *8.2.2. Measuring changes in viscosity at a constant shear rate as the sample is aged*

The mean viscosity change (+/- standard deviation) was plotted with aging time at a constant shear rate of 150 $s^{-1}$. This is shown in figure 63.

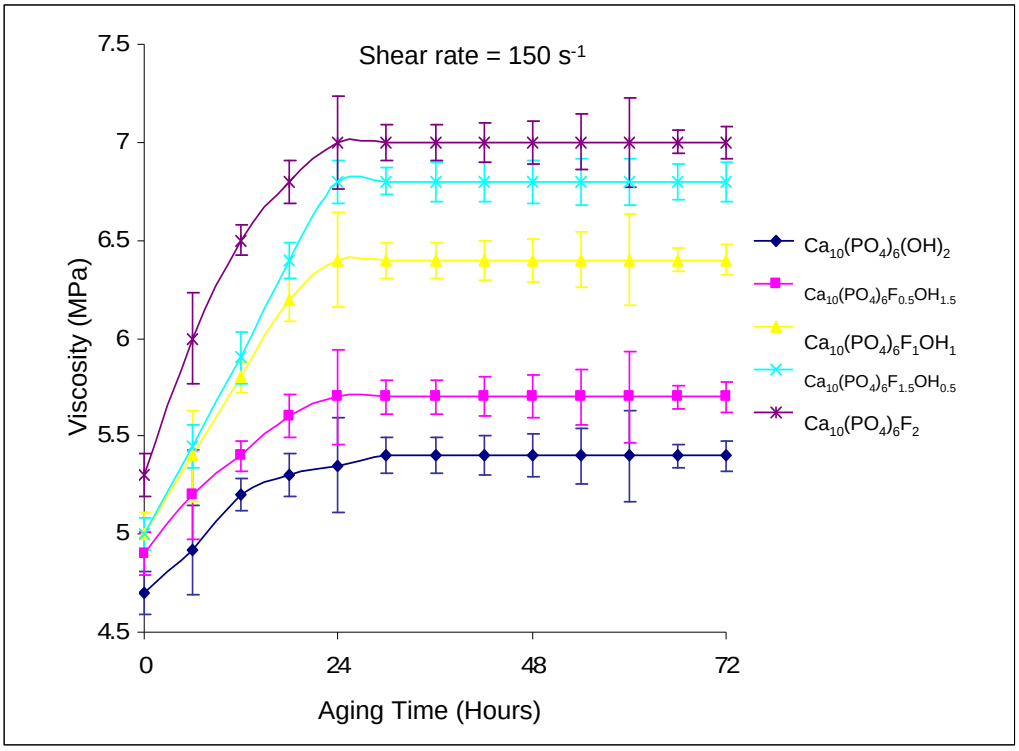


**Figure 63:** Viscosity changes in HA, FA and FHA sol-gels measured at shear rate of 150$s^{-1}$, as represented with respect to aging (mean +/- SD).

With reference to figure 63 the viscosity of all the sol-gels increased with aging time, there were two clear patterns to be seen. Firstly, all the sol-gels showed a rapid increase in viscosity over the first 24 hours, this subsequently stabilised and saw minimal changes over the next 48 hours. Secondly, once again there is a clear pattern in the viscosity of the sol-gels; the higher the concentration of Fluoride in the sol-gel the higher the viscosity i.e. the viscosity of the sol-gels was as follows; $Ca_{10}(PO_4)_6F_2$ > $Ca_{10}(PO_4)_6OH_{0.5}F_{1.5}$ > $Ca_{10}(PO_4)_6OH_1F_1$ > $Ca_{10}(PO_4)_6OH_{1.5}F_{0.5}$ > $Ca_{10}(PO_4)_6(OH)_2$.

### *8.2.3. Contact angle measurement*

The overall mean contact angles, plus and minus the standard deviation for each of the sol-gels is shown in table 22.

| **Mean (+/- SD) Contact Angle Apatite Sol-gel ($Ca_{10}(PO_4)_6$..)** | | | | |
|---|---|---|---|---|
| **$(OH)_2$** | **$(F_{0.5}OH_{1.5})_2$** | **$(F_1OH_1)_2$** | **$(F_{1.5}OH_{0.5})_2$** | **$F_2$** |
| 55.34 (+/- 0.35) | 56.36 (+/- 0.48) | 57.32 (+/- 0.37) | 58.12 (+/- 0.44) | 60.34 (+/- 0.46) |

**Table 22**: Mean contact angle of each of the sol-gels

Figure 64 graphically shows the contact measurement as a result of time of the HA, FA and FHA sol-gels.

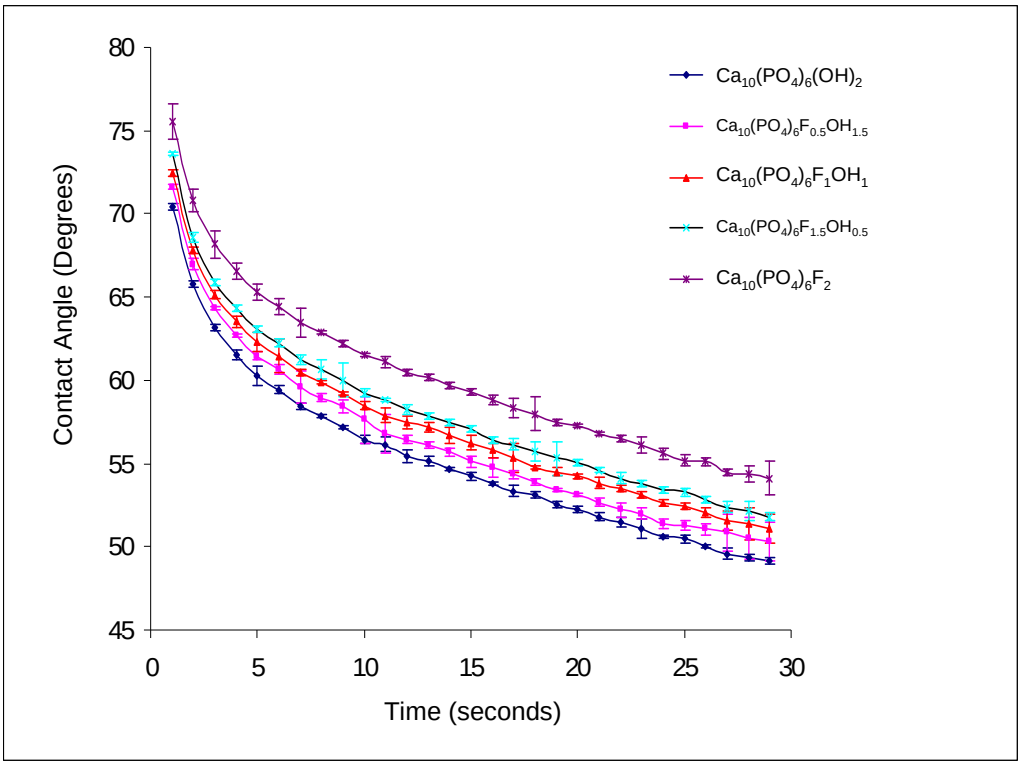


**Figure 64:** Contact angle measurements for each of the sol-gels.

With reference to figure 64 it can be seen that there were clear patterns. Initially on dropping the sol-gel for approximately the first four second there is rapid decrease in contact angle, subsequently the reduction starts to slow. There is a clear pattern in that the contact angle is higher with the increasing fluoride concentration such that the contact angles are as follows; $Ca_{10}(PO_4)_6F_2$ > $Ca_{10}(PO_4)_6OH_{0.5}F_{1.5}$ > $Ca_{10}(PO_4)_6)OH_1F_1$ > $Ca_{10}(PO_4)_6OH_{1.5}F_{0.5}$ > $Ca_{10}(PO_4)_6(OH)_2$.

## 8.3. Discussion of rheology of HA, FA and FHA sol-gels

### *8.3.1. Rheology*

Rheology is concerned with the flow and deformation of materials experiencing an applied force. It is important to have a basic understanding of the rheology of the sol-gels in this thesis as one of the potential planned future uses are as a coating material.

### *8.3.2. Varying viscosity of the sol-gels after a set aging time at various shear rates*

The first parameter chosen for investigation in this thesis was varying the viscosity of the sol-gels after a set aging time at various shear rates. A period of testing after 24 hours of aging was chosen because from the previous data found in this thesis we know that 24 hours was the optimum aging time for formation of the sol-gels. Each sol-gel i.e. $Ca_{10}(PO_4)_6(OH)_2$, $Ca_{10}(PO_4)_6OH_{1.5}F_{0.5}$, $Ca_{10}(PO_4)_6)OH_1F_1$, $Ca_{10}(PO_4)_6OH_{0.5}F_{1.5}$ and $Ca_{10}(PO_4)_6F_2$ was measured at various shear rates (from 20 to 200 $s^{-1}$ with intervals of $10s^{-1}$), each for 20 seconds at a constant temperature of 25$^{o}$C. This was repeated 3 times to allow a mean and standard deviation to be calculated.

With reference to figure 62 it can be seen that after aging for 24 hours, the viscosity of all the sol-gels showed an exponential decrease at short shear rates and stabilised with the higher shear rates. This behaviour is characteristic of sol-gels. As the shear rate is initially increased the viscosity of the sol-gel falls as there is a breakdown in the sol structure (Ben-Nissan & Choi, 2006). As the shear rates become higher, this effect becomes reduced such that any additional increases in shear rate cause negligible effects on the viscosity (Ben-Nissan & Choi, 2006).

There is a clear pattern that can be seen throughout; the higher the concentration of fluoride in the sol-gel the higher the viscosity i.e. the viscosity of the sol-gels was as follows; $Ca_{10}(PO_4)_6F_2$ > $Ca_{10}(PO_4)_6OH_{0.5}F_{1.5}$ > $Ca_{10}(PO_4)_6)OH_1F_1$ > $Ca_{10}(PO_4)_6OH_{1.5}F_{0.5}$ > $Ca_{10}(PO_4)_6(OH)_2$. This is a novel finding to this thesis. A potential theory to explain this is that there could be stronger cross links within the sol-gel with higher fluoride content. As a result of these stronger links the viscosity is increased.

Clearly the rheological results obtained here are novel and may have implications when coating the sol-gels on to titanium i.e to achieve the same coating with increasing fluoride concentration, different coating speeds may have to be adopted.

### *8.3.3. Measuring changes in viscosity at a constant shear rate as the sample is aged*

The second parameter chosen for investigation in this thesis was measuring the changes in viscosity at a constant shear rate as the sample is aged. The first 24 hours of aging was chosen as it is known from the previous results in this thesis that this is when the sol-gel process is occurring.

With reference to figure 63 the viscosity of all the sol-gels increased with aging time, there were two clear patterns to be seen. Firstly, all the sol-gels showed a rapid increase in viscosity over the first 24 hours, this subsequently stabilised and saw minimal changes over the next 48 hours. This seems to tie in with the initial results found in the optimisation and characterisation of the sol-gels. Establishing the initial protocol it was found that the optimal time to mix the hydrolysed triethyl phosphite [$P(C_2H_50)_3$], calcium nitrate [$Ca(NO_3)_2.4H_20$] and ammonium hydroxide ($NH_4OH$) for was 24 hours. Less mixing than this and the reaction had not been completed. Mixing for longer periods made no difference.

Secondly, once again there is a clear pattern in the viscosity of the sol-gels; the higher the concentration of fluoride in the sol-gel the higher the viscosity i.e. the viscosity of the sol-gels was as follows; $Ca_{10}(PO_4)_6F_2$ > $Ca_{10}(PO_4)_6OH_{0.5}F_{1.5}$ > $Ca_{10}(PO_4)_6OH_1F_1$ > $Ca_{10}(PO_4)_6OH_{1.5}F_{0.5}$ > $Ca_{10}(PO_4)_6(OH)_2$.

Again a possible theory that can be suggested for the reason for the increasing viscosity as more fluoride is substituted in to the sol-gel structure could be that there could be stronger cross links within the sol-gel with higher fluoride content. As a result of these stronger links this may have an overall effect on the viscosity.

### *8.3.4. Contact angle measurement*

Contact angle measurement is a simple technique for surface analysis and is directly related to surface energy and tension. Contact angle describes the shape of a liquid droplet resting on a solid surface. When drawing a tangent line from the droplet to the touch of the solid surface, the contact angle is the angle between the tangent line and the solid surface. When a droplet of high surface tension is placed on a solid of low surface energy, the liquid surface tension will cause the droplet to form a spherical shape (lowest surface energy). The measurement provides information regarding the bonding energy of the solid surface and the surface tension of the droplet. Because of its simplicity, contact angle measurement has been broadly accepted for material surface analysis related to wetting, adhesion, and absorption.

Drop shape analysis has been adopted in this thesis and is a convenient way to measure contact angles and thereby determine surface energy. The principal assumption is that the drop is symmetrical about a central vertical axis; this means it is irrelevant from which direction the drop is viewed.

The CAM 200 used in this thesis was set up to measure the contact angle every second for 30 seconds (dynamic contact angle measurement). This allowed a range of data to be viewed of the contact angle following pipetting the droplet on to the titanium disks. The experiment was repeated three times for each sol gel so a mean and standard deviation could be calculated for each sol-gel at each time point.

With reference to figure 64 it can be seen that there were clear patterns in the contact angle data obtained. Initially on dropping the sol-gel for approximately the first four seconds there was a rapid decrease in contact angle, subsequently the reduction start to plateau off. This is normal of contact angle measurements and is the reason why multiple measurements were recorded over the first 30 seconds as the surface tension of the sample forms an equilibrium with the titanium disk.

Throughout all contact angle measurements, at all times, there was a pattern with the contact angle being higher with increasing fluoride concentration such that the contact angles were as follows; $Ca_{10}(PO_4)_6F_2$ > $Ca_{10}(PO_4)_6OH_{0.5}F_{1.5}$ > $Ca_{10}(PO_4)_6)OH_1F_1$ > $Ca_{10}(PO_4)_6OH_{1.5}F_{0.5}$ > $Ca_{10}(PO_4)_6(OH)_2$. This suggests that increasing the concentration of fluoride seems to increase the hydrophobicity (contact angle) of the sol-gel. This finding is novel to this thesis and it can be proposed that this is related to the fluoride producing stronger cross linking within the sol-gel structure. With increasing fluoride substitution it can be proposed that there will be stronger cross links per unit area in each comparable sol-gel and as a result the hydrophobicity is increased.

This finding may have implications when coating the sol-gels on to titanium. It can be proposed, that because of the altered rheological characteristics with higher levels of fluoride substitution, in the apatite structure produced by the

sol-gel technique, different coating speeds / protocols may have to be adopted when coating the sol-gels on to titanium.

# Chapter 9:

# Dissolution Behaviour Of

# Hydroxyapatite $Ca_{10}(PO_4)_6OH_2$,

# Fluorapatite $Ca_{10}(PO_4)_6F_2$ &

# Fluor-hydroxyapatite $Ca_{10}(PO_4)_6OH_xF_y$

# Powders from Sol-gels

## 9.1. Methods & Materials

### *9.1.1. Preparation of samples*

Samples of the $Ca_{10}(PO_4)_6(OH)_2$, $Ca_{10}(PO_4)_6F_{0.5}OH_{1.5}$, $Ca_{10}(PO_4)_6F_1OH_1$ $Ca_{10}(PO_4)_6F_{1.5}OH_{0.5}$ and $Ca_{10}(PO_4)_6F_2$ sol-gels were heated to 600$^oC$ for 2 hours in a hot air oven (Lenton Furnace, Lenton Thermal Designs Limited, UK) with a ramp of 5$^oC$ per minute, dwell time of 60 minutes and cool down rate of 10$^oC$ per minute. They were subsequently ball milled and passed through a sieve to a particle size of approximately 20 µm.

1.0g of the ball milled samples was subsequently placed in a jig and pressed to 7 tons. The pressing weight was determined by trial and error to produce a solid sample. The solid samples were then placed in 100ml of ultra pure water in a sealed container. A 10ml sample of the ultra pure water within which the sample was contained was removed at a predetermined time for ion chromatography analysis. To ensure that there was no dilution effect there was a sample produced for each time analysis period.

All samples were analysed in triplicate and a mean and standard deviation calculated.

### *9.1.2. Sample analysis protocol - $Ca^{2+}$ and $PO_4^{3-}$ ion release*

$Ca^{2+}$ and $PO_4^{3-}$ ion release for all the prepared samples was analysed daily for the first 7 days and then at weekly intervals for 7 weeks.

### *9.1.3. Effect of sol-gel heating temperature on $Ca^{2+}$ and $PO_4^{3-}$ ion release*

Three of the sol-gels were selected here for investigation. $Ca_{10}(PO_4)_6(OH)_2$, $Ca_{10}(PO_4)_6F_1OH_1$ and $Ca_{10}(PO_4)_6F_2$ sol-gels were heated to 600, 700, 800 and

1000$^{o}$C for 2 hours in a hot air oven (Lenton Furnace, Lenton Thermal Designs Limited, UK) with a ramp of 5$^{o}$C per minute, dwell time of 60 minutes and cool down rate of 10$^{o}$C per minute. They were subsequently ball milled to a particle size of approximately 20 µm, pressed and prepared as above.

### *9.1.4. Ion release*

Ion release profiles were investigated using a Dionex ICS – 1000 (Dionex Ltd, Surrey, UK) and a Dionex ICS – 2500 Ion Chromatograpy system (Dionex Lts, Surrey, UK). The ICS – 1000 with attached autosampler was used for the routine analysis calcium ($Ca^{2+}$) cations. The ICS – 2500 was used for the analysis of $PO_4^{3-}$.

#### *9.1.4.1. Cation release analysis:*

A 20mM Methanesulfonic acid (MSA, BDH, UK) solution was used as the eluent. The ICS – 1000 is an integrated and preconfigured system that performs isocratic IC separations using suppressed conductivity detection.

In this method, cations were eluted using a 4 x 250 mm IonPac® CS12A separator column. All results were calculated against a 4 –point calibration curve using the predefined calibration route. The samples were injected onto the system using a AS50 Autosampler (Dionex, Surrey, UK). The Chromeleon® software package was used for data analysis.

#### *9.1.4.2. Standard solution preparation*

To ensure the accuracy of the measuring system standard solutions were prepared which were analysed along with each run of the samples. Calcium chloride (Sigma, UK) was used as the base for the standard solutions. A 100 parts per million stock solution was prepared, from which three serially diluted

50, 20 and 1 part per million solutions were made. These four solutions acted as the standards.

#### *9.1.4.3. Anion release analysis*

The phosphate ($PO_4^{3-}$) anion measurements were conducted on a Dionex ICS – 2500 ion chromatography system (Dionex, Surrey, UK), consisting of a gradient pump with a 25 µl sample loop.

In this method the phosphates were eluted using a 4 x 250 mm IonPac® AS16 anion-exchange column packed with anion exchange resin. A Dionex ASRS® (Anion Self-Regenerating Suppressor) was used at 242 mA.

The Dionex EG50 eluent equipped with a KOH (potassium hydroxide) cartridge was used in conjuction with the ASRS®. The EG50 eluent generator system electronically produced high-purity KOH eluents using deionised water as the carrier stream to the point of use. On analysis the samples were injected onto the system using an AS50 Autosampler (Dionex, Surrey, UK). The Chromelon® softward package was used for data analysis.

#### *9.1.4.4. Standard solution preparation*

To ensure the accuracy of the measuring system standard solutions were prepared which were analysed along with each run of the samples. Sodium phosphate tribasic – $Na_3PO_4$ (Sigma-Aldrich, UK) was used as the base for the standard solutions. A 100 parts per million stock solution was prepared, from which three serially diluted 50, 20 and 1 part per million solutions were made. These four solutions acted as the standards.

## 9.2. Results

### *9.2.1. Ca $^{2+}$ and $PO_4^{3-}$ ion release*

The data obtained for the Ca $^{2+}$ ion release is shown graphically in figure 65.

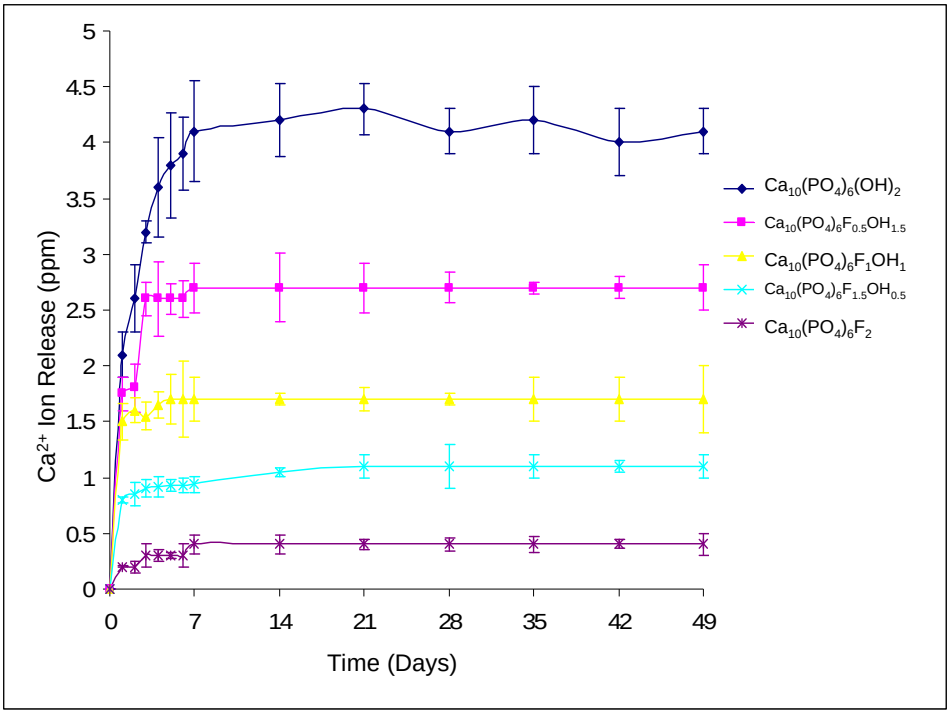


**Figure 65**: Calcium (Ca $^{2+}$) ion release from sol-gels heated to 600$^{o}$C, mean +/- standard deviation.

For all the powdered sol-gel samples there was a clear pattern to the dissolution behaviour of the $Ca^{2+}$ ions. There was a rapid increase in release of the $Ca^{2+}$ ions over the first seven days, this then stabilised to a similar level for the next seven weeks.

Throughout the periods the dissolution rates were markedly different between the different powdered sol-gels. The highest release of $Ca^{2+}$ ions was seen with $Ca_{10}(PO_4)_6(OH)_2$. Increase in the fluoride substitution of the apatite structure resulted in less $Ca^{2+}$ ions throughout, such as that the $Ca^{2+}$ ion release was $Ca_{10}(PO_4)_6(OH)_2$>$Ca_{10}(PO_4)_6F_{0.5}OH_{1.5}$>$Ca_{10}(PO_4)_6F_1OH_1$>$Ca_{10}(PO_4)_6F_{1.5}OH_{0.5}$> $Ca_{10}(PO_4)_6F_2$.

The data obtained for the $PO_4^{3-}$ ion release is shown graphically in figure 66.

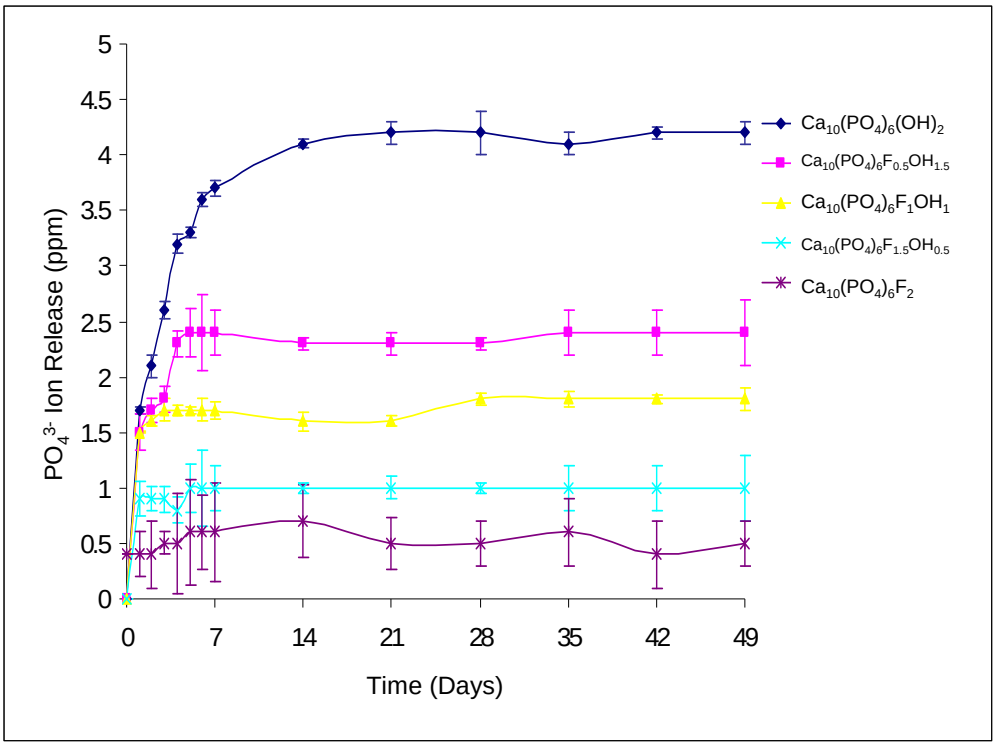


**Figure 66**: Phosphate ($PO_4^{3-}$) ion release from sol-gels heated to 600°C mean +/- standard deviation.

The pattern of the $PO_4^{3-}$ Ion release was very similar to the $Ca^{2+}$ release, as might be expected. For all the powdered sol-gel samples there was a clear pattern to the dissolution behaviour of the $PO_4^{3-}$ ions. There was a rapid increase in release of the $PO_4^{3-}$ ions over the first seven days, this then stabilised to a similar level for the next seven weeks.

Throughout the periods the dissolution rates were markedly different between the different powdered sol-gels. The highest release of $PO_4^{3-}$ ions was seen with $Ca_{10}(PO_4)_6(OH)_2$. Increase in the fluoride substitution of the apatite structure resulted in less $PO_4^{3-}$ ions throughout, such as that the $PO_4^{3-}$ ion release was $Ca_{10}(PO_4)_6(OH)_2$ > $Ca_{10}(PO_4)_6F_{0.5}OH_{1.5}$ > $Ca_{10}(PO_4)_6F_1OH_1$ > $Ca_{10}(PO_4)_6F_{1.5}OH_{0.5}$ > $Ca_{10}(PO_4)_6F_2$.

### *9.2.2. Effect of sol-gel heating temperature on $Ca^{2+}$ and $PO_4^{3-}$ ion release*

The data obtained for the $Ca^{2+}$ ion release for the $Ca_{10}(PO_4)_6(OH)_2$, $Ca_{10}(PO_4)_6F_1OH_1$ and $Ca_{10}(PO_4)_6F_2$ sol-gel heated to 600, 700, 800 and 1000°C is shown graphically in figures 67, 68, 69, 70, 71 and 72.

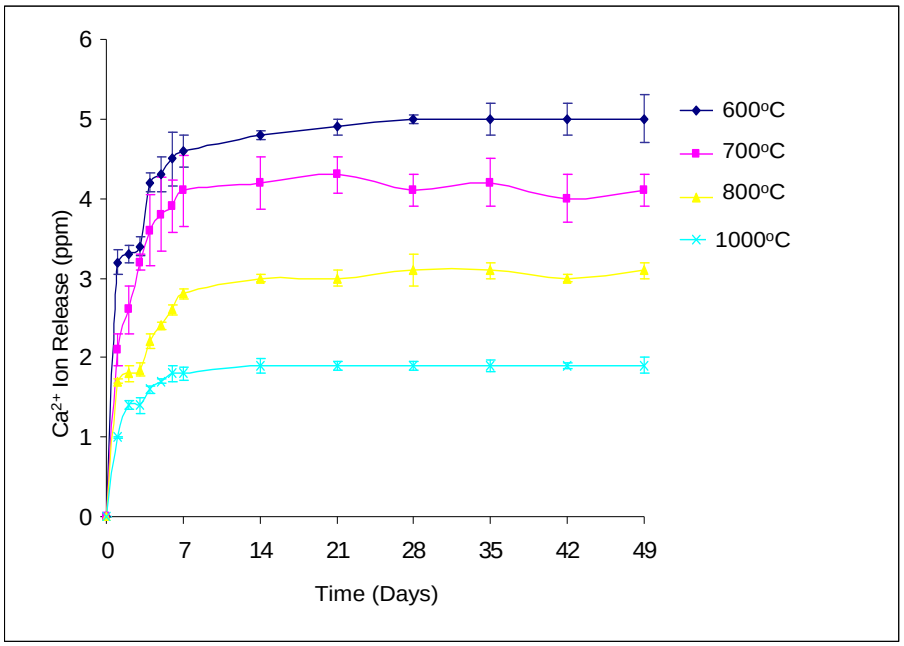


**Figure 67**: Graph to show mean (+/-SD) $Ca^{2+}$ ion release for the $Ca_{10}(PO_4)_6(OH)_2$ produced sol-gel heated to 600, 700, 800 and 1000°C

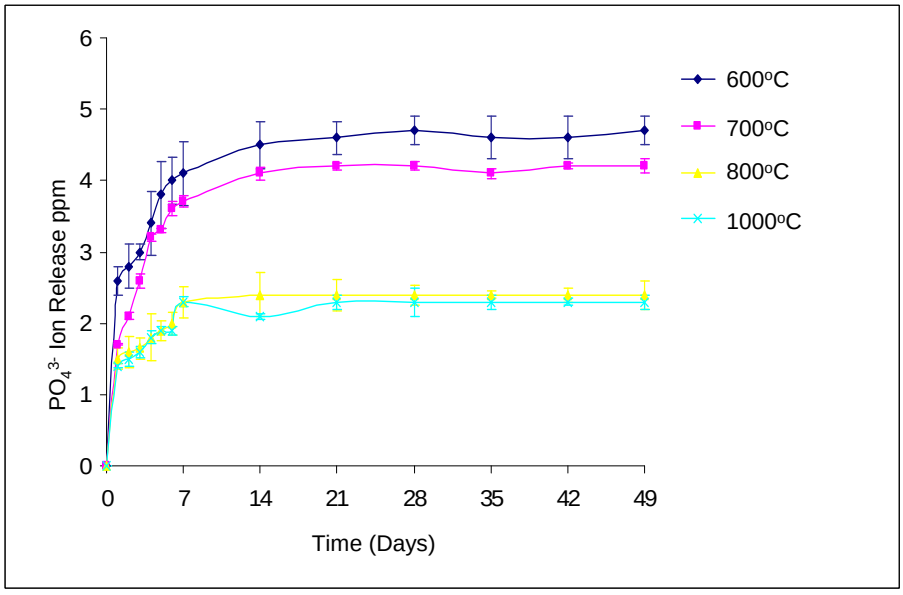


**Figure 68**: Graph to show mean (+/- SD) $PO_4^{3-}$ ion release for the $Ca_{10}(PO_4)_6(OH)_2$ produced sol-gel heated to at 600, 700, 800 and 1000°C.

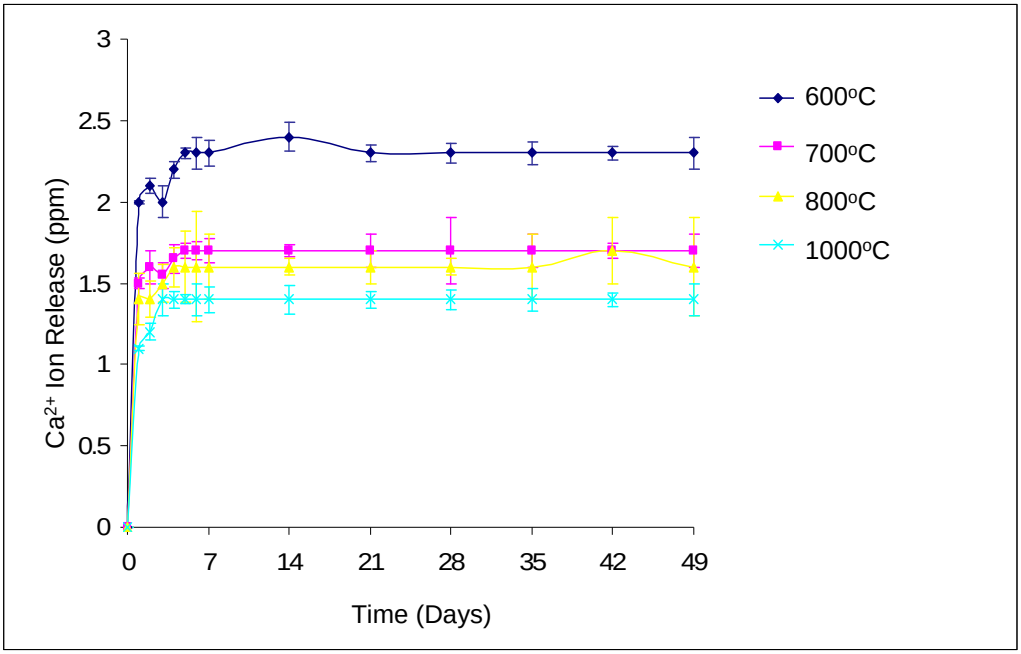


**Figure 69**: Graph to show mean (+/- SD) $Ca^{2+}$ ion release for the $Ca_{10}(PO_4)_6F_1OH_1$ produced sol-gel heated to 600, 700, 800 and 1000°C.

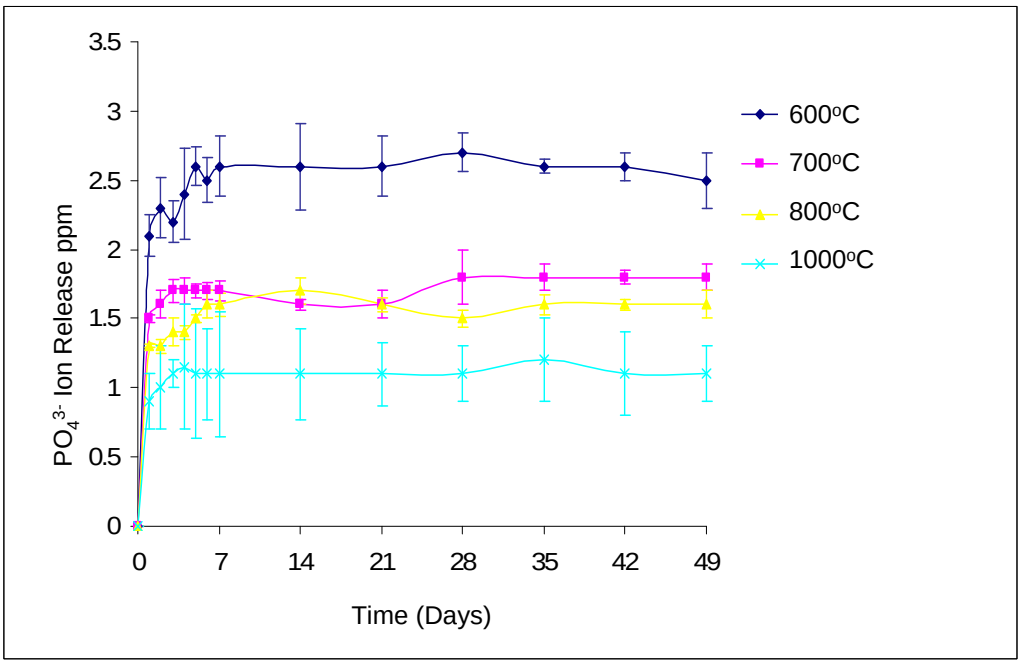


**Figure 70**: Graph to show mean (+/- SD) $PO_4^{3-}$ ion release for the $Ca_{10}(PO_4)_6F_1OH_1$ produced sol-gel heated to at 600, 700, 800 and 1000°C.

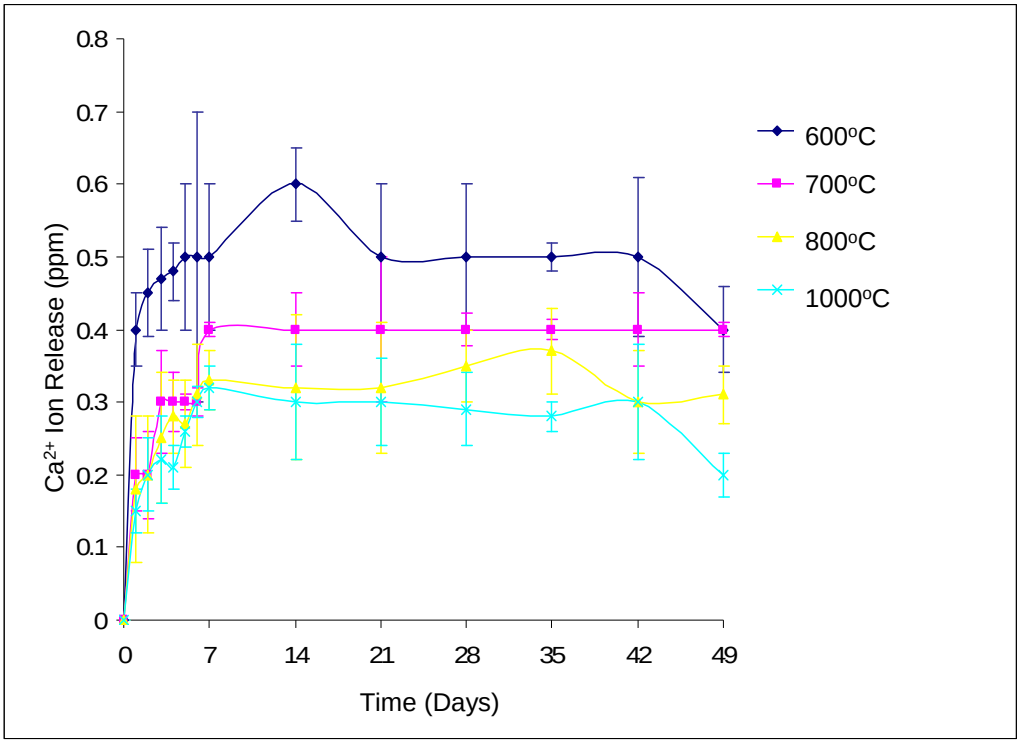


**Figure 71**: Graph to show mean (+/- SD) $Ca^{2+}$ ion release for the $Ca_{10}(PO_4)_6F_2$ produced sol-gel heated to 600, 700, 800 and 1000°C.

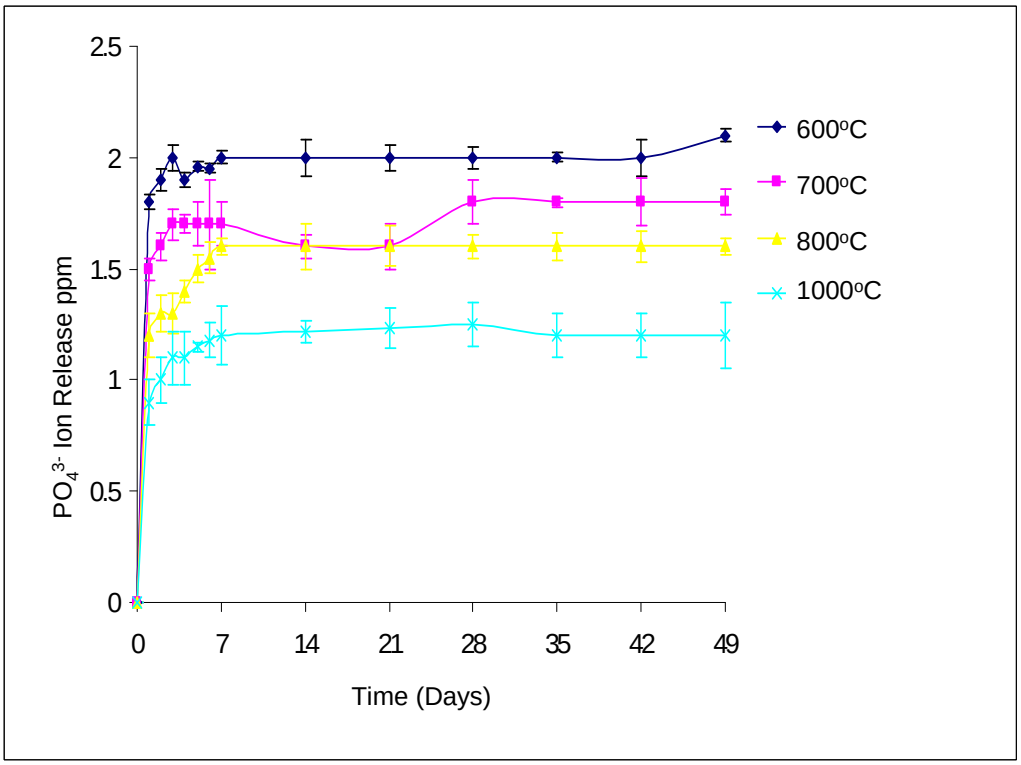


**Figure 72**: Graph to show mean (+/- SD) $PO_4^{3-}$ ion release for the $Ca_{10}(PO_4)_6F_2$ produced sol-gel heated to at 600, 700, 800 and 1000°C.

The pattern of the $Ca^{2+}$ and $PO_4^{3-}$ Ion release with different heating temperatures was very similar for all the samples. There was a rapid increase in release of the $PO_4^{3-}$ ions over the first seven days (as already discussed), this then stabilised to a similar level for the next seven weeks.

Throughout the periods the dissolution rates were markedly different within the sol-gels at different heating temperatures. The higher the temperature the sol-gel was heated to the lower to ion release. The ion release followed the pattern of $600^oC > 700^oC > 800^oC > 1000^oC$.

## 9.3. Discussion of ion release

### *9.3.1. Ion release*

One of the most important issues when considering hydroxyapatite (HA) for biological coatings is the dissolution rate in an environment where human body fluids exist. It has been reported that plasma-sprayed HA coatings dissolve and degrade quickly, resulting in the weakening of the coating-substrate bonding or the implant fixation to the host tissues (Jarcho, 1992; Bloebaum & Dupont, 1993; Overgaard et al., 1996). For this reason any changes to the HA that result in a higher chemical stability would be an advantage.

The ion release experimental methodology adopted, allows a possible insight to be gained of how the powders obtained by the sol-gels manufactured in this thesis, may behave in an environment where human body fluids exist. Despite many attempts it was not possible to record the fluoride ion release with the equipment available, therefore only $Ca^{2+}$ and $PO_4^{3-}$ ions were investigated in this thesis. $Ca^{2+}$ and $PO_4^{3-}$ ion release were chosen to observe the dissolution behaviour of each powder since the apatite structure is known to collapse by the release of these ions.

### *9.3.2. $Ca^{2+}$ and $PO_4^{3-}$ ion release*

For all the sol-gel powdered samples there was a clear pattern to the dissolution behaviour and release of the $Ca^{2+}$ and $PO_4^{3-}$ ions. The dissolution of all the powders showed an initial rapid increase over the first seven days, this then stabilised to similar level for the next seven weeks. Importantly, the fluoride substitution decreased the dissolution of the $Ca^{2+}$ and $PO_4^{3-}$ ions, that is with the dissolution rate in the order $Ca_{10}(PO_4)_6(OH)_2$ > $Ca_{10}(PO_4)_6F_{0.5}OH_{1.5}$ > $Ca_{10}(PO_4)_6F_1OH_1$ > $Ca_{10}(PO_4)_6F_{1.5}OH_{0.5}$ > $Ca_{10}(PO_4)_6F_2$.

Such a decrease in the dissolution rate of an apatite driven by the fluoride substitution can be potentially explained by the compositional and structural stability of each powder. In the powdered HA, the presence of any TCP and nonstoichiometric apatite can accelerate the dissolution rate. However, not only the phase-related parameters but also the size and crystallinity of the powder play a crucial role in the dissolution behaviours. When considering the improvement in the crystallinity and crystallite size of the fluoride substituted powders, such a retarded dissolution can be partially effected by the improvement in crystallisation. As a result of the observations in this thesis it is deduced that the fluoride substitution effectively controls the dissolution rate of an apatite powder and suggest the possibility of tailoring the solubility of any coatings made from the sol-gels through fluoride ion substitution.

The degree to which fluoride ion substitution has been able to be controlled in this study is novel and in combination with the above results suggests the potential for a whole new type of coating with different dissolution properties based on the level of fluoride substitution in the apatite structure. Moreover it can be proposed that the apatite powder substituted by the fluoride, may find a

use in systems that require controlled release rates, that is, systems delivering drugs and requiring low solubility.

### *9.3.3. Discussion of sol-gel heating temperature on $Ca^{2+}$ and $PO_4^{3-}$ ion release*

The dissolution behaviour and resultant $Ca^{2+}$ and $PO_4^{3-}$ Ion release with different heating temperatures was very similar for all the samples. There was a rapid increase in release of the $PO_4^{3-}$ ions over the first seven days (as already discussed), this then stabilised to a similar level for the next seven weeks. Importantly, the heating temperature was able to decrease the dissolution of the $Ca^{2+}$ and $PO_4^{3-}$ ions with all the samples obtained, that is with the dissolution rate in the order $600^oC > 700^oC > 800^oC > 1000^oC$.

Such a decrease in the dissolution rate of an apatite driven by the temperature to which the apatite has been heated can again be explained by the compositional and structural stability of each powder. In the powdered HA, the presence of any TCP and nonstoichiometric apatite can accelerate the dissolution rate. The previous results in this thesis have shown that increasing the heating temperature from 600 to $1000^oC$ improves the crystallinity and decreases the crystal size of the HA/FHA/FA powders, such a retarded dissolution can be partially affected by the improvement in crystallisation. As a result of the observations in this thesis it is deduced that heating of the apatite structure from 600 to $1000^oC$ is effectively able to control the dissolution rate of an apatite powder and suggest the possibility of tailoring the solubility of any coatings made from the sol-gels through controlled heating.

As already discussed any change to HA that results in a higher chemical stability would be an advantage. In all cases the higher the temperature the sol-gel was heated to, the lower the ion release. This has not been reported before

and again excitingly this suggests the possibility of tailoring the solubility of any coatings made from the sol-gels through increasing the firing temperature. Moreover it can again be proposed that the apatite powders produced by the sol-gel technique investigated in this study, may find a use in systems that require controlled release rates, that is, systems delivering drugs and requiring low solubility.

# Chapter 10 :

# Hydroxyapatite $Ca_{10}(PO_4)_6OH_2$,

# Fluorapatite $Ca_{10}(PO_4)_6F_2$ &

# Fluor-hydroxyapatite $Ca_{10}(PO_4)_6OH_xF_y$

# Sol-gel Coatings on Titanium

# Scanning Electron Microscopy

## 10.1. Methods & Materials

### *10.1.1. Protocol for preparation of titanium disks*

8mm disks of commercially pure titanium were prepared using the standardised protocol;

Samples were mounted using Struers (Struers Ltd, UK) tape on a mounting block such that 7 would fit on a 30mm block.

#### *10.1.1.1. Grinding*

Initial grinding was undertaken using 1200 grit paper on a Struers RotoPol (Struers Ltd., UK) for 5 minutes using a 5 N force and 300 rpm under water spray to cool and remove debris. Samples were then placed upside down in a beaker with water in an ultrasonic bath for 30 seconds and subsequently rinsed under running water for 30 seconds.

Further grinding was undertaken on the Struers RotoPol (Struers Ltd., UK) with 2400 grit paper for 5 minutes using a 5 N force and 300rpm. Samples were then placed upside down in a beaker with water in an ultrasonic bath for 30 seconds and subsequently rinsed under running water for 30 seconds. Care was taken to ensure that all particles were removed as transfer of any to the subsequent polishing cloth would be detrimental to the polishing process.

#### *10.1.1.2. Polishing*

100ml of silica suspension was placed in a beaker and 10 ml of 30% hydrogen peroxide was added. This solution was dispensed onto a polishing cloth. The polishing cloth was placed on the Struers RotoPol (Struers Ltd., UK) and the samples polished for 10 minutes using a 5 N force and 150 rpm. Samples were

then placed upside down in a beaker with water in an ultrasonic bath for 30 seconds and subsequently rinsed under running water for 30 seconds.

#### *10.1.1.3. Cleaning*

A sharp metal blade was slid under each disk to prise it from the mounting tape. The disks were placed in a beaker of acetone in an ultra-sonic bath for 1 minute. The disks were removed, dried and added to another beaker containing propan-2-ol (IPA, UK) in the ultra-sonic bath for 1 minute. The disks were removed from this solution, dried and then placed in a beaker containing ultra-pure water in the ultra-sonic bath for 1 minute. On removal the disks were dried, placed in a sealed container and were ready for coating.

### *10.1.2. Establishment of sol-gel coating technique*

#### *10.1.2.1. Motor*

To establish a spinning platform a motor (Dell, UK) was wired to a power supply (Weir, 403D, UK, Ltd.). The titanium disks were adhered to this platform with Struers tape (see figure 73).


**Figure 73**: Fan motor wired to Weir 403D power supply.

A small white dot was placed on top of the platform and with a strobe the voltage and corresponding revolutions per minute (rpm) of the platform established. When the dot became fixed in one position under the strobe this was directly correlated to the rpm.

The central point of the platform was determined and marked. This allowed identical placement of the prepared 8mm Titanium disks attached with Struers tape in the centre.

#### *10.1.2.2. Coating protocol*

1ml of the sol-gels [$Ca_{10}(PO_4)_6(OH)_2$, $Ca_{10}(PO_4)_6F_{0.5}OH_{1.5}$, $Ca_{10}(PO_4)_6F_1OH_1$, $Ca_{10}(PO_4)_6F_{1.5}OH_{0.5}$ or $Ca_{10}(PO_4)_6F_2$] were drawn up in to a pipette. Using a clamp the pipette tip was centred over the spinning disk and set at a distance of 20mm.

The rpm of the disk was set at different speeds and 0.5ml of the sol-gels dispensed on to the disk. The disks were then heated to 1000$^{o}$C in a furnace (Lenton Furnace, Lenton Thermal Designs Limited, UK) with a ramp of 5$^{o}$C per minute, dwell time of 60 minutes and cool down rate of 10$^{o}$C per minute.

### *10.1.3. Scanning Electron Microscopy*

#### *10.1.3.1. Surface morphology*

Once the sol-gels had been coated onto the titanium disks and heated in the hot air oven, they were prepared for analysis with scanning electron microscopy.

All samples were mounted onto 0.5 inch aluminium SEM stubs (Agar Scientific, Essex, UK) with 12 mm conducting carbon tabs (Agar Scientific, Essex, UK). Subsequently they were sputter coated with gold/palladium (Polaron E5000,

Quorum Technology, UK) at 1.5kV and 2mA for 90 seconds. Samples were examined in a JEOL 5410LV SEM (JEOL UK, Herts, UK) operating at 10kV. Each sample was viewed at a working distance of 15mm and at x50, x100, x200, x500 x1,000 and x2,000 magnifications. All digital images were acquired using INCA 300 software (Oxford Instruments, Berks. UK)

### *10.1.3.2 Coating thickness and surface interaction*

To assess the coating thickness, six of each group of the sol-gel titanium disks [$Ca_{10}(PO_4)_6(OH)_2$, $Ca_{10}(PO_4)_6F_{0.5}OH_{1.5}$, $Ca_{10}(PO_4)_6F_1OH_1$, $Ca_{10}(PO_4)_6F_{1.5}OH_{0.5}$, $Ca_{10}(PO_4)_6F_2$] were placed in a multi-clip holder (Struers Ltd., UK), which was subsequently placed in to pots (Struers Ltd., UK ) and filled with Specifix-20 epoxy resin (Struers Ltd., UK). Using a band saw (Exact, UK) the disks were then sectioned through the middle (see figure 74 to 76).

**Figure 74**: Coated Ti disks mounted in epoxy resin.

**Figure 75**: Sectioning through disks with band saw

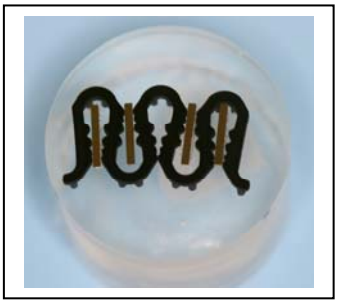

**Figure 76**: Picture of coated disks after sectioning.

The surface of the embedded samples was then ground and polished using the same protocol as for the titanium disks in sections 10.1.1.1. and 10.1.1.2. The samples were prepared for SEM analysis by mounting onto 0.5 inch aluminium SEM stubs (Agar Scientific, Essex, UK) with 12 mm conducting carbon tabs (Agar Scientific, Essex, UK). Subsequently they were sputter coated with carbon (Polaron E5000, Quorum Technology, UK) at 1.5kV and 2mA for 90 seconds. Samples were examined in a JEOL 5410LV SEM (JEOL UK, Herts,

UK) operating at 10kV. Each sample was viewed at a working distance of 15mm and at x50, x100, x200, x500 x1,000 and x2,000 magnifications. All digital images were acquired using INCA 300 software (Oxford Instruments, Berks. UK). The thickness was measured using scanning electron microscopy at 5 random areas.

The interaction between the surface of the titanium and the coating was investigated using INCA 300 software (Oxford Analytical, Berks, UK). This software allowed the precise chemical constituents and their relative levels at different areas to be investigated.

## 10.2. Results

### *10.2.1. Coating protocol*

Table 23 summarises the voltage of the power supply and corresponding rpm determined with the strobe.

| VOLTAGE (v) | Revs / Minute (rpm) |
|---|---|
| 4 | 850 |
| 5 | 1215 |
| 6 | 1640 |
| 7 | 2035 |
| 8 | 2430 |
| 9 | 2825 |
| 10 | 3220 |
| 11 | 3615 |
| 12 | 4010 |

**Table 23**: Voltage of the power supply and corresponding rpm of the table on the motor as determined by a strobe.

From the data in table 23 it can be seen that after 4 volts for every 1 volt increase the rpm is increased by 395. The maximum voltage the set up would run to was 12 volts / 4010 rpm.

Due to the viscosity of the sol-gels voltages up to 7 volts (2035 rpm) proved to be insufficient to centrifuge the coating over the entire 8mm diameter of the disk. Voltages of 8 volts (2430 rpm) produced a visually uniform coating on the Titanium.

### *10.2.2. Surface morphology of coatings*

Examples of the scanning electron micrographs obtained for the surface morphology are shown in figures 77, 78, 79 and 80.

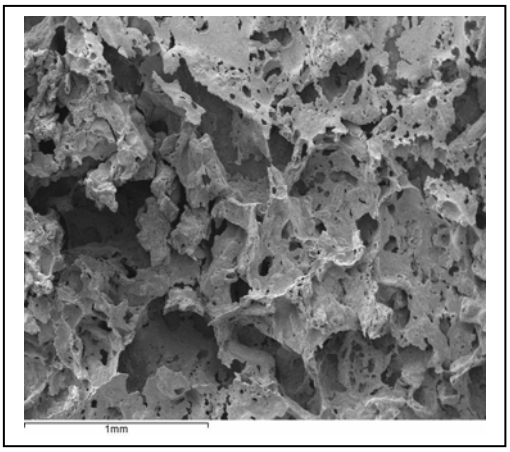


**Figure 77**: SEM of typical coating at 2430 rpm

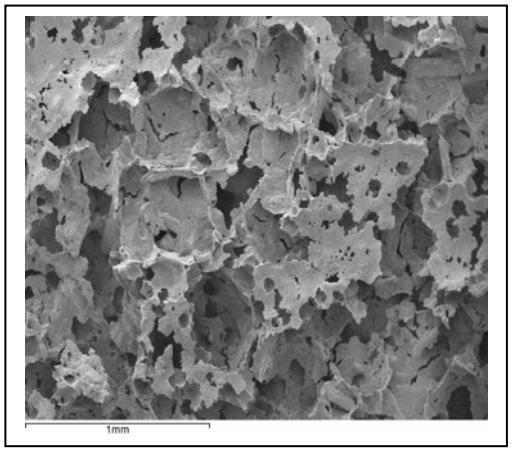


**Figure 78**: SEM of typical coating at 2825 rpm

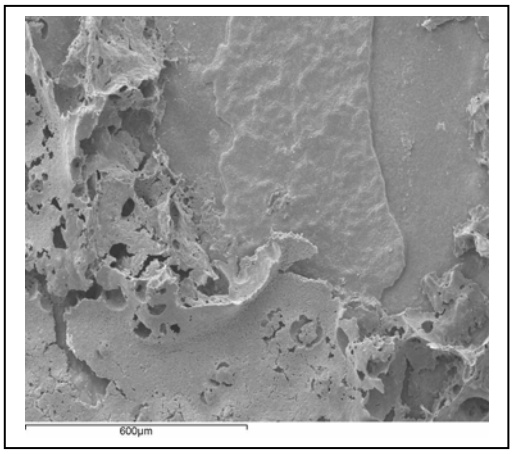


**Figure 79**: SEM of typical coating at 3220 rpm

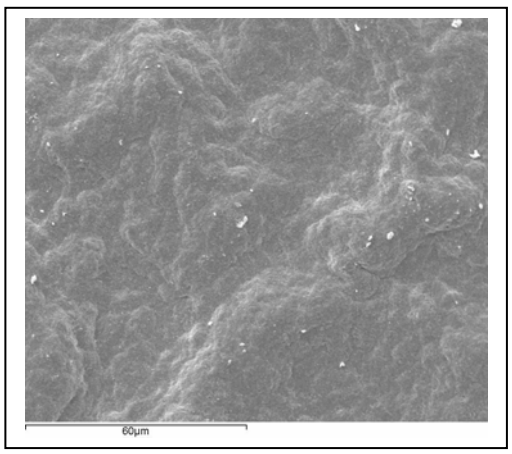


**Figure 80**: SEM of typical coating at 3615 rpm

With reference to the SEM's in figures 77 - 80 the following can be seen;

- At low spinning speeds i.e. 2430 and 2825, the coatings are very porous.
- As the spinning speed increased the coating becomes more uniform.
- At speeds of 3615 and above all of the sol-gels resembled the uniform smooth surface seen in figure 80.

The patterns noted above were similar with all the sol-gels [$Ca_{10}(PO_4)_6(OH)_2$, $Ca_{10}(PO_4)_6F_{0.5}OH_{1.5}$, $Ca_{10}(PO_4)_6F_1OH_1$, $Ca_{10}(PO_4)_6F_{1.5}OH_{0.5}$, $Ca_{10}(PO_4)_6F_2$].

There were no individual features noticed that were different under SEM of the five different sol-gels tested.

### *10.2.3. Coating thicknesses*

Table 24 summarises the mean and standard deviation (from 5 readings) of data obtained for the sol-gel coating thickness obtained with rpm.

| rpm | Sol-gel Coating, $Ca_{10}(PO_4)_6$… Thickness (μm) Mean (+/- Standard Deviation) | | | | |
|---|---|---|---|---|---|
| | $(OH)_2$ | $F_{0.5}OH_{1.5}$ | $F_1OH_1$ | $F_{1.5}OH_{0.5}$ | $F_2$ |
| **2430** | 24.6(+/-2.81) | 25.7(+/-3.26) | 25.9 (+/-2.94) | 27.3(+/-3.61) | 28.1(+/-3.14) |
| **2825** | 18.3(+/-0.68) | 21.1(+/-2. | 22.6(+/-2.05) | 22.8(+/-1.86) | 23.1(+/-1.67) |
| **3220** | 5.41(+/-0.44) | 5.65(+/-2.11) | 6.99(+/-1.44) | 7.01(+/-1.89) | 8.36(+/-1.77) |
| **3615** | 1.32(+/-0.22) | 1.48 (+/-0.16) | 1.38 (+/-0.38) | 1.52(+/-0.16) | 1.46 (+/-0.22) |
| **4010** | 1.21 (+/-0.10) | 1.31 (+/- 0.16) | 1.37(+/-0.22) | 1.41(+/-0.08) | 1.43(+/-0.21) |

**Table 24**: Mean and standard deviation obtained for the sol-gel coating thickness with different rpm.

There are some clear trends that can be seen in table 24:

(1) As the spinning speed is increased overall the coating thickness decreases.

(2) In general the coating thickness increases with increasing substitution of fluoride, such that the coating thickness of the sol-gel derived apatites was $Ca_{10}(PO_4)_6F_2$ > $Ca_{10}(PO_4)_6OH_{0.5}F_{1.5}$ > $Ca_{10}(PO_4)_6OH_1F_1$ > $Ca_{10}(PO_4)_6OH_{0.5}F_{1.5}$ > $Ca_{10}(PO_4)_6(OH)_2$.

(3) Throughout there were large decreases in the coating thickness from 2430 – 3220 rpm.

(4) There were minimal differences between the coating thicknesses between 3615 and 4010 rpm.

### *10.2.4. SEM's of different coating thicknesses*

Figures 81 – 84 show examples of SEM's obtained with different coating speeds. Note the faster the spinning speed the thinner the coating

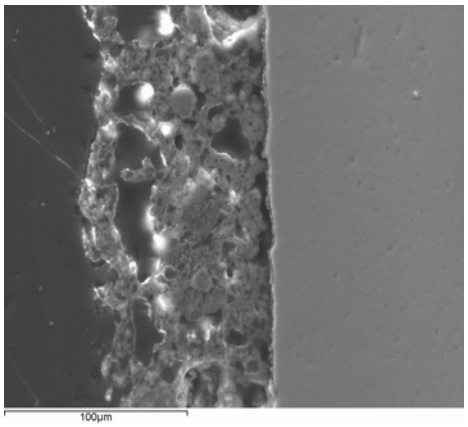


**Figure 81**: $Ca_{10}(PO_4)_6F_2$ coated at 2430 rpm.

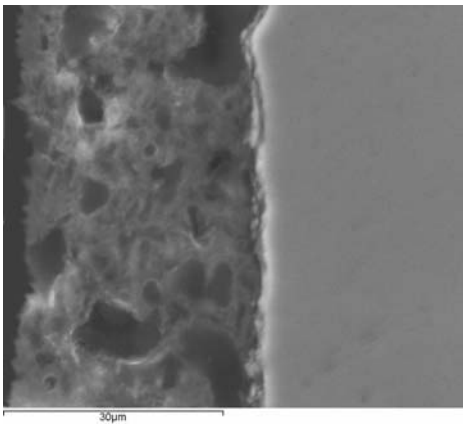


**Figure 82**: $Ca_{10}(PO_4)_6F_2$ coated at 2825 rpm.

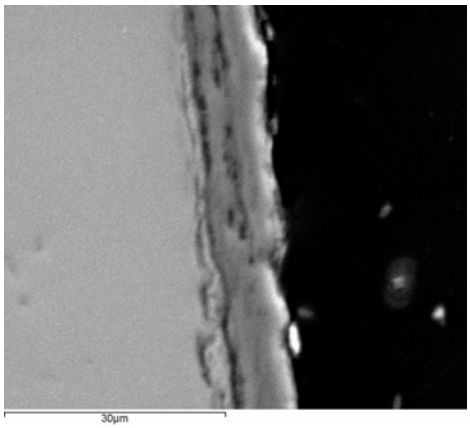


**Figure 83**: $Ca_{10}(PO_4)_6F_2$ coated at 3220 rpm.

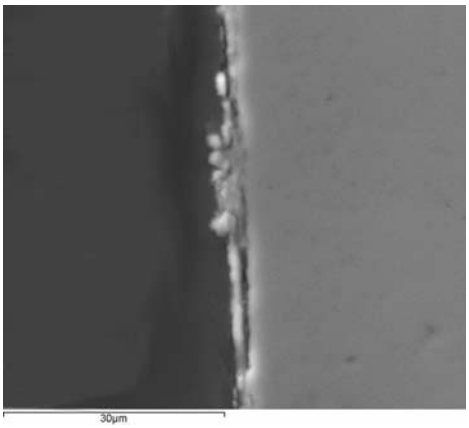


**Figure 84**: $Ca_{10}(PO_4)_6F_2$ coated at 4010 rpm.

### *10.2.5. Surface interaction*

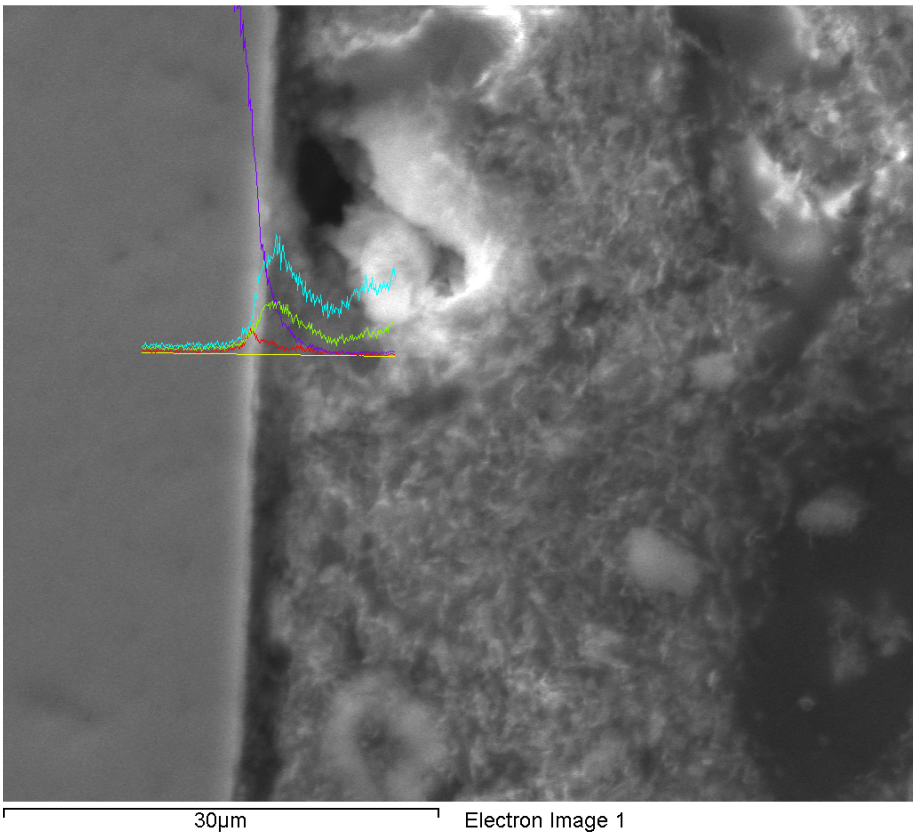


**Figure 85:** SEM and use of INCA software to explore surface interaction – $Ca_{10}(PO_4)_6(OH)_2$.

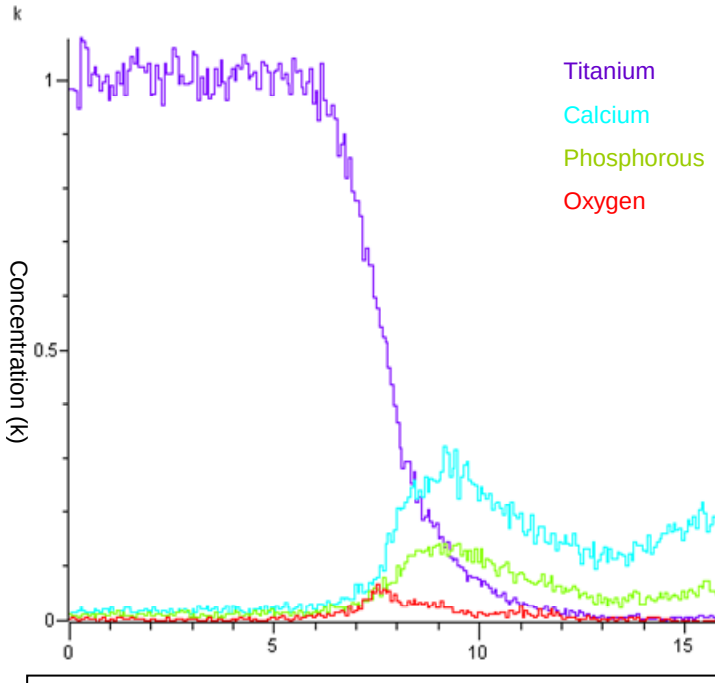


**Figure 86:** Enlargement of graph in Figure 85 showing interaction between titanium and $Ca_{10}(PO_4)_6(OH)_2$ coating.

The SEM and INCA software proved to be an excellent method of exploring the surface interactions between the hydroxyapatite and titanium. With reference to figures 85 and 86 there are several observations that can be seen. On the surface of the titanium there is a thin white band approximately 1µm in width this represents the titanium dioxide layer ($TiO_2$). There is diffusion of both calcium (Ca) and phosphorous (P) and titanium (Ti) in to the dioxide layer.

There appears to be diffusion of titanium ions not only into the oxide layer but beyond into the hydroxyapatite. There is a reaction zone which is present around the oxide layer where the levels of both calcium and phosphorous are increased. The coexistence of the Ca and P ions within the titanium dioxide suggests the possible occurrence of chemical bonds between the Ca and P from the hydroxyapatite coating and the Ti substrate.

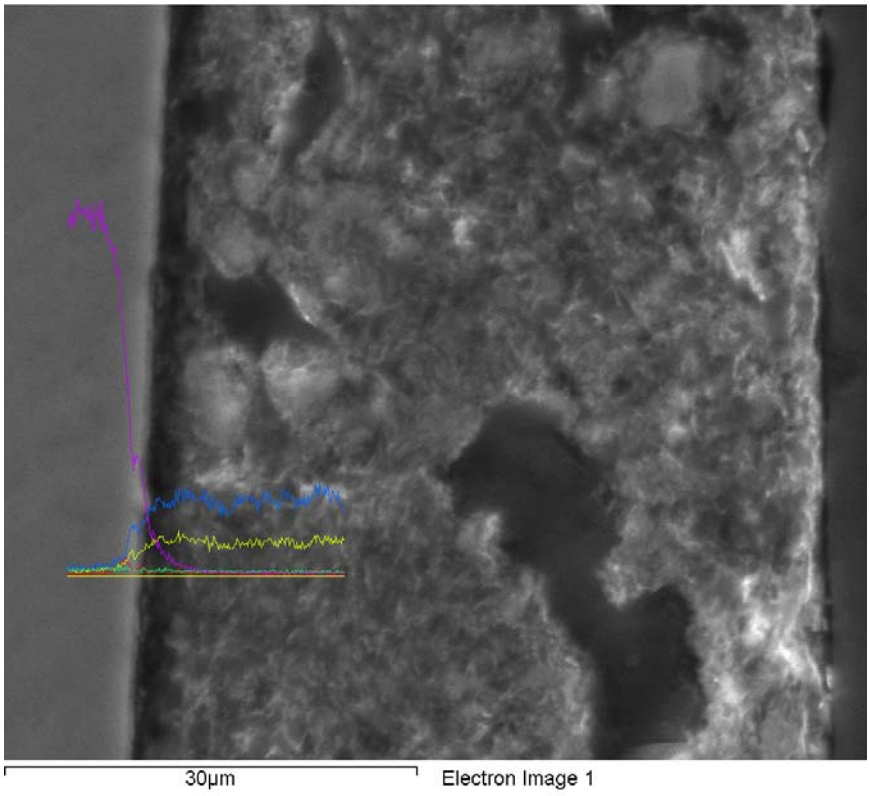


**Figure 87:** SEM and use of INCA software to explore surface interaction – $Ca_{10}(PO_4)_6F_2$.

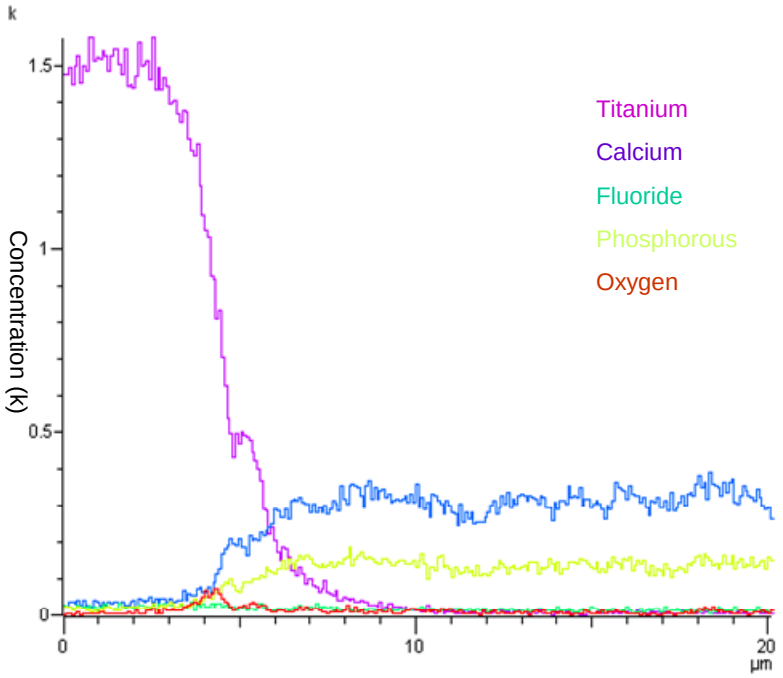


**Figure 88:** Enlargement of graph in Figure 87 showing interaction between titanium and $Ca_{10}(PO_4)_6F_2$ coating.

The SEM and INCA software were used to investigate the surface interaction between fluorapatite and titanium. The results of this are shown in figures 87 and 88, with reference to these there are several observations that can be seen. The presence of the oxide layer can again be seen as a thin white band approximately 1µm in width. There is diffusion of Ca, P and Ti into the oxide layer again forming a reaction zone, however this is much less well pronounced than that found with the hydroxyapatite. The levels of fluoride (F) do not appear to be changing at any point, this suggests that the F does not contribute to any form of chemical bonding with the Ti substrate and that any chemical bonding occurring is solely the result of Ca and P.

## 10.3. Discussion of sol-gel coating technique

### *10.3.1. Preparation of titanium disks*

To standardise all the coating techniques it was essential that the substrate surface i.e. the surface of the titanium disks were identical. To ensure this a protocol was adopted, firstly to the grind the surface and then to polish the surfaces using an identical technique. The protocol adopted was successful and resulted in a mirror finish which was identical for all the titanium surfaces.

### *10.3.2. Sol-gel coating technique*

There were two potential possibilities for coating with sol-gels, these are dip-coating and spin-coating. When coating implants it has been suggested that a thin uniform coating is desirable (Gan & Ben-Nissan, 1997) and that a spin coating technique offers the best way to achieve this type of coating (Kim et al., 2005). It was for this reason that a spin coating protocol was adopted.

A simple and cheap, but effective method was sought to achieve the spin coating. It was decided that a simple motor could be useful for this purpose. The motor was wired to a power supply and it could be clearly seen that the spinning speed of the platform could be altered by changing the voltage in the power supply.

The titanium disks could be adhered to the motor platform, directly in the central portion. The next problem to solve was to relate exactly the voltage and corresponding spinning speed. To achieve this, a small white dot was placed on top of the motor platform and with a strobe, the voltage and corresponding revolutions per minute (rpm) of the platform was established. This showed that after 4 volts for every 1 volt increase the spinning speed increased by 395rpm.

By trial and error it was established that a distance of 20mm from the motor platform resulted in suitable administration of the coating. Due to the viscosity of the sol-gels up to 7 volts (2035rpm) was insufficient to centrifuge the coating.

The simple technique of spin coating adopted here proved to be an effective, efficient, simple and cheap method of coating the sol-gels on to the titanium disks. It is novel and has not been reported before.

### *10.3.3. Surface morphology of coatings*

The scanning electron micrographs obtained showed clearly that the spinning speed had an effect on the surface morphology of the coating. This appears not to have been reported in the literature before with specific regards to coating titanium.

At low spinning speeds it was found that coatings were very porous and would probably be of insufficient strength to be of clinical use as a coating. As the spinning speed increased the coating became more uniform, with a speed of 3615 rpm being optimal to produce a uniform smooth coated surface. Speeds in excess of 4010 rpm resulted in the sol-gel coating being centrifuged and almost entirely removed from the surface of the titanium.

There are no differences noted between the actual surface morphology obtained with all the sol-gels [$Ca_{10}(PO_4)_6(OH)_2$, $Ca_{10}(PO_4)_6F_{0.5}OH_{1.5}$, $Ca_{10}(PO_4)_6F_1OH_1$, $Ca_{10}(PO_4)_6F_{1.5}OH_{0.5}$, $Ca_{10}(PO_4)_6F_2$]. The pattern of surface morphology obtained with 3615 rpm is consistent with other spin coating patterns of hydroxyapatite that have been seen in the literature (Gan & Pillar, 2004; Kim et al., 2004c; Zreiqat et al., 2005)

### *10.3.4. Coating thickness*

From the results it can be clearly seen that the spinning speed (within certain parameters) could be used to dictate the coating thickness. This is an extremely useful finding using the sol-gel technique to coat titanium.

The parameters for coating speed ranged from 2430 rpm to 4010 rpm. Any speed less that 2430rpm was insufficient to centrifuge the sol-gel coating, any speed over 4010rpm was too fast and all the coating was centrifuged off – this was without exception regardless of type of coating. The optimum spinning speed appeared to be 3615 rpm – increasing the speed above this caused little change in the coating thickness.

There was a general trend that the coating thickness increased with increasing substitution of fluoride, such that the coating thickness of the sol-gel derived apatite's was $Ca_{10}(PO_4)_6F_2$ > $Ca_{10}(PO_4)_6OH_{0.5}F_{1.5}$ > $Ca_{10}(PO_4)_6OH_1F_1$ > $Ca_{10}(PO_4)_6OH_{1.5}F_{0.5}$ > $Ca_{10}(PO_4)_6(OH)_2$. This could well be related to the earlier reported differences in contact angle and rheological properties of the fluoride substituted apatite's when compared to hydroxyapatite. It was found that the higher the level of fluoride substitution the higher the viscosity and contact angle – as a result with all other variables the same, the higher level of substitution of fluoride, the higher the sol-gel viscosities.

The actual thicknesses of coating are in line with what has been previously reported for hydroxyapatite in the literature using a spin coating technique (Gan & Pillar, 2004; Hsieh et al., 2002).

### *10.3.5. Surface interaction*

The results of the surface interaction showed the presence of an oxide layer on the surface of the titanium with both the $Ca_{10}(PO_4)_6(OH)_2$ and the $Ca_{10}(PO_4)_6F_2$ tested. The oxide layer was seen to be approximately 1µm in thickness. It is well established that titanium oxidises rapidly on exposure to air (Albrektsson et al., 1985) and this is confirmed in the results seen here.

With both the coatings tested the calcium and phosphorous could be seen to be interacting with the titanium oxide surface. The coexistence of the calcium and phosphorous ions within the titanium oxide suggests the occurrence of chemical bonds between the coatings and titanium substrate and supports the finding of an earlier study (Ong & Lucas, 1998). Furthermore this is suggestive that the bond strengths achieved between the apatites and the titanium are not just by micromechanical retention. The idea of some form of chemical / ionic bond between hydroxyapatite and titanium dioxide ($TiO_2$) seem to be supported by the results of this thesis.

In both cases the calcium concentration is greater than the phosphorous concentration at the surface. This may suggest that the calcium has a more significant role in the bonding than the phosphorous, although this needs further investigation.

On further investigation of the surface interaction found with the $Ca_{10}(PO_4)_6F_2$ it is interesting to note that the levels of fluoride ions are always around the zero mark, this clearly indicated that the fluoride content has no role in the chemical interaction between the titanium and the fluorapatite coating, and that in the fluoride substituted coatings, the chemical bonding / interchange seen can be solely attributed to the calcium and phosphorus ions.

# Chapter 11 :

# Hydroxyapatite $Ca_{10}(PO_4)_6OH_2$,

# Fluorapatite $Ca_{10}(PO_4)_6F_2$ &

# Fluor-hydroxyapatite $Ca_{10}(PO_4)_6OH_xF_y$

# Sol-gel Coatings on Titanium

# Shear Bond Strengths

## 11. Bond strength of sol-gel coatings

### *11.1. Methods & materials*

The commercially pure titanium disks were prepared using the protocol previously described. The disks were then sandblasted with 50μm aluminium oxide for 5 seconds at a set distance of 10mm at 2.5 bar pressure, they were subsequently steam cleaned for 30 seconds at a distance of 10mm. 0.5ml of the sol-gels [$Ca_{10}(PO_4)_6(OH)_2$, $Ca_{10}(PO_4)_6F_{0.5}OH_{1.5}$, $Ca_{10}(PO_4)_6F_1OH_1$, $Ca_{10}(PO_4)_6F_{1.5}OH_{0.5}$, $Ca_{10}(PO_4)_6F_2$] was centred over the disks spinning at 3615 rpm and dispensed at a distance of 20mm. The disk was allowed to spin for a further 30 seconds and then removed from the platform (see figures 89, 90 and 91).

**Figure 89**: 0.5ml of sol-gel being drawn up in syringe

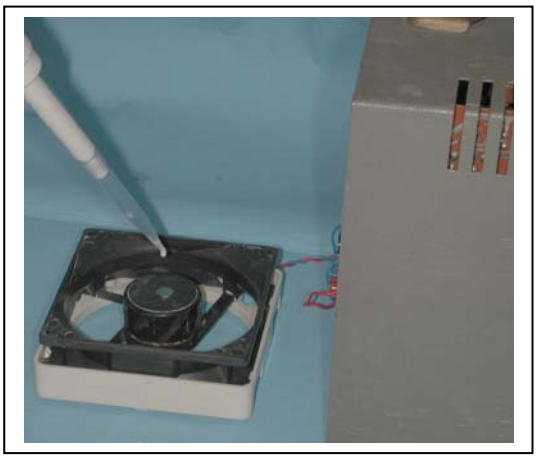

**Figure 90**: Set up for coating disk.

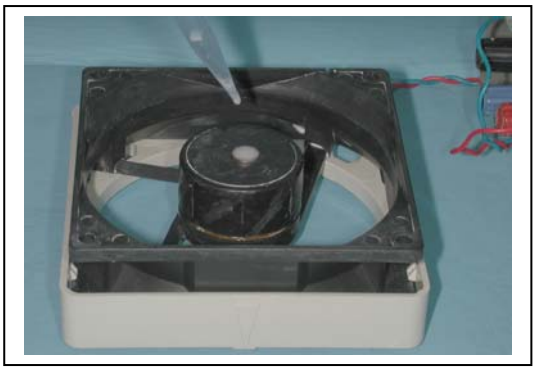

**Figure 91**: Sol-gel coated disk

The disks were then heated to 600, 700, 800 & 1000$^{o}$C in a hot air oven (Lenton Furnace, Lenton Thermal Designs Limited, UK) with a ramp of 5$^{o}$C per minute, dwell time of 60 minutes and cool down rate of 10$^{o}$C per minute (see figure 92).

**Figure 92**: Coated titanium disks after firing

4mm diameter titanium alloy (Ti-6Al4V) rods were prepared to a cylindrical length of 3mm and one of the end surfaces sandblasted with 50µm aluminium oxide. Using cyanoacrylate adhesive (GS, UK Ltd.) the sandblasted end of the disk attached to the centre of the coated disk (see figures 93 and 94).

**Figure 93:** Cyanoacrylate attached to sandblasted Ti-6Al4V rod.

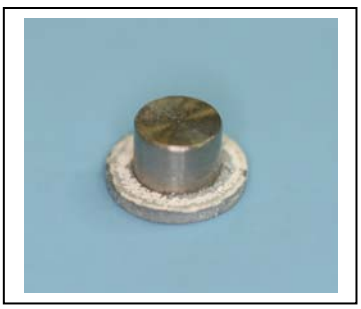

**Figure 94:** Ti-6Al4V rod attached to coated Ti disk.

A mounting assembly was designed and made to hold the disk for shear testing in an Instron Universal load testing machine (Instron Corporation, Buckinghamshire, UK) [see figure 95 and 96].

**Figure 95**: Assembly for mounting disk in Instron Universal load testing machine.

**Figure 96**: Constructed assembly ready for shear testing.

The Instron Universal load testing machine was connected to a computer installed with a soft ware package (series 1x automated materials testing system, version 5.34.09), and activated to apply a compressive load to the shearing blade at a crosshead speed of 5.0 mm per minute. The mounting assembly was positioned in the machine (see figures 97 and 98).

**Figure 97**: Assembly mounted in Instron machine.

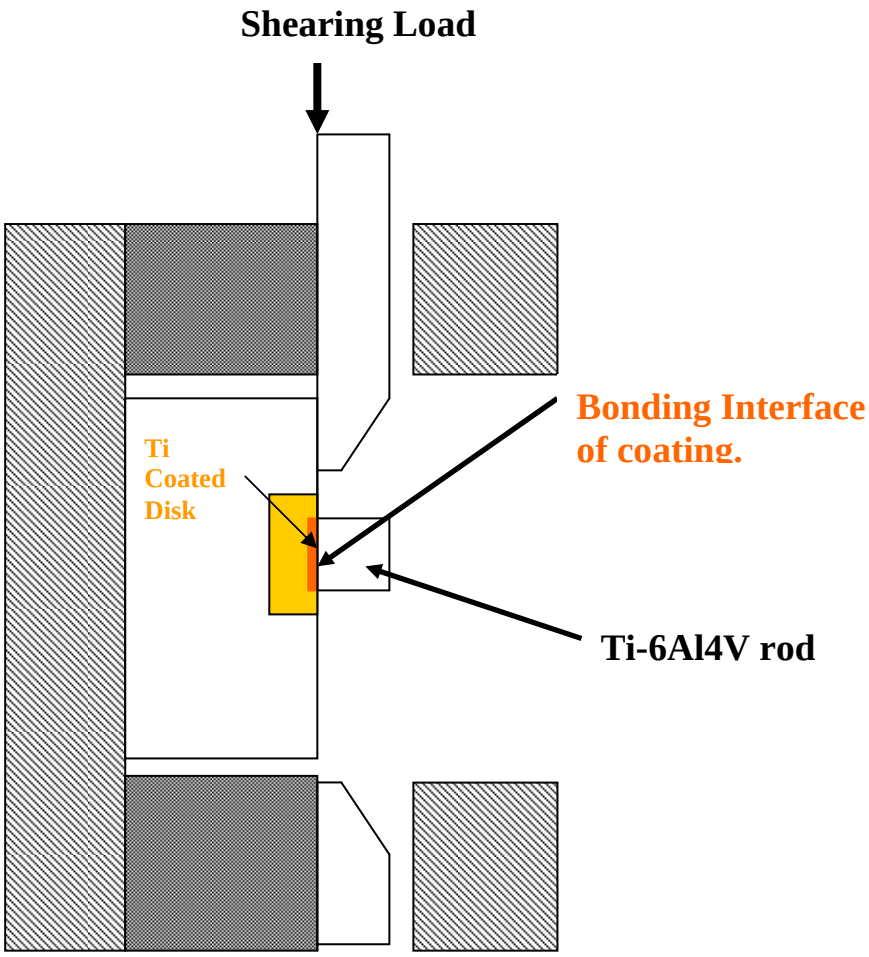


**Figure 98**: Schematic representation of mounting in Instron Machine.

Each test run was carried out having reset the computer to zero. The test was started via the keyboard and was observed on the computer screen. It was possible to observe the separation as a defined event where the peak force fell away rapidly.

Fifteen coated samples were prepared in each of the sol-gel groupings [$Ca_{10}(PO_4)_6(OH)_2$, $Ca_{10}(PO_4)_6F_{0.5}OH_{1.5}$, $Ca_{10}(PO_4)_6F_1OH_1$, $Ca_{10}(PO_4)_6F_{1.5}OH_{0.5}$, $Ca_{10}(PO_4)_6F_2$] at each heating temperature (600, 700, 800 and 1000$^oC$) giving a total of 300 test samples.

The load at failure was recorded in Kilonewtons (KN) and then converted to shear bond strength in Megapascals (MPa), using the formula:

$$\frac{\text{Kilonewtons} \times 1000}{\pi r^2} = \text{MPa}$$

(r = radius in millimetres)

### *11.1.1. Analysis*

#### *11.1.1.1.Optical microscope*

The de-bonded surfaces were then observed under an optical microscope (Wild Heerbrug optical microscope, Bracon Dental, Forest Green, Sussex, U.K.) at x12 magnification, and the location of each failure was recorded i.e between the titanium disk and the coating (adhesive), within the coating (cohesive), between the coating and cyanoacrylate adhesive, or between the cyanoacrylate adhesive and the sandblasted Ti-6Al4V titanium rod.

### *11.1.2. Statistical treatment of the data*

The data was tabulated in Microsoft Excel Worksheet. Statistical package for social sciences (SPSS) Version 14 was used to analyze the data. A two way analysis of variance was undertaken and if appropriate poc hoc testing with a Bonferroni correction.

## 11.2 Results

### *11.2.1. Force/displacment graph*

The crosshead was positioned to be in light contact with the Instron jig / specimen set up in such a way that it did not come into contact with the coating surface. On commencement of the compressive shear force test the lower assembly moved upwards at a speed of 5 mm per minute. The patterns of all the force displacement graphs were very similar and figure 99 shows a typical force displacement graph obtained. There is a gradual ride in force until the peak load, followed by a sharp drop to zero.

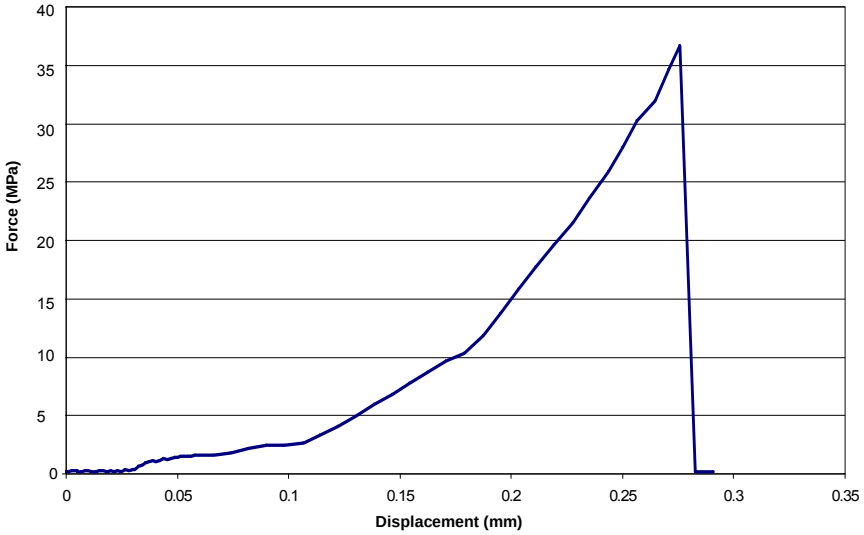


**Figure 99**: Typical force/displacement graph obtained.

### *11.2.2. Descriptive statistics for all specimens*

| Material | Temp (°C) | Mean Bond Strength (MPa) | Standard Deviation | n |
|---|---|---|---|---|
| $Ca_{10}(PO_4)_6(OH)_2$ | 600 | 31.960 | .6197 | 15 |
| | 700 | 33.153 | .2900 | 15 |
| | 800 | 36.540 | .8609 | 15 |
| | 1000 | 39.640 | 1.5519 | 15 |
| | Total | 35.323 | 3.1694 | 60 |
| $Ca_{10}(PO_4)_6F_{0.5}OH_{1.5}$ | 600 | 32.847 | .7558 | 15 |
| | 700 | 34.120 | .6816 | 15 |
| | 800 | 37.467 | 1.1586 | 15 |
| | 1000 | 40.487 | 1.4677 | 15 |
| | Total | 36.230 | 3.1801 | 60 |
| $Ca_{10}(PO_4)_6F_1OH_1$ | 600 | 33.767 | 1.0688 | 15 |
| | 700 | 34.947 | 1.5090 | 15 |
| | 800 | 38.980 | 1.8139 | 15 |
| | 1000 | 41.433 | 1.9452 | 15 |
| | Total | 37.282 | 3.4832 | 60 |
| $Ca_{10}(PO_4)_6F_{1.5}OH_{0.5}$ | 600 | 35.160 | 2.3231 | 15 |
| | 700 | 36.553 | 1.9766 | 15 |
| | 800 | 40.207 | 2.1786 | 15 |
| | 1000 | 42.647 | 2.7669 | 15 |
| | Total | 38.642 | 3.7472 | 60 |
| $Ca_{10}(PO_4)_6F_2$ | 600 | 37.207 | .8884 | 15 |
| | 700 | 37.753 | .8114 | 15 |
| | 800 | 42.827 | 1.5332 | 15 |
| | 1000 | 46.093 | 2.1562 | 15 |
| | Total | 40.970 | 3.9731 | 60 |

**Table 25**: Mean shear bond strengths

This data is represented graphically in Figure 100.

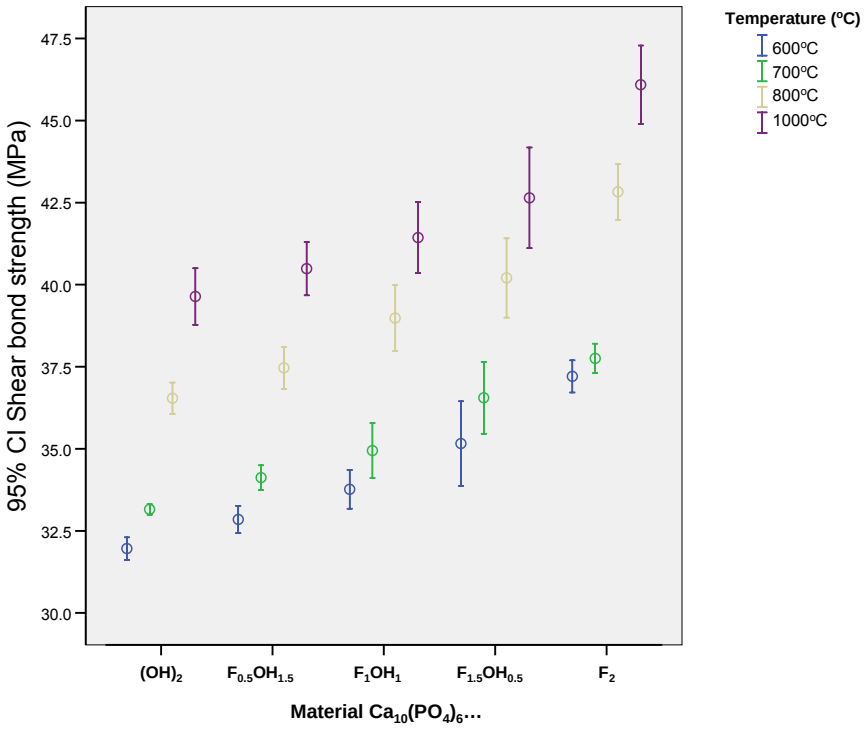


**Figure 100**: Graph to show mean with 95% confidence intervals exploring material / heating temperature (°C).

### *11.2.3. Statistical analysis of the results*

A two-way analysis of variance was undertaken. Initially the effect of the independent variables to peak shear bond strength was determined both individually and in combination. This is shown in Table 26.

| Source | Type III Sum of Squares | Degrees of Freedom | Mean Square | F | Significance |
|---|---|---|---|---|---|
| **Corrected Model** | 4155.635(a) | 19 | 218.718 | 89.645 | <0.001 |
| **Intercept** | 426145.754 | 1 | 426145.754 | 174662.511 | <0.001 |
| **Material** | 1173.811 | 4 | 293.453 | 120.276 | <0.001 |
| **Temperature** | 2950.480 | 3 | 983.493 | 403.100 | <0.001 |
| **Material and interaction with Temperature** | 31.344 | 12 | 2.612 | 1.071 | 0.385 |
| **Error** | 683.151 | 280 | 2.440 | | |
| **Total** | 430984.540 | 300 | | | |
| **Corrected Total** | 4838.786 | 299 | | | |

a $R^2$ = 0.759 (Adjusted R Squared = 0.749)

**Table 26**: Tests of between-subjects effects.

The corrected model indicates that the factors under investigation are predictive for the peak shear bond strength.

The $R^2$ explains how much variation can be explained by the statistical model. In this case 75.9% is explained by the model and 24.1% by chance or other factors not explored by the model.

The intercept compares the values of shear bond strength required to zero when all the model parameters are set to zero (the baseline case) and significantly shows that a positive force is required.

The material and temperature rows indicate that individually the material and temperature are statistically significant in explaining differences in shear bond strength. When combined there is no statistically significant evidence that these variables interact in affecting the peak shear bond strength.

### *11.2.4. Post hoc multiple comparison tests*

Post hoc multiple comparison tests using the Bonferroni correction were peformed. These compared differences in type of material (table 27) and temperature (table 28)

| Type of Surface | | Mean Difference (I-J) | Standard Error | Significance | 95% Confidence Intervals | |
|---|---|---|---|---|---|---|
| I | J | | | | Lower bound | Upper bound |
| $Ca_{10}(PO_4)_6(OH)_2$ | $Ca_{10}(PO_4)_6F_{0.5}OH_{1.5}$ | -0.907 | 0.285 | 0.016 | -1.714 | -0.1 |
| | $Ca_{10}(PO_4)_6F_1OH_1$ | -1.958 | 0.285 | <0.001 | -2.765 | -1.151 |
| | $Ca_{10}(PO_4)_6F_{1.5}OH_{0.5}$ | -3.318 | 0.285 | <0.001 | -4.125 | -2.511 |
| | $Ca_{10}(PO_4)_6F_2$ | -5.647 | 0.285 | <0.001 | -6.454 | -4.840 |
| $Ca_{10}(PO_4)_6F_{0.5}OH_{1.5}$ | $Ca_{10}(PO_4)_6F_1OH_1$ | -1.052 | 0.285 | 0.003 | -1.859 | -0.245 |
| | $Ca_{10}(PO_4)_6F_{1.5}OH_{0.5}$ | -2.412 | 0.285 | <0.001 | -3.219 | -1.605 |
| | $Ca_{10}(PO_4)_6F_2$ | -4.740 | 0.285 | <0.001 | -5.547 | -3.933 |
| $Ca_{10}(PO_4)_6F_1OH_1$ | $Ca_{10}(PO_4)_6F_{1.5}OH_{0.5}$ | -1.360 | 0.285 | <0.001 | -2.617 | -0.563 |
| | $Ca_{10}(PO_4)_6F_2$ | -3.688 | 0.285 | <0.001 | -4.495 | -2.881 |
| $Ca_{10}(PO_4)_6F_{1.5}OH_{0.5}$ | $Ca_{10}(PO_4)_6F_2$ | -2.328 | 0.285 | <0.001 | -3.135 | -1.521 |

**Table 27**: Multiple comparisons between sol-gel coating material.

Table 27 shows that there is a statistically significant difference ($p<0.01$) in mean shear bond strengths between all the sol-gel coatings except $Ca_{10}(PO_4)_6(OH)_2$ and $Ca_{10}(PO_4)_6F_{0.5}OH_{1.5}$. The mean shear bond strengths are $Ca_{10}(PO_4)_6F_2 > Ca_{10}(PO_4)_6OH_{0.5}F_{1.5} > Ca_{10}(PO_4)_6)OH_1F_1 > Ca_{10}(PO_4)_6OH_{1.5}F_{0.5} = Ca_{10}(PO_4)_6(OH)_2$.

| Temperature (°C) | | Mean Difference (I-J) | Standard Error | Significance | 95% Confidence Intervals | |
|---|---|---|---|---|---|---|
| I | J | | | | Lower bound | Upper bound |
| 600 | 700 | -1.117 | 0.255 | p<0.001 | -1.795 | -0.44 |
| | 800 | -5.018 | 0.255 | p<0.001 | -5.984 | -4.388 |
| | 1000 | -7.872 | 0.255 | p<0.001 | -8.550 | -7.194 |
| 700 | 800 | -3.899 | 0.255 | p<0.001 | -4.576 | -3.221 |
| | 1000 | -6.755 | 0.255 | p<0.001 | -7.432 | -6.077 |
| 800 | 1000 | -2.856 | 0.255 | p<0.001 | -3.534 | -2.178 |

**Table 28:** Multiple comparisons between different temperatures.

Table 28 shows that there were significant differences between all heating temperatures of the sol-gel coatings tested. With all coatings, the higher the heating temperature, the greater the bond strength.

### *11.2.5. Mode of failure*

After examination all the failures noted were found to be adhesive i.e. between the coating and the titanium disk (an example can be seen in figure 101).

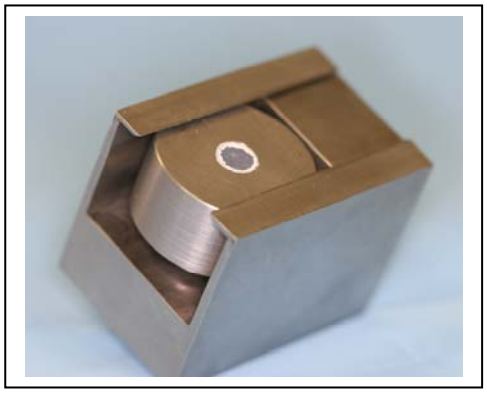

**Figure 101:** Photograph of assembly after shear testing of Instron showing adhesive failure (between coating and titanium disk).

## 11.3. Discussion of bond strengths with sol-gel coatings

### *11.3.1. Experimental protocol*

To optimise the chance of micromechanical retention it was decided to sandblast the titanium disks in a standardised manner prior to application of the sol-gels. Sandblasting with 50μm aluminium oxide is a well established technique in dentistry for increasing surface areas on metals prior to bonding procedures.

The spin coating protocol used here provided a successful method for coating the sol-gels to titanium disks. A spinning speed of 3615 rpm and dispersion of the sol-gel from at set distance of 20mm was chosen as this as been established as the optimum spinning speed and distance previously in this thesis.

Heating temperatures of 600, 700, 800 and 1000$^{o}$C were chosen for investigation as all these materials had been previously characterised in these temperature ranges in this thesis.

### *11.3.2. Shear bond strength testing*

The shear bond strength for each specimen was tested using the Instron Universal Load Testing machine. This machine was calibrated for identical test settings between testing of each specimen to ensure that data generated was accurate and related. The shear testing alignment jig allowed seating of the specimen, with the shearing blade resting perpendicularly to the specimen. The crosshead of the Instron machine was calibrated to close at a rate of five millimetres per minute, and proved a successful method of investigating the shear bond strength of the specimens. Shear bond strength testing is well documented in the literature. However, a study by DeHoff et al., 1995

concluded that experimentally derived shear bond values based on average loads at failure can be grossly underestimated, because of the failure to compensate for severe stress concentrations that exist near the loading site.

Clearly the larger the sample size the more valid the results of the study. A sample size estimation was calculated using N-query advisor statistical software, using data from a similar published study (Yang & Ong, 2003). This suggested that to gain a power of 90%, there should be a sample size of 15 per group. Each of the samples were allocated a number and the order in which the shear bond strength testing was carried out was randomly determined using a random number generator, this was undertaken in an effort to minimise any potential bias.

On commencement of the Instron machine, a compressive shear force was applied, the force displacement patterns obtained were all consistent, and showed a gradual rise in force with respect to displacement until a peak load was reached. This was followed by an immediate sharp drop to zero, indicating a catastrophic failure of the apatite / titanium interface. This is characteristic of the type of failure to be expected, where stress is applied to one or more brittle materials (Anusavice et al., 1986). After examination all the failures noted were found to be adhesive i.e. between the coating and the titanium disk. This is extremely important as if the failure was not occurring at this interface, but between the cyanoacrylate and apatite coating, or, titanium disk and cyanoacrylate then the results would be invalid.

### *11.3.3. Descriptive statistics for all specimens*

Table 25 gives the overall mean shear bond strengths for all specimens, which are represented graphically in Figure 100. Generally all the mean shear bond strength figures (31-46 MPa) compare favourably with those in the literature

observed with the hydroxyapatite plasma-sprayed coatings (≈ 10 – 40 MPa) [Wang et al., 1993; Yang et al., 1997; Ferraz et al., 1999; Strnad et al., 2000; Kweh et al., 2002; Mandl et al., 2002; Lee et al., 2004; Nurhaerani et al., 2006]. This is an extremely encouraging result for the sol-gel materials produced in this study. It is possible that pre-treatment of the titanium surface with 50μm aluminium oxide optimised the surface area and micromechanical interlocking of the apatite coating and the titanium surface.

### *11.3.4. Significant differences in bond strength*

Increasing the fluoride substitution significantly increased the bond strength such that the bond strengths were as follows; $Ca_{10}(PO_4)_6F_2$ > $Ca_{10}(PO_4)_6OH_{1.5}F_{1.5}$ > $Ca_{10}(PO_4)_6)OH_1F_1$ > $Ca_{10}(PO_4)_6OH_{1.5}F_{0.5}$ = $Ca_{10}(PO_4)_6(OH)_2$. The mean bond strength of $Ca_{10}(PO_4)_6F_2$ was approximately 40MPa, which is higher than or comparable to those usually observed with the hydroxyapatite plasma-sprayed coatings (≈ 10 – 40 MPa) [Wang et al., 1993; Yang et al., 1997; Ferraz et al., 1999; Strnad et al., 2000; Kweh et al., 2002; Mandl et al., 2002; Lee et al., 2004; Nurhaerani et al., 2006]. When considering one of the problems associated with the plasma-sprayed coatings, that is, the weak coating strength, the high strengths found using this sol-gel method are quite promising. The thin and dense structure as well as the good interfacial properties of the sol-gel film would result in such a high strength value.

It can be suggested that the greater bond strengths achieved may be related to greater diffusion of the fluoride substituted apatites across the interface. The more the fluoride substitution, the greater diffusion across the interface, and as a result the greater bonding interaction with the titanium surface.

The bond strength data showed here that the temperature that the sol-gels were fired on to the titanium was also a factor in determining the overall bond

strength. Uniformly with all the sol-gel coatings the bond strength significantly increased as the temperature increased such that bond strengths 1000$^{o}$C > 800$^{o}$C > 700$^{o}$C > 600$^{o}$C. This increase in bond strength may again be attributable to greater diffusion occurring across the interface.

These findings are novel to this thesis, and clearly the ability to optimise the bond strength by increasing the substitution of fluoride or increasing the temperature that the sol-gel is fired on to the titanium as important and useful findings.

# Chapter 12 :

# Hydroxyapatite $Ca_{10}(PO_4)_6OH_2$,

# Fluorapatite $Ca_{10}(PO_4)_6F_2$ &

# Fluorhydroxyapatite $Ca_{10}(PO_4)_6OH_xF_y$

# Biological Properties

## 12. Biological properties of HA, FHA and FA derived via the Sol-gel technique

### *12.1. Methods & Materials*

#### *12.1.1 Cell culture*

##### *12.1.1.1 Maintenance of primary Human Osteosarcoma Cells (HOC)*

HOC were obtained from the Eastman Dental Institute archive. These cells were in cryogenic storage and had been previously obtained from a culture from a gingival tissue mucosal biopsy after obtaining ethical approval. Frozen vials of HOC were retrieved from storage and defrosted in a 37 ºC water bath. The exterior of the vial was wiped with a tissue soaked with 70 % ethanol to remove any contamination. The content of the vial was then transferred with a sterile pipette into a 150 $cm^2$ tissue culture flask ($T_{150}$) (BD Bio-Sciences, UK). Fifteen ml of standard growth medium [Dulbecco's Modified Eagle's Medium (DMEM), 10% Foetal calf serum (FCS), 1% L-Glutamine (L-Glut), 1% Penicillin (100 IU/ml)/ Streptomycin (100 µg/ml) and, 1% Amphotericin B] (Gibco, Life Technologies, UK) was then added, and the cells were incubated in a humidified incubator at 37 ºC and 5 % $CO_2$. The growth medium was changed every three days.

##### *12.1.1.2. Cell subculture*

The cells were trypsinized during the log phase of growth. The growth medium was removed from the flask; 10 ml of 0.5 % trypsin-0.02 % ethylene diamine triacetic acid (EDTA) solution (Gibco, Life Technologies, UK) was added, and the flask was incubated for 5 min at 37 ºC during which the cells become rounded and detached. The cell suspension was gently triturated with a 10 ml

pipette before being transferred into a sterile 50 ml graduated centrifuge tube. An aliquot of growth medium, approximately 10 ml, was added to the cell suspension to terminate the action of trypsin/EDTA. The cells were then collected by centrifugation at 1000 rpm for 5 min at room temperature; a balance weight was used when required. Once centrifuged, the supernatant was discarded, and the cell pellet was resuspended into 4 ml of standard growth medium for reseeding into 4 tissue culture flasks ($T_{150}$). Cells used for the experiments were collected from $15^{th}$ to $18^{th}$ passages.

#### *13.1.1.3. Cell counting*

HOC were detached from the flasks, as described in cell subculture, and resuspended into growth medium. Then the cell number was determined using a haemocytometer, which is a thick glass slide with a central area designed as a counting platform for cells. Before the haemocytometer was loaded with cells, the cell clumps were dispersed by pipetting up and down. Then, 20 µl of cell suspension was transferred into a 1.5 ml micro-centrifuge tube and 20 µl of 0.4% trypan blue solution was added and homogenously mixed together. Trypan blue is metabolised by viable cells, and hence they will not stain blue, while dead cells will take up the stain and turn blue. About 10 µl of stained cell suspension was transferred to the edge of each filling notch of the two counting chambers. A microscope was used to view the cells for counting.

#### *13.1.1.4. Cryopreservation of cells*

For preserving surplus cells to be used as required, HOC were detached from the flasks, as described in cell subculture, and the cell pellet having a cell density of $1x10^6$ cells/ml was prepared for freezing. The cell pellet was then resuspended in a freezing medium [90% of FCS and 10 % of dimethyl sulfoxide (DMSO) (Gibco, Life Technologies, UK). One ml aliquots were placed in

cryovials that were labelled with the cell type/passage number and date of freezing. The cryovials were then placed in a cooled 'Mr. Frosty', a Styrofoam insulated container filled with isopropanol. The container was then transferred into a freezer at -80 ºC with a cooling rate of -1 ºC.min$^{-1}$ for 24 h. The cryovials was then preserved in liquid nitrogen (-196 ºC) until needed.

### *12.1.2 Production of samples for investigation*

Samples of the $Ca_{10}(PO_4)_6(OH)_2$, $Ca_{10}(PO_4)_6F_{0.5}OH_{1.5}$, $Ca_{10}(PO_4)_6F_1OH_1$ $Ca_{10}(PO_4)_6F_{1.5}OH_{0.5}$ and $Ca_{10}(PO_4)_6F_2$ sol-gels were heated to 600$^o$C for 1 hour in a hot air oven (Lenton Furnace, Lenton Thermal Designs Limited, UK) with a ramp of 5$^o$C per minute, dwell time of 60 minutes and cool down rate of 10$^o$C per minute. They were subsequently ball milled to a particle size of approximately 20 µm.

0.5g of the ball milled samples was subsequently placed in a die (13mm wide) and pressed to 4 tons. The pressing weight and amount of sample used was determined by trial and error to produce a flat solid sample (see figure 102).

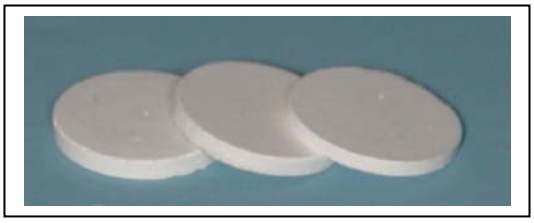

**Figure 102**: Photograph to illustrate example of pressed disks produced

The surfaces were polished using the protocol in section (10.1.1). The samples were made in triplicate for each powder type. As a comparison polished titanium disks (as produced in section 10.1.1) were also included for use in the experiment. All samples wrapped in tin foil (Sainsbury's, UK) sealed with sterilisation tape (3M, UK) and heated to 200$^o$C in a hot air oven (Gallenkamp,

Weiss, UK) for 3 hours to ensure that they were sterile prior to commencement of the cellular work.

### 12.1.3 *Cell proliferation assay – Human Osteosarcoma Cells*

Human Osteosarcoma (HOS) cells were used to obtain a preliminary estimate of biological compatibility of $Ca_{10}(PO_4)_6(OH)_2$, $Ca_{10}(PO_4)_6F_{0.5}OH_{1.5}$, $Ca_{10}(PO_4)_6F_1OH_1$ $Ca_{10}(PO_4)_6F_{1.5}OH_{0.5}$ and $Ca_{10}(PO_4)_6F_2$ and to compare it with both Titanium and tissue culture plastic (TCP) as a positive control. The samples were all prepared in triplicate and pre-treated by incubation in a growth medium described below for 24 hours at 37ºC humidified atmosphere incubator of 5% $CO_2$ in air.

HOS cells were cultured at 37 ºC humidified atmosphere incubator of 5% $CO_2$ in air; in a growth medium [Dulbecco's modified Eagles Medium (DMEM, Gibco), 10% fetal calf serum, and 1% penicillin and streptomycin solution (Gibco)]. The medium was changed every three days. The cells were seeded at a density of 5 $x10^3$ cells/disc. Three wells contained growth medium as a control (-ve) – see figure 103.


**Figure 103**: HOS cells seeded in growth medium on the samples ($F_2$, $F_{1.5}$, $F_1$, $F_{0.5}$, HA, Ti, TCP and –ve control [just growth medium]).

The measurement of HOS proliferation was based on measuring the metabolic activity of these cells using alamarBlue™ assay. Cell growth results in a chemical reduction of alamarBlue, and continued growth maintains a reduced environment while inhibition of growth maintains an oxidized environment. Reduction related to growth causes the redox indicator to change from oxidized non-fluorescent, blue form to reduced fluorescent, red form; the intensity of the colour produced is directly related to the number of metabolically active cells.

At 1, 3, and 7 days time point, the culture media was removed and the samples were washed three times with warm PBS. Five hundred microlitres of 10% Alamar Blue in warm Hanks Balanced Salt Solution was then added to each well and incubated for 90 minutes. The fluorescence was then measured at 530 nm excitation, and 590 nm emission using a Fluroskan Ascent plate reader (Labsystems, Helsinki, Finland). The fluorescence measurement was repeated twice for each sample. A background fluorescence reading was also taken from Alamar Blue at each occasion.

In summary two readings were taken from each of the three samples in each group – giving a total of six readings per group. At the same time two fluorescence readings were taken from the wells containing only Alamar Blue, these values were then subtracted from the sample readings to give a true value of fluorescence from the samples and thus cell proliferation that had occurred.

### *12.1.4. Cell attachment*

HOS attachment was conducted using scanning electron microscopy (SEM). Samples for SEM were overnight fixed with 3% glutaraldehyde in 0.1 M sodium cacodylate buffer (Agar Scientific Ltd., Essex, UK) at 4ºC, then dehydrated in graded alcohol (20, 50, 70, 90, and 100%). The dehydrated samples were

critically dried in hexamethyldisilazane (HMDS, Taab Laboratories Ltd., Berkshire, UK) for 5 minutes, and then left to air dry. The dried samples were then mounted on aluminium stub; sputter coated with gold-palladium alloy, and viewed using JEOL 5410LV Scanning electron microscope (JEOL UK Ltd, UK).

### 12.1.5 *Statistical treatment of the data*

The data was tabulated in Microsoft Excel Worksheet. Statistical package for social sciences (SPSS) Version 14 was used to analyze the data. A two way analysis of variance was undertaken and when appropriate post hoc testing with a Bonferroni correction.

## 12.2 Results

**12.2.1.** ***Descriptive statistics for all specimens - Raw data -*** Fluorescence 530 nm excitation and 590 nm emission (Flurometric Units) – Table 29.

| **Reading on Day 1** | | | | | | | | |
|---|---|---|---|---|---|---|---|---|
| **Disk** | **Reading** | **$Ca_{10}(PO_4)_6$…** | | | | | **Ti** | **TCP** |
| | | **$F_2$** | **$F_{1.5}OH_{0.5}$** | **$F_1OH_1$** | **$F_{0.5}OH_{1.5}$** | **$(OH)_2$** | | |
| **1** | **1** | 38.7 | 23.0 | 4.0 | 13.0 | 9.1 | 20.3 | 18.7 |
| | **2** | 44.8 | 26.8 | 6.2 | 14.0 | 10.8 | 24.2 | 21.5 |
| **2** | **1** | 39.9 | 25.8 | 5.6 | 6.1 | 0 | 16.3 | 14.8 |
| | **2** | 43.0 | 26.6 | 7.3 | 7.0 | 0 | 21.2 | 14.2 |
| **3** | **1** | 42.1 | 17.3 | 4.7 | 4.0 | 2.7 | 4.5 | 18.7 |
| | **2** | 45.2 | 20.1 | 3.9 | 3.7 | 1.7 | 5.1 | 20.6 |
| **Reading on Day 3** | | | | | | | | |
| **1** | **1** | 226.3 | 51.8 | 61.9 | 24.5 | 20.0 | 10.8 | 23.6 |
| | **2** | 210.4 | 67.2 | 64.7 | 26.0 | 21.3 | 11.1 | 24.6 |
| **2** | **1** | 173.7 | 59.4 | 8.3 | 20.2 | 11.1 | 20.8 | 11.8 |
| | **2** | 99.9 | 41.9 | 26.4 | 20.1 | 20.2 | 20.7 | 21.3 |
| **3** | **1** | 158.4 | 25.5 | 20.8 | 20.6 | 20.1 | 20.3 | 17.4 |
| | **2** | 145.4 | 22.1 | 20.7 | 20.2 | 19.6 | 19.8 | 19.2 |
| **Reading on Day 3** | | | | | | | | |
| | | **$F_2$** | **$F_{1.5}OH_{0.5}$** | **$F_1OH_1$** | **$F_{0.5}OH_{1.5}$** | **$(OH)_2$** | | |
| **1** | **1** | 226.3 | 51.8 | 61.9 | 24.5 | 20.0 | 10.8 | 23.6 |
| | **2** | 210.4 | 67.2 | 64.7 | 26.0 | 21.3 | 11.1 | 24.6 |
| **2** | **1** | 173.7 | 59.4 | 8.3 | 20.2 | 11.1 | 20.8 | 11.8 |
| | **2** | 99.9 | 41.9 | 26.4 | 20.1 | 20.2 | 20.7 | 21.3 |
| **3** | **1** | 158.4 | 25.5 | 20.8 | 20.6 | 20.1 | 20.3 | 17.4 |
| | **2** | 145.4 | 22.1 | 20.7 | 20.2 | 19.6 | 19.8 | 19.2 |

**12.2.2 *Mean and standard deviation* -** Fluorescence 530 nm excitation and 590 nm emission (Flurometric Units) – Table 30.

| | | | | | | | |
|---|---|---|---|---|---|---|---|
| **Day 1** | | | | | | | |
| | **$Ca_{10}(PO_4)_6$…** | | | | | **Ti** | **TCP** |
| | **$F_2$** | **$F_{1.5}OH_{0.5}$** | **$F_1OH_1$** | **$F_{0.5}OH_{1.5}$** | **$(OH)_2$** | | |
| **Mean** | 42.3 | 23.2 | 5.3 | 8.0 | 3.7 | 15.3 | 18.1 |
| **SD** | 2.6 | 3.9 | 1.3 | 4.5 | 5.1 | 8.5 | 2.97 |
| **Day 3** | | | | | | | |
| **Mean** | 169.0 | 44.7 | 33.8 | 21.9 | 18.7 | 17.2 | 19.6 |
| **SD** | 47.8 | 18.2 | 23.6 | 2.6 | 3.8 | 4.9 | 4.8 |
| **Day 7** | | | | | | | |
| **Mean** | 532.3 | 169.2 | 88.1 | 87.8 | 65.4 | 50.1 | 94.8 |
| **SD** | 78.8 | 80.4 | 24.8 | 24.4 | 11.2 | 22.6 | 15.7 |

This data is represented graphically in Figure 104.

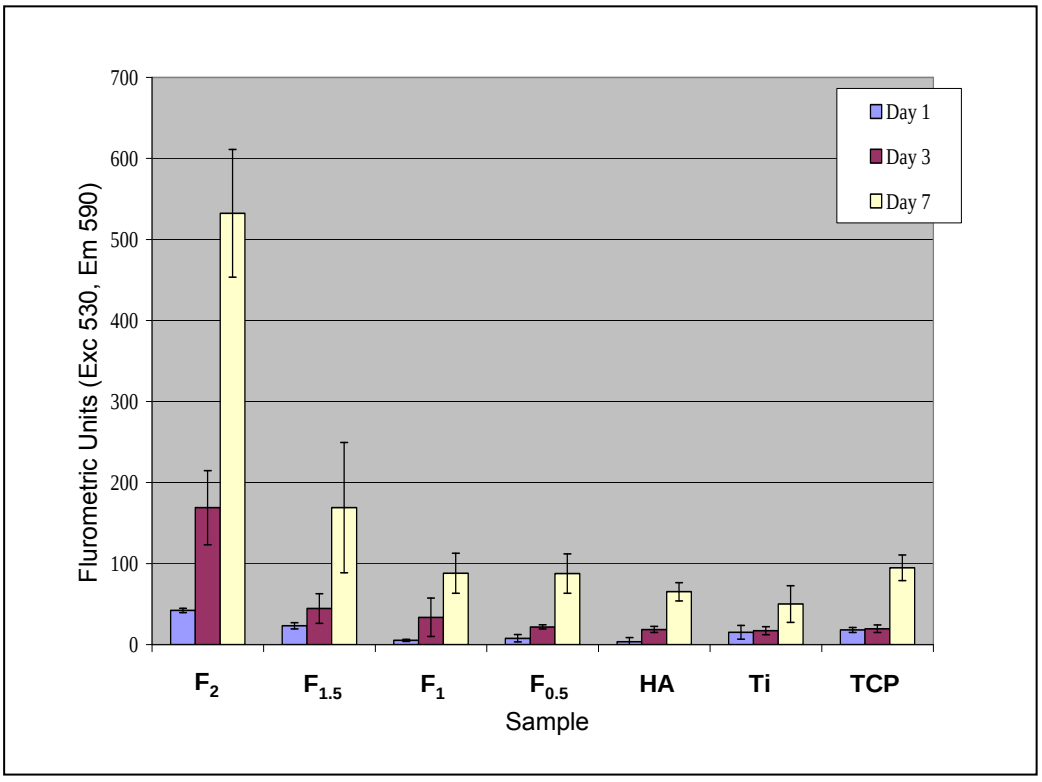


**Figure 104:** Bar graph to show mean (+/- SD) proliferation of Human Osteosarcoma Cells over a seven day period.

### 12.2.3 *Statistical analysis of the results*

A two-way analysis of variance was undertaken. Initially the effect of the independent variables to fluorescence was determined both individually and in combination. This is shown in table 31.

| Source | Type III Sum of Squares | Degrees of Freedom | Mean Square | F | Significance |
|---|---|---|---|---|---|
| **Corrected Model** | 1691441.5 | 62 | 27281.3 | 237.263 | <0.001 |
| **Intercept** | 667542.9 | 1 | 667543 | 5805.5 | <0.001 |
| **Sample** | 674955.1 | 6 | 112492.5 | 978.33 | <0.001 |
| **Day** | 448574.3 | 2 | 224287.1 | 1950.6 | <0.001 |
| **Sample and interaction with day** | 9209.8 | 12 | 2302.5 | 20.02 | <0.001 |
| **Error** | 7243.969 | 63 | 114.984 | | |
| **Total** | 2366228.4 | 126 | | | |
| **Corrected Total** | 1698685.4 | 125 | | | |

a R Squared = 0.996 (Adjusted R Squared = 0.992)

**Table 31:** Two way ANOVA of fluorescence values obtained.

The corrected model indicates that the factors under investigation are predictive for the fluorescence.

The $R^2$ explains how much variation can be explained by the statistical model. In this case 99.6% is explained by the model and 0.4% by chance or other factors not explored by the model.

The intercept compares the values of fluorescence required to zero when all the model parameters are set to zero (the baseline case) and significantly shows that a positive fluorescence (i.e. cell proliferation) is taking place.

The sample and day rows indicate that individually the sample type and day are statistically significant in explaining differences in fluorescence. When

combined there is statistically significant evidence that these variables interact in affecting the fluorescence.

### 13.2.4 *Post hoc multiple comparison tests*

Post hoc multiple comparison tests using the Bonferroni correction were performed. These were used to compare differences in fluorescence for the different materials at each time point i.e. if there was a difference in cellular proliferation on any of the materials on day 1 (table 32), 3 (table 33), 7 (table 34).

| Type of Material | | Mean Difference (I-J) | Standard Error | Significance | 95% Confidence Intervals | |
|---|---|---|---|---|---|---|
| I | J | | | | Lower bound | Upper bound |
| **$Ca_{10}(PO_4)_6F_{0.5}OH_{1.5}$** | $Ca_{10}(PO_4)_6F_1OH_1$ | 2.664 | 2.675 | 1.000 | -6.09 | 11.43 |
| | **$Ca_{10}(PO_4)_6F_{1.5}OH_{0.5}$** | **-15.273** | **2.675** | **<0.001** | **-24.03** | **-6.51** |
| | **$Ca_{10}(PO_4)_6F_2$** | **-34.313** | **2.675** | **<0.001** | **-43.08** | **-25.55** |
| | $Ca_{10}(PO_4)_6(OH)_2$ | 4.234 | 2.675 | 1.000 | -4.52 | 12.99 |
| | TCP | -10.132 | 2.675 | 0.0563 | -18.89 | -1.36 |
| | Titanium | -7.304 | 2.675 | 0.207 | -16.07 | 1.45 |
| **$Ca_{10}(PO_4)_6F_1OH_1$** | **$Ca_{10}(PO_4)_6F_{1.5}OH_{0.5}$** | **-17.937** | **2.675** | **<0.001** | **-26.70** | **-9.17** |
| | **$Ca_{10}(PO_4)_6F_2$** | **-36.977** | **2.675** | **<0.001** | **-45.74** | **-28.21** |
| | $Ca_{10}(PO_4)_6(OH)_2$ | 1.569 | 2.675 | 1.000 | -7.19 | 10.33 |
| | **TCP** | **-12.797** | **2.675** | **<0.001** | **-21.56** | **-4.03** |
| | **Titanium** | **-9.968** | **2.675** | **<0.001** | **-18.73** | **-1.21** |
| **$Ca_{10}(PO_4)_6F_{1.5}OH_{0.5}$** | **$Ca_{10}(PO_4)_6F_2$** | **-19.040** | **2.675** | **<0.001** | **-27.80** | **-10.28** |
| | **$Ca_{10}(PO_4)_6(OH)_2$** | **19.507** | **2.675** | **<0.001** | **10.74** | **28.2** |
| | TCP | 5.140 | 2.675 | 1.000 | -3.62 | 13.90 |
| | Titanium | 7.968 | 2.675 | 0.110 | -0.79 | 16.73 |
| **$Ca_{10}(PO_4)_6F_2$** | **$Ca_{10}(PO_4)_6(OH)_2$** | **38.547** | **2.675** | **<0.001** | **18.25** | **35.77** |
| | **TCP** | **24.180** | **2.675** | **<0.001** | **15.42** | **32.94** |
| | **Titanium** | **27.009** | **2.675** | **<0.001** | **18.25** | **35.77** |
| **$Ca_{10}(PO_4)_6(OH)_2$** | **TCP** | **-14.369** | **2.675** | **<0.001** | **-23.12** | **-5.60** |
| | **Titanium** | **-11.538** | **2.675** | **<0.001** | **-20.30** | **-2.78** |
| TCP | Titanium | 2.828 | 2.675 | 1.000 | -5.93 | 11.59 |

**Table 32**: Multiple comparisons between cell proliferation on materials, day 1.

| Type of Material | | Mean Difference (I-J) | Standard Error | Significance | 95% Confidence Intervals | |
|---|---|---|---|---|---|---|
| I | J | | | | Lower bound | Upper bound |
| **$Ca_{10}(PO_4)_6F_{0.5}OH_{1.5}$** | $Ca_{10}(PO_4)_6F_1OH_1$ | -11.86 | 12.054 | 1.000 | -51.34 | 27.63 |
| | $Ca_{10}(PO_4)_6F_{1.5}OH_{0.5}$ | -22.737 | 12.054 | 1.000 | -62.22 | 16.75 |
| | **$Ca_{10}(PO_4)_6F_2$** | **-147.106** | **12.054** | **<0.001** | **-186.6** | **-107.6** |
| | $Ca_{10}(PO_4)_6(OH)_2$ | 3.192 | 12.054 | 1.000 | -36.29 | 42.68 |
| | TCP | 2.277 | 12.054 | 1.000 | -37.21 | 41.76 |
| | Titanium | 4.676 | 12.054 | 1.000 | -34.81 | 44.16 |
| **$Ca_{10}(PO_4)_6F_1OH_1$** | $Ca_{10}(PO_4)_6F_{1.5}OH_{0.5}$ | -10.880 | 12.054 | 1.000 | -50.36 | 28.61 |
| | **$Ca_{10}(PO_4)_6F_2$** | **-135.249** | **12.054** | **<0.001** | **-174.7** | **-95.8** |
| | $Ca_{10}(PO_4)_6(OH)_2$ | 15.049 | 12.054 | 1.000 | -24.43 | 54.54 |
| | TCP | 14.135 | 12.054 | 1.000 | -25.35 | 53.62 |
| | Titanium | 16.532 | 12.054 | 1.000 | -22.95 | 56.02 |
| **$Ca_{10}(PO_4)_6F_{1.5}OH_{0.5}$** | **$Ca_{10}(PO_4)_6F_2$** | **-124.370** | **12.054** | **<0.001** | **-163.9** | **-84.88** |
| | $Ca_{10}(PO_4)_6(OH)_2$ | 25.929 | 12.054 | 0.808 | -13.56 | 65.42 |
| | TCP | 25.014 | 12.054 | 0.953 | -14.47 | 64.50 |
| | Titanium | 27.412 | 12.054 | 0.613 | -12.07 | 66.90 |
| **$Ca_{10}(PO_4)_6F_2$** | **$Ca_{10}(PO_4)_6(OH)_2$** | **150.299** | **12.054** | **<0.001** | **110.8** | **189.8** |
| | **TCP** | **149.383** | **12.054** | **<0.001** | **109.9** | **188.9** |
| | **Titanium** | **151.782** | **12.054** | **<0.001** | **112.3** | **191.3** |
| $Ca_{10}(PO_4)_6(OH)_2$ | TCP | -0.915 | 12.054 | 1.000 | -40.40 | 38.57 |
| | Titanium | 1.483 | 12.054 | 1.000 | -38.01 | 40.97 |
| TCP | Titanium | 2.398 | 12.054 | 1.000 | -37.09 | 41.89 |

**Table 33**: Multiple comparisons between cell proliferation on materials, day 3.

| Type of Material | | Mean Difference (I-J) | Standard Error | Significance | 95% Confidence Intervals | |
|---|---|---|---|---|---|---|
| I | J | | | | Lower bound | Upper bound |
| **$Ca_{10}(PO_4)_6F_{0.5}OH_{1.5}$** | $Ca_{10}(PO_4)_6F_1OH_1$ | -0.311 | 26.506 | 1.000 | -87.14 | 86.52 |
| | $Ca_{10}(PO_4)_6F_{1.5}OH_{0.5}$ | -81.384 | 26.506 | 0.086 | -168.2 | 5.44 |
| | **$Ca_{10}(PO_4)_6F_2$** | **-444.473** | **26.506** | **<0.001** | **-531.3** | **-357.6** |
| | $Ca_{10}(PO_4)_6(OH)_2$ | 22.452 | 26.506 | 1.000 | -64.38 | 109.3 |
| | TCP | -7.004 | 26.506 | 1.000 | -93.83 | 79.83 |
| | Titanium | 37.665 | 26.506 | 1.000 | -86.52 | 87.14 |
| **$Ca_{10}(PO_4)_6F_1OH_1$** | $Ca_{10}(PO_4)_6F_{1.5}OH_{0.5}$ | -81.073 | 26.506 | 0.089 | -167.9 | 5.75 |
| | **$Ca_{10}(PO_4)_6F_2$** | **-444.161** | **26.506** | **<0.001** | **-530.9** | **-357.3** |
| | $Ca_{10}(PO_4)_6(OH)_2$ | 22.764 | 26.506 | 1.000 | -64.07 | 109.6 |
| | TCP | -6.692 | 26.506 | 1.000 | -93.51 | 80.14 |
| | Titanium | 37.976 | 26.506 | 1.000 | -48.85 | 124.8 |
| **$Ca_{10}(PO_4)_6F_{1.5}OH_{0.5}$** | **$Ca_{10}(PO_4)_6F_2$** | **-363.089** | **26.506** | **<0.001** | **-449.9** | **-276.3** |
| | **$Ca_{10}(PO_4)_6(OH)_2$** | **103.84** | **26.506** | **<0.001** | **17.01** | **190.7** |
| | TCP | 74.381 | 26.506 | 0.171 | -12.45 | 161.2 |
| | **Titanium** | **119.049** | **26.506** | **<0.001** | **32.22** | **205.9** |
| **$Ca_{10}(PO_4)_6F_2$** | **$Ca_{10}(PO_4)_6(OH)_2$** | **466.925** | **26.506** | **<0.001** | **380.1** | **553.8** |
| | **TCP** | **437.470** | **26.506** | **<0.001** | **350.6** | **524.3** |
| | **Titanium** | **482.138** | **26.506** | **<0.001** | **395.3** | **568.9** |
| $Ca_{10}(PO_4)_6(OH)_2$ | TCP | -29.456 | 26.506 | 1.000 | -116.3 | 57.37 |
| | Titanium | 15.212 | 26.506 | 1.000 | -71.62 | 102.4 |
| TCP | Titanium | 44.668 | 26.506 | 1.000 | -42.16 | 131.5 |

**Table 34**: Multiple comparisons between cell proliferation on materials, day 7.

Table 32 shows that there is a statistically significant difference ($p<0.001$) in fluorescence and thus cell proliferation on day 1 as follows:

- $Ca_{10}(PO_4)_6F_2$ (fluorapatite) had significantly greater cellular proliferation than all the other materials, including hydroxyapatite [$Ca_{10}(PO_4)_6(OH)_2$], titanium and TCP.
- $Ca_{10}(PO_4)_6F_{1.5}OH_{0.5}$ had significantly greater cellular proliferation than hydroxyapatite[$Ca_{10}(PO_4)_6(OH)_2$], $Ca_{10}(PO_4)_6F_1OH_1$ and $Ca_{10}(PO_4)_6F_{0.5}OH_{1.5}$.
- $Ca_{10}(PO_4)_6F_1OH_1$ had significantly less cellular proliferation than TCP and titanium.
- Hydroxyapatite [$Ca_{10}(PO_4)_6(OH)_2$] had significantly less cellular proliferation than TCP and titanium.

Table 33 shows that there is a statistically significant difference ($p<0.001$) in fluorescence and thus cell proliferation on day 3 as follows:

- $Ca_{10}(PO_4)_6F_2$ (fluorapatite) had significantly greater cellular proliferation than all the other materials, including hydroxyapatite [$Ca_{10}(PO_4)_6(OH)_2$], titanium and TCP.

Table 34 shows that there is a statistically significant difference ($p<0.001$) in fluorescence and thus cell proliferation on day 7 as follows:

- $Ca_{10}(PO_4)_6F_2$ (fluorapatite) had significantly greater cellular proliferation than all the other materials, including hydroxyapatite [$Ca_{10}(PO_4)_6(OH)_2$], titanium and TCP.
- $Ca_{10}(PO_4)_6F_{1.5}OH_{0.5}$ had significantly greater cellular proliferation than hydroxyapatite [$Ca_{10}(PO_4)_6(OH)_2$].

### *12.2.5. Cell attachment*

Figures 105, 106, 107 and 108 show examples of scanning electron micrographs of cells cultured on $Ca_{10}(PO_4)_6F_2$, $Ca_{10}(PO_4)_6F_{1.5}OH_{0.5}$, $Ca_{10}(PO_4)_6(OH)_2$ and titanium respectively after 3 days.

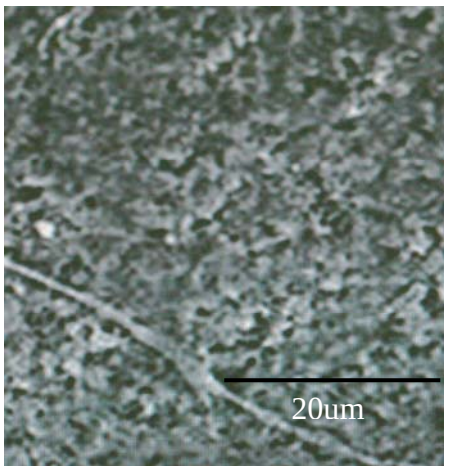


**Figure 105**: SEM of cells cultured on $Ca_{10}(PO_4)_6F_2$ after 3 days.

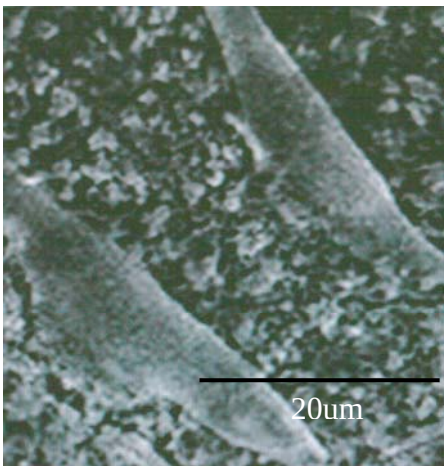


**Figure 106**: SEM of cells cultured on $Ca_{10}(PO_4)_6F_{1.5}OH_{0.5}$ after 3 days.

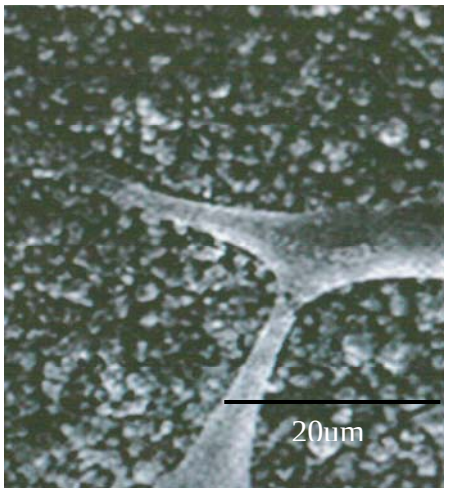


**Figure 107**: SEM of cells cultured on $Ca_{10}(PO_4)_6(OH)_2$ after 3 days.


**Figure 108**: SEM of cells cultured on titanium after 3 days.

## 12.3 Discussion of cell results

### *12.3.1 Use of Human Osteosarcoma Cells*

Osteoblasts are mononucleate cells that are responsible for bone formation, in *in vitro* studies osteoblasts are slow and difficult to culture and grow, clearly any cells that mimic the effect of these cells, but as less fickle to grow and can grow at a faster rate can be useful to test the biocompatibility of a material.

The osteosarcoma cell line has been well characterised and validated as a model to test biocompatibility of various materials (Francheschi et al., 1985; Boyan et al., 1989). Osteosarcoma cell lines have been used in many studies, particularly with in vitro work with titanium surface topographies, potential bone grafting materials and implant coating materials. Despite being a tumour cell line, which proliferates more rapidly than human bone derived cells, osteosarcoma cells exhibit many osteoblastic traits which are characteristic for bone forming cells (Bachle & Kohal, 2003). Osteosarcoma cells exhibit an increased alkaline phosphatase activity following I,25-dihydroxyvitamin $D_3$ ($I,25(OH)_2D_3$) administration, which is a characteristic for bone derived cells (Clover & Gowen, 1994). These cells are thought to be relatively immature osteoblasts. However they exhibit a number of osteoblast-like phenotypic markers, including response to parathyroid hormone (Aisa et al., 1996) and inhibition of proliferation with $I,25(OH)_2D_3$ (Boyan et al., 1989).

The osteosarcoma cell line in this study was used to provide an estimate of the biocompatibility of $Ca_{10}(PO_4)_6(OH)_2$, $Ca_{10}(PO_4)_6F_{0.5}OH_{1.5}$, $Ca_{10}(PO_4)_6F_1OH_1$ $Ca_{10}(PO_4)_6F_{1.5}OH_{0.5}$ and $Ca_{10}(PO_4)_6F_2$ prepared disks, both compared to each other and to titanium and tissue culture plastic (TCP). It was possible to culture cells successfully on all the samples.

### *12.3.2. Use of Alamar Blue*

Alamar blue was successfully used to monitor cellular proliferation of the osteosarcoma cell line used in this study. Alamar blue monitors the reducing environment of proliferating cells, without altering the viability of the cells (Ahmed et al., 1994), this was important in this study as multiple readings were required over the seven day period. The reduction of Alamar blue was monitored by measuring fluorescence. The measurements were made by exciting at 530nm and measuring the emission at 590nm. This is a well known technique and was used successfully in this study.

### *12.3.3. Surface roughness / topography*

The influence of surface topography of implant materials on biomolecule or cell adherence and on morphogenesis has been widely reported and plays an important role (Meyle et al., 1995; Cochran et al., 1997; Nanci et al., 1998). Surface characteristics (topography, chemistry or surface energy) influence the cell/material interaction.

As a result of this it was essential that all the surfaces of the samples that were tested in this study were the same. Any difference in surface topography could clearly result in spurious results. To achieve this, the same protocol was used to prepare the surfaces of the specimens in this study prior to the cell culture. This was the case for all the samples and the titanium and tissue culture plastic used in this study.

### *12.3.4 Proliferation results - cell number over time*

Without failure all cell numbers increased between day 1 and 7 indicating that the cells were able to proliferate on all the surfaces in the experimental protocol.

### *12.3.5. Trends in cellular proliferation*

The data obtained in this study showed clear trends in the cellular proliferation with the different materials used. Without failure at each of the periods tested (1, 3 and 7 days) the cellular proliferation values were significantly high for $Ca_{10}(PO_4)_6F_2$ (pure fluorapatite). Furthermore there was a general trend that can be seen very clearly in the graph in figure 100 that the more Fluoride substitution that occurred in the apatite structure the more the cells proliferated. This is a significant and important finding and potentially paves the way for fluorapatite coatings to supersede hydroxyapatite coatings.

The data throughout the experiment shows that there was a clear trend for the fluorhydroxyapatite and fluorapatite to outperform the hydroxyapatite coatings in terms of cellular proliferation. On inspection of figure 104 there is clear trend for increased cellular proliferation with increasing fluoride content, this was only actually significantly different with the highest concentrations of fluoride substitution. $Ca_{10}(PO_4)_6F_2$ had significantly greater cellular proliferation than HA at 1, 3 and 7 days, $Ca_{10}(PO_4)_6F_{1.5}OH_{0.5}$ had significant greater cellular proliferation on days 1 and 7.

Considering the known clinical biocompatibility of titanium and hydroxyapatite, the results of this study are very encouraging indeed. The hydroxyapatite [$Ca_{10}(PO_4)_6(OH)_2$] had significantly worse cellular proliferation on day 1 when compared with titanium, while on day 3 and 7 there was no significantly difference. In contrast the cellular proliferation results for higher level of

substitution of the fluoride coating were significantly better than both titanium and hydroxyapatite. Postulating this forward to the clinical situation suggests that cellular proliferation and hence the first stages of healing could potentially be faster with fluoride substitute apatite coatings than with hydroxyapatite coatings or titanium itself.

Further encouragement from these results is that the higher level of fluoride substitution coatings performed significantly better than the tissue culture plastic. It must be understood that tissue culture plastic is specifically designed to support and encourage cellular growth, for the $Ca_{10}(PO_4)_6F_2$ and $Ca_{10}(PO_4)_6F_{1.5}OH_{0.5}$ to significantly outperform this shows great potential for use *in vivo* as a highly compatible material.

The results of this study provide support and build on the current knowledge in the literature. Fluorapatite coatings have attracted a great deal of attention in areas requiring long-term chemical and mechanical stability (Legeros et al., 1983; Okazaki et al., 1998; Kim et al., 2002b). Previous studies have suggested that fluorapatite ($Ca_{10}(PO_4)_6F_2$) has a similar biocompatibility with HA in terms of its fixation to bone and bone in-growth (Heling et al., 1981; Slosarczyk et al., 1996; Overgaard & Lind, 1997). Qu & Wei (2006) studied discs doped with various amounts of fluorine ion ($F^-$) to investigate the effect of $F^-$ content on oesteoblastic cell behaviour. They concluded that FHA is biocompatibile and that the amount of $F^-$ affects cell attachment, proliferation, morphology and differentiation of osteoblastic cells.

The first study to suggest that fluorapatite may have superior biological properties to HA was Kim et al., (2004). This current study takes this work further and suggests that fluorapatite ($Ca_{10}(PO_4)_6F_2$) and highly substituted

fluorhydroxyapatites ($Ca_{10}(PO_4)_6F_{1.5}OH_{0.5}$) have a far superior biocompatibility than HA itself.

These fluoride substituted apatites produced by the sol-gel method in this study, have the potential to offer themselves as highly biocompatible titanium implant coating materials, furthermore because of their high biocompatibility they could offer the potential as an alloplastic bone grafting material.

Currently clinically one of the most commonly used bone grafting materials is BioOss$^{TM}$ (Geistlich, Austria), this is made from deproteinised bovine bone. It may be possible to produce a highly biocompatible osteoconductive material made from Fluorapatite / fluoride substituted hydroxyapatite that could be used as a bone grafting material. The materials could be made in blocks or differing particle sizes and offer a range of properties depending on the level of fluoride substitution.

# Chapter 13:

# Future Studies

## 13. Future Studies

Based on the results of the work found in this thesis there are many avenues for future work and potential future clinical uses of the materials developed.

### *13.1. Further in vitro experiments*

The results of this thesis have generated several findings which need further in vitro investigation:

(a) The Rheology results have shown that increasing the amount of fluoride in the sol-gel increases the viscosity and contact angle measurement. The exact mechanism for this needs to be investigated further.

(b) The lower dissolution rates for the fluoride-substituted powders require further investigation. Furthermore it would be highly desirable to develop a technique to record the fluoride ion release.

(c) The exact mechanism for the lower dissolution rates for the higher temperature the sol-gel was heated to needs further investigation.

(d) The suggested chemical bond that the heated sol-gels formed with the titanium is important and the nature of this bond requires further investigation.

(e) The fluoride substituted apatite's showed excellent biocompatibility. The reason for the effect of fluoride substitution on cell growth should be investigated further.

### *13.2. Animal studies*

The results of this work have clearly suggested *in vitro* that the higher substitution fluorhydroxyapatite or phase pure fluorapatite coatings produced by the sol-gel technique can be manufactured to have superior properties to hydroxyapatite coatings, both in terms of bond strength, dissolution rate and biocompatibility. Clearly *in vitro* experiments have their limitations and the next stage for these new materials must be investigation in an in vivo animal model.

Using an animal model dental implant shaped titanium rods could be coated with; $Ca_{10}(PO_4)_6F_2$, $Ca_{10}(PO_4)_6OH_{0.5}F_{1.5}$, $Ca_{10}(PO_4)_6)OH_1F_1$, $Ca_{10}(PO_4)_6OH_{1.5}F_{0.5}$ and $Ca_{10}(PO_4)_6(OH)_2$ and the time and stages of healing compared to an un-coated titanium control. It would be imperative, that as has been done in the *in vitro* experiments, the surfaces are controlled to ensure that the surface topography is identical for each of the variables.

As well as the differing fluoride content of the coatings the other variables that could be tested in an animal model are:

(1) The dissolution rate of the different coatings.

(2) The effect of different heating temperatures on the *in vivo* dissolution rate and biocompatibility of the coatings.

(3) The effect of coating thickness on the biocompatibility of the coatings.

If the results of these *in vivo* animal studies confirm the results of the data from this *in vitro* study then the use of fluoride-substituted hydroxyapatite / fluorapatite coatings may have a very useful role in the clinical situation. For example:

- Use of a fluorapatite coating when the bone is compromised to optimise the biocompatibility and osteoconductivity of the implant material. Figure 109 shows an implant being immediately inserted into an extraction site, the buccal plate is very thin and compromised and use of a fluorapatite coating could potentially optimise the healing and help to ensure that the buccal plate does not undergo further resorption.

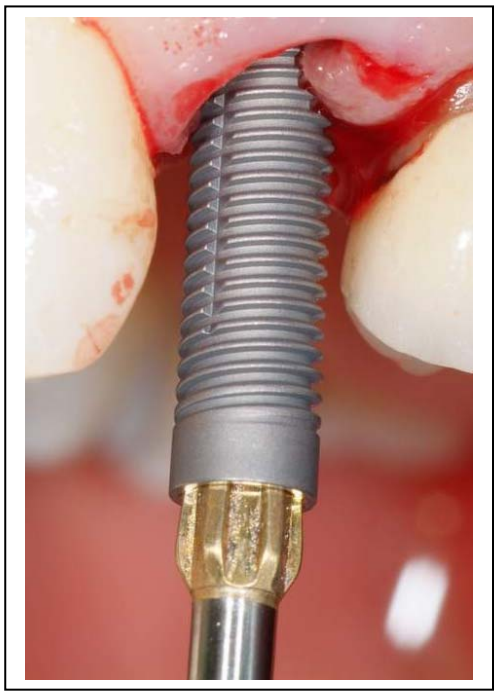

**Figure 109**: Titanium dental implant being inserted into compromised bone site (compromised buccal plate).

- This study has shown that the dissolution rate of all the sol-gel synthesised materials can be controlled by the firing temperature and relative substitution of the apatite structure with fluoride. This could potentially be clinically useful.

To give an example; if the available bone is of good quality e.g. type I bone – mainly cortical bone, but it is wished to increased the speed of osseointegration then use of a fluorapatite that was fired to 600$^{o}$C, would allow for excellent

biocompatibility and a more rapid dissolution rate so that following increasing the speed of intergration the coating could dissolve rapidly leaving the titanium integrated with the bone.

If the bone was of lower quality e.g. type IV bone – mainly cancellous bone and it was wished to allow time for optimal bone growth around the implant then use of a fluorapatite that was fired to 1000$^{o}$C, would allow for excellent biocompatibility but a slower dissolution rate allowing time for optimal bone formation around the apatite scaffold.

### *13.3. Abutment coating materials*

The biocompatibility of the fluorapatite coatings has solely focused on hard tissue i.e. bone formation. It is possible that other cells e.g. fibroblasts would also have an increased affinity for these materials. Additional *in vitro* work could be undertaken to assess this. If it is shown that other cells such as fibroblasts also have an affinity for these materials this may provide a further potential clinical use for them.

Once the implant has been placed there is often a clinical scenario where additional soft tissue is required. Figure 110 shows a clinical scenario where the soft tissues have been manipulated at second stage surgery to try and offer an additional bulk of tissue on the buccal surface for aesthetic purposes

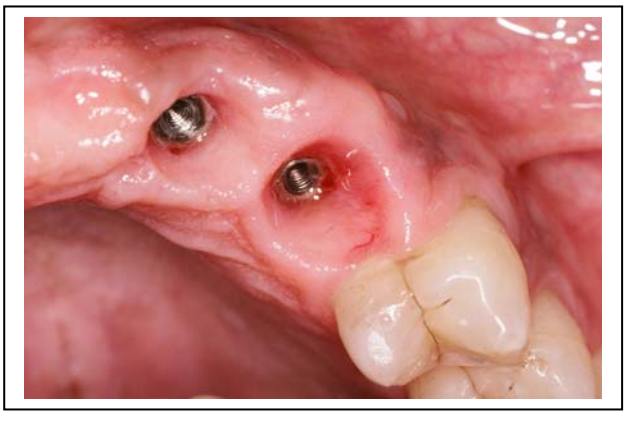

**Figure 110**: Soft tissue profile from implants.

It could be possible to coat the under surface of implant healing abutments or implant abutments to encourage soft tissue proliferation and potentially soft tissue regeneration, this would allow optimal aesthetics in a case where the soft tissues are currently suboptimal.

Figure 111 and 112 shows a case where a procedure has been undertaken to attempt to increase the soft tissue bulk to improve the emergence profile of the fixed implant retained restorations. Clearly it could be of significant benefit if the implant healing abutments could be coated with a material that encouraged epithelial growth and proliferation. Potentially the fluorapatite made in this study from the sol-gel technique could be simply coated on to the desired areas of the titanium abutments and maintained in place to initially stimulate the healing phase and subsequent cellular proliferation phase.

**Figure 111**: Pre-operative view – note lack of soft tissues.

**Figure 112**: Post-operative after stage II surgery – using flap design attempt has been made to increase the soft tissues.

### *13.4. Bone grafting materials*

While observing the SEM's from this study it became very clear that following spin coating at lower speeds the patterns that were seen were extremely similar to one of the current bone grafting materials that is used commonly with dental implants – Bio-Oss (Geistlich Pharma AG, Switzerland). Bio-Oss is made from deproteinised bovine bone.

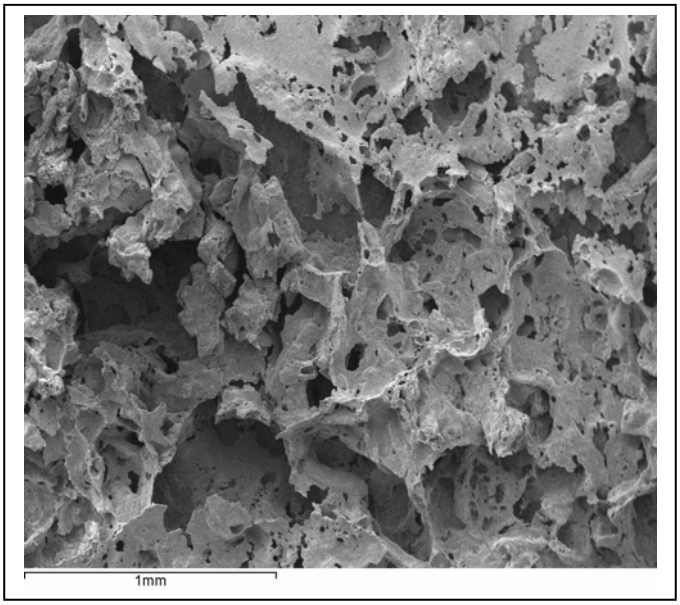


**Figure 113**: SEM of typical coating at 2430 rpm

Figure 113 shows the SEM pattern obtained when fluorapatite was coated at speed of 2430rpm. Higher coating speeds than this resulted in a much more dense coating. The pattern seen immediately suggests that the materials that have been made from the sol-gel technique in this study could potentially offer themselves as osteoconductive bone grafting materials.

The first potential role as a bone grafting material could be in the form of alloplastic bone crystals. Figures 114 - 117 show a sinus lift being undertaken clinically, using a mixture of Bio-Oss and harvested bone scraping to provide the bone for the graft.

**Figure 114**: Pre-operative radiograph – note large sinus

**Figure 115**: Bio-Oss (left) to be mixed with harvested bone.

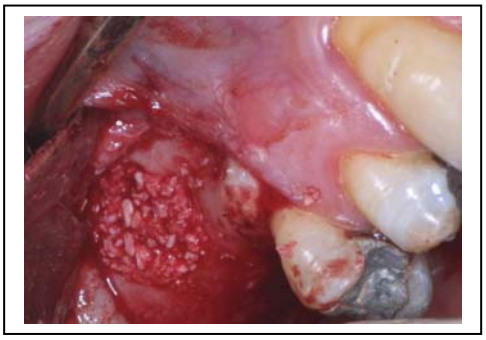

**Figure 116**: Bio-Oss and harvested bone in the sinus.

**Figure 117**: Post operative radiograph after sinus lift procedure.

The results from this study suggest that because of the excellent biocompatibility of fluorapatite made from the sol-gel method and the simple method of constructing it from the sol-gel route – this may be able to provide a synthetic clinical alternative to current materials.

The second potential role as bone grafting material could be by moulding and making the sol-gel into a specific shape as a bulk material – then use of the entire material as a bone graft.

Figure 118, shows the sol-gel as received. The gel like properties of this material could be used to mould the material into a desired shape.

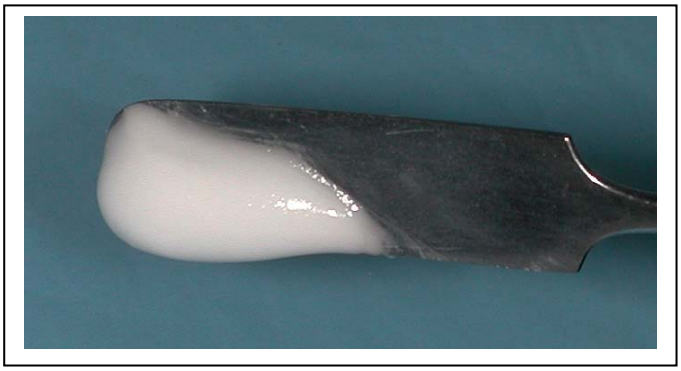

**Figure 118**: Consistency of the sol-gel as received.

Figures 119 to 121, show a block bone graft being undertaken clinically. The donor bone is harvested from the mandible and cut to the correct size to match the region to which it is being harvested.

**Figure 119**: Harvesting bone graft from the mandible

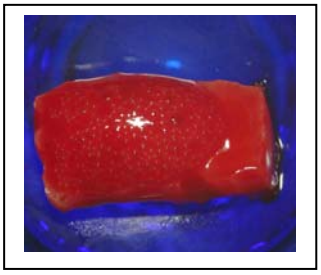

**Figure 120**: Harvested bone graft.

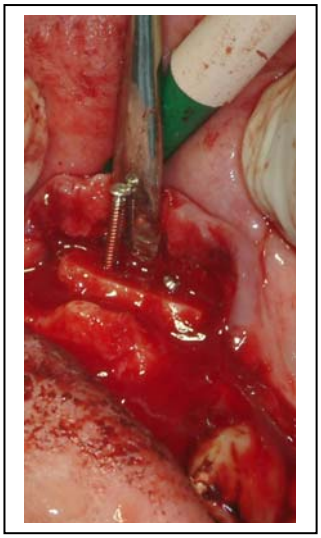

**Figure 121**: Harvested bone graft being placed in donor site (maxilla).

Clearly harvesting the bone is a procedure which requires a prolonged surgical intervention and has its own risks and side effects.

Following establishment of the size of the defect, by building on the results of this study it may be possible to get a fluorapatite sol-gel, mould it to the desired shape, cure it to that shape e.g. by rapid heating under pressure, open a flap clinically then place it directly in to the harvest site. Here it could be osteoconductive to new bone growth.

# Chapter 14 :

# Summary

## 14. Summary

The investigation and results of this study have revealed the following:

- The following protocol has been established for the production of hydroxyapatite sol-gels:

  (1) Triethyl phosphite ([$P(C_2H_50)_3$], Aldrich, USA) of 0.1 moles is hydrolyzed in ethanol with distilled water for 72 hours.

  (2) The hydrolysed TEP is then slowly added to a 0.16 mole solution of calcium nitrate [$Ca(NO_3)_2.4H_20$, Aldrich USA] and allowed to mix for 24 hours.

  (3) A 5% solution of ammonium hydroxide ($NH_4OH$, BDH, UK) and 100ml water is added to the solution in order to improve gelation and the polymerization of an apatite structure.

  (4) Subsequent aging is allowed for 24 hours at room temperature.

  (5) Oven drying is undertaken for a further 24 hours.

- With the use of an ammonium fluoride ($NH_4F$) precursor fluoride substitution can be controlled into the apatite structure such that it is possible to make; $Ca_{10}(PO_4)_6F_2$, $Ca_{10}(PO_4)_6OH_{0.5}F_{1.5}$, $Ca_{10}(PO_4)_6OH_1F_1$ and $Ca_{10}(PO_4)_6OH_{1.5}F_{0.5}$.

- The sol-gel technique used produced hydroxyapatite (HA), fluorapatite (FA) and fluorhydroxyapatite (FHA) that showed varying thermally stabilities.

- Heating from 500°C to 1000°C caused a decrease in the unit cell size of the apatite structure for HA, FA and FHA obtained from the sol-gel technique used.

- Increasing fluoride ion substitution in the apatite structure caused a decrease in the unit cell size. This can be solely attributed to changes in the a – axis of the apatite structure.

- The higher the concentration of fluoride in the sol-gel the higher the viscosity i.e. the viscosity of the sol-gels was as follows; $Ca_{10}(PO_4)_6F_2$ > $Ca_{10}(PO_4)_6OH_{0.5}F_{1.5}$ > $Ca_{10}(PO_4)_6)OH_1F_1$ > $Ca_{10}(PO_4)_6OH_{1.5}F_{0.5}$ > $Ca_{10}(PO_4)_6(OH)_2$.

- The higher the concentration of fluoride in the sol-gel the higher the contact angle i.e. the contact angle of the sol-gels on titanium was as follows; $Ca_{10}(PO_4)_6F_2$ > $Ca_{10}(PO_4)_6OH_{0.5}F_{1.5}$ > $Ca_{10}(PO_4)_6OH_1F_1$ > $Ca_{10}(PO_4)_6OH_{1.5}F_{0.5}$ > $Ca_{10}(PO_4)_6(OH)_2$.

- The dissolution rates of the fluoride-substituted powders from the sol-gels were considerably lower than that of HA. The observed dissolution rates ($Ca_{10}(PO_4)_6(OH)_2$ > $Ca_{10}(PO_4)_6F_{0.5}OH_{1.5}$ > $Ca_{10}(PO_4)_6F_1OH_1$ > $Ca_{10}(PO_4)_6F_{1.5}OH_{0.5}$ > $Ca_{10}(PO_4)_6F_2$) suggest the possibility of tailoring the solubility of any coatings made from the sol-gels through fluoride ion substitution.

- The higher the temperature the sol-gel was heated to, the lower to ion release and thus dissolution rate. The dissolution rate followed the pattern of 600°C > 700°C > 800°C > 1000°C suggesting the possibility of tailoring the solubility of any coating made from this sol-gel route by increasing the firing temperature.

- The sol-gels can be coated onto titanium using a spin coating method.

- At low spinning speeds i.e. 2430 and 2825, the coatings are very porous. As the spinning speed increased the coating becomes more uniform. At speeds of 3515 rpm and above all of the sol-gels resembled uniform smooth surface.

- Increasing the fluoride substitution significantly increased the bond strength such that the bond strengths were as follows; $Ca_{10}(PO_4)_6F_2$ > $Ca_{10}(PO_4)_6OH_{0.5}F_{1.5}$ > $Ca_{10}(PO_4)_6OH_1F_1$ > $Ca_{10}(PO_4)_6OH_{1.5}F_{0.5}$ = $Ca_{10}(PO_4)_6(OH)_2$.

- Uniformly with all the sol-gel coatings the bond strength significantly increased as the firing temperature increased such that bond strengths 1000$^oC$ > 800$^oC$ > 700$^oC$ > 600$^oC$.

- The mean bond strength of $Ca_{10}(PO_4)_6F_2$ was approximately 40MPa, which is higher than or comparable to those usually observed with the hydroxyapatite plasma-sprayed coatings (≈ 10 – 40 MPa).

- In general the coating thickness increases with increasing substitution of fluoride, such that the coating thickness of the sol-gel derived apatites was $Ca_{10}(PO_4)_6F_2$ > $Ca_{10}(PO_4)_6OH_{0.5}F_{1.5}$ > $Ca_{10}(PO_4)_6OH_1F_1$ > $Ca_{10}(PO_4)_6OH_{1.5}F_{0.5}$ > $Ca_{10}(PO_4)_6(OH)_2$.

- Throughout there were large decreases in the coating thickness from 2430 – 3220 rpm. There were minimal differences between the coating thicknesses between 3615 and 4010 rpm.

- $Ca_{10}(PO_4)_6F_2$ (fluorapatite) had significantly greater cellular proliferation than all the other materials, including hydroxyapatite [$Ca_{10}(PO_4)_6(OH)_2$], titanium and TCP.

- Fluoride substituted hydroxyapatites synthesised by the sol-gel protocol established in this thesis may offer a highly biocompatible alternative to hydroxyapatite for coating titanium implants and as an alloplastic osteoconductive bone grafting materials. The physical and biological properties of these coatings / bone grafting materials may be altered by; level of fluoride substitution in the apatite structure and temperature the sol-gel is heated to after crystallisation.

# Chapter 15:

# References

## 15. References


Abe, Y., Hiasauzuki, K. & Akagawa, Y. (2005) New surface modification of titanium implant with phospho-amino acid. *Dental Materials Journal* **24**: 536-540.

Abrahams, I. & Knowles, J.C. (1994) Effects of sintering conditions on hydroxyapatite for use in medical applications - A powder diffraction study. *Journal of Materials Chemistry* **4**: 185-188.

Adell, R., Lekholm, U., Rockler, B. & Branemark, P.I. (1981) A 15-year study of osseointegrated implants in the treatment of the edentulous jaw. *International Journal of Oral Surgery* **10**: 387-461.

Ahmed, S.A., Gogal, R.M. & Walsh, J.E. (1994) A new rapid and non-radioactive assay to monitor and determine the proliferation of lymphocytes: an alternative to 3H thymidine incorporation assay. *Journal of Immunological Methods* **170**: 211-224.

Aisa, M.C., Rahman, S., Senin, U., Maggio, D. & Russell, R.G. (1996) Cathepsin B activity in normal human osteoblas-like cells and human osteoblastic osteosarcoma cells (MG-63): regulation by interleukin-I beta and parathyroid hormone. *Acta Biochemistry and Biophysics* **1290**: 29-36.

Albrektsson, T. & Hansson, H.A. (1986) An ultrastructural characterization of the interface between bone and sputtered titanium or stainless steel surfaces. *Biomaterials* **7**: 201-5.

Albrektsson, T., Hansson, H.A. & Ivarsson, B. (1985) Interface analysis of titanium and zirconium bone implants. *Biomaterials* **6**: 97-101.

Anderson. P. & Klein, L.C. (1987) Shrinkage of lithium aluminosilicate gels during drying. *Journal of Non Crystal Science* **93**: 415-422.

Anderson, J., Areva, S., Spliethoff, B. & Linden, M. (2005) Sol-gel synthesis of a multifunctional, hierarchically porous silica/apatite composite. *Biomaterials* **26**: 6827-6835.

Anusavice, K.J., Hojjatie, B. & Dehoff, P.H. (1986) Influence of metal thickness on stress distribution in metal-ceramic crowns. *Journal of Dental Research* **65**: 1173-1178.

Aoki, H. (1991) *Science and Medical Applications of Hydroxyapatite* Japanese Association of Apatite Science, Takayama Press System Center Co, Inc,.

Athanasou, N.A. (1999) *Colour Atlas of Bone, Joint, and Soft Tissue Pathology*. Oxford University press.

Bachle, M. & Kohal, R.J. (2004) A systematic review of the influence of different titanium surfaces on proliferation, differentiation and protein synthesis of osteoblast-like MG63 cells. *Clinical Oral Implant Research* **15**: 683-692.

Baier, R.E & Meyer, A.E. (1988) Implant surface preparation. *International Journal of Oral and Maxillofacial Implants* **3**: 9-20.

Balas, F., Perez-Pariente, J. & Vallet-Regi, M. (2003) In vitro Bioactivity of Silicon Subsituted Hydroxyapatites. *Journal of Biomedical Materials Research* **66A**:364.

Baleani, M. Viceconti, M. & Toni, A. (2000) The effect of sandblasting treatment on endurance properties of titanium alloy hip prostheses. *Artificial Organs* **24**: 296-299.

Barralet, J., Best, S. & Bonfield, W. (1998) Carbonate substitution in precipitated hydroxyapatite: an investigation into the effects of reaction temperature and bicarbonate ion concentration. *Journal of Biomedical Materials Research* **41**: 79-86.

Ben-Nissan, B. & Choi, A.H. (2006) Sol-gel production of bioactive nanocoatings for medical applications. *Nanomedicine* **1**: 311-319.

Bigi, A., Falini, G., Foresti, E., Gazzano, M., Ripamonti, A. & Roveri, N. (1996) Structure Refinements of Calcium Hydroxyapatite Containing Magnesium. *Acta Crystallographica* **B52**: 87-92.

Binon, P. (2000) Implant and components: Entering the new millennium. *International Journal of Oral and Maxillofacial Implants* **15**: 76-94.

Biosource Handbook – alamarBlue (2003) www.biosource.com.

Bloebaum, R.D. & Dupont J.A. (1993) Osteolysis from a Press-Fit Hydroxyapatite-Coated Implant. *Journal of Arthroplasty* **8**:195-197.

Block, M.S., Finger. I.M., Fontenot, M.G. & Kent J.N. (1989) Loaded hydroxyapatite-coated proximal ingrowth femoral stems. A matched pair control study. *Clinical Orthopaedics* **4**: 219-225.

Bogdanoviciene, I., Beganskiene, A., Tonsuaadu, K., Glaser, J., Meyer., H.J. & Kareiva, A. (2006) Calcium hydroxyapatite $Ca_{10}(PO_4)_6(OH)_2$ prepared by aqueaous sol-gel processing. *Materials Research Bulletin* **41**: 1754-1762.

Boyan, B.D., Schwartz, Z., Bonewald, L.F. & Swain, L.D. (1989) Localization of 1,25-(OH)2D3- responsive alkaline phosphatise in osteoblast-like cells (ROS 17/2.8, MG63 and MC3T3) and growth cartilage cells in culture. *Journal of Biological Chemistry* **264**: 11879-11886.

Boyan, B.D., Hummert, T.W., Kieswetter, K., Schraub, D., Dean, D. & Schwartz, Z. (1995) Effect of titanium surface characteristics on chondrocytes and osteoblasts *in vitro*. *Cells and Materials* **5**: 323-334.

Braun R.D. (1987) *Introduction to Instrumental Analysis*, McGraw-Hill Book Company, New York.

Breithaupt, J. (1990) *Understanding Physics For Advanced Level,* Second Edition, Stanley Thornes (Publishers) Limited.

Brett, P.M., Harle, J., Salih, V., Mihoc, R., Olsen, I., Jones, F.H. & Tonetti, M. (2004) Roughness response genes in osteoblasts. *Bone* **35**: 124-133.

Brinker, C.J. & Scherer, G.W. (1990) *Sol-gel science: The Physics and Chemistry of Sol-Gel Processing.* Academic Press, London, UK.

Brunski, J.B. (2003) *In vivo* response to biomechanical loading at the bone/dental-implant interface. *Advanced Dental Research* **13**: 99-119.

Buser, D. Nydegger, T. Oxland, T. Cochran, D.L. Schenk, R.K., Hirt, H.P. Snetivy, D. & Nolte, L.P. (1999) Interface shear strength of titanium implants with a sandblasted and acid-etched surface: A biomechanical study in the maxilla of miniature pigs. *Journal of Biomedical Materials Research* **45** (2): 75-83.

Chai, C.S. & Ben-Nissan, B. (1999) Bioactive nanocrystalline sol-gel hydroxyapatite coatings. *Journal of Material Science and Materials in Medicine* **10** : 465-469.

Cheng, K., Shen, G., Weng. W.J., Han, G.R., Ferreira, J.M.F & Yang, J. (2001) Synthesis of hydroxyapatite/fluoroapatite solid solution by a sol-gel method. *Materials Letters* **51**: 37-41.

Cheng, K., Weng, W.J., Du P.Y., Shen, G. Han, G.R. & Ferreira, J.M.F. (2004) Synthesis and characterisation of fluoridated hydroxyapatite with a novel fluorine containing reagent. *Key Engineering Materials* **254**: 331-334.

Cheng, Z.H., Yasukawa, A., Kandori, K. & Ishikawa, T. (1998) FTIR Study on incorporation of $CO_2$ into calcium hydroxyapatite. *Journal of the Chemical Society, Faraday Transactions* **94**: 1501-1505.

Chiang, Y.-M., Birnie I.D. & Kingery, D.W. (1997) *Physical Ceramics: Principles for Ceramic Science and Engineering*. John Wiley & Sons, Inc.

Clover, J. & Gowen, M. (1994) Are MG63 and HOS TE85 human osteosarcoma cell lines representative models of the osteoblastic phenotype? *Bone* **15**: 585-591.

Cochran, D.L (1999) A comparison of endosseous dental implant surfaces. *Journal of Periodontology* **70**: 1523-1539.

Cochran, D.L., Hermann, J., Schenk, R., Higginbottom, F. & Buser, D. (1997) Biologic width around titanium implants. A histometric analysis of the implanto-gingival junction around unloaded and loaded nonsubmerged implants in the canine mandible. *Journal of Periodontology* **68**: 186-198.

Collier, J.P., Surprenant, V.A., Mayor, M.B., Wrona, M., Jensen, R.E. & Surprenant, H.P. (1993) Loss of hydroxyapatite coating on retrieved, total hip components. *Jourrnal of Arthroplasty* **8**: 389-395.

Connors, K. (1990) Chemical Kinetics. *VCH Publishers, 14-28.*

Cullity, B.D. (1978) *Elements of X-Ray Diffraction* 2nd edition. Addison-Wesley.

Degasne, I. Basle, M.F. Demais, V. Hure, G. Lesourd, M. Grolleau, B. Mercier, L. & Chappard, D. (1999) Effects of roughness, fibronectin and vitronectin on attachment, spreading, and proliferation of human osteoblast-like cells (Saos-2) on titanium surfaces. *Calcified Tissue Interface* **64**: 499-507.

DeHoff P.H., Anusavice, K.J., Wang, Z. (1995) Three-dimensional finite element analysis of the shear bond test. *Dental Materials* **11**: 126-131.

De Lambilly, H.,Klein, L.C. (1989) Effect of methanol concentration on lithium aluminosilicate. *Journal of Non Crystal Solutions* **109**: 69-78.

De Maetzu, M.A., Braceras, I., Alava, J.I., Sanchez-Garces, M.A. & Gay-Escoda, C. (2007) Histomorphometric study of ion implantation and diamond-like carbon as dental implant surface treatments in beagle dogs. *International Journal of Oral and Maxillofacial Implants* **22**: 273-279.

Dionex. (2003) ICS-*1000 Ion Chromatography System Operators Manual*.

Dislich, H. (1988) Thin films from the sol-gel process. In: *Sol-Gel Technology for Thin Films, Fibers, Preforms, Electronics and Speciality Shapes.* Klein LC (Ed.) Noyes Pub., NJ, USA: 50-77.

Doremus, R.H. (1992) Review of Bioceramics. *Journal of Materials Science* **27**: 285-297.

Driskell, T.D. (1994) *Early history of calcium phosphate. Materials and Coatings*, ASTM publication, Philadelphia: 3-17.

Ducheyne P, & Cuckler J.M. (1992) Bioactive Ceramic Prosthetic Coatings. *Clinical Orthopaedic Related Research* **27**:102-14.

Elliot, J.C. (1994) Structure and Chemistry of the Apatites and other Calcium Orthophosphates. *Studies in Inorganic Chemistry* **18**: 48-87.

Esposito, M., Hirsch, J.M., Lekholm, U. & Thomsen, P. (1998) Biological factors contributing to failures of osseointegrated oral implants. *European Journal of Oral Science* **106**: 527-551.

Evans, G., Behiri, J., Currey, J. & Bonfield, W. (1990) Microhardness and Young's modulus in cortical bone exhibiting a wide-range of mineral volume fractions and in a bone analogue. *Journal of Materials Science-Materials in Medicine* **1**: 38-43.

Feki, H.E., Savariault, J.M. & Salah, A.B. (1999) Structure refinement by the Rietveld method of partially substituted hydroxyapatite: $Ca_9Na_{0.5}(PO_4)_{4.5}(CO_3)_{1.5}(OH)_2$. *Journal of Alloys and Compounds* **287**: 114-120.

Ferraz, M.P., Fernandes, M.H., Cabral, A.T., Santos, J.D. & Monteiro, F.J. (1999) In vitro growth and differentiation of osteoblast-like human bone marrow cells on glass reinforced hydroxyapatite plasma- sprayed coatings. *Journal of Materials Science-Materials in Medicine* **10**: 567-576.

Floch, H.G., Belleville P.F., Priotton, J.J., Pegon, P.M., Dijonneau, C.S. & Guerain, J. (1995) Sol gel coatings for lasers III. *American Ceramic Society Bulletin* **74**: 48-52.

Finklea, H.O. & Murry, R.W. (1979) Effects of silanization on titanium dioxide electrodes. *Journal of Physical Chemistry B* **83**: 353-359.

Fraker, A.C. Ruff, A.W., Sung, P. Van Orden A.C. & Speck K.M. (1983) *Titanium alloys in surgical implants*. In: H.A. Luckey and F. Kubli, Editors, ASTM Special Technical Publication 796, Philadephia : 206–219.

Francheschi, R.T., James, W.M. & Zerlough. Dihydroxyvitamin $D_3$ specific regulation of growth, morphology and fibronectin in a human osteosarcoma cell line. *Journal of Cellular Physiology* **123**: 401-409.

Freund, F. & Knobel, R.M. (1977) Distribution of fluorine in hydroxyapatite studied by infrared spectroscopy. *Journal of the Chemical Society* **15**: 1136-1140.

Frost, H.M. (1989) The biology of fracture healing. An overview for clinicians. *Clinical Orthopaedic Related Research* **248**: 294-309.

Gabriel, A.O. & Riedal, R. (1997) Novel non-oxide sol-gel process to Si-C-N ceramics. *Ceramic Engineering Scientific Proceeds* **18** : 713-720.

Gadaleta, S.J., Pascahalis, E.P., Betts, F., Mendelsohn, R. & Boskey, A.L. (1996) Fourier transform infrared spectroscopy of the solution-mediated conversion of amorphous calcium phosphate to hydroxyapatite: New correlations between x-ray diffraction and infrared data. *Calcified Tissue International* **58**: 9-16.

Gan, L. & Ben-Nissan, B. (1997) The effect of mechanical properties of think films on nano-identation data: Finite Element Analysis. *Compendium of Materials in Science* **8**: 273-381.

Gan, L. & Ben-Nissan, B. (2006) Sol gel production of bioactive nanocoatings. *Nanomedicine* **1**:311-319.

Gan, L. & Pilliar R. (2004) Calcium phosphate sol-gel derived films on porous-surfaced implants for enhanced osteoconductivity. Part 1: synthesis and characterization. *Biomaterials* **25**: 5303-5312.

Georgiou, G. & Knowles, J.C. (2001) Glass reinforced hydroxyapatite for hard tissue surgery-Part 1: mechanical properties. *Biomaterials* **22**: 2811-2815.

Gibson, I.R., Best, S.M. & Bonfield W. (1999) Chemical characterization of silicon-substituted hydroxyapatite. *Journal of Biomedical Material Research* **44**: 422-8.

Golden, D.C. & Ming, D.W. (1999) Nutrient-substituted hydroxyapatites: Synthesis and characterisation. *Soil Science Society of America Journal* **63**: 657-664.

Haddow D.B, Kothari, S., James P.F., Short R.D., Hatton P.V. & Van Noort R. (1996) Synthetic implant surfaces. 1. The formation and characterization of sol-gel films. *Biomaterials* **17**: 501-7.

Han, Y.C., Li, S.P., Wang X.Y. & Chen X.M. (2004) Synthesis and sintering of nanocrystalline hydroxyapaptite powders by citric acid sol-gel combustion method. *Materials Research Bulletin* **39**: 25-32.

Harris, M.T., Byers, C.H. & Brunson, R.R. (1988) A study of solvent effects on the synthesis of pure component and composite ceramic powders by metal alkoxide hydrolysis. In: *Better Ceramic Through Chemistry (3rd Edition)* Brinker CJ, Clark DE, Ulrich DR (Eds) Materials Research Societry, PA, USA: 287-292.

Hasegawa, I., Nakamura, T., Motojima, S. & Kajiwara, M. (1997) Synthesis of silicon carbide fibers by sol-gel processing. *Journal of Sol-Gel Science Technology* **8**: 577-579.

Heling, I., Heindel, R. & Merin, B. (1981) Calcium-fluorapatite. A new material for bone implants. *Journal of Oral Implantology.* **9**: 548-555.

Hench, L.L. (1991) Bioceramics from Concept to Clinic. *Journal of the American Dental Association* **74**:1485-510.

Hench, L.L. & Andersson, Ö. (1993) *Bioactive glass*. In: L.L. Hench and J. Wilson, Editors, *An Introduction to Bioceramics*, World Scientific, Singapore: 41–62.

Hermansson, L., Kraft, L. & Engqvist, H. (2003) Chemically bonded ceramics as biomaterials. *Key Engineering Materials* **247**: 437-442.

Hollas, J.M. (1996) *Modern Spectroscopy* 3rd edition. John Wiley & Sons..

Hignett, B., Andrew, T. C., Downing, W., Duwell, E.J., Belanger, J. & Tulinski, E.H. (1987) *Surface cleaning, finishing and coating*. In: W.G. Wood, Editors, *Metals Handbook* vol. **5**, American Society for Metals, Metals Park, OH: 107–127.

Hsieh, M.F., Perng, L.H. & Chin, T.S. (2002) Hydroxyapatite coatings on Ti6Al4V alloy using a sol-gel derived precursor. *Materials in Chemistry and Physics* **74**: 245-250.

Ikoma, T., Yamazaki, A., Nakamura, S. & Akao, M. (1999) Preparation and dielectric property of sintered monoclinic hydroxyapatite. *Journal of Materials Science Letters* **18**, 1225-1228.

Iwasaki, Y. & Saito, N. (2003) Immobilization of phosphorylcholine polymers to Ti supported vinyldimethylsilyl monolayers and reduction of albumin adsorption. Colloids Surfaces B *Biointerfaces* **32**: 77-83.

Jackson, M.J., Robinson, G.M., Ali, N., Kousar, Y., Mei, S., Gracio, J., Taylor, H. & Ahmed, W. (2006) Surface engineering of artificial heart valve disks using nanostructured thin films deposited by chemical vapour deposition and sol-gel methods. *Journal of Medical Engineering and Technology* **30**: 323-329.

Jackson, M.J., Sein, H., Ahmed, W. & Woodwards, R. (2007) Novel diamond-coated tools for dental drilling applications. *Journal of Medical Engineering and Technology* **31**: 81-93.

Jarcho, M. (1992) Retrospective analysis of hydroxyapatite development for oral implant applications. *Dental Clinics of North America* **36**: 19-26.

Jimenez, C. & Langlet, M. (1994) Formation of TiN by nitration of $TiO_2$ films deposited by ultrasonically assisted sol-gel technique. *Surface Coating Technology* **68**: 249-252.

Joa, L.J., Best, S.M., Knowles, J.C., Rehman, I. & Santos,J.D. (1997) Preparation and characterization of fluoride-substituted apatites. *Journal of Materials Science-Materials in Medicine* **8**: 185-191.

Kanno, T., Horiuchi, J.-I., Kobayashi, M., Motogami, Y. & Akazawa,T. (1999) Characteristics of the Carbonate Ions Incorporated into Calcium-Partially-Strontium-Substituted and Strontium Apatites. *Journal of Materials Science Letters* **18**: 1343-1345.

Karlsson, K.H. Fröberg K. & Ringbom, T. (1989) A structural approach to bone adhering of bioactive glasses. *Journal Non-Crystalline Solids* **112**: 69-77.

Kasemo B (1983) Biocompatibility of Titanium Implants: Surface Science aspects. *Journal of Prosthetic Dentistry* **49**: 832-837.

Kasemo, B. & Lausmaa, J. (1986) Surface science aspects on inorganic biomaterials. *CRC Critical Review of Biocompatibility* **2**: 335-380.

Kay, M.I., Young, R.A. & Posner, A.S. (1964) Crystal Structure of Hydroxyapatite. *Nature* **204**: 1050-1052.

Kilpadi, D.V., Lemons, J.E., Liu, J., Ganesh, N. & Raikar, N. (2000) Cleaning and heat – treatments effects of unalloyed titanium implant surfaces. *International Journal of Oral and Maxillofacial Implants* **15**: 219-230.

Kim, H.W., Long-Hao, L., Koh, T.H., Knowles, J.C. & Kim, H.E (2004) Sol-gel Preparation and Properties of Fluoride-Substituted Hydroxyapatite Powders. *Journal of the American Ceramic Society* **87**: 1939-1944.

Kim, H.W., Kim, H.E. & Knowles JC. (2004) (a) Fluor-hydroxyapatite sol-gel coatings on titanium substrate for hard tissue implants. *Biomaterials* **27**: 3351-8.

Kim, H.W., Kim, H.E. & Knowles J.C. (2005) Improvement of Hydroxyapatite Sol-Gel Coatings on Titanium with Ammonium Hydroxide Addition. *Journal of the American Ceramic Society* **88**: 154-159.

Kim, H.W., Knowles, J.C., Salih. V. & Kim, H.E. (2004) (b) Hydroxyapatite and fluor-hydroxyapatite layered film on titanium processed by a sol-gel route for hard-tissue implants. *Journal of Biomedical Material Research* **71B**: 66-76.

Kim, H.W., Kim, H.E., Salih, V. & Knowles, J.C. (2005) Hydroxyapatite and titania sol-gel composite coatings on titanium for hard tissue implants and *in vitro* biological performance. *Journal of Biomaterials Research B: Applied Biomaterials* **72B**: 1-8.

Kim, H.W., Koh, Y.H., Li, L.H., Lee, S. & Kim, H.E (2004) (c) Hydroxyapatite coating on titanium substrate with titania buffer layer processed by sol-gel method*. Biomaterials* **25**: 2533-2546.

Kim, H.W., Koh, Y.H., Yoon, B.H. & Kim, H.E. (2002) Reaction Sintering and Mechanical Properties of Hydroxyapatite-Zirconia Composite with $CaF_2$ Additions. *Journal of the American Ceramic Society* **85**: 1634-1636.

Kim, H.W., Noh, Y.J., Koh, Y.H., Kim, H.E., & Kim, H.M. (2002b) Effect of CaF2 on densification and properties of hydroxyapatite-zirconia composites for biomedical applications. *Biomaterials* **23**: 4113-4121.

Kim, H.M. Miyaji, F., Kokubo, T. & Nakamura, T. (1996) Preparation of bioactive Ti and its alloy via simple chemical surface treatment. *Journal of Biomedical Materials Research* **32**: 409-417.

Kim, H.M. Miyaji, F., Kokubo, T. & Nakamura, T. (1996) In situ measurements of ion-exchange processes in single polymer particles: laser trapping microspectroscopy and confocal fluorescence microspectrosopy. *Journal of Biomedical Materials Research* **33**: 524-531.

Knowles, J.C., Talal ,S. & Santos, J.D. (1996) Sintering effects in a glass reinforced hydroxyapatite. *Biomaterials* **17,** 1437-1442.

Kokubo, T., Kim, H.M. & Kawashta, M. (2003) Novel bioactive materials with different mechanical properties. *Biomaterials* **24**: 2161-2175.

Kweh, S.W.K., Khor, K.A. & Cheang, P. (2002) An in vitro investigation of plasma sprayed hydroxyapatite (HA) coatings produced with flame-spheroidized feedstock. *Biomaterials* **23**: 775-785.

Lacefield, W.R. (1993) *An introduction to Bioceramics. World Scientific, Singapore* In: L.L. Hench and J. Wilson, Editors 223-233.

Lajeunesse, D., Kiebzak, G.M., Frondoza, C.G. & Sacktor, B. (1991) Regulation of osteocalcin secretion by human primary bone cells and by the human osteosarcoma cell line MG-63. *Bone and Mineral* **14**: 237-250.

Larsen, M.J. & Jensen, S.J. (1989) Solubility, Unit Cell Dimensions and Crystallinity of Fluoridated Human Dental Enamel. *Archives of Oral Biology* **34**:969-73.

Larson, A.C., Von Dreele, R.B. & Lujan, M. (1990) GSAS *Generalised Structural Analysis System,* Neutron Scattering Centre, Los Alamos National Library, CA.

Larsson, C., Thomsen, P., Aronsson, B.O., Rodhal, M., Lausmaa, J., Kasemo, B. & Ericsson, L.E. (1996) Bone response to surface modified titanium implants: studies on the early tissue response to machined and electropolished implants with different oxide thicknesses. *Biomaterials* **17**: 605-616.

Lausmaa, J., Kasemo, B. & Mattsson, H. (1990) Surface spectroscopic characterization of titanium implant materials. *Applied Surface Science* **44**: 133-147.

Lausmaa, J., Lofgren, P. & Kasemo, B. (1999) Adsorption and coadsorption of water and glycine on $TiO_2$. *Journal of Biomedical Materials Research* **44**: 227-242.

Layrolle, P., Ito, A. & Tateishi, T. (1998) Sol-gel synthesis of amorphous calcium phosphate and sintering into microporous hydroxapatite bioceramics. *Journal of the American Ceramic Society* **81**: 1421-1428.

Layrolle, P. & Lebugle, A. (1994) Characterization and reactivity of nanosized calcium phosphate prepared in anhydrous ethanol. *Chemistry Materials* **6**: 1996-2004.

Lazzara, R.J., Testori, T., Trisi, P., Porter, S.S. & Weinstein, R.L. (1999) A human histological analysis of osseotite and machined surfaces using implants with two opposing surfaces. *International Journal of Periodontics and Restorative Dentistry* **19**: 117-129.

Lee, J.W., Won, C.W., Chun, B.S. & Sohn (1993) Dip-coating of alumina films by the sol-gel method. *Journal of Materials Research* **8**: 3151-3157.

Lee, B.H., Kim, J.K., Kim, Y.D., Choi, K. & Lee, K.H. (2004) In vivo behaviour and mechanical stability of surface-modified titanium implants by plasma spray coating and chemical treatments. *Journal of Biomedical Materials Research* **69 A**: 279-284.

LeGeros, R.Z. (1965) Effect of carbonate on the lattice parameters of apatite. *Nature* **205**: 403-404.

Legeros R.Z., Lee, D., Quirolgico, G. & Shirra, W.P. (1983) In vitro caries-like formation in fluorine-containing tooth enamel. *Journal of Dental Research* **62**: 138-144.

LeGeros, R.Z. & LeGeros, J.P. (1993) *Dense Hydroxyapatite*, in: Hench, L. L., Wilson, J., editors. *An Introduction to Bioceramics, Chapter 9* World Scientific: Singapore, 139-180.

Li, H., Khor, K.A. & Cheang, P. (2003) Impact formation and microstructure characterization of thermal sprayed hydroxyapatite/titania composite coatings. *Biomaterials* **24**: 949-957.

Lim, Y.M., Hwang, K.S. & Park, Y.J. (2003) Sol-gel derived functionally graded $Ti0_2$/Hap films on Ti-6Al-4V. *Journal Sol-Gel Science and Technology* **21**:123-128.

Liu, X., Chu, P. & Ding, C. (2004) Surface modification of titanium, titanium alloys, and related materials for biomedical applications. *Material Science and Engineering* **47**: 49-61.

Loong, C.-K., Rey, C., Kuhn, T., Combes, C., Wu, Y., Chen, S.-H. & Glimcher, M.J. (2000) Evidence of Hydroxyl-Ion Deficiency in Bone Apatites: An Inelastic Neutron-Scattering Study. *Bone* **26**, 599-602.

Lopes, M.A., Knowles, J.C. & Santos, J.D. (2000) Structural insights of glass-reinforced hydroxyapatite composites by Rietveld refinement. *Biomaterials* **21**, 1905-1910.

Lu, G., Bernasek, S. I. & Schwartz, J. (2000) Oxidation of a polycrystalline titanium surface by oxygen and water. *Surface Science* **458**: 80-90.

Lucchini, J. P., Aurelle, J. L., Therin, M., Donath, K. & Becker, W. (1996) A pilot study comparing screwshaped implants. Surface analysis and histologic evaluation of bone healing. *Clinical Oral Implants Research* **7**: 397-404.

Majewski, P.J. & Allidi, G. (2006) Synthesis of hydroxyapatite on titanium coated with organic self-assembled monolayers. *Materials Science and Engineering A* **420**: 13-20.

Mandl, S., Sader, R., Thorwarth, G., Krause, D., Zeilhofer, H.F., Horch, H.H. & Rauschenbach, B. (2002) Investigation on plasma immersion ion implantation treated medical implants. *Biomedical Engineering* **19**: 129-132.

Mani, G., Johnson, D.M., Marton, D., Feldman, M.D., Patel, D., Ayon, A.A. & Agrawal, C.M. (2008) Drug delivery from gold and titanium surfaces using self-assembled monolayers. *Biomaterials* **29**: 4561-4573.

Marie, P.J. & Hott, M. (1986) Short Term Effects of Fluoride and Strontium on Bone Formation and Resorption in the Mouse. *Metabolism* **35**:547-51.

Marinucci, L., Balloni, S., Becchetti, E., Belcastro, S., Guerra, M., Calvitti, M., Lilli, C., Calvi, E. M. & Locci, P. (2006) Effect of titanium surface roughness on human osteoblast proliferation and gene expression *in vitro*. *International Journal of Oral and Maxillofacial Implants* **21**: 719-725.

Mazdiyasni, K.S. (1982) Powder synthesis from metal-organic precursors. *Ceramics International* **8**: 42-56.

McPherson, E.J., Dorr, L.D., Gruen, T.A. & Saberi, M.T. (1995) Hydroxyapatite-Coated Proximal Ingrowth Femoral Stems. *Clinical Orthopaedics* **315**: 223-30.

Meirelles, L., Currie, F., Jacobsson, M., Albrektsson, T. & Wennerberg, A. (2008) The effect of chemical and nanotopographical modifications on the early stages of osseointegration. *International Journal of Oral Maxillofacial Implants* **23(4)**: 641-7.

Meretoja, V. V., Tirri, T., Aaritalo, V., Jansen, J. A. & Narhi, T. O. (2007) Titania and Titania-Silica Coatings for Titanium: Comparison of Ectopic Bone Formation within Cell-Seeded Scaffolds. *Tissue Engineering* **13(4)**: 855-863.

Merry, J.C., Gibson, I.R., Best, S.M. & Bonfield, W. (1998) Synthesis and characterization of carbonate hydroxyapatite. *Journal of Materials Science-Materials in Medicine* **9**: 779-783.

Meyle, J., Gultig, K. & Nisch, W. (1995) Variation in contact guidance by human cells on microstructured surface. *Journal of Biomedical Materials Research* **29**: 81-88.

Misch, C.E. (1999) *Contemporary implant dentistry* 2nd Ed. Mosby, St. Louis.

Mittal, K.L. (1979) *Surface Contamination: Genesis, Detection and Control* Vol. **1**. In: K.L. Mittal, Editors Plenum Press, New York: 3–46.

Mobasherpour, I., Soulati Heshajin, M., Kazemzadeh, A. & Zakeri. M. (2007) Synthesis of nanocrystalline hydroxyapatite by using precipitation method. *Journal of Alloys and Compounds* **430**: 330-333.

Morgan, H., Wilson, R.M., Elliot, J.C., Dowker, S.E.P. & Anderson, P. (2000) Preparation and Characterisation of Monoclinic Hydroxyapatite and its Precipitated Carbonate Apatite Intermediate. *Biomaterials* **21**: 617-627.

Morono, E.C., Kresak, M. & Zahradnik, R.T. (1974) Fluoridated Hydroxyapatite Solubility and Caries Formation. *Nature* **247**: 64-65.

Mossman, T. (1983) Rapid colorimetric assay for cellular growth and survival: application to proliferation and cytotoxic assays. *Journal of Immunological Methods* **65**: 55-63.

Nanci, A., Wuest, J.D., Peru, L., Brunet, P., Sharma, V., Zalzal, S. & McKee, M.D. (1998) Chemical modification of titanium surfaces for covalent attachment of biological molecules. *Journal of Biomedical Material Research* **40**: 324-335.

Narasaraju, T.S.B. & Phebe, D.E. (1996) Some physico-chemical aspects of hydroxyapatite. *Journal of Materials Science* **31**, 1-21.

Nurhaerani, V., Arita, K., Shinonaga, Y. & Nishino, M. (2006) Plasma-based fluorine ion implantation into dental materials for inhibition of bacterial adhesion. *Dental Materials Journal* **25**: 684-692.

Ohtsuki, C., Iida, H., Hayakawa, S. & Osaka, A. (1997) Bioactivity of titanium treated with hydrogen peroxide solutions containing metal chlorides. *Journal of Biomedical Materials Research* **35**: 39-47.

Okazaki, M., Miake, H., Tohda, H. & Yanagisawa, T. (1998) Differences in solubility of two types of heterogenous fluoridated hydroxyapatites. *Biomaterials* **19**: 611-616.

Ong, J.L. & Lucas, L.C. (1998) Auger electron spectroscopy and its uses for the characterisation of titanium and hydroxyapatite surfaces. *Biomaterials* **19**: 455-464.

Overgaard, S., Soballe, K., Hansen, E.S., Josephsen, K. & Bunger, C. (1996) Implant Loading Accelerates Resorption of Hydroxyapatite Coating. *Journal of Orthopaedic Research* **14**: 888-94.

Overgaard, S., Lind, M., Grundvig, H., Biinger, C. & Soballe, K. (1997) Hydroxyapatite and Fluoroapatite coatings for fixation of weight loaded implants. *Clinical Orthopaedic Related Research* **336**: 286-296.

Patsi, M., Hautaniemi, J. A., Rahiala, H., Peltola, T. & Kangasiemi, I. (1998) Bonding Strengths of Titania Sol-Gel Derived Coatings on Titanium. *Journal of Sol–Gel Science and Technology* **11**: 55-61.

Powder Diffraction File (PDF) (1998) ICDD Powder Diffraction File, PDF-2, ICDD, Pennsylvanis, USA.

Penel, G., Leroy, G., Rey, C. & Bres, E. (1998) MicroRaman Spectral Study of the $PO_4$ and $CO_3$ Vibrational Modes in Synthetic and Biological Apatites. *Calcified Tissue International* **63**: 475-481.

Pettet, R.B., Ashley, C.S., Reed, S.T. & Brinker, C.J. (1988) Antireflective films from sol-gel process. In: *Sol-Gel Technology for Thin Films, Fibers, Preforms, Electronics and Speciality Shapes.* Klein LC (Ed.). Noyes Pub., NJ, USA: 80-109.

Piveteau, L.D., Girona, M.I., Schlapbach, L., Barboux, P., Boilot, J.P. & Gasser, B. (1999) Thin films of calcium phosphate and titanium dioxide by a sol-gel route: a new method for coating medical implants. *Journal of Science and Materials in Medicine* **10**: 161-167.

Price, B., Borland, J.O. & Selbrede, S. (1993) Properties of chemical-vapour-deposited titanium nitride. *Thin Solid Films* **236**: 311-318.

Puleoa, D .A., Kissling, R. A. & Sheu, M. S. (2002) A technique to immobilize bioactive proteins, including bone morphogenetic protein-4 (BMP-4) on titanium alloy. *Biomaterials* **23**: 2079-2087.

Qu, H.B. & Wei, M. (2006) The effect of fluoride contents in fluoridated hydroxyapatite on oesteoblast behaviour. *Acta Biomaterials* **2**: 113-119.

Rangavittal, N., Landa-Canovas, A.R., Gonzalez-Calbet, J.M. & Vallet-Regi, M. (2000) Structural study and stability of hydroxyapatite and beta- tricalcium phosphate: Two important bioceramics. *Journal of Biomedical Materials Research* **51**: 660-668.

Ratner, B.D. (1993) New ideas in biomaterials science - A path to engineered biomaterials. *Journal of Biomedical Material Research* **27**: 837-850.

Ratner, B.D. (1996) *Surface Properties of Materials*. In: Ratner BD, Hoffman AS, Schoen FJ, Lemons, JE, Editors. Biomaterial Science: An Introduction to Materials and Methods. California: Academic Press: 21-35.

Raynaud, S., Champion, E., Bernache-Assollant, D. & Thomas, P. (2002) Calcium phosphate apatites with variable Ca/P atomic ratio 1. Synthesis, characterisation and thermal stability of powders. *Biomaterials* **23**: 1065-72.

Rehman, I. & Bonfield. W (1997) Characterization of hydroxyapatite and carbonated apatite by photo acoustic FTIR spectroscopy. *Journal of Materials Science: Materials in Medicine* **8**: 1-4.

Rendon-Angeles, J.C., Yanagisawa, K., Ishizawa, N. & Oishi, S. (2000) Topotaxial conversion of chlorapatite and hydroxyapatite to fluorapatite by hydrothermal ion exchange. *Chemistry Materials* **12**: 2143-2150.

Rey, C. (2000) Calcium phosphate biomaterials and bone mineral. Difference in composition, structure and properties. *Biomaterials* **11**: 5-13.

Richerson, D.W. (1992) *Modern Ceramic Engineering*, Second edition, Marcel Dekker, Inc.

Rietveld H.M. (1968) A profile refinement method for nuclear and magnetic structures. *Journal of Applied Crytsallography* **2**, 65-71.

Ring, T.A. (1996) *Fundamentals of Ceramic Powder Processing and Synthesis,* Academic Press.

Rupp, F., Scheideler, L., Olshanska, N., de Wild, M., Wieland, M. & Geis-Gerstorfer, J. (2005) Enhancing surface free energy and hydrophilicity through chemical modification of microstructured titanium implant surfaces. *Journal of Biomedical Materials Research* **76**: 323-334.

Sakka, S., Kamiya, K., Makita, K. & Tamamoto, Y. (1984) Formation of sheets and coating films from alkoxide solutions. *Journal of NonCrystal Solutions* **63**: 223-235.

Samuneva, B., Kozhukharov, V., Trapalis, C. & Kranold, R. (1993) Sol-gel processing of titanium-containing thin coatings Part I: Preparation and Structure. *Journal of Material Science* **28**: 2353-2361.

Schramm, D.U., Rossi, A.M. & Bemski, G. (1998) Electron spin resonance, electron-nuclear double resonance and general triple resonance studies on the contributions to line broadening of CO2- in A-type carbonated apatites and biocarbonates. *Japanese Journal of Applied Physics* **37**: 502-508.

Schroder, H. (1966) New sun-shielding glasses for architectural purposes. *New Silicates* **10**: 10-14.

Schuler, M., Owen, G.R., Hamilton, D.W., de Wild, M., Textor, M., Brunette, D.M. & Tosatti, S.G.P. (2006) Biomimetic modification of titanium dental implant model surfaces using the RGDSP-peptide sequence: A cell morphology study. *Biomaterials* **27**: 4003-4015.

Schwartz, I., Anderson, P., de Lambilly, H. & Klein, L.C. (1986) Stability of lithium silicate gels. *Journal of Non Crystal Solutions* **83**: 391-399.

Scotchford, C.A., Cooper, E., Legget, G. J. & Downes, S.1998) Growth of human osteoblast-like cells on alkanethiol on gold self-assembled monolayers: The effect of surface chemistry. *Journal of Biomedical Materials Research* **41**: 431-439.

Scriven, F., Wlasichuk, K.B. & Palcic, M.M. (1988) A continual spectrophotometric assay for sol gels. *Annals of Biochemistry* **170**: 367-371.

Sepulveda, P., Bressiani A.H., Bressiani, J.C., Meseguer, L. & Konig, B. (2002) In vivo evaluation of hydroxyapatite foams. *Journal of Biomedical Materials Research* **62**: 587-592.

Shanon, R.D. (1976) Revised effective ionic radii and systematic studies of interatomic distances in halides and chalcogenides. *Acta Crystallography* **A32**: 751-757.

Shriver, D.F., Atkins, P.W. & Langford, C.H. (1995) *Inorganic Chemistry,* Second Edition, Oxford University Press.

Sigal, G. B., Mrksics, M. & Whitesides, G.M. (1998) Effect of surface wettability on the adsorption of proteins and detergents. *Journal of American Chemical Society* **120**: 3464-3472.

Skartveit, L., Selvig, K.A., MykleBust, S. & Tveit, A.B. (1990) Effect of TiF4 solutions on bacterial growth in vitro and on tooth surfaces. *Acta Odontological Scadanavia* **48**: 169-174.

Slosarczyk, A., Stobierska, Z., Paszkiewicz, Z. & Gawlicki, M. (1996) Calcium phosphate materials prepared from precipitates with various calcium: phosphorous molar ratios. *Journal of the American Ceramic Society.* **79**: 2539-2544.

Smith, D.K. (1994) Calcium Phosphate Apaptites in Nature, in *Hydroxyapatite and Related Materials.* Edited by P.W. Brown and B. Constantz, CRC Press, London, UK: 29-44.

Steinmann, S.G (2000) Titanium - the material of choice? *Periodontology* **17**: 7-21.

Strawbridge, I. & James, P.F. (1986) Thin silica films prepared by dip coating. *Journal of NonCrystal Solutions* **82**: 366-372.

Stringa, E., Filanti, C., Giunciuglio, D., Albini, A. & Manduca, P. (1995) Osteoblastic Cells from Rat Long Bone. I. Characterization of their Differentiation in Culture. *Bone* **16**: 663-670.

Stoch, A., Jastrzebski, W. & Dlugon, E. (2005) Sol-gel derived hydroxyapatite coatings on titanium and its alloy Ti6AL4V. *Journal of Molecular Structures* **744**: 633-640.

Strnad, Z., Strnad, J. & Urban, K. (2000) Effect of plasma- sprayed hydroxyapatite coating on the osteoconductivity of commercially pure titanium implants. *International Journal of Oral and Maxillofacial Implants* **15**: 483-490.

Sunny, M.C. & Sharma, C.P. (1991) Titanium-protein interaction: changes with oxide layer thickness. *Journal of Biomaterial Application* **6**: 22-29.

Surowska, M., Kiles, K. & Hughes P. (2004) Thin silica films prepared by dip coating. *Journal of NonCrystal Solutions* **82**: 366-372.

Sze, S.M. (1985) *Diffusion and ion implantation*, In: Sze, S.M. Semiconductor devices, Physics and Technology Wiley & Sons, New York: 381-427.

Taborelli, M., Jobin, M.,Francois, P.,Vaudaux, P., Tonetti, M., Szmucler-Moncler, S. & Simpson, J.P. (1997) Influence of surface treatments developed for oral implants on the physical and biological properties of titanium. *Clinical Oral Implant Research* **8(3)**: 208-216.

Tanahashi, M. & Matsuda, T. (1997) Surface functional group dependence on apatite formation on self-assembled monolayers in a simulated body fluid. *Journal of Biomedical Materials Research* **34**: 305-312.

Tegoulia, V. A., Rao, W., Kalambur, A. T., Rabolt, F. & Cooper, S.L. (2001) Surface properties, fibrinogen adsorption, and cellular interactions of a novel phosphorylcholine-containing self-assembled monolayer on gold. *Langmuir* **17**: 4396-4403.

Thomas, I.M. (1988) Multicomponent glasses from the sol-gel process. In: *Sol-Gel Technology for Thin Films, Fibers, Preforms, Electronics and Speciality Shapes.* Klein LC (Ed.). Noyes Pub., NJ, USA: 2-15.

Tkalcec, E., Sauer, M., Menninger, R. & Schmidt, H. (2001) Sol-gel derived hydroxyapatite powders and coatings. *Journal of Material Science* **36**: 5253-5263.

Tonsuaada, K., Peld, M., Leskela, T., Mannonen, R., Niinisto, L. & Veiderma, M. (1995) A thermoanalytical study of synthetic carbonate-containing apatites. *Thermochimica Acta* **256**: 55-65.

Tosatti, S., De Paul, S. M., Askendal, A., Van de Vondele, S., Hubbell, J. A., Tengvall, P. & Textor, M. (2003) Peptide functionalized poly(lysine)-*g*-poly(ethylene glycol) on titanium: resistance to protein adsorption in full heparinized human blood plasma. *Biomaterials* **24**: 4949-4958.

Townsend, P. D., Chandler, P. J. & Zhang, L. P. (1994) *Optical effects of ion implantation*. Cambridge University Press.

Trapalis, C., Kozhukharov, V., Samuneva B. & Stefanov, P. (1993) Sol-gel processing of titanium-containing thin coatings Part II : XPS Studies. *Journal of Material Sciences* **28**: 1276-1281.

Upasani, V.V., Farnsworth, C.L., Tomlinson, T., Chambers, R.C., Tsutsui, S., Slivka, M.A., Mahar, A.T. & Newton, P.O. (2009) Pedicle screw surface coatings improve fixation in nonfusion spinal constructs. *Spine* **34**: 335-343.

Vallet-Regi, M. (2001) Ceramics for medical applications. *Journal of the Chemistry Society* **2**: 97-108.

Van Noort., R. (2006) Principles of Adhesion. *Introduction to Dental Materials*: 61-5.

Verbeeck, R.M.H., De Maeyer, E.A.P. & Driessens, F.C.M. (1995) Stoichiometry of Potassium and Carbonate-Containing Apatites Synthesised by Solid Sate Reactions. *Inorganic Chemistry* **34**, 2084-2088.

Vercaigne, S., Wolke, J.G., Naert, I. & Jansen, J.A. (1998) Bone healing capacity of titanium plasma-sprayed and hydroxylapatite-coated oral implants. *Clinical Oral Implant Research* **9(4)**: 261-271.

Wang, C., Karlis, G.A., Anderson, G.I., Dunstan, C.R., Carbone, A., Berger, G., Ploska, U. & Zreiqat (2008) Bone growth is enhanced by novel bioceramic coatings on Ti alloy implants. *Journal of Biomaterial Research A* June 3 (Epub ahead of print).

Wang, B. C., Lee, T. M., Chang, E. & Yang, C. Y. (1993) The shear strength and the failure mode of plasma-sprayed hydroxyapatite coating to bone: the effect of coating thickness. *Journal of Biomedical Materials Research* **27**: 1315-1327.

Wen, F., Dai, H. N., Huang, H., Sun, Leng, Y. X. & Chu, P. K. (2002) Controlling synthesis of Ti–O/Ti–N gradient films by PIII. *Surface and Coatings Technology* **156**: 208-213.

Wen, H.B., Liu, Q., Wijn, J.R. & de Groot, K. (1998) Preparation of bioactive microporus titanium surface by a new two-step chemical treatment. *Journal of Material Science: Materials in Medicine* **9**: 121-128.

Wen, H.B,. Wolke, J.G., Wijn, J.R., Liu, Q., Cui, F.Z. & de Groot, K. (1997) Fast precipitation of calcium phosphate layers on titanium induced by simple chemical treatments. *Biomaterials* **18**: 1471-1478.

Wennerberg, A., Albrektsson, T. & Lausmaa, J. (1996) Torque and histomorphometric evaluation of cp titanium screws blasted with 25 and 75 µm sized particles of $Al_2O_3$. *Journal of Biomedical Materials Research* **30**: 251-260.

Willard, H.H, Merritt, L.L. & Dean, J.A. (1981) *Instrumental Methods of Analysis*. Wadsworth Publishing Group, New York.

Williams, D.H. & Fleming, I. (1995) *Spectroscopic Methods in Organic Chemistry* 5th edition. McCraw-Hill.

Worrall, W.E. (1975) *Clays and Ceramic Raw Materials,* Applied Science Publishers.

Xiao S.J., Kenausis, G. & Textor M. (2001) *Titanium in Medicine*. In: D.M. Brunette, P. Tengvall, M. Textor and P. Thomsen, Editors, Springer, Berlin: 417–455.

Xiao, S.J., Textor, M., Spencer, N.D. & Sigrist, H. (1998) Covalent attachment of cell-adhesive, (Arg-Gly-Asp)-containing peptides to titanium surfaces. *Langmuir* **14**: 5507-5512.

Xiao, S.J., Textor, M., Spencer, N.D., Wieland, M., Keller, B. & Sigrist, H. (1997) Immobilization of the cell-adhesive peptide Arg–Gly–Asp–Cys (RGDC) on titanium surfaces by covalent chemical attachment. *Journal of Material Science: Materials in Medicine* **8**: 867-875.

Xynos, I.D., Edgar, A.J., Buttery, L.D., Hench, L.L. & Polak, J.M. (2001) Gene-expression profiling of human osteoblasts following treatment with the ionic products of Bioglass. *Journal of Biomedical Materials Research* **55**: 151-157.

Yang, X., Han, Y., Lin, K., Tian, G., Feng, Y., Meng, X., Di, Y., Du, Y., Zhang, Y. & Xiao, F.S. (2004) Catalytically stable titanium sites. *Chemistry* **21**: 2612-2615.

Yang, Y. & Ong, J.L. (2003) Bond strength, compositional and structural properties of hydroxyapatite coatings on Ti, ZrO2-coated Ti, and TPS-coated Ti substrate. *Journal of Biomedical Materials Research A* **64**: 509-516.

Yang, C. Y., Wang, B. C. & Lee, T. M. (1997) Intramedullary implant of plasma-sprayed hydroxyapatite coating: An interface study. *Journal of Biomedical Materials Research* **36**: 39-48.

Yoldas, B.E. (1984) Wide-spectrum anti-reflective coatings for fused silica and other glasses. *Applied Optics* **23**: 1418-1420.

Yoshida, K., Kamada, K., Sato, K., Hatada, R., Baba, K. & Atsuta, M. (1999) Thin sol-gel-derived silica coatings on dental pure titanium casting. *Journal of Biomedical Materials Research B Applied Biomaterials* **48**: 778-785.

Yoshinari, M., Oda, Y., Kato, T., Okuda, K. & Hirayama, A. (2001) Influence of surface modifications to titanium on antibacterial activity in vitro. *Biomaterials* **22**: 2043-2048.

Zheng, H., Colby,M.W. & Mackenzie J.D. (1988) *The control of precipitation in sol-gel solutions*. In: Better Ceramic Through Chemistry (3rd Edition). Brinker CJ, Clarke DE, Ulrich DR (Eds). Materials Research Society, PA, USA: 537-540.

Zhou, J., Zhang, X., Chen, J., Zeng, S. & Groot, K. (1993) High temperature characteristics of synthetic hydroxyapatite. *Journal of Materials Science: Materials in Medicine* **4**: 83-85.

Zreiqat, H., Valenzuela, S.M. & Ben-Nissan, B. (2005) The effect of surface chemistry modification of titanium alloy on signalling pathways in human osteoblasts. *Biomaterials* **26**: 7579-7586.